Distribution Agreement

In presenting this thesis or dissertation as a partial fulfillment of the requirements for an advanced degree from Emory University, I hereby grant to Emory University and its agents the non-exclusive license to archive, make accessible, and display my thesis or dissertation in whole or in part in all forms of media, now or hereafter known, including display on the world wide web. I understand that I may select some access restrictions as part of the online submission of this thesis or dissertation. I retain all ownership rights to the copyright of the thesis or dissertation. I also retain the right to use in future works (such as articles or books) all or part of this thesis or dissertation.

Signature:

_____ _____

Timothy Nguyen Hoang Date

Lessons from One Pandemic to Another: HIV and SARS-CoV-2

By

Timothy Nguyen Hoang
Doctor of Philosophy

Graduate Division of Biological and Biomedical Science
Immunology and Molecular Pathogenesis

_____
Mirko Paiardini, Ph.D.
Advisor

_____
Rafi Ahmed, Ph.D.
Committee Member

_____
Haydn Kissick, Ph.D.
Committee Member

_____
Joshy Jacob, Ph.D.
Committee Member

_____
Jason Brenchley, Ph.D.
Committee Member

Accepted:

_____
Kimberly J. Arriola, Ph.D.
Dean of the James T. Laney School of Graduate Studies

_____
Date

Lessons from One Pandemic to Another: HIV and SARS-CoV-2

By

Timothy Nguyen Hoang

B.S., Drexel University, 2015

Advisor: Mirko Paiardini, Ph.D.

An abstract of
A dissertation submitted to the Faculty of the
James T. Laney School of Graduate Studies at Emory University
In partial fulfillment of the requirements for the degree of
Doctor of Philosophy

Program in Immunology and Molecular Pathogenesis
Graduate Division of Biological and Biomedical Sciences

2021

Abstract

Lessons from One Pandemic to Another: HIV and SARS-CoV-2

By Timothy N. Hoang

The latent HIV reservoir is comprised of a subset of long-lived HIV-infected $CD4^+$ T cells that can persist during antiretroviral therapy (ART) and constitutes the main barrier to achieving HIV remission. Understanding the anatomical residence of the viral reservoir and the nature of the cells that harbor latent virus would aid in the design of therapeutics targeted at the 37.6 million people worldwide living with HIV. Using the clinically relevant non-human primate model for HIV infection and clinical specimens, we sought to investigate the poorly characterized role played by the bone-marrow (BM) compartment in HIV pathogenesis and viral persistence.

We tracked the longitudinal kinetics of BM derived $CD4^+$ T cells before and following SIV infection and evaluated their contribution to the viral reservoir during ART. We found that BM derived memory $CD4^+$ T cells were rapidly depleted following SIV infection, expressed high levels of PD-1 and CTLA-4, recently proliferated (Ki-67^+), and harbored SIV-DNA and SIV-RNA at levels akin to that of circulating memory $CD4^+$ T cells. In summation, the BM compartment is a site of viral persistence that remains largely understudied and has a vital contribution to HIV viral persistence.

During late 2019 and the beginning of 2020, there was a rapid emergence and dissemination of a viral infection that caused pneumonia. This virus was then named SARS-CoV-2 and determined to be the causative agent behind the COVID-19 pandemic. Infection with SARS-CoV-2 is rapidly followed by induction of systemic inflammation, disease pathogenesis, and infiltration of immune cells into the respiratory tract. Using non-human primates, we sought to understand the underlying mechanisms driving systemic inflammation, disease pathogenesis, and evaluate the efficacy of immune modulators.

We tested baricitinib, which is a Janus Kinase (JAK) 1 and 2 inhibitor that is approved for treatment of active rheumatoid arthritis. It was reported that baricitinib could have two beneficial treatment modalities: anti-viral and anti-inflammatory properties. Viral shedding patterns in the bronchoalveolar lavage and nasal/throat swabs were not reduced with baricitinib. However, animals treated with baricitinib exhibited a profound decrease in inflammation, lung pathology, infiltration of inflammatory cells, and NETosis activity. These data support a beneficial role for using baricitinib during acute infection and elucidate the mechanism of action to mitigate disease severity.

In addition, we were interested in the role that type-I interferons (IFN-I) play following SARS-CoV-2 infection. To understand this, we modulated IFN-I signaling using an IFN-I antagonist (IFNant) prior to infection through day 2 of infection in non-human primates. Remarkably, IFNant treatment resulted in a highly significant and consistent reduction in viral load in the lower and upper airways. Furthermore, treatment with IFNant potently reduced soluble markers of inflammation in bronchoalveolar lavage (BAL) fluid, expansion of inflammatory monocytes, and pathogenesis in the lung. Thus, IFNant treatment resulted in limited viral replication and reduction of inflammation and pathogenesis in SARS-CoV-2-infected RMs. These data indicate a vital and early role of IFN-I in regulating COVID-19 progression and emphasize the importance of identifying and understanding IFN-I pathways in COVID-19 for the development of therapeutic strategies.

These studies highlight the importance of non-human primates as models to understand infectious disease dynamics and therapeutic modalities. Taken together, these diverse studies

across two different infection models underlie the importance of understanding the immune response following infection, the key determinants of pathogenesis, and how to target these pathways for therapeutic benefit.

Lessons from One Pandemic to Another: HIV and SARS-CoV-2

By

Timothy Nguyen Hoang

B.S., Drexel University, 2015

Advisor: Mirko Paiardini, Ph.D.

A dissertation submitted to the Faculty of the
James T. Laney School of Graduate Studies at Emory University
In partial fulfillment of the requirements for the degree of
Doctor of Philosophy

Program in Immunology and Molecular Pathogenesis
Graduate Division of Biological and Biomedical Sciences

2021

Acknowledgements

I would first like to thank my mentor, Mirko Paiardini, for giving me the opportunity to be one of the first PhD students in his lab. I am absolutely grateful for his support, guidance, trust and encouragement during my time in his lab. I value the freedom that was afforded to me to pursue my interests and take the lead on projects well outside the scope of the lab. Mirko, you have taught me to be the best scientist that I can be and to always challenge the status quo with exciting scientific questions, this is something that I will carry with me wherever I go. I would also like to thank all current and former members of the Paiardini lab for their support, encouragement, critiques, and friendship over the years. I would like to especially thank Justin Harper, Maria Pino, Zachary Strongin, Elise Viox and Kevin Nguyen for being a constant source of advice, banter, and support during my time. In addition, I would like thank all members of the Yerkes National Primate Research Center veterinary and research staff, without which none of this would have been possible.

I also must thank my family. My parents (Thanh Hoang and Thien Nguyen) who have raised me to be the best version of myself and always supported my goals and dreams. I would also like to thank the friends I made along the journey: starting at Drexel University, to the Vaccine Research Center at the NIH, and here at Emory University.

Thank you all!

Table of Contents

Table Index

Figure Index

Figure 3.S1. Baricitinib was well-tolerated and detectable in the central nervous system in SARS-CoV-2-infected RMs, related to Figure 3.1

Figure 3.S2. Baricitinib reduced lung neutrophil and macrophage infiltration, preserved IFN responses but did not reduce SARS-CoV-2 replication in RMs, related to Figures 3.1 and 3.2.

Figure 3.S3. Baricitinib Suppressed the expression of inflammatory mediators and neutrophil degranulation genes in BALs from SARS-CoV-2-infected RMs, related to Figure 3.3.

Figure 3.S4. Baricitinib inhibited the expression of inflammatory and macrophage/neutrophil chemokine genes while preserving ISGs in lung macrophages from SARS-CoV-2-infected RMs, related to Figure 3.4.

Figure 3.S5. Baricitinib reduced the expression of inflammatory and chemokine genes while maintaining ISGs in BALs from SARS-CoV-2- infected RMs, related to Figure 3.4.

Figure 3.S6. Flow cytometry gating strategy for innate and adaptive cells, related to Figures 3.5 and 3.6.

Figure 3.S7. Baricitinib treatment did not affect the immune T cell responses in SARS-CoV-2-infected RMs, related to Figure 3.6.

Figure 4.1. Early expansion of inflammatory cells in the blood following infection with SARS-CoV-2.

Figure 4.2. Early pro-inflammatory and ISG response observed in airways and peripheral blood by bulk transcriptomics.

Figure 4.3. Influx of pro-inflammatory macrophages in BAL

Figure 4.4. Baricitinib reduced the influx of pro-inflammatory macrophages in addition to the pro-inflammatory gene expression profile.

Figure 4.S1. Flow sorting strategy for different immune cell populations.

Figure 4.S2. Longitudinal flow cytometric analysis in BAL and blood following SARS-CoV-2 infection.

Figure 4.S3. Bulk transcriptomic analysis of airways and peripheral blood.

Figure 4.S4. Reference used for annotating macrophage/monocyte subsets.

Figure 4.S5. Cell annotation using bulk sorted cells as reference.

Figure 4.S6. Expression of DE genes in different macrophage/monocyte subsets

Figure 5.1 IFNant treated RMs have lower levels of viremia during treatment phase.

Figure 5.2. Reduced disease pathogenesis and lower levels of lung pathology in IFNant-treated RMs.

Figure 5.3. Decreased expansion of pro-inflammaotry monocytes and Siglec-1 expression in IFNant-treated RMs.

Chapter One: Introduction – HIV and SARS-CoV-2

Discovery and origins of HIV/AIDS

Human immunodeficiency virus (HIV) is the causative agent that results in individuals developing acquired immune deficiency syndrome (AIDS) [1, 2]. Currently, there are 37 million people living with HIV, with 1.8 million new infections and 1 million HIV-related deaths due to complications occurring each year. The first cases of AIDS in the U.S. were reported in 1981 when a group of previously healthy, homosexual men in New York City and Los Angeles perished due to Pneumocystis pneumonia and Kaposi's sarcoma respectively, which only occur in individuals who are severely immunocompromised [2, 3]. Shortly after these events, Drs. Luc Montagnier and Françoise Barré-Sinoussi identified HIV as the virus that caused AIDS for which they won the Nobel Prize in Physiology or Medicine in 2008 [1, 2].

HIV is subdivided into two species; HIV-1 and HIV-2. HIV-1 is characterized by its high virulence and infectivity, global distribution, whereas, HIV-2 is less virulent and infectious and confined to West Africa [4]. Sequencing of HIV-1 and HIV-2 has revealed that HIV-1 is closely related to SIV_{cpz} (common chimpanzee) and HIV-2 is closely related to SIV_{SMM} (sooty mangabey) [5-7]. It is thought that SIV was able to jump the species barrier on at least four different occasions, resulting in the four groups (M, N, O, and P) [8-10]. There is also supportive evidence that individuals who participated in the bushmeat trade (hunters or vendors) were infected by SIV, leading to the evolution of HIV and subsequent spread across the globe.

Group M is the most common type of HIV-1, as it currently accounts for >90% of HIV/AIDS cases [11]. Group M viruses are further divided into nine clades (A, B, C, D, F, G, H, J, and K), in addition to the nine clades there are also hybrid viruses (circulating recombinant form; CRFs) [11]. Subtypes A and D are predominantly found in Eastern Africa, subtype C is found in Southern

Africa and parts of Asia, and subtype B is the dominant form in the Americas, Europe, and Australia [12, 13].

Viral properties and lifecycle of HIV

HIV is a single-stranded, positive-sense, enveloped RNA (+ssRNA) virus belonging to the lentivirus group and a part of the *retroviridae* family [14]. HIV primarily targets cells of the human immune system such as $CD4^+$ T cells, macrophages, and dendritic cells [15]. The HIV genome is 9.2 kilobases (kb) in length and can encode genes for structural and accessory proteins. Within each HIV virion are two copies of the genome, reverse transcriptase, integrase and protease. The three main structural proteins are *gag*, *pol*, and *env* and the accessory proteins are *tat*, *rev*, *nef*, *vpr*, *vif*, and *vpu* [16]. *Gag* encodes for core and matrix proteins which are necessary components of the viral core. *Pol* encodes proteins for viral infection and replication. *Env* will encode the transmembrane glycoproteins gp120 and gp41, that assemble as trimers on the surface of the virion and serve to bind to target cell receptors and co-receptors for viral entry. The accessory proteins are utilized for viral production and dampening host response, such as *nef* downregulating CD4, MHC-I, and MHC-II molecules; whereas, *Tat* enhances efficiency of viral transcription.

In order for HIV to enter a target cell, gp120 on the surface of the virion binds to its target receptor, CD4, which induces a conformational shift in gp120 exposing its co-receptor binding site which then binds to either CCR5 or CXCR4 depending on the tropism of the virus [17-23]. Gp41 is the fusion peptide acting as a hydrophobic harpoon that allows for fusion of the viral envelope to the cell membrane where the virus can then enter the cell and uncoat [24, 25]. Upon entry into its target cell, HIV will utilize reverse transcriptase that it shuttles in to convert its RNA genome into double-stranded DNA (dsDNA). The resulting dsDNA is then translocated to the nucleus and integrates into host DNA, with increased frequency at activated genes, via integrase and other co-factors. Reverse transcriptase is also highly error prone, which allows for rapid viral evolution

and the establishment of viral diversity as there is an average one nucleotide swapped per replication [26-28]. Once inside the host cell, HIV will hijack host machinery to replicate and disseminate to infect other cells.

HIV/SIV pathogenesis and immune dysregulation

HIV infection occurs via the transfer of bodily fluids (blood, semen, vaginal secretions, and breastmilk) from an infected individual. Based on current statistics, most occurrences of HIV transmission are due to heterosexual transmission [29-31]. However, there is a sizable rate of transmission in homosexual populations and intravenous (IV) drug users, with a small proportion of transmission occurring in mother-to-child settings [32, 33].

The risk of transmission following an exposure event has been deemed to be relatively low, with 1 transmission event per 200-2000 exposures in male-to-female and 1 transmission per 700-3000 exposures in female-to-male heterosexual transmission [34]. Viral transmission can be achieved either by free virus present in fluids or alternatively the transfer of infected cells between partners[35]. A study by Derdeyn et al. showed that primary infection is achieved by one viral variant termed the 'transmitted founder' virus that is able to establish the infection in the mucosa, this variant is classically described to have the highest viral fitness [36, 37]. After this initial transmission event, the virus that seeds the infection rapidly expands to infect other target cells and then disseminates to lymphoid tissue and inducing a systemic infection. HIV replicates continuously throughout the course of an untreated and uncontrolled infection, where it is able to evade host immune response via accessory proteins and rapid mutations to epitopes that can be targeted by $CD8^+$ T cells and antibodies [38-41].

HIV is able to disrupt the adaptive immune response as it primarily targets $CD4^+$ T cells, or helper T cells, which play vital roles in aiding cytotoxic T cells and the development of antibody responses [42]. During acute HIV and SIV infection, there is a preferential and significant loss of memory $CD4^+$ T cells from mucosal sites [43, 44]. At the height of infection, 30-60% of memory $CD4^+$

T cells are infected, with most infected cells dying within four days of infection [44]. Mucosal site memory $CD4^+$ T cells are highly infected due to their high expression of CCR5 and being in a relatively activated state, thus are the ideal target cells for HIV [17, 18, 20, 45, 46]. In pathogenesis studies of SIV infection, it has been seen that after infection is established within the mucosa, SIV is rapidly disseminated to local and distant tissues including lymph nodes, spleen, thymus, and mucosal tracts [42, 47-50]. *In situ* hybridization of SIV and HIV RNA probes also shows that there is a higher frequency of infected $CD4^+$ T cells within lymph nodes and mucosal tracts during the chronic phase of infection [42, 50-53]. In the absence of any ART, HIV establishes itself as a chronic and progressive infection that over the span of several years leads to destruction of the adaptive immune system and fatal immunodeficiency [42].

Clinical symptoms of an HIV infection are similar to that of flu with indications that include a high fever, sore throat, rash, and lymphadenopathy. These symptoms tend to resolve if immediate medical attention is sought. In the acute symptomatic phase of HIV infection, which lasts for a few weeks, there is an association with high viremia, significant decline in levels of peripheral $CD4^+$ T cells, establishment of a viral reservoir, and development of an HIV-specific immune response [42, 54-67]. Early infection results in rapid depletion of $CD4^+$ T cells in the gastrointestinal tract, leading to microbial translocation and results in systemic immune activation and inflammation [42]. Following this acute phase, the plasma viremia decreases to set point, there is a slight increase to numbers of peripheral $CD4^+$ T cells, followed by an asymptomatic phase of chronic infection lasting on average of 10 years [42]. Following this chronic phase, is a marked but steady decline of peripheral $CD4^+$ T cells and increased plasma viremia. During this phase, $CD4^+$ T cell counts can decline to <200 cells/μL (AIDS), at which point, opportunistic infections and tumors that are AIDS related take hold [42].

Immune response to HIV

Prior to triggering any sort of adaptive immune response, HIV induces a rapid response from the innate immune system. We have germline encoded host-restriction factors that serve to rapidly respond to viral antigen, with the primary role being to limit viral replication. TRIM5α which is present within the cytoplasm can recognize specific motifs present on viral capsid proteins and prevents the virus from uncoating, thereby preventing reverse transcription and transport into the nucleus [68-70]. Another restriction factor, tetherin, prevents spreading of infection by preventing viral particles from budding and is able to promote an inflammatory response [71]. APOBEC3G interferes with viral replication by acting as an activation-induced cytidine deaminases (AID) to induce deoxycytidine to deoxyuridine mutations of the negative strand of the viral DNA [72-74].

The innate immune response is not limited to just restriction factors, but there is also a cellular response that occurs prior to the adaptive response. Studies in SIV infected rhesus macaques (RMs) have elucidated the early events following infection, particularly at mucosal sites. After infection, there is a rapid expansion of plasmacytoid dendritic cells (pDCs), and a large induction of pro-inflammatory cytokines and chemokines, such as IFNα and TNFα [75-77]. All together, these early events result in the recruitment of innate and adaptive immune cells following infection. There is also a rapid induction of genes related to innate immune signaling and inflammation [78-83]. Acting differently from restriction factors, pathogen recognition receptors (PRRs) of the innate immune system recognize different components of viruses (viral particles, intracellular virus, and endogenous viral elements) to induce a rapid response. If activated on an antigen-presenting cell (APC), these PRRs will induce the upregulation of MHC molecules and costimulatory molecules to induce the activation and differentiation of naïve T cells. Viral RNA can also trigger TLR7 and TLR8 responses [84].

A phenomenon termed ‘microbial translocation’ has been described by Brenchley et al. that links damage of the gut mucosa to systemic inflammation during chronic infection and progression

to AIDS [85]. $CD4^+$ T cells within the gut are targeted and depleted during infection [86, 87]. Within the $CD4^+$ T cell populations, T_H17 $CD4^+$ T cells play a vital role in the maintenance of barrier integrity, and their depletion results in a 'leaky gut' where bacterial and bacterial products such as lipopolysaccharide (LPS) can escape and induce systemic inflammation and immune activation by binding to TLR4 [85]. Several SIV studies have shown that viral replication within lymphoid organs, such as lymph nodes, induces a robust and rapid IFN-I response in both pathogenic and non-pathogenic conditions [88, 89]. This upregulation of interferon stimulated genes (ISGs) is resolved in non-pathogenic infections, but remains elevated in pathogenic conditions, which could be a mechanism of viral persistence [78-83]. Natural killer (NK) cells have also been described to have a vital role in the control of non-pathogenic infection. Huot et al. demonstrated that the depletion of NK cells by blocking IL-15 resulted in viral replication and $CD4^+$ T cell depletion in African Green Monkeys (AGMs), which have been shown to natural hosts who can control viral replication without the administration of ART [90].

HIV and SIV will also induce activation and expansion of Ag-specific $CD8^+$ T cells (cytotoxic T cells) that can be seen after ~2-4 weeks of infection. The importance of $CD8^+$ T cells has been demonstrated in several studies where $CD8^+$ T cells were depleted pre-ART and during ART. The depletion of $CD8^+$ T cells during ART resulted in viremia in RMs and viral suppression was established once $CD8^+$ T cells returned. The activation and differentiation have been linked to the large expansion of HIV/SIV specific $CD8^+$ T cells as well as the expansion of bystander $CD8^+$ T cells due to systemic immune activation [91-96]. The presence of HIV/SIV-specific $CD8^+$ T cells has been strongly correlated with the decline in viremia and studies have shown that it also coincides with a lower setpoint and the seeding of the viral reservoir [63, 93, 97]. $CD8^+$ T cells of HIV controllers have been shown to possess higher proliferative capacity and survivability, are more differentiated, greater expression of CD127 (needed for generation of a memory pool), and heightened cytolytic potential (more granules and perforin) [98-104]. Recent work by Buggert et al.

showed that HIV controllers had higher levels of tissue resident memory (T_{RM}) $CD8^+$ T cells and these T_{RMs} were enriched for effector-related genes and signatures when compared to non-T_{RMs} $CD8^+$ T cells [105]. Taken together, Buggert et al. show that previous studies of peripheral $CD8^+$ T cells do not fully capture the nature of $CD8^+$ T cells within lymphoid tissue. However, the robust $CD8^+$ T cell response is unable to control the infection. This is due to viral escape due to selective pressure by $CD8^+$ T cells and immune exhaustion (See section 'Chronic infection and immune exhaustion') allowing the virus to escape and continue replicating [106, 107].

HIV-specific $CD4^+$ T cells have been shown to expand during the acute phase of infection. Studies have shown that HIV-specific $CD4^+$ T cells with cytolytic and proliferative potential has been associated with lower levels of viremia [66, 108]. However, HIV-specific $CD4^+$ T cells are preferentially infected by HIV and contain higher levels of HIV-DNA compared to memory $CD4^+$ T cells during all stages of infection [109]. As mentioned previously, the loss of T_H17 $CD4^+$ T cells within the mucosa results in microbial translocation and systemic immune activation. This occurs as T_H17 $CD4^+$ T cells produce IL-17 and IL-22, which are critical to maintaining gut barrier integrity [110]. IL-22 mainly acts on stromal and epithelial cells for survival, proliferation, and production of antimicrobials and plays a role in wound healing. Studies by Paiardini et al. have shown infusion with recombinant IL-21 in SIV-infected RMs restored levels of T_H17 $CD4^+$ T cells, resulting in decreased inflammation and reduction in plasma viremia and viral reservoir size [110, 111].

IgM antibodies are generated very early on during acute HIV infection, but these antibodies have no capacity to neutralize HIV [112]. Neutralizing antibodies to HIV are generally derived from class switching and through affinity maturation to have more specific antibodies. This is generally a very arduous process that can take several months to years to generate potent antibodies via somatic hypermutation, V_H replacement, receptor editing, and class switch recombination [113]. The development of antibodies with neutralizing capabilities seems to be delayed during HIV infection, this could be attributed to presence of multiple quasi-species, further enhancing HIV's

ability to escape immune detection and the virus' ability to quickly adapt to the host environment and the depletion of T_{FH} cells [112, 114]. There have been instances in select individuals where the antibody response co-evolved with the virus, resulting in the generation of antibodies with broad neutralizing capacity (broadly neutralizing antibodies; bnAbs) [114]. These bnAbs can target conserved residues on the HIV *env* trimer, such as the CD4 binding site (VRC01, 3BNC117, and VRC07) or the fusion peptide [24, 25, 115]. The ability to generate these bnAbs remains elusive, but some studies suggest that the development of these bnAbs can be attributed to high antigen load, as bnAbs have been more readily found in individuals who have been untreated for several years or in subjects with high levels of viremia [116]. The difficulty in generating bnAbs in a large population of individuals has been linked to bnAbs needing a large accumulation of mutations in order to be able to neutralize multiple strains of HIV [117, 118]. HIV replicating within secondary lymphoid organs may also alter the development of antibodies. B cells have been shown to undergo 'exhaustion' that is linked to the cytokine profile generated during HIV infection [119-122]. T follicular helper (T_{FH}) $CD4^+$ T cells are also preferential targets of HIV, and have been shown to sustain HIV replication within the lymph node [123-126]. The loss of T_{FH} cells could delay the development of antibodies, allowing HIV infection to continue if left untreated.

Antiretroviral therapy

The advent of antiretroviral therapy (ART) has resulted in a substantial reduction in HIV-related morbidities and mortalities and reduced transmission. However, the interruption of ART results in rapid viral recrudescence due to a reservoir of latently infected $CD4^+$ T cells [55, 59, 123, 126-129]. Thus, adherence to a daily ART regimen is crucial in maintaining viral suppression and preventing transmission to uninfected individuals.

ART has been designed to target all aspects of the viral lifecycle to prevent the spread of infection to neighboring cells. Current ART drugs target three main proteins of viral replication: reverse transcriptase, integrase, and protease. Reverse transcriptase is targeted by either

nucleoside analogs (nucleoside transcriptase inhibitors, NRTIs) or non-nucleoside analogs (nonnucleoside transcriptase inhibitors, NNRTIs) to inhibit the function of reverse transcriptase and production of new virus. Examples of NRTIs are emtricitabine (FTC) or tenofovir disoproxil fumarate (TDF). NNRTIs commonly used are efavirenz (EFV) and etravirine (ETR). Integrase inhibitors, such as Dolutegravir (DTG) and Raltegravir (RAL), prevent the integration of the viral genome into host DNA [130-132]. The last class of ART drugs target viral protease, saquinavir and darunavir, and these drugs act to prevent the final stages of viral processing and budding of viruses. Protease inhibitors are generally only used in 2nd or 3rd line regimens. Some other less common drugs target the CCR5 co-receptor or block HIV fusion (enfuvirtide or T20). However, these drugs are more expensive compared to the classic drug regimen and only used in salvage therapy once multi-drug resistance has been developed [133]. In 1997, a combination of three ART drugs were shown to be able to robustly suppress plasma viremia to undetectable levels based on the assays at the time, which is consistent with the cessation of viral replication [134-136].

Currently, there is a large push for the use of pre-exposure prophylaxis (PrEP) to mitigate transmission risk among vulnerable and high-risk populations [137, 138]. Truvada (2 drug combination of FTC and TDF) is currently recommended by the Centers for Disease Control (CDC) as studies have shown that taking Truvada decreased the risk of contracting HIV by 51% [139].

In the absence of a scalable treatment able to functionally cure or eradicate HIV, ART remains a lifelong treatment placing an excessive onus on individuals and public health systems. Individuals living with HIV face several challenges such as readily available access to ART and affordability, side effects due to long-term ART administration, and complications due to residual immune activation that persists during therapy that has been associated with maintenance of the viral reservoir [140-144]. Long-term ART administration also has side effects such as development of hypersensitivity/allergies, nausea, bone degeneration, and heart disease [145]. Lack of

adherence to the prescribed ART regimen can lead to the development of HIV-drug resistance, that necessitates the migration to 2nd or 3rd line regimens that are considerably more toxic with increased instances of adverse events.

The viral reservoir and immune escape

ART is highly effective at reducing HIV plasma viremia to undetectable levels, however, once ART is interrupted there is rapid recrudescence of HIV resulting in increased viremia and depletion of $CD4^+$ T cells as ART alone is unable to clear the viral reservoir. This viral rebound is due to a reservoir of resting $CD4^+$ T cells that contain latent HIV-1 proviruses that are replication competent. The ability for HIV to achieve a state of latency and remain quiescent in long-lived memory $CD4^+$ T cells is the main obstacle to achieving a sterilizing cure [55, 56, 59, 60, 127, 128, 146, 147]. Latency is described as a reversible non-productive state of infection, and a reservoir is defined as a cell that shows long-term maintenance and persistence of replication-competent/inducible virus while on suppressive ART. The cessation of ART can reactivate one or multiple latently infected $CD4^+$ T cells that results in viral production, new infection of previously uninfected $CD4^+$ T cells, and exponential viral rebound within two weeks of ART interruption [127, 148].

In individuals on suppressive ART, HIV remains persistent as measured by integrated viral DNA within resting $CD4^+$ T cells, with little to no expression of viral RNA while the cells are in a quiescent state [146]. Multiple studies have been performed, and they have shown that $CD4^+$ T cells containing HIV genomes are essentially indistinguishable from an uninfected cell, thus the field is currently elucidating potential markers of the reservoir. Hill et al. demonstrated that latency and quiescence are not permanent, as cells containing intact proviral genomes can be reactivated upon stimulation [149]. Studies by Siliciano et al. have shown that the latent reservoir decays at a slow rate, with a half-life ($t_{1/2}$) of 3.6 years, thus in order to eradicate HIV with ART alone would take in excess of 70 years of therapy due to the size of the reservoir (10^5-10^7 $CD4^+$ T cells) [59, 150-153]. Recent findings have elucidated key details about the state of the latent reservoir. Using full

viral genome sequencing, Ho et al. and others showed that ~93% of proviruses in resting $CD4^+$ T cells of ART-suppressed individuals were defective, meaning that there were large deletions or mutations within the viral genome rendering it unable to replicate once ART is stopped [154-160]. Defining the total burden of the reservoir is also another area that has studied recently. Before ART is initiated, lymphoid tissues contain >98% if SIV-RNA^+ and SIV-DNA^+ cells [161]. On ART, the majority of infected cells were in lymphoid tissues with the largest proportion being the gastrointestinal compartment [161].

To date, latency induction and seeding of the viral reservoir remains unclear. There are multiple models and theories presented, however, the simplest explanation or Occam's razor is that latency occurs as an accident of timing. Based on what we know about HIV infection and target cells, it is unclear why the latent reservoir is established within resting memory $CD4^+$ T cells. Resting $CD4^+$ T cells do not express CCR5, the necessary co-receptor required for viral entry [17, 18, 20, 162]. Abortive infection of resting $CD4^+$ T cells has also been shown to induce cell death [163]. The most likely scenario for latency induction is the infection of an activated $CD4^+$ T cell that is reverting to a resting state [136, 164-166]. While productive infection of an activated $CD4^+$ T cell normally results in cell death, the transition of an activated cell to a resting state could convert the cell to a long-lived quiescent cell. This scenario provides the optimal conditions for latency establishment as there is high expression of CCR5/CXCR4, dNTP pools for reverse transcription, and reduction in viral gene expression due to downregulation of host derived activation transcription factors (NFAT and NFκB) [166]. These cells can undergo replication and integration of the viral genome, but since they are not actively producing viral particles they can escape immune detection and enter latency. Studies using SIV have shown that latency and the reservoir can be seeded in as little as 3 days after infection [167-169]. Reports in HIV infected individuals also showed that a latent reservoir of 10^5-10^7 cells is seeded during acute infection and early chronic infection [55, 56].

The reservoir has been described as being stable with little turnover, and this can be attributed to the longevity of resting $CD4^+$ T cells [43, 128, 170]. $CD4^+$ T cells in a resting state can undergo homeostatic proliferation or antigen-stimulated proliferation to maintain their numbers [171-180]. Recent efforts have shown that HIV persistence is due to clonal expansion of infected cells. The first papers showed that there were predominant clones detectable in plasma of HIV infected individuals on suppressive ART [181, 182]. This demonstrated for that the first time that HIV was able to persist over several years without undergoing any evolution to its genome. The next line of evidence for clonal expansion came from studies looking at integration sites. Since HIV integrates randomly into transcriptionally active regions of host DNA, integration sites can serve as 'barcodes' to determine if the infected cell comes from an infected clone. Multiple studies described finding HIV-DNA^+ $CD4^+$ T cells with the same integration site and full-length vital sequence from a given subject on ART, further confirming that HIV persists via clonal expansion [183-190]. IL-7 and IL-15 driven homeostatic proliferation has also been described to increase the number of infected cells [170, 191].

A study by Boritz et al. tracked HIV replication and persistence of infected $CD4^+$ T cells in study subjects with natural virologic control (controllers) or viremics via viral sequencing, TCR repertoire genes, integration site analysis, and whole transcriptomic analysis [124]. They described three distinct mechanisms of viral persistence that occur within different anatomic and functional compartments. Within lymph nodes, they saw that viruses had genetic and transcriptional characteristics of active replication within T_{FH} and non- T_{FH} memory $CD4^+$ T cells. In the blood compartment, they were able to detect inducible proviruses with an archival origin among differentiated and clonally expanded $CD4^+$ T cells. They were able to link the blood and lymph node via a small pool of circulating $CD4^+$ T cells containing proviruses of recent origin [124]. They concluded that in individuals with an active antiviral immune response, HIV was able to persist via active replication within lymphoid tissues, clonal expansion of infected cells, and recirculation

of recently infected cells. Lymphoid tissues are currently thought to be the primary anatomical reservoir harboring replication competent virus during suppressive ART [123, 129, 161, 192]. Quantification of HIV-DNA has shown that there was a higher proportion of infected cells within lymph nodes as compared to blood [193]. Studies have also shown that within lymph nodes, there are no infiltrating $CD8^+$ T cells, further enhancing the environment for viral persistence.

A surface marker that is able to delineate an infected cell from an uninfected cell has proven difficult to find. Several groups have demonstrated that the expression of exhaustion markers on the surface of $CD4^+$ T cells could identify infected cells, however, there is no one marker that is able to discern all infected cells within a host. In lymph nodes, T_{FH} cells ($CXCR5^+$) expressing PD-1 were shown to contain inducible proviruses [123, 124, 126]. One caveat of these cells could be that they remain activated, thus not the true latent reservoir. A study by McGary et al. in SIV infected RMs showed that CTLA-4^+ PD-1^- memory $CD4^+$ T cells were enriched for replication competent virus in all anatomically tissues that were sampled (blood, lymph node, spleen, and gut) [129]. Descours et al. showed that CD32a, an F_C receptor not usually expressed on $CD4^+$ T cells was enriched for inducible and replication competent virus [194]. However, since the initial publication, several groups of followed up with CD32a with conflicting results stating that CD32a is not a marker of the reservoir [155, 195-197].

Chronic infection and immune exhaustion

One of the first studies looking at cytolytic T cell responses during HIV infection led by Lieberman et al. showed that $CD8^+$ T cell function was compromised during chronic HIV infection, with lower levels of granzyme and perforin [198, 199]. This idea was further explored and the field of $CD8^+$ T cell exhaustion during chronic infection was formed, leading to new insights into other chronic diseases and cancer and resulted in the development of new immunotherapies [200]. The first of the 'exhaustion' markers to be described was PD-1. PD-1 was discovered by Tasuku Honjo's group, where they show that PD-1 activation was involved in programmed cell death,

hence the name 'Program cell death protein 1 or PD-1' [201]. Honjo went one to win a Nobel Prize in Medicine in 2018 along with James Allison for his discovery of CTLA-4 [202]. T cell exhaustion is defined as having poor effector functions, continued expression of inhibitory receptors, and having a transcriptional and epigenetic state that is unique when compared to functional effector or memory T cells. T cell exhaustion was first described in the 1990s as dysfunction and subsequent deletion of antigen-specific T cells in the setting of chronic viral infection in mice [203-205].

During an acute infection, naïve $CD8^+$ T cells will undergo proliferation and clonal expansion to differentiate into effector $CD8^+$ T (T_{EFF}) cells are then able to directly target and kill infected cells [206, 207]. T_{EFF} cell differentiation is characterized by transcriptional, epigenetic, and metabolic reprogramming and the ability to generate cytokines and cytotoxic granules [200, 208]. After the infection is cleared, the majority of these T_{EFF} die during the contraction phase of an immune response. However, a small fraction of T_{EFF} persist and differentiate into memory T (T_{Mem}) cells. T_{Mem} downregulate the effector programs and begin to develop a stem-cell like program that allows them to survive for an extended period of time without the need for antigen stimulation, and persists as long-lived memory that continue to maintain their numbers via IL-7 and IL-15 driven homeostatic proliferation [209]. T_{Mem} cells are poised to rapidly reactivate and generate effector molecules upon re-encountering antigen and are able to home to lymphoid tissues [210-217].

In a setting of chronic viral infection or cancer, where the antigen is unable to be cleared and there is continued stimulation, there is a failure to develop an effective memory pool and the T cells become exhausted. Antigen load has been linked to the severity of T cell exhaustion, as higher viral loads correlates with more T cell dysfunction [218-221]. The duration of infection and loss of $CD4^+$ T cells results in increased severity of immune exhaustion [216, 222]. The loss of effector functions in exhausted cells is not stochastic but rather follows a hierarchical pattern, where loss of IL-2 production occurs first followed by loss of TNFα production [223, 224]. Defects in cytotoxicity

and production of IFNγ occurs during more severe exhaustion and correlate with the emergence of terminally differentiated exhausted cells [224-228]. Exhausted T cells also lose the capacity to respond to IL-7 and IL-15, which normally maintains homeostatic proliferation of T_{Mem} cells [205, 229-234]. Exhausted T cells are instead maintained by persistent antigen stimulation that drives their ongoing proliferation [232, 235]. This continued proliferation drives the production of 'stem-like' exhausted cells that were defined by Im et al., where these cells are defined as being PD-1^+ CXCR5^+ TIM-3^- Tcf-1^+ and they retain proliferative capacity and able to self-renew and respond to PD-1 blockade [236]. In the same article, they defined 'terminally exhausted' $CD8^+$ T cells as being PD-1^+ CXCR5^- TIM-3^+ Tcf-1^-, and since this population have recently divided, lose the ability to respond to additional stimuli [235-237]. Since the initial paper defining the subsets of exhausted $CD8^+$ T cell populations, several groups have gone on to further characterize these cells [238-249].

The pathways that drive the development of T cell exhaustion are still incompletely understood as there are currently debates whether it is a predetermined fate decision or a result of overstimulation from antigen or driven by other factors. IL-10 has been implicated in the establishment of T cell exhaustion. In settings of chronic infection, IL-10 production results in suppression of immune responses to limit pathology, but several studies have shown that blockade of IL-10 or infection of IL-$10^{-/-}$ mice reverses T cell exhaustion or prevents the establishment of exhaustion [250-253]. In studies of LCMV Cl13 infection, blocking IL-10 signaling in conjunction with PD-1 blockade resulted in a robust T_{EFF} response, development of T_{Mem} cells, and enhanced virologic control [250, 251, 254]. Our lab has shown that plasma levels of IL-10 are elevated during acute SIV infection and remain elevated during chronic infection and during ART (unpublished). We have also shown that levels of plasma IL-10 correlates with the size of the reservoir and that IL-10 signaling drives the persistence of SIV infected $CD4^+$ T cells in the lymphoid compartment.

The sustained expression of inhibitory receptors could also be driving T cell exhaustion. PD-1 is normally expressed after a T cell is activated and on functional T_{EFF} cells, with its expression returning to baseline after activation or an antigen is cleared. In chronic infections, PD-1 expression is sustained and demarcates exhausted T cells [218, 255-259]. In a groundbreaking study by Barber et al., they showed that T cell exhaustion could be reversed trough the blockade of PD-1, resulting in reduction in LCMV viral load and a reinvigoration of T cell effector function in exhausted T cells [255]. This showed for the first time that exhausted T cells were in an exhausted or differentiated state, rather than being in an anergic state and unable to respond to TCR signaling. Day et al. showed similar findings in chronically HIV-infected individuals, where blockade of the PD-1/PD-L1 axis yielded expansion of Ag-specific $CD8^+$ T cells and production of IFNγ [256]. Other surface markers of T cell exhaustion include CTLA-4, TIM-3, Lag-3, and TIGIT. Recent work by Rafi Ahmed's group [260] has described a novel surface marker, CD101, as marking terminally differentiated and exhausted T cells. CD101 expression on Ag-$CD8^+$ T cells in a B16-OVA tumor model identifies a population of 'non-reprogrammable' PD-1^+ exhausted T cells, indicating a terminally differentiated state of exhaustion in these cells [247, 261, 262].

Recent efforts have been directed towards the understanding of transcriptional and epigenetically linked programs that could drive T cell exhaustion. In a series of five papers, authors identify the nuclear factor *Tox* mediating transcriptional and epigenetic changes that are vital for $CD8^+$ T cells responses during chronic infection and cancer [263-267]. The expression of *Tox* is crucial for the formation of the 'stem-like' pool of $CD8^+$ T cells and the subsequent differentiation into terminally exhausted cells described above, as without *Tox,* the 'stem like' pool of Ag-specific $CD8^+$ T cells wanes over time during chronic infection. *Tox* programs a wide array of epigenetic changes and activates the transcription of transcription factors (*Tcf7* and *Eomes*) and drives upregulation of inhibitory receptors (PD-1, Lag-3, 2B4, and TIM-3). *Tox* expression does have benefits outside of inducing T cell exhaustion, as the studies show that *Tox* can enhance the

length of a T cell response and reduce immunopathology to the host. Without *Tox*, the exhaustion program is not initiated, rather $CD8^+$ T cells become terminal effector ($KLRG1^+$) cells and then contract immediately once the antigen is cleared and cannot persist as long-lived memory cells. In mice that received $Tox^{-/-}$ $CD8^+$ T cells, they were subjected to prolonged instances of immunopathology and experienced increased weight loss and organ damage. The idea of targeting *Tox* provides an interesting conundrum, as *Tox* clearly drives the T cell exhaustion pathway so targeting it can enhance anti-viral or anti-tumor responses, but deletion or blockade of *Tox* could result in severe immunopathology.

Strategies towards HIV remission

Due to the overall complexity of HIV infection and the nature of the viral reservoir, a sterilizing cure for HIV remains a daunting task for researchers. A more realistic cure for HIV could be through reducing the reservoir size enough to allow for remission, otherwise termed a 'functional cure'. To date, there have been two cases of patients with durable HIV remission upon cessation of ART. Timothy Ray Brown (the Berlin Patient) was the first case of an individual with long-term control of HIV [(268)]. He was an HIV infected individual, who upon diagnosis with acute myeloid leukemia underwent an allogeneic hematopoietic stem-cell transplant (HSCT) from a donor homozygous for the CCR5Δ32/Δ32 mutation. In short, this genetic mutation renders the donor cells non-permissive to HIV infection and confers protection against any CCR5 tropic HIV virus. After transplantation and immune reconstitution, Timothy Ray Brown was taken off ART remained without aviremic until his death. A second occurrence of long-term remission took place in 2019. Adam Castillejo (the London patient), was diagnosed with Hodgkin's lymphoma and underwent an allogeneic HSCT from a CCR5Δ32/Δ32 donor. Similar to what was seen in Timothy Ray Brown's case, the Adam Castillejo has remained aviremic since 2016 [(269)]. These two unique cases show that a cure is possible via the eradication of the entire viral reservoir, but this type of

therapeutic approach is not feasible for 37 million people currently living with HIV. Thus, more scalable approaches need to be explored in the field.

Several studies have looked at the timing of ART administration and how that relates to the establishment and size of the viral reservoir. Early administration of ART is linked with lowered immune activation, smaller reservoir, and lower viral diversity as there is less time for the virus to escape and mutate. ART is most effective with when started within the first few weeks of infection, but reports have shown that up to six months post-infection still results in smaller reservoir sizes [270-273]. Several clinical trials have studied whether early ART results in delayed viral rebound or enhanced viral control. They saw that after analytical ART interruption the subjects with earlier ART administration had enhanced viral control, but all patients rebounded, signifying that this was not a curative approach [274-277]. SIV studies have also shown that ART administration very early on infection could prevent the reservoir from seeding [168, 169].

A considerable effort has been directed at targeting the latent reservoir, as it is the main barrier to cure. Current approaches towards HIV remission involve using single-agent immunotherapy, however, it is being clear that future strategies will likely utilize combinatory approaches to target the reservoir. The use of latency reversing agents (LRAs) has been proposed in 'shock and kill' approaches to purge the reservoir. The 'shock' is intended to induce viral production from infected cells that can then be 'killed' by $CD8^+$ T cells or other cytopathic cells. LRAs are intended to be used in conjunction with ART to prevent the spread of new infection. Some examples of LRAs include histone deacetylase inhibitors (HDACi), STING pathway agonists, SMAC mimetics, and protein kinase C (PKC) agonists. A recent study used TLR7 agonists as an LRA, the authors showed that they were able to induce transient viremia and reduced SIV-DNA content within $CD4^+$ T cells [278]. Recent work by Guido Silvestri's group has elucidated the roles of non-cytolytic $CD8^+$ T cell mediated viral suppression during ART [279, 280]. They show that in SIV-infected RMs on ART, depletion of $CD8^+$ T cells with an anti-$CD8\alpha$ results in robust viral rebound in all treated RMs

[281]. They have since followed up with the initial study and combined anti-CD8α with N-803, an IL-15 super agonist, and showed that depletion of $CD8^+$ T cells in conjunction with an LRA enhanced the effects of the LRA in inducing a robust and sustained viremia.

As mentioned above, immunotherapy directed at inhibitory receptors has become a viable therapeutic strategy in reinvigorating 'exhausted' $CD8^+$ T cells to restore immune function and potentially target the reservoir of latently infected cells. Previous studies mentioned above have shown that $CD4^+$ T cells expressing 'exhaustion' markers were enriched for HIV/SIV DNA content, thus targeting these molecules could lead to clearance of the reservoir. CTLA-4 blockade using ipilimumab in a melanoma and HIV-infected individual on ART resulted in activation of $CD4^+$ T cells and induced cell-associated unspliced HIV-RNA that correlated with a subsequent decline in plasma HIV-RNA [282]. PD-1 blockade (nivolumab) in an ART-suppressed individual with non-small cell lung cancer resulted in transient increase in plasma viremia and an overall decrease in 'exhausted' $CD4^+$ and $CD8^+$ T cells [283]. Similar results were seen in a clinical trial of PD-L1 blockade [284], however some adverse events were noted in study participants. Several ongoing clinical trials are studying the efficacy of immune checkpoint blockade in persons who have also been diagnosed with cancer and are HIV-infected (NCT02408861, NCT03354936). In the NHP model of SIV infection, immune checkpoint blockade has shown variable degrees of success. The first study to test PD-1 blockade was done by Velu et al. in chronically infected RMs that were ART naïve [285]. They showed that after PD-1 therapy, there was an expansion of SIV-specific $CD8^+$ T cells with an enhanced effector profile. They also saw a significant reduction in plasma viral load and prolonged survival of treated RMs. A follow up study to this was to test the efficacy in ART-treated RMs. They again showed enhanced effector function in Ag-specific $CD8^+$ T cells and a reduction in ISGs, however, no major effect was seen in the size of the reservoir [286]. Following ART interruption, it was also noted that where was expansion of $CXCR5^+$ $CD8^+$ T cells within lymphoid tissue, these cells have been associated with enhanced viral clearance [192, 286,

[287]. Recently published results in Mirko Paiardini's lab have shown that PD-1 blockade alone was able to induce transient viremia in 50% of treated RMs. They have also seen that blockade of CTLA-4 resulted in robust plasma viremia and enhanced $CD4^+$ T cell activation. Combinations of PD-1 and CTLA-4 saw synergistic effects and an overall increase in viremia [288]. However, there was not significant reduction to the size of the reservoir, thus different approaches must continue to be investigated.

Another avenue that is being studied is the use of a therapeutic vaccine that could elicit and immune response and enhance anti-viral immunity when subjects are no longer on ART. A dendritic cell (DC) based vaccine was tested in chronically infected individuals, he authors saw that after vaccination, viral loads declined by 80% with some individuals suppressing for almost one year [289]. NHP studies have used a recombinant adenovirus serotype 26 (Ad26), modified vaccinia Ankara (MVA) boost and stimulation with TLR7 to drive immune responses towards viral control [290]. In this study, they show that after the prime/boost and stimulation there was a delay in viral rebound following ART cessation and a decrease to levels of viral DNA within lymph nodes, peripheral blood. However, no therapeutic vaccine has been able to elicit long-term HIV remission following interruption of ART, this is most likely due to how diverse the escape variants are and that no vaccination strategy has been to stimulate a broad response.

Recently, broadly neutralizing antibodies (bnAbs) have been brought into the clinics as another means to induce virologic control without ART. A phase 1b clinical trial using two bnAbs (3BNC117 and 10-1074), targeting the CD4 binding site (CD4bs) and the V3 glycan showed that treated individuals were able to maintain viral suppression for between 15-30 weeks after analytical treatment interruption [291, 292]. The RV397 study utilized VRC01, which also targets the CD4bs, to study if a single bnAb was able to confer protection after ART was withdrawn [293]. Only one individual was able to become aviremic for greater than 24 weeks, all other participants reached >1000 copies/mL of HIV-1 RNA prior to 24 weeks. In Lynch et al. they show that a single

infusion with VRC01 was able to significantly reduce plasma viremia and preferentially suppress neutralization sensitive virus in HIV-untreated individuals [294]. There were two individuals who saw no response, however, upon studying the nature of the virus present, they discovered that the virus in these individuals were resistant to VRC01. This shows that bnAbs could have a robust and profound impact in maintaining viral suppression, however, this highlights a crucial need to develop combination strategies to maintain that suppression. The generation of bnAbs through *Env* vaccination remains a challenging endeavor. This is due to the unusual nature of bnAb formation, as bnAbs are formed via high levels of mutation driven by activation-induced cytidine deaminase (AID) and the overall structure of *Env* is masked by high levels of glycans covering sites of vulnerability [295]. Other approaches include immunizing with *Env* proteins and addition of immunogens to drive somatic hypermutation to enhance bnAb generation [25, 296-298]. Combination of structural biology and immunological information has led to a new strategy termed 'germline targeting', which is the idea of generating bnAb precursor cells that are more likely to form bnAbs upon immunogen vaccination [299].

The field is also shifting efforts into developing vaccines to confer protection against HIV infection. The first truly successful vaccine came from Louis Picker's group using rhesus cytomegalovirus (RhCMV) vectors that were able to elicit robust SIV-specific effector memory (T_{EM}) responses at sites of infections [300]. They show that 13/24 RMs were protected from SIV_{mac239} challenge for >1 year. This showed that persistent vectors such as CMV, could be used to generate a HIV vaccine. They followed up this study, and showed that RhCMV/SIV vector elicited immune responses can control SIV after viral dissemination [301]. Recently, they utilized a RhCMV vector that was live-attenuated, thus unable to spread, and again showed protection and clearance from SIV_{mac239} challenge [302, 303].

Non-human primate models of HIV infection

As explained above, non-human primate models of SIV infection have allowed researchers to study the pathogenesis of SIV and determine how this is similar to HIV infection in humans. This has shed light on the rapid and preferential depletion of $CD4^+$ T cells within the mucosa, the rapid onset of inflammation, and eventual immune exhaustion that occurs. SIV models have also allowed researchers to investigate the nature and anatomical distribution of the latent viral reservoir, and to test novel and sometimes risky interventions to potentially eradicate infected cells. The NHP model allows researchers to study SIV infection in a controlled setting, with the added ability to finely study the kinetics of pathogenesis and viral rebound in multiple anatomical sites. The RMs are tightly controlled, adherence to the prescribed ART regimen is regulated, and ART interruptions can be planned to study viral rebound kinetics. NHP studies also allow us to test the safety and efficacy of experimental therapeutic approaches prior to moving on to phase I and II trials in humans.

Initial studies to identify a suitable animal model of HIV infection focused mainly on using chimpanzees. However, researchers quickly realized that infection rates of chimpanzees were low as they are natural hosts [304-307]. Sooty mangabeys are also natural hosts (SIV_{SMM}) of SIV, they have high levels of plasma viremia but do not experience a dramatic decline in levels of $CD4^+$ T cells [308-313]. Studies of sooty mangabeys has yielded insight on how natural hosts can confer protection from highly pathogenic SIV infections, such as T_{CM} of sooty mangabey's expressing lower levels of CCR5 and that sooty mangabeys have a frameshift in the TLR-4 gene that is associated with decreased inflammation [314, 315].

Macaques of Asian origin, such as rhesus (*M. mulatta*), pigtailed (*M. nemestrina*), and cynomolgus (*M. fascicaluris*), are the NHPs used as models to study pathogenesis and persistence of HIV-1 [316-318]. In our lab, we routinely use *rhesus macaques* in our studies as they are readily infected with SIV and SHIV variants, undergo the same kinetics of $CD4^+$ T cell

depletion as seen in humans, and if left untreated will progress to AIDS. As seen in our previous studies, the administration of ART in RMs results in rapid viral decay and reconstitution of $CD4^+$ T cells [111, 129, 281].

Summary for HIV

Since the discovery that HIV was the virus that caused AIDS, HIV/AIDS has taken the life of 35 million infected individuals, and infected over 77 million people in total. The discovery and prescription of antiretroviral therapy (ART) has resulted in a substantial reduction in HIV-related morbidities and mortalities and reduced transmission, however, ART is a lifelong treatment and not a cure. A cure for HIV is hindered by the presence of the viral reservoir, a pool of latently infected $CD4^+$ T cells that is able to evade immune detection indefinitely and is indiscernible from an uninfected cell. Nevertheless, there is hope for a cure, as referenced by two patients that have achieved durable HIV remission upon cessation of ART (Berlin and London Patients). Therapeutic strategies will need to be studied in detail to identify the best means to rid the body of the reservoir. There remain critical gaps in our knowledge as to what is maintaining the viral reservoir and how an infected cell can persist for years in an infected individual. The identification of those mechanisms will allow the design of specific therapeutic strategies aimed at HIV remission.

SARS-CoV-2 background, properties, and viral life cycle

Severe acute respiratory syndrome coronavirus 2 (SARS-CoV-2) is a highly transmissible and pathogenic coronavirus that emerged in late 2019 in Wuhan, China and has caused a global pandemic termed “coronavirus disease 2019” (COVID-19) [319, 320]. Coronaviruses are diverse in nature, and have been shown to be able to infect various animals, with bats being the primary animal host prior to zoonotic spread. Typically, infection via a coronavirus results in a mild to severe respiratory tract infection in humans. However, infection with coronaviruses has been lethal to humans such as infection with Severe acute respiratory syndrome coronavirus (SARS-CoV) and Middle Eastern respiratory syndrome coronavirus (MERS-CoV), making coronaviruses

a large public health concern. In a relatively short period of time, SARS-CoV-2 has rapidly surpassed both SARS-CoV and MERS-CoV in number of total cases and deaths.

In December of 2019, local health officials in the Wuhan, China began describing multiple clusters of patients exhibiting symptoms of pneumonia of unknown cause [319, 320]. These patients symptoms included : fever, cough, bilateral pneumonia, dyspnea, and opacity in the lungs [319, 320]. These symptoms are largely consistent with those seen in people infected with SARS-CoV and MERS-CoV [320, 321]. Early viral sequencing from bronchoalveolar lavage fluid of these patients in Wuhan showed that the "unknown agent" of this rapidly developing scenario belonged to the betacoronavirus family that has never been seen before [320, 322, 323]. While the early clusters of cases were linked to the Huanan Seafood Wholesale Market, it was becoming clear that subsequent clusters in Wuhan were caused through human-to-human interaction and spread transmitted via respiratory droplets. Within 30 days of the first reported cases, it had spread to all provinces in China with thousands of confirmed daily cases. On January 30th, the WHO declared a public health emergency. By the middle of February, the novel coronavirus was named SARS-CoV-2 and the subsequent disease as COVID-19. Following the events in China, large clusters of infections began appearing internationally due to the transmissibility and ease of travel [324]. By the second week of March 2020, the WHO declared COVID-19 to be a global pandemic [324].

SARS-CoV-2 is a betacoronavirus (+ssRNA virus) and shares 79% of its genome with SARS-CoV and 50% with MERS-CoV [325], with similar genome organization to other betacoronaviruses. It has six functional open reading frames (ORFs): replicase (ORF1a/ORF1b), spike (S), envelope (E), membrane (M), and nucleocapsid (N). In addition, there are seven ORFs coding for accessory proteins that are intermingled with the structural proteins. SARS-CoV-2 shares 90% amino acid homology in the structural genes with SARS-CoV, with SARS-CoV-2 diverging with the spike gene.

Genome analysis indicates that SARS-CoV-2 is clustered with SARS-CoV and related SARS-related coronaviruses, and a part of the subgenus Sarbecovirus of the genus betacoronavirus. Of note, viruses in this subgenus are found in bats. Bats have been shown to be natural hosts for alpha- and betacoronaviruses. Analysis has shown that the closest relative to SARS-CoV-2 to a bat coronavirus that was initially discovered in *Rhinolophus affinis* in Yunnan province, China called "RaTG13" where they share 96.2% sequence homology [323]. This evidence hints that SARS-CoV-2 originated in bats [323, 326]. Pangolins were also linked as a intermediate host for SARS-CoV-2, with multiple SARS-CoV-2 like viruses isolated from pangolins with identical receptor binding domains (RBD).

Angiotensin-converting enzyme 2 (ACE2) was determined to be the entry receptor for SARS-CoV-2 and SARS-CoV [323, 327]. In addition to human ACE2, SARS-CoV-2 has been shown to have recognition to ACE2 of rhesus macaques, ferrets, pigs, civets, cats, pangolin, rabbits and dogs, suggesting that there may be a wide range of hosts [323, 328-331]. As with other coronaviruses, SARS-CoV-2 needs proteolytic processing of the spike protein to active the endocytic route. Studies have shown that host proteases can cleave the S protein and activate entry into the host cell. Transmembrane protease serine protease 2 (TMPRSS2), cathepsin L, and furin have been shown to initiate this process [327, 332]. Interestingly, TMPRSS2 has been shown to be highly expressed with ACE2 in nasal epithelial cells, lungs and bronchial branches [333].

SARS-CoV-2 will bind to a target cell using the spike (S) protein to bind to host ACE2 to mediate attachment, and in addition may bind to co-receptors such as NRP1 or Siglec-1 to enhance infection. Host derived TMPRSS2 will then cleave the S protein to S1 (RBD) and S2 (fusion peptide) domains which will then initiate viral fusion to host cell whereby the virus is taken up and uncoats. Once SARS-CoV-2 is released into the host cell, the process of replication begins. Translation of ORF1a and ORF1b from the genomic RNA produces pp1a and pp1ab. From this, 16 non-structural proteins (NSPs) are co-translationally and post-translationally

released from NSP1-11 (pp1a) and NSP1-10/NSP12-16 (pp1ab) after proteolytic cleavage by papain-like protease (PL^{pro}) and chymotrypsin-like protease ($3CL^{pro}$). NSP1 release occurs rapidly to disrupt host cell translation. RNA synthesis will then be mediated by nsp12, the RNA-dependent polymerase (RdRp). Viral replication organelles consisting of double-membrane vesicles, convoluted membranes, and small open double-membrane spherules will create a protective environment for the viral genomic RNA replication and transcription of sgRNA. The translated structural proteins (spike, envelope, and membrane) translocate into the endoplasmic reticulum membranes and travel through the ER-to-Golgi intermediate compartment where they interact with N-encapsidated gRNA results in budding into vesicular compartments. The virions are then secreted by an infected cell via exocytosis to continue the infection cycle in additional host cells [334].

SARS-CoV-2 clinical features

It was evident early on that SARS-CoV-2 can infect all ages of the human population, however, clinical manifestation and disease severity was worst in older patients, whereas younger patients had mild infections or were asymptomatic. In addition, patients with co-morbidities, such as hypertension or obesity, were far more likely to experience severe disease [335, 336].

Following infection, the most common symptoms were fever, dry cough, and nausea in a majority of patients [335, 336]. However, some people also experienced headache, hemoptysis, diarrhea, chest pain, chills, loss of taste and smell. Signs of infection were evident anywhere from 1-14 days following infection, with most symptoms resent by day 7, with pneumonia developing at day 7-10, and peak viremia occurring at about day 10 post-infection. On admission to the hospital, ground glass opacity in lungs were seen with chest x-rays or computer tomography (CT) scans. Patients presented with severe COVID-19 often required mechanical ventilation and in extreme cases the use of extracorporeal membrane oxygenation (ECMO).

SARS-CoV-2 Pathogenesis

Common circulating coronaviruses such as 229E, NL63, OC43, and HKU1 have been shown to cause disease in humans and animals [337]. Typically, only the upper respiratory is affected with patients showing mild symptoms, and rarely progress beyond that [337]. To date, there have been three coronaviruses that have been able to infect and robustly replicate in the lower respiratory tract: SARS-CoV, MERS-CoV, and SARS-CoV-2. The pathophysiological response following SARS-CoV-2 infection mimics that of SARS-CoV where there is a rapid and strong pro-inflammatory response resulting in cytokine storm and infiltration of immune cells into the lung milieu driving immunopathology [338-341]. Thus, the damage seen in the lungs of patients is partially due to the viral infection, but primarily driven by the over-exuberant immune response. Acute respiratory distress syndrome (ARDS), whereby the patient has difficulty breathing and low blood oxygenation levels may lead to respiratory failure and death. Also, the induction of cytokine release may drive hypercytokinemia and symptoms associated with sepsis which can be fatal. In these instances, with cytokine storm and uncontrolled inflammation can lead to multi-organ failure, with effects seen in cardiac, hepatic, and renal systems [335, 342].

Work following the SARS-CoV outbreak highlighted that the primary cells that were infected were airway epithelial cells, alveolar epithelial cells, vascular endothelial cells, and macrophages in the lung, where all of these cells express ACE2 and the primary targets of SARS-CoV-2 [323, 327, 343, 344]. Following infection, ACE2 expression is reduced which has been associated with lung injury, and ACE2 has also been shown to regulate the renin-angiotensin system (RAS). SARS-CoV-2 causing downregulation of ACE2 could impact RAS driving dysfunction of blood pressure, electrolyte balance, and enhancement of inflammation and increase vascular permeability [345].

SARS-CoV-2 infection of the lower respiratory tract and the destruction of lung epithelial cells results in a local and systemic inflammatory response, characterized by the recruitment of macrophages and monocytes, release of cytokines and chemokines, and priming of T and B cell

responses [338-341]. These early innate and adaptive responses will normally be enough to resolve the primary infection; however, an abhorrent, dysfunctional and over-exuberant immune response can drive immunopathology leading to death. SARS-CoV-2 is a cytopathic virus and induces death of infected cells, and can induce pyroptosis and the release of IL-1beta, which has been well documented following infection [338, 346, 347]. Alveolar epithelial cells and macrophages can use pattern recognition receptors (PRRs) to detect pathogen-associated molecular patterns (PAMPs) and damage-associated molecular patterns (DAMPs) to induce signaling. This is followed with local and systemic inflammation and the production and secretion of pro-inflammatory cytokines and chemokines such as: IL-6, IL-10, IP-10, CXCL8, TNFalpha, IFNgamma, MIP1alpha and MCP1 [329, 338]. The secretion of these cytokines and chemokines results in the recruitment of immune cells from the periphery to the lung, which can be explained by the lymphopenia and increased neutrophil-lymphocyte ratio seen in COVID-19 patients [329, 338-341, 348]. Typically, the initiation of the immune response will be enough to clear the viral infection and the generation of immunological memory. However, in a subset of individuals with a misfiring to the immune response results in hypercytokinemia or cytokine storm resulting in inflammation of the lungs driving additional pathology [338].

The infiltration of inflammatory cells into the lung can induce damage through the secretion of proteases and reactive oxygen species (ROS), resulting in alveolar damage, hyaline membrane formation, and pulmonary edema. As a result, the normal gas exchange within the lung is impaired, causing breathing difficulty and low blood oxygen levels leading to organ failure. Cytokine storm will drive systemic inflammation, as elevated levels of cytokines in the blood can mimic septic shock resulting in organ damage and failure.

SARS-CoV-2 T Cell immunity

T cell play a pivotal role in the adaptive immune response to mediate helper functions and clearance of viral infections. T cell responses against SARS-CoV-2 can be detected as early as

1-week following the onset of symptoms during acute infection, with the majority of patients developing a memory response following viral clearance. Both the $CD4^+$ and $CD8^+$ T cell responses are directed against various SARS-CoV-2 antigens, but primarily elicited against nucleocapsid and spike [349-351]. $CD4^+$ T cell responses are skewed towards a T_H1 response, with $CD8^+$ T cell responses exhibiting effector phenotypes with increased cytotoxicity and increased activation, similar to other acute and chronic viral infections [105, 352-354]. There have also been several studies published describing early upregulation of T cell exhaustion markers (PD-1, TIM-3, CTLA-4, and CD39), suggesting that acute SARS-CoV-2 infection was driven by hyper-activation, resulting in early T cell dysfunction [340, 355, 356]. However, other studies have shown in SARS-CoV-2 that T cells expressing these exhaustion markers remain fully functional, and that upregulation of these markers is likely due to activation [357]. Currently, the data published suggest that an early induction of a functional $CD4^+$ and $CD8^+$ T cell response strongly correlates with early viral control and mild COVID-19, whereas a delayed or dysfunctional response results in severe disease and delayed clearance [351, 358, 359].

Nearly 100% of convalescent patients show a durable and detectable $CD4^+$ and $CD8^+$ T cell response following recovery of COVID-19 [353, 360, 361]. Early on, numerous studies showed that there were polyfunctional $CD4^+$ and $CD8^+$ T cell responding to structural and non-structural proteins [354, 362]. Asymptomatic patients exhibit polyfunctional $CD4^+$ and $CD8^+$ T cell responses, albeit to a lower extent than symptomatic patients, however, whether this is enough to confer protection from re-infection remains to be determined [354, 363-367].

Cross-reactive T cells have also been shown to exist in peripheral blood of uninfected individuals that are able to recognize structural and non-structural proteins [354, 361, 368-376]. Cross-reactive $CD4^+$ T cell responses are more prevalent compared to $CD8^+$ T cells in the blood [361, 368]. The generation of these cross-reactive T cell responses could be due to prior exposure of common human coronaviruses which all share some sequence homology to SARS-CoV-2 [368, 369,

[371-373]. The cross-reactive T cell responses detected in people are typically directed against highly conserved epitopes [372, 374, 377]. The presence of pre-existing T cell immunity against SARS-CoV-2 and impact on disease severity and outcome remains debated within the field. While having an early and active memory response could generate a potent antiviral response, but could be involved in enhancing immunopathology [378-381].

While peripheral T cell responses can persist for at least 8 months following recovery or vaccination, there is interest in the status of resident T cells (T_{RMs}) [382-384]. T_{RMs} have been shown to rapidly control viral infection upon re-infection through killing of infected cells and secretion of cytokines to recruit immune cells to site of infection. Recent work has shown that T_{RMs} can persist in the lung and nasal passages for 2-10 months following SARS-CoV-2 infection, but their numbers and persistence remains to be elucidated [382-384]. Intranasal administration of vaccines has been shown to generate local T_{RMs} establishment, whereas intramuscular administration has systemic effects with less induction of T_{RMs}.

Studies of T cell depletion have also sown the importance of $CD4^+$ and $CD8^+$ T cells in the context of SARS-CoV-2 infection. Depletion of $CD8^+$ T cells in convalescent macaques partially hinders their ability to protect against re-infection, suggesting that cellular immunity to natural infection plays a major role in protecting the host following primary infection in cases of waning antibody titers [385]. Others have also shown that depletion of T cells results in delayed viral clearance and recovery, however there was no changes to disease severity [386]. This highlights the importance of T cells in viral clearance.

SARS-CoV-2 B Cell immunity

Antibodies are a vital part of the immune system that responsible for neutralizing viral infection. Patients who recover from SARS-CoV-2 have detectable titers of neutralizing antibodies against the various epitopes on SARS-CoV-2 [360, 387-395]. Neutralizing antibodies against the S protein are typically begin developing 2-3 weeks following infection. However, there are patients

that upon viral clearance do not generate antibodies against SARS-CoV-2, and remain at risk for re-infection [396]. The use of mRNA and adenovirus vectored vaccines also results in the generation of high titers of neutralizing antibodies, resulting in protection from subsequent infections.

Pre-pandemic samples and specimens from SARS-CoV-2 naïve individuals have shown that there are people with pre-existing antibodies against SARS-CoV-2 antigens that may have arisen due to exposure of circulating human coronaviruses (HCoVs) [397, 398]. Most of these antibodies bind to endemic HCoV S antigen, and <1% bind to SARS-CoV-2 RBD, thus conferring little to no protection against SARS-CoV-2 [399-401]. The S protein of SARS-CoV-2 is proteolytically cleaved into two subunits: S1 (containing the RBD and N-terminal domain) and S2 (responsible for host-viral membrane fusion). Pre-existing antibodies tend to target S2 as this subunit shares greater sequence homology with circulating HCoVs [399, 400, 402, 403]. The RBD is the primary target for neutralization, but some antibodies that bind to the N-terminal domain can prevent protease cleavage and conformation change thus exhibiting some protective effects [404-406].

Within the first two weeks of infection, IgG, IgA and IgM responses against SARS-CoV-2 can be detected, with seroconversion occurring between 10-13 days following symptom onset [407, 408]. IgA and IgM levels wane relatively rapidly, whereas IgG antibody against S levels remain quite stable 3months following infection and modest decline 5-8 months out [407]. Anti-RBD and -N responses have also been reported to wane more rapidly [360, 409, 410]. Interestingly, the magnitude of the anti-SARS-CoV-2 correlates with disease severity, patients with severe COVID-19 tend to generate a larger antibody response [365, 393]. There is also evidence that patients with delayed neutralizing antibody production is associated with fatal COVID-19 [411].

The advent of the COVID-19 vaccines has halted the spread, with all vaccines primarily targeting the S protein to induce high levels of neutralizing antibodies [412]. The mRNA platforms utilized by Moderna and Pfizer/BioNtech induce high titers of anti-S and anti-RBD antibodies, with

peak titers similar to that seen in severely ill patients. Recent data hints that the Pfizer/BioNtech vaccinated individuals have antibodies that wane quicker compared to Moderna, which could be attributed to timing between dose 1 and 2, or the amount of mRNA administered [413]. Which suggests the need for boosters in the near future.

The rise of variants of concern has raised questions whether the antibodies generated from natural infection or vaccination will be enough to confer protection. New viral variants would likely evolve to have increased pathogenicity, transmissibility, or escape from humoral and cellular immune responses [414-416]. E484 on RBD has been identified as an amino acid position that could have the largest effect on antibody neutralization. The P.1 (gamma) and B.1.351 (beta) share a mutation (E484K), and is associated with resistance to neutralization [417-420]. The N501Y, found in the gamma, beta, and alpha variant has also been selected in emerging variants as it has been described to enhance affinity for ACE2 [421, 422]. The delta variant (B.1.617.2) has several substitutions within the RBD, and has been shown to have decreased neutralization in sera from vaccinated individuals [423]. Thus, it will be interesting to see the effects of boosting against ancestral strains and how the effects the ability to neutralize the variants of concern.

Deficiency to interferons can lead to severe COVID

Gaining insight to what drives the development of severe COVID-19 is a topic that has been widely researched since the onset of the pandemic. As mentioned above, the majority of people infected with SARS-CoV-2 experience asymptomatic or mild disease, with only a small fraction of individuals experiencing severe disease. However, some young otherwise healthy people do develop severe disease, and understanding what causes this would be of clinical benefit. The Casanova group at The Rockefeller University made two seminal findings during the early part of the pandemic and highlight a key factor that could result in severe COVID-19. In two separate studies, Zhang et al. and Bastard et al. implicate that deficiencies to type I interferons (IFN-I) is highly associated with severe COVID-19 [424, 425].

IFN-I are the primary responders following viral infection and form the basis of the innate immune response. IFN-I are induced when a cell detects viral RNA via TLR3/TLR7/TLR8 that are found in cellular endosomes. The IFN-I molecules will bind to IFNAR1 and IFNAR2 that will lead to downstream signaling of antiviral and pro-inflammatory genes [426].

In Zhang et al., they describe inherited mutations to genes that encode for antiviral signaling molecules are more prevalent in individuals with severe COVID-19 that were previously found in people who experienced severe disease following influenza infection. They found enrichment in rare variants that are predicted to be loss-of-function (LOF) at 13 human loci that encode for *TLR3* and *IRF7*, two key genes involved in the antiviral response. Thus, inborn errors to *TLR3* and *IRF7* dependent IFN-I immunity may result in severe and life-threatening COVID-19 [425]. In Bastard et al., they report that ~10% of patients with life-threatening COVID-19 had neutralizing IgG auto-antibodies against IFNalpha, IFNbeta, IFNkappa, IFNepsilon, and IFNomega. Interestingly, these auto-antibodies were not found in individuals with asymptomatic or mild disease, and presented in <1% of healthy individuals [424]. The most direct consequence of having a deficient IFN-I response may be the uncontrolled viral replication that may occur following infection. However, there are other potential outcomes such as the loss of suppression of immune-signaling-complexes called inflammasomes and increased production of pro-inflammatory cytokines [427]. Previous work in mice with knockouts to IFN-I signaling have shown that following influenza infection they die of inflammasome activation, rather than uncontrolled viral infection [428].

Hadjadj also show that individuals with severe COVID-19 have impaired production of IFNalpha and IFNbeta, which is associated with increased viremia and a pro-inflammatory response[429]. Blanco-Melo et al. were one of the first groups to show that the immune response follow SARS-CoV-2 infection was defined with low type I and III IFNs levels, and high expression of IL-6 [430]. Max Krummel's group show that in patients with mild COVID-19 there was a robust pattern of ISGs across all cell types, whereas this ISG signature was not present in patients with

severe COVID-19. Functional analysis of these patients show that they produce antibodies that block production of ISG-expressing cells and dampen interferon pathways [431]. Wang et al. show that patients with mild or asymptomatic disease have increased occurrences of autoantibodies when compared to naïve individuals. The autoantibodies tend to target immunomodulatory proteins (cytokines, chemokines, complement proteins, and cell surface proteins), suggesting that SARS-CoV-2 infection drives production of autoantibodies that disrupt normal immune function [432].

Sposito et al. show that patients with high levels of IFN-III characterize the upper repository tract of people with COVID-19 with high viral burden and reduced disease risk and severity [433]. The production of IFN-III was found in patients with mild pathology and was able to drive the transcription of genes that protect against severe disease. However, they also noted that IFNs were overrepresented in the lower airways of patients with severe COVID-19, and these patients had genes that were enriched for apoptosis and decreased proliferation. These data suggest that the roles of IFNs are localized anatomically and can play opposing roles based on the anatomic site [433]. Kramer et al. found elevated levels of IFNalpha in the plasma of early severe COVID-19 patients, and increased NK cell expression of ISGs and genes downstream of IFNalpha [434]. They also associated prolonged IFN-I signatures with dysfunction in NK cells, which may lead to worst disease outcomes. In addition, two papers published in *Science* in 2020 show that proloned Type I IFN production may be detrimental to lung epithelial tissue repair following influenza infection. Whereas, Type III IFNs (IFNlambda) was beneficial in clearing the infection without disrupting tissue repair pathways [435, 436].

In summation, multiple studies have linked the deficient IFN-I response with exacerbating disease pathogenesis and driving disease severity. The loss of a proper IFN-I response may lead to uncontrolled viral infection and prolonged inflammatory signaling via the presence of inflammasomes. However, additional work has shown that early and prolonged IFN-I signaling

may be detrimental to disease prognosis. Taken together, the timing and duration of IFN-I will be critical to developing therapeutics utilizing these pathways.

SARS-CoV-2 Therapeutics

As of today, there are several therapeutics approved for treatment following SARS-CoV-2 infection, these include monoclonal antibodies, antivirals and anti-inflammatories.

SARS-CoV-2 primarily uses ACE2 as the entry receptor, and others have recently shown that other receptors, such as Siglec-1 and DC-SIGN, can act to enhance infection and blockade of these can decrease viremia [437]. Monoclonal antibodies (mAbs) that bind and "neutralize" virus have been used with wide success in treating disease such as Ebola and HIV through passive immunization. The use of neutralizing mAbs such as bamlanivimab, etesevimab, casirivimab, imdevimab, and sotrovimab have shown promise and been granted emergency use authorization [417, 438-446]. Several of these mAbs are used in combination to mitigate the risk of loss of efficacy dude to viral evolution and escape from these binding epitopes. The use of mAbs in treating COVID-19 has resulted in reduced time in hospitals and incidences of death. As such, mAbs alone or in combination with other therapeutic approaches remain attractive and effective in mitigating disease severity. Early clinical trial results support the use of mAbs, however, more data is needed to determine if the use of mAbs against variants of concern remain and the optimum dosage and timing of giving mAbs.

Other approaches target inhibition of viral replication, such as remdesivir, favilavir, ribavirin, lopinavir, ritonavir, PF-07321332, and molnupiravir. The majority of antivirals listed above target 3CLpro or RdRp [447-450], whereas molnupiravir is a synthetic nucleoside derivative that will disrupt viral replication through the introduction of copying errors [451]. Remdesivir showed good efficacy against SARS-CoV-2 *in vitro* and *in vivo* and was the first drug tested in a large clinical trial, Adaptive COVID-19 Treatment Trial (ACTT) [452]. Early reports indicated that patients treated with remdesivir had shorten recovery time in the hospital, whereas there was no meaningful difference

in mortality. Remdesivir was also included in the ACTT2 trial with baricitinib, and the combination of remdesivir was superior to remdesivir alone and placebo [453]. The Pfizer drug PF-07321332 targeting 3CLProteases has also shown promise *in vitro* and *in vivo* [447] and concluded the clinical trials early due to high efficacy and reducing hospitalization by 80%.

SARS-CoV-2 infection drives a pro-inflammatory response and can trigger cytokine storm, thus, the use of immunomodulatory agents were thought to have promise in treating COVID-19. Dexamethasone which is a corticosteroid with potent anti-inflammatory properties was tested, and results indicated that treated patients had reduced mortality [454]. Tocilizumab and sarilumab, two antibodies targeted against IL-6 showed some early efficacy, however subsequent trials showed that there was no significant reduction in disease pathogenesis [455]. Baricitinib, a JAK 1 and 2 inhibitor showed early promise, and results from ACTT2 and CoV-BARRIER showed that monotherapy or combined with remdesivir resulted in decreased time in the hospital and reduced mortality [329, 453, 456]. Studies have also identified type I interferons as candidate therapeutics for SARS-CoV-2 [457-459], with ongoing trials testing IFNalpha and IFNbeta in patients with COVID-19.

SARS-CoV-2 Vaccines

To date, there are several vaccines that have been approved by the FDA for use to prevent COVID-19 with the mRNA platform achieving >90% efficacy [460-462]. The rapid development of COVID-19 vaccines was a collaborative effort between the U.S. government, pharmaceutical companies, biotech, and academic institutions based on decades of research behind the best vaccine platform, structure-based vaccine design, viral immunology, and scale-up processes.

Traditional vaccine approaches were to use live-attenuated, inactivated, or a subunit of the pathogen that was delivered as recombinant protein or protein particle with much success [463-466]. Recent developments to gene-based approaches have gained interest as of late, where vectors encoding proteins were administered to allow the host to produce the vaccine antigen. Gene-based approaches include nucleic acids (DNA and RNA), as well as recombinant adenoviruses.

Using the host to generate the response will mimic a natural infection, whereby robust humoral and $CD4^+/CD8^+$ T cell responses are established. Previous work has shown that adenovirus vectors (human Ad26 or ChAd – Chimpanzee vector) can be used to insert genes of interest into the vector and can be rapidly manufactured, scaled-up, and ready for clinical evaluation. mRNA platforms can readily incorporate genes of interest, but have the benefit of delivery of lipid nanoparticles, thus bypassing the need to for large cell cultures and simplifying the overall production process [467]. For COVID-19, both mRNA (Moderna and Pfizer) and adenovirus vector (Johnson & Johnson and Astrazeneca) vaccine platform were used.

The majority of vaccine platforms were designed to target the spike (S) protein and the receptor binding domain (RBD), as this is the primary feature on coronavirus virions that mediates attachment and entry into a host cell making it the ideal target for neutralizing antibodies [468-471]. The three vaccines used in the U.S. (Moderna, Pfizer, and J&J) targeted the prefusion stabilized (S-2P) transmembrane anchored full-length spike protein, whereas the Astrazeneca target was not the prefusion spike [412]. Initially, Moderna and Pfizer required 2 doses 28 and 21 days apart respectively, whereas J&J was a single-shot vaccine approach. However, due to recent data regarding variants of concern and waning antibody titers, it has been proposed to receive a booster for all vaccines. Data has shown that vaccinated individuals maintain detectable levels of neutralizing antibodies for at least 6 months following the 2^{nd} dose, however data for 1 year and beyond are currently being prepared [472-474]. In addition, neutralizing titers against variants of concern will need to be monitored as there has been data showing varying degrees of loss of titers [475].

As with any RNA virus, random mutations will tend to accumulate over time, and as cases continued to climb throughout the world, variants of concern began to appear for SARS-CoV-2 [476-479]. Numerous studies have shown that these new variants are able to evade neutralizing antibodies and infect vaccinated individuals. Variations to the spike protein will result in less

efficient binding of neutralizing mAbs, with some titers being 5-10-fold less for variants of concern [475, 480-482]. However, data shows that there are still detectable levels of neutralizing mAbs, and the vaccinated individuals are >95% protected against severe disease [483].

Immunogenicity studies for Moderna, Pfizer/BioNTech, J&J, and Astrazenca vaccines showed a robust induction of $CD4^+$ and $CD8^+$ T cell response [484-488]. $CD4^+$ and $CD8^+$ T cell responses are generated after the prime dose, and increase following the boost 3-4 weeks after the prime. $CD4^+$ T cell responses following vaccination are skewed towards a T_H1 and T_{FH} profile, akin to that seen following natural infection [485, 487, 488]. $CD8^+$ T cell responses following vaccination exhibit an effector phenotype, with some studies showing that $CD8^+$ responses following natural infection are more differentiated profile.

The rate at which these vaccines were developed was unprecedented, but was aided through a global collaborative effort and years of planning and develop of technologies to provide these breakthrough discoveries. For COVID-19, the use of structure-based vaccine design resulted in vaccines that generated neutralizing antibodies to a much higher degree than following natural infection.

Non-human primate models of SARS-CoV-2 infection

As with NHP models of HIV/SIV infection, NHPs have allowed for the rapid understanding of disease prognosis, and development of vaccines and therapeutics for SARS-CoV-2. The use of NHPs for SARS-CoV-2 has led to detailed analysis of viral pathogenesis, pathology associated following acute SARS-CoV-2, inflammatory pathways, and immune responses during acute and after clearance. In addition, NHPs have allowed researchers to comprehensively define and locate where SARS-CoV-2 infection takes place besides the upper and lower respiratory track. Similar to SIV studies, SARS-CoV-2 research with NHPs were in controlled settings allowing for the study of viral kinetics and dynamics of the acute immune response that cannot be done with human subjects.

Summary for SARS-CoV-2

Since the onset of the COVID-19 pandemic in late 2019, there have been over 250 million cases and 5 million deaths. While the past two years have generated a great deal of research regarding SARS-CoV-2 and COVID-19, much remains to be understood. The rapid development of multiple viable vaccines against COVID-19 has halted the exponential number of cases, but the emergence of variants of concern remain a global health concern. These variants have been shown to evade antibody responses, thus the need for therapeutics remains a top priority. Research into the immune response during acute infection and after recovery will provide key insights into the mechanism of action and provide clues for therapeutics against SARS-CoV-2.

Chapter Two: Bone Marrow-Derived CD4+ T Cells Are Depleted in Simian Immunodeficiency Virus-Infected Macaques and Contribute to the Size of the Replication-Competent Reservoir

Timothy N. Hoang[1], Justin L. Harper[1], Maria C. Pino[1], Hong Wang[1], Luca Micci[1], Colin T. King[1], Colleen S. McGary[1], Julia B. McBrien[1], Barbara Cervasi[2], Guido Silvestri[1,3], and Mirko Paiardini[1,3]

[1] Division of Microbiology and Immunology, Yerkes National Primate Research Center, Atlanta, GA

[2] Flow Cytometry Core, Emory Vaccine Center, Emory University, Atlanta, GA

[3] Department of Pathology and Laboratory Medicine, Emory University, Atlanta, GA

Published in *Journal of Virology* Volume 93, No. 1, December 10th, 2018, PMID: 30305357

Abstract

The bone marrow (BM) is the key anatomic site for hematopoiesis and plays a significant role in the homeostasis of mature T cells. However, very little is known on the phenotype of BM-derived $CD4^+$ T cells, their fate during simian immunodeficiency virus (SIV) infection, and their contribution to viral persistence during antiretroviral therapy (ART). In this study, we characterized the immunologic and virologic status of BM-derived $CD4^+$ T cells in rhesus macaques prior to SIV infection, during the early chronic phase of infection, and during ART. We found that BM memory $CD4^+$ T cells are significantly depleted following SIV infection, at levels that are similar to those measured in the peripheral blood (PB). In addition, BM-derived memory $CD4^+$ T cells include a high frequency of cells that express the coinhibitory receptors CTLA-4 and PD-1, two subsets previously shown to be enriched in the viral reservoir; these cells express Ki-67 at levels similar to or higher than the same cells in PB. Finally, when we analyzed SIV-infected RMs in which viral replication was effectively suppressed by 12 months of ART, we found that BM $CD4^+$ T cells harbor SIV DNA and SIV RNA at levels comparable to those of PB $CD4^+$ T cells, including replication-competent SIV. Thus, BM is a largely understudied anatomic site of the latent reservoir which contributes to viral persistence during ART and needs to be further characterized and targeted when designing therapies for a functional or sterilizing cure to HIV.

Importance

The latent viral reservoir is one of the major obstacles in purging the immune system of HIV. It is paramount that we elucidate which anatomic compartments harbor replication-competent virus, which upon ART interruption results in viral rebound and pathogenesis. In this study, using the rhesus macaque model of SIV infection and ART, we examined the immunologic status of the BM and its role as a potential sanctuary for latent virus. We found that the BM compartment undergoes a similar depletion of memory $CD4^+$ T cells as PB, and during ART treatment the BM-derived

memory $CD4^+$ T cells contain high levels of cells expressing CTLA-4 and PD-1, as well as amounts of cell-associated SIV DNA, SIV RNA, and replication- competent virus comparable to those in PB. These results enrich our understanding of which anatomic compartments harbor replication virus and suggest that BM- derived $CD4^+$ T cells need to be targeted by therapeutic strategies aimed at achieving an HIV cure.

Keywords

CTLA-4, HIV-1, PD-1, SIV, bone marrow, coinhibitory receptors, viral reservoir

Introduction

Recent advancements in antiretroviral therapy (ART) have effectively been able to suppress human immunodeficiency virus type 1 (HIV-1) replication and have reduced HIV-related morbidities and mortalities [489, 490]. Despite these successes, individuals infected with HIV must remain on a lifelong ART regimen due to viral persistence of latently infected cells which contain intact and transcriptionally silent proviruses that are able to evade the host immune system [59]. Within the latent population, a fraction of these integrated proviruses are replication competent, and upon ART interruption, this replication competence results in recrudescence of virus. Therefore, identifying the cellular and anatomic nature of the latent viral reservoir is paramount in achieving a functional or sterilizing cure for HIV.

In healthy individuals and mice, the bone marrow (BM) compartment contains mature T cells [491], with T cells comprising 3% to 8% of total nucleated BM cells, and has a reduced CD4/CD8 ratio compared with that of peripheral blood (PB) mononuclear cells [491-493]. After priming of T cells in mice, contraction has been shown to be less pronounced in the BM compartment than in other lymphoid organs and blood, leading to persistence of BM antigen (Ag)-specific memory T cells [494-496]. Within mouse BM, there resides a large proportion of memory T cells, as defined by

expression of $CD44^{hi}$, that increases with age and Ag encounter [491, 497, 498]. BM-derived memory T cells are primarily comprised of central memory (T_{CM}) and effector memory (T_{EM}), two subsets of circulating T cells found in the blood [499]. Others have also shown that in human BM there exists a reservoir for $CD4^+$ $CD25^+$ T regulatory (T_{Reg}) cells [500]. A large majority of human and mouse BM memory T cells are nonproliferative and in a quiescent state; however, there is a small fraction of memory T cells that proliferate under steady-state conditions [494, 501]. It has been postulated that proliferation of T cells is stimulated by the BM microenvironment, where high levels of cytokines regulating T cell homeostasis, such as interleukin-7 (IL-7) and IL-15, are present [502-505]. $CD4^+$ T cells in the BM have also been shown to be enriched for CCR5, the necessary coreceptor for HIV infection [506]. Previous studies with nonhuman primates (NHPs) showed early BM hematopoietic defect after simian immunodeficiency virus (SIV) or simian-human immunodeficiency virus (SHIV) infection, which resulted in an impaired T cell production [507, 508]. A recent study looking at myeloid-derived suppressor cells (MDSC) revealed that depletion of these cells in BM could contribute to systemic immune activation and exacerbate SIV pathogenesis [509]. In our paper, we focus on the $CD4^+$ T cell contribution to viral persistence; however, others have shown that other cellular subsets in the bone marrow may harbor virus as well [510].

The above-listed immunologic features suggest that the BM compartment can be an important anatomic location targeted by HIV and in which HIV can persist. Indeed, resting memory $CD4^+$ T cells are considered the main cellular reservoir for HIV, and homeostatic proliferation of $CD4^+$ T cells is considered a central mechanism for viral persistence during ART. However, the BM remains largely understudied in regard to its potential contribution to HIV pathogenesis and viral persistence, both in humans and in NHPs, with most published work focusing on other anatomic locations such as the PB, lymph node, gut, spleen, and brain.

In this study, using the well-established model of SIV infection in rhesus macaques (RMs), we characterized the immunologic and virologic status of BM and compared it with that of PB before and after SIV infection as well as after 12 months of ART. In accordance with previous studies, we show that the BM compartment indeed has a lower CD4/CD8 ratio than PB. In contrast to previous studies, we show a paucity of T_{Reg} cells ($CD25^+$ $CD127^-$ $FoxP3^+$) in the BM. During the course of SIV infection, BM memory $CD4^+$ T cells undergo a severe depletion, similar to what occurs in the periphery and lymphoid organs. Recently, we and others have shown that CTLA-4^+ and PD-1^+ memory $CD4^+$ T cells are enriched in the viral reservoir [123, 129, 511, 512]; here we show that BM-derived $CD4^+$ T cells contain high levels of cells expressing CTLA-4 and PD-1 during early chronic infection and after ART. Finally, after 12 months of ART, BM $CD4^+$ T cells harbor SIV DNA and SIV RNA at levels comparable to those found in PB $CD4^+$ T cells, including similar amounts of replication-competent SIV. In conclusion, the BM is an additional, previously unappreciated site for the viral reservoir that needs to be further characterized and considered when designing therapies for a functional or sterilizing cure for HIV.

Results

Immunologic characterization of BM-derived T cells in healthy RMs. For this study, we used bone marrow (BM) aspirate and peripheral blood (PB) longitudinally collected from 41 RMs before and after experimental intravenous (i.v.) infection with SIV_{mac239}. An ART regimen consisting of tenofovir (TDF), dolutegravir (DTG), and emtricitabine (FTC) was initiated at day 60 post-infection (p.i.) and was maintained for up to 12 months, with all animals achieving undetectable levels (<60 copies/ml) of plasma viremia. Microscopic examination after Wright-Giemsa staining was performed to exclude major blood contamination in the BM aspirate (see “Sample collection and processing” below).

Immunophenotypic analysis shows that in healthy uninfected RMs, the BM contained a mean of 46% ± 8.23% $CD4^+$ T cells and 35.6% ± 6.97% $CD8^+$ T cells among $CD3^+$ lymphocytes, as opposed to 60.1% ± 6.91% $CD4^+$ ($P < 0.0001$) and 26.8% ± 6.19% $CD8^+$ ($P < 0.0001$) cells among $CD3^+$ lymphocytes seen in PB (**Fig. 2.1A**), with a significant decrease in the CD4/CD8 ratio compared to that in PB (**Fig. 2.1B**; $P < 0.0001$). Representative CD4-by-CD8 staining in BM and PB is shown in **Fig. 2.1C**. We then analyzed the frequencies of $CD4^+$ (**Fig. 2.1D**) and $CD8^+$ (**Fig. 2.1E**) T cells with a naive ($CD28^+$ $CD95^-$ $CCR7^+$), central memory (CM; $CD95^+$ $CCR7^+$), or effector memory (EM; $CD95^+$ $CCR7^-$) phenotype; the gating strategy for the different T cell subsets is shown in **Fig. 2.1F** for BM. BM-derived $CD4^+$ T cells have significantly lower levels of CM (BM, 17.35% ± 5.51%; PB, 21.66% ± 6.37%; $P = 0.0010$) and higher levels of EM (BM, 14.55% ± 7.09%; PB, 9.15% ± 3.62%; $P < 0.0001$) cells than blood (**Fig. 2.1D**). Similar to the case with $CD4^+$ T cells, the frequency of CM $CD8^+$ T cells was also lower in BM than PB (BM, 4.29% ± 1.86%; PB, 7.09% ± 2.13%; $P < 0.0001$), with no significant difference for EM (BM, 43.82% ± 16.21%; PB, 39.5% ± 12.98%; $P = 0.2545$) or naive cells.

The expression of coinhibitory receptors (co-IRs), such as CTLA-4 and PD-1, on Ag-specific T cells defines an exhausted T cell population that has impaired effector function and diminished production of effector cytokines [255]. Recently, it has been shown that $PD\text{-}1^+$ as well as $CTLA\text{-}4^+$ $PD\text{-}1^-$ memory $CD4^+$ T cells critically contribute to viral persistence during ART in humans and nonhuman primates [123, 129, 511, 512]. Thus, we looked at CTLA-4 and PD-1 expression in the BM and PB of healthy RMs. In the $CTLA\text{-}4^+$ $PD\text{-}1^-$ population, we saw similar expression patterns between BM-derived $CD4^+$ T cells and PB-derived CD4+ T cells, except for BM having a higher frequency of $CTLA\text{-}4^+$ $PD\text{-}1^-$ CD4+ CM cells (BM, 4.95% ± 1.09%; PB, 4.03% ± 0.91%, $P < 0.0001$) (**Fig. 2.2A**). We also saw similar expression levels of $CTLA\text{-}4^-$ $PD\text{-}1^+$ and $CTLA\text{-}4^+$ $PD\text{-}1^+$ $CD4^+$ T cell subsets between BM- and PB-derived cells (**Fig. 2.2B and C**). Representative PD-1

by-CTLA-4 staining in BM and PB is shown in **Fig. 2.2D**. The levels of expression of Ki-67 within memory $CD4^+$ T cells expressing CTLA-4 and/or PD-1 were comparable between BM and PB (**Fig. 2.2E**). Since PD-1 and CTLA-4 are highly expressed on T follicular helper (T_{FH}) and T_{Reg} $CD4^+$ T cells, respectively, we measured and compared the frequencies of these two functional subsets between BM and PB. For both T_{FH}-like ($CXCR5^+$ $PD\text{-}1^+$; BM, 1.32% ± 1.42%; PB, 12.24% ± 3.94%; $P < 0.0001$) and T_{Reg} cells ($CD25^+$ $CD127^-$ $FoxP3^+$; BM, 0.13% ± 0.29%; PB, 5.15% ± 1.30%; $P < 0.0001$), we saw a lower frequency of each subset within memory $CD4^+$ cells in the BM compartment (**Fig. 2.2F**); the gating strategy for the memory $CD4^+$ T cell subsets is shown in **Fig. 2.2G** for PB. Of note, although BM harbored a population of memory $CD4^+$ T cells with a $CD25^+$ $CD127^-$ phenotype, the paucity of T_{Reg} cells in BM described above derived from the lack of expression of FoxP3, the master regulator of T_{Reg} cells (**Fig. 2.2F**). We also saw lowers levels of T follicular regulatory (T_{FReg}) cells in the BM, but this can be attributed to the lack of FoxP3 expression as seen with conventional T_{Reg} cells.

Immunologic characterization of BM-derived T cells in SIV-infected and ART- treated RMs. SIV infection in RMs is normally pathogenic and results in a massive depletion of $CD4^+$ T cells, particularly those with a memory phenotype, during the viremic phase of infection. Here, we showed that BM memory $CD4^+$ T cells were depleted during the early chronic phase of infection (day 52 p.i.), similarly to the depletion seen in PB, with the frequency of BM memory $CD4^+$ T cells going from 33.67% ± 10.19% before infection to 13.8% ± 8.61% at day 52 p.i. ($P < 0.0001$) (Fig. 2.3A). After 12 months of ART administration, memory $CD4^+$ T cells were reconstituted in both BM and PB (**Fig. 2.3A**); however, in BM they remained at levels still significantly lower than those at pre-infection (pre-infection, 33.67% ± 10.19%; ART, 25.46% ± 8.45%; $P < 0.0008$). BM memory $CD8^+$ T cells were increased in frequency during early chronic infection, comparable to what was seen in the PB, going from 48.65% ± 15.67% prior to infection to 58.48% ± 13.63% following

infection (P = 0.0052) (**Fig. 2.3A**). Following ART, BM memory $CD8^+$ T cells were slightly lower than pre-infection levels (pre-infection, 48.65% ± 15.67%, ART, 38.41% ± 15.21%; P = 0.0062), whereas in the PB no difference was seen between pre-infection and on-ART levels (P = 0.9279). The CD4/CD8 ratio was decreased during the course of SIV infection and restored during ART, although at all phases of infection it remained lower in the BM than in the PB (**Fig. 2.3B**). During the course of infection, the frequency of BM CM and EM $CD4^+$ T cells was diminished and was restored upon ART administration, but to a lower level than pre-infection levels, whereas, in the PB, the levels returned to pre-infection levels (**Fig. 2.3C**). BM and PB CM $CD8^+$ T cells were increased during infection, but after ART, they returned to levels lower than baseline (**Fig. 2.3D**). In BM EM, $CD8^+$ T cells were slightly elevated during infection, and similarly to CM cells, they returned to levels below baseline during ART, whereas, in PB, the levels remained constant throughout (**Fig. 2.3D**). Similar to what can be seen for uninfected animals (**Fig. 2.2F**), throughout the course of SIV infection and ART T_{FH} -like and T_{Reg} cells were present at lower frequencies in the BM than in PB (**Fig. 2.3E**). The combined ART regimen was very effective in suppressing plasma viremia in all RMs (**Fig. 2.3F**).

Next, we examined the expression of CTLA-4 and PD-1 throughout the course of infection (**Fig. 2.4A to C**). We saw comparable frequencies of CTLA-4^+ PD-1^- or CTLA-4^+ PD-1^+ cells among BM and PB CD4+ subsets during viremia and ART (**Fig. 2.4A and C**). The frequencies of CTLA-4^- PD-1^+ cells among BM and PB $CD4^+$ subsets were equivalent throughout, except for the EM population during viremia (BM, 22.86% ± 9.68%; PB, 45.35% ± 11.37%; P < 0.0001) (**Fig. 2.4B**). Expression of Ki-67 was overall similar within CTLA-4^+ and/or PD-1^+ memory $CD4^+$ T cells in the BM to that in PB, with the exception of a higher frequency of cycling CTLA-4^+ PD-1^+ cells at day 36 p.i. (**Fig. 2.4D to F**). To avoid quantification of Ki-67 on very few events, we opted to show cell cycling for memory $CD4^+$ T cells expressing CTLA-4 and/or PD-1 and not for the CM or EM subsets.

Overall, these data indicate that BM-derived memory $CD4^+$ T cells are depleted during SIV infection of RMs and reconstituted during ART to lower levels than those measured in blood; furthermore, BM contains a high frequency of $CD4^+$ T cells expressing co-IRs, which have been previously shown to be enriched in the HIV reservoir [123, 129, 511, 512].

BM $CD4^+$ T cells harbor SIV DNA and SIV RNA as well as replication-competent virus at levels comparable to those in PB. The finding that BM contains subsets of memory $CD4^+$ T cells previously shown to critically contribute to the viral reservoir, such as those expressing coinhibitory receptors, led us to hypothesize that the BM may significantly contribute to viral persistence during ART. To test this hypothesis, we sorted paired BM- and PB-derived $CD4^+$ T cells from 6 SIV-infected RMs treated with suppressive ART for 12 months and performed quantitative PCR (qPCR) to detect cell-associated SIV DNA and SIV RNA levels. Consistent with our hypothesis, we found that in the BM the amount of SIV DNA was 2,162 $\pm$ 1,234 copies/1 x 10^6 $CD4^+$ T cells, which was comparable to the levels seen in the PB, at 2,220 $\pm$ 1,177 copies/1 x 10^6 $CD4^+$ T cells (P = 0.8182) (**Fig. 2.5A**). Similar results were obtained for SIV RNA in the BM and PB, with levels at 581.8 $\pm$ 340.5 copies/1 x 10^6 $CD4^+$ T cells and 419 $\pm$ 187.6 copies/1 x 10^6 $CD4^+$ T cells, respectively (P = 0.3095) (**Fig. 2.5B**). As a result, the ratios of SIV RNA to SIV DNA were also very similar in BM and PB (P = 0.8182) (**Fig. 2.5C**). Importantly, as determined by viral outgrowth assays (VOA) performed with BM and PB of two ART-treated, SIV-infected RMs, a subset of BM $CD4^+$ T cells harbors replication- competent virus at levels that are at least comparable to those seen in the PB (**Fig. 2.5D**).

Discussion

Reduction of the HIV reservoir is paramount for the development of a sterilizing or functional cure for HIV. However, this goal has been hampered by the inability to properly quantify and identify the anatomic location of latently infected cells. In humans, the bone marrow compartment

contains a high proportion of memory T cells, with T cells representing 3% to 8% of total nucleated BM cells [491]. The BM microenvironment has been shown to have high levels of IL-7 and IL-15, both shown to be important for T cell proliferation and maintenance of homeostasis [502-505]. Expression of CCR5, the coreceptor for HIV, has also been shown to be enriched in BM $CD4^+$ T cells [506]. These findings suggest that the BM compartment could serve as a potential anatomic location targeted and exploited by HIV and can serve as a sanctuary of latent infection. To test this hypothesis, we performed a comprehensive study of BM as an anatomic site of viral persistence, its role in maintaining the viral reservoir, and studied the phenotypical features of BM-derived $CD4^+$ and $CD8^+$ T cells during the course of SIV infection and ART treatment in 41 rhesus macaques. To the best of our knowledge, this is the first detailed, longitudinal characterization of the immunologic and virologic features of BM following SIV infection and ART.

In the healthy RMs, we found that BM was characterized by a lower ratio of CD4 to CD8 than in PB, aligning with what others have shown [491-493]; lower levels of CM $CD4^+$ and $CD8^+$ T cells in BM, with higher levels of EM $CD4^+$ T cells; and similar levels of expression of CTLA-4 and PD-1, except for higher levels of CTLA-4 expressed on CM $CD4^+$ T cells. Furthermore, BM harbors significantly lower levels of T_{FH} and T_{Reg} cells than does blood. Of note, we saw very low expression of FoxP3 in the BM, even though the $CD25^+$ $CD127^-$ population was present. Although a previous study with mice reported the BM being enriched in T_{Reg} cells, quantification of T_{Reg} cells in that study was limited to $CD4^+$ $CD25^+$ T cells and to mRNA levels of FoxP3 [500].

SIV infection in RMs normally leads to a severe depletion of memory $CD4^+$ cells. In our study, we saw that the memory $CD4^+$ cells in BM undergo a depletion similar to that in PB. Upon 12 months of ART, the levels of BM memory $CD4^+$ T cells is restored, but not to the levels seen during pre-infection and to a lesser extent than in PB. Although our study was not designed to formally prove it, one possible explanation for the lower reconstitution of $CD4^+$ T cells seen in the BM during ART

is cells trafficking to the periphery. The CD4/CD8 ratio, an important immunologic marker of disease progression, remains significantly lower in BM than PB following SIV infection and ART [513-515].

Recent studies highlight $CD4^+$ T cells expressing coinhibitory receptors, including PD-1 and/or CTLA-4, as the main cellular reservoirs in blood and lymphoid tissues of HIV- and SIV-infected subjects [123, 129, 170, 511, 512, 516]. Importantly, BM-derived $CD4^+$ T cells express PD-1 or CTLA-4 at levels comparable to those found in blood $CD4^+$ T cells during the course of infection and ART. Furthermore, BM $CD4^+$ T cells that are CTLA-4^+ PD-1^+ express Ki-67 at levels significantly higher than in the same cells in the PB in untreated, SIV-infected RMs. Thus, not only does BM contain $CD4^+$ T cell subsets that have been identified as critical to viral persistence, but also these cells seem to be of a phenotype which may favor viral infection and, potentially, viral persistence. Indeed, consistent with the immunologic data showing BM harboring subsets of $CD4^+$ T cells in which HIV and SIV can persist during ART, we found comparable levels of cell- associated SIV DNA and SIV RNA among $CD4^+$T cells of the two anatomic sites after 12 months of suppressive ART. Unfortunately, due to low cell yield from a BM aspirate and the fact that BM $CD4^+$ T cells are depleted during infection, we were unable to quantify the levels of cell-associated SIV DNA and SIV RNA during the pre-ART phase of the study. Finally, by performing viral outgrowth assays, we showed that the BM $CD4^+$ T cells harbor replication-competent virus. Although we were unable to perform quantitative viral outgrowth assays (QVOA), as we were limited in cell numbers isolated from BM, our VOA results indicate that a fraction of BM-derived $CD4^+$ T cells harbored replication-competent virus during ART, supporting the presence of latent HIV-infected cells in a previously understudied anatomic location.

In summary, our results highlight that SIV is able to establish and maintain viral persistence within the BM. Thus, the BM compartment represents an additional viral reservoir that needs to be targeted for a functional or sterilizing cure.

Materials and Methods

Study approval. All animal experiments were conducted following the guidelines established by the Animal Welfare Act and the *Guide for the Care and Use of Laboratory Animals* and performed in accordance with institutional regulations after review and approval by the Institutional Animal Care and Usage Committee (IACUC, 3000065, 2003297, 2003470, and PROTO201700665) at the Yerkes National Primate Research Center (YNPRC; Atlanta, GA). Anesthesia was administered prior to performing any procedure, and the proper steps were taken to minimize any suffering the animals may have experienced.

Animals. Forty-one male Indian rhesus macaques (RMs; *Macaca mulatta*) (aged 2 to 3.5 years at time of assignment), all housed at the YNPRC, were included in this study. All RMs were HLA*B08$^-$ and HLA*B17$^-$. Prior to study assignment, all RMs were screened for SIV, cercopithecine herpesvirus 1 (B virus), simian T-lymphotropic virus (STLV), respiratory syncytial virus (RSV), and tuberculosis (TB) and dewormed. After experimental infection, animals were housed in isolation, in order to lower the risk of superinfection, in metal wire cages at an ambient temperature of 72°F. RMs were fed a diet consisting jumbo biscuits supplemented with 15% protein, half an orange per day, and produce enrichment and foraging material (cereals, grains, seeds, etc.) five times per week. All procedures were approved by the Emory University IACUC, and animal care facilities are accredited by the U.S. Department of Agriculture (USDA) and the Association for Assessment and Accreditation of Laboratory Animal Care (AAALAC) International.

All RMs were intravenously (i.v.) infected with 300 50% tissue culture infective doses ($TCID_{50}$) of SIV_{mac239}. An ART regimen, consisting of tenofovir (TDF; 5.1 mg/kg of body weight/day), dolutegravir (DTG; 2.5 mg/kg/day), and emtricitabine (FTC; 40 mg/kg/day), was initiated at day 60 p.i. and was maintained for up to 12 months. Animals remained on ART until plasma viremia was undetectable (limit of detection 60 copies/ml of plasma) for at least 3 months. Ages of RMs

pre-ART ranged from 2.1 to 3.6 years, and ages during ART measurement ranged from 2.7 to 4.2 years. The expression of Ki-67 among the CTLA-4 and/or PD-1 memory $CD4^+$ T cell subsets was determined in a different cohort of animals, specifically in 22 Indian RMs at pre-infection and at day 36 after SIV_{mac239} infection (i.v., 300 $TCID_{50}$), as well as in 14 of these 22 animals after 12 months of ART (day 399 p.i.). Ages of these 22 animals at pre-infection ranged from 3 years and 10 months to 9 years and 2 months.

Sample collection and processing. BM and PB were collected pre-infection, during early chronic infection, and during ART. Animals were anesthetized with either intramuscular (i.m.) ketamine (5 to 10 mg/kg) or tiletamine- zolazepam (Telazol; 3 to 5 mg/kg) prior to BM collection. The animals were placed in either dorsal or lateral recumbency. The area over the iliac crest was clipped and surgically scrubbed with 3 alternating applications of chlorhexidine or betadine scrub and alcohol before aseptic introduction of a 14- to 20-gauge needle connected to a syringe (with or without heparin coating) into the bone.

The desired volume was aspirated into the syringe. Suction was released before removing the bone marrow needle. Bone marrow aspirations were limited to a volume of 1 to 1.5 ml to avoid contamination with PB. The quality of our samples was assessed by performing a Wright-Giemsa stain on a glass slide smear. Samples were accepted and further processed only if the stained smear showed the cellular morphology typical of a BM aspirate, including a sufficient number of bone spicules and significant representation of all hematopoietic lineages with normal distribution of hematopoietic precursors. BM- and PB-derived cells were isolated by density gradient (Ficoll-Paque Premium; GE Healthcare) centrifugation.

Determination of viral load RNA. Quantitative real-time reverse transcription (RT)-PCR was per- formed to determine SIV plasma viral load as previously described [(517)].

Flow cytometric analysis. Eighteen-parameter flow cytometric analysis was performed on peripheral blood- and bone marrow-derived cells according to procedures using a panel of monoclonal antibodies that we and others have shown to be cross-reactive with RMs [111, 129]. The following antibodies were used at predetermined optimal concentrations: anti-FoxP3-allophycocyanin (APC) (clone 150D), anti-CD4-APC-Cy7 (clone OKT4), anti-CD95-BV605 (clone DX2), anti-CD25-BV711 (clone BC96), and anti-PD-1–BV785 (clone EH12.2H7), all from Biolegend; anti-CXCR5-phycoerythrin (PE) (clone MU5UBEE) and anti-CD127-PE-Cy5 (clone eBioRDR5), both from eBioscience; anti-CCR7-PE-Cy7 (clone 3D12), anti- Ki-67-Alexa700 (clone B56), anti-CTLA-4-BV421 (clone BNI3), anti-CD3-BUV395 (clone SP34-2), anti-CD8- BUV496 (clone RPA-T8), and anti-CD28-BUV737 (clone CD28.2), all from BD Biosciences; and Aqua LIVE/DEAD amine dye-AmCyan from Invitrogen. To detect the expression of FoxP3 intracellularly, mononuclear cells were fixed and permeabilized with FoxP3 fixation/permeabilization solution (Tonbo) and subsequently stained intracellularly with FoxP3. Flow cytometric acquisition was performed on at least 100,000 CD3 T cells on an LSRFortessa (BD Biosciences) cytometer driven by fluorescence- activated cell sorting (FACS) DIVa software. The data acquired were analyzed using FlowJo software (version 10.4.2; TreeStar).

Flow cytometry cell sorting. Mononuclear cells isolated from blood and bone marrow were sorted on a FACSAria II (BD Biosciences) driven by FACS DIVa software. The following antibodies were used at predetermined optimal concentrations: anti-CD8-fluorescein isothiocyanate (FITC) (clone RPA-T8), anti- CD3-APC-Cy7 (clone SP34-2), anti-CD4-BV650 (clone OKT4), and Aqua LIVE/DEAD amine dye-AmCyan from Invitrogen. Sorted cells, with a purity higher than 95%, were used to determine the content of cell-associated SIV DNA and RNA or for viral outgrowth assay.

Quantitation of cell-associated SIV DNA and SIV RNA. Cellular DNA and RNA were extracted from at least 50,000 $CD4^+$ T cells lysed in RLT Plus buffer (Qiagen) and isolated using the AllPrep DNA/RNA minikit (Qiagen) per the manufacturer's manual.

Viral outgrowth assay. BM- and PB-derived $CD4^+$ T cells were sorted using a FACSAria II using the protocol described above. Cells were stimulated with CD3 and CD28 and allowed to incubate for 12 h. Sorted $CD4^+$ T cells were plated at a 1:1 ratio and supplemented with IL-2. At weeks 2, 4, and 6, supernatant was taken for RNA analysis.

Statistical analysis. All analyses were performed using GraphPad Prism 7 software. Prior to implementation of any specific statistical analysis for each outcome, assumptions were assessed (i.e., normality and homogeneity of variance). If the underlying assumptions were met, a two-sided two-sample equal-variance *t* test was performed to compare the differences. If the assumptions were violated, the two-sample Mann-Whitney U test was used. Error bars in figures represent standard deviations. A *P* value of □0.05 was considered significant.

ACKNOWLEDGMENTS

We thank Stephanie Ehnert and Christopher Souder (Research Resources) as well as Sherrie Jean (Veterinary Medicine) at YNPRC for providing animal and veterinary care. The $SIVmac_{239}$ strain used to infect the RMs was kindly provided by Chris Miller of UC-Davis. Cell-associated SIV DNA and SIV RNA levels were quantified by Jeffrey Lifson, AIDS and Cancer Virus Program, Leidos Biomedical Research, Inc., Frederick National Laboratory for Cancer Research.

This work was supported by the NIAID, NIH, under award numbers R01AI116379, R33AI116171, and R33AI104278 to M.P. This work was also supported by ORIP/OD P51OD011132 (to the YNPRC).

The content of this publication does not necessarily reflect the views or policies of the Department of Health and Human Services, nor does mention of trade names, commercial products, or organizations imply endorsement by the U.S. government.

Chapter Two Figures

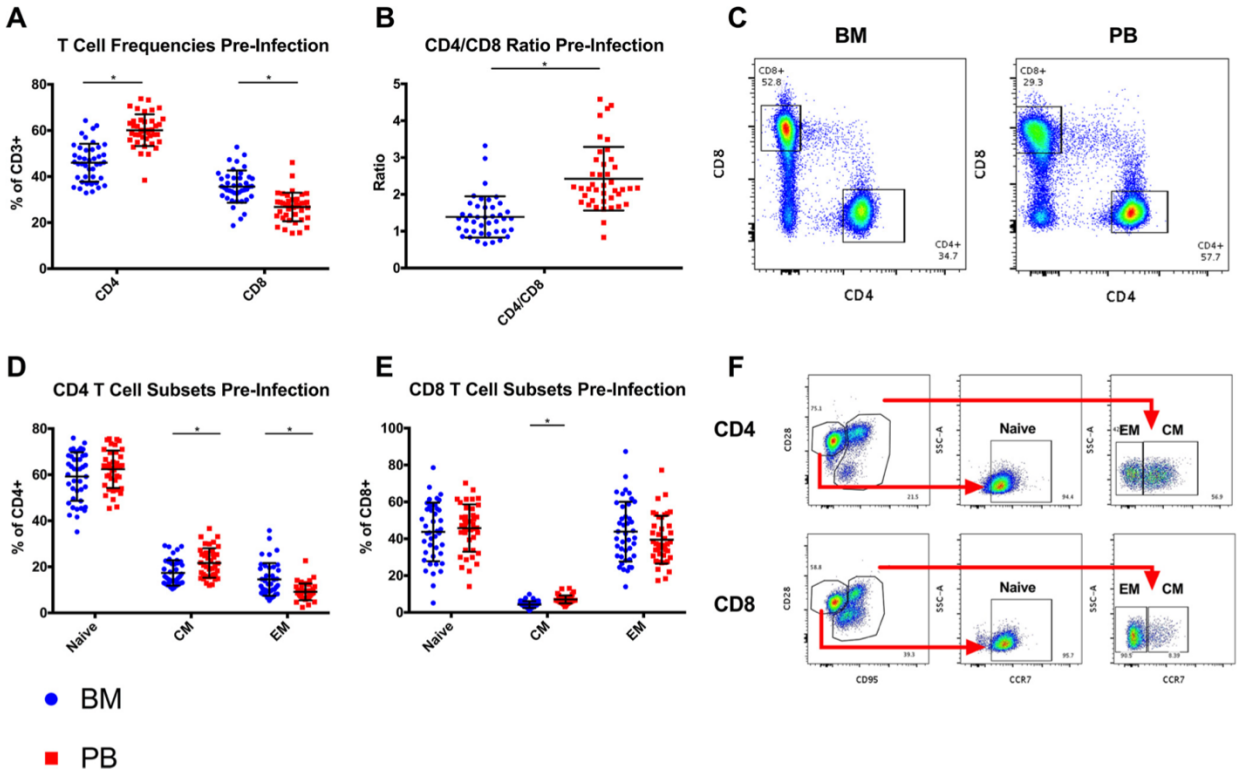

Figure 2.1 $CD4^+$ and $CD8^+$ T cell subset frequencies in BM and PB of healthy RMs. (A) Frequencies of $CD4^+$ and $CD8^+$ T cells within live $CD3^+$ lymphocytes were measured from uninfected RMs. (B) Ratios of $CD4^+$ to $CD8^+$ were determined by calculating the ratio of paired $CD4^+$ and $CD8^+$ T cells. (C) Representative CD4-by-CD8 staining in BM and PB. (D and E) Frequencies of naive, central memory (CM), and effector memory (EM) $CD4^+$ and $CD8^+$ T cells were measured for uninfected RMs. (F) Representative staining in BM and defining subsets of $CD4^+$ and $CD8^+$ T cells (n = 41 RMs). *, $P < 0.0001$.

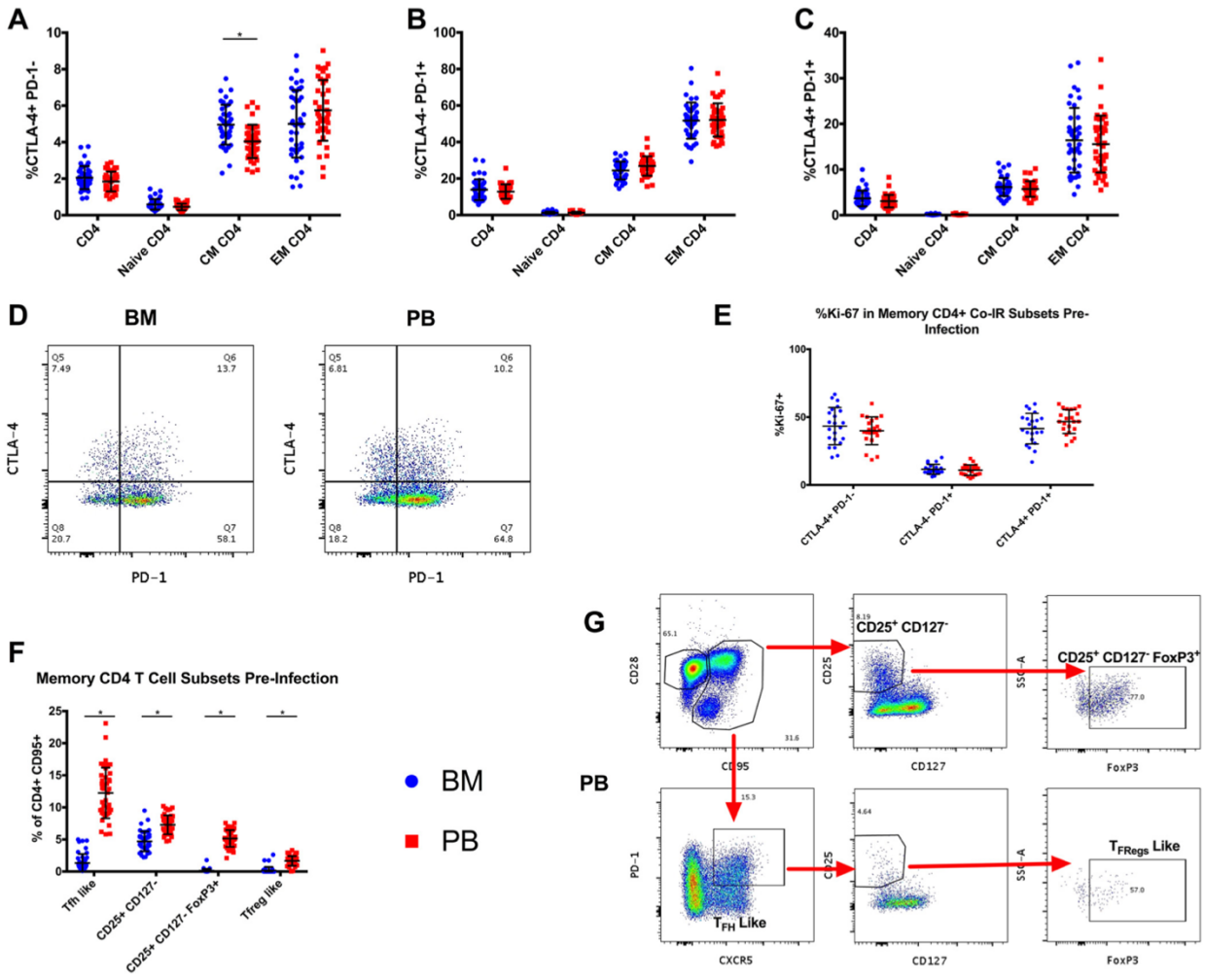

Figure 2.2 Expression of coinhibitory receptors (co-IRs) and frequencies of T_{FH}-like and T_{Reg} subsets in BM and PB of healthy RMs. (A to C) Frequencies of $CD4^+$ T cell subsets with CTLA-4^+ PD-1^- (A), CTLA-4^- PD-1^+ (B), and CTLA-4^+ PD-1^+ (C) phenotypes. (D) Representative CTLA-4-by-PD-1 staining in BM and PB CM $CD4^+$ T cells. (E) Expression of Ki-67 in CTLA-4^+ PD-1^+, CTLA-4^+ PD-1^+, and CTLA-4^+ PD-1^+ memory $CD4^+$ T cell subsets. Ki-67 expression was measured in a different cohort of 22 RMs (see Materials and Methods). (F) Frequencies of memory $CD4^+$ ($CD95^+$) T cell subsets: T_{FH}-like ($CXCR5^+$ PD-1^+), $CD25^+$ $CD127^-$, T_{Reg} ($CD25^+$ $CD127^-$ $FoxP3^+$), and T_{FReg}-like ($CXCR5^+$ PD-1^+ $CD25^+$ $CD127^-$ $FoxP3^+$). (G) Representative staining of subsets in PB (n = 41 RMs). *, $P < 0.0001$.

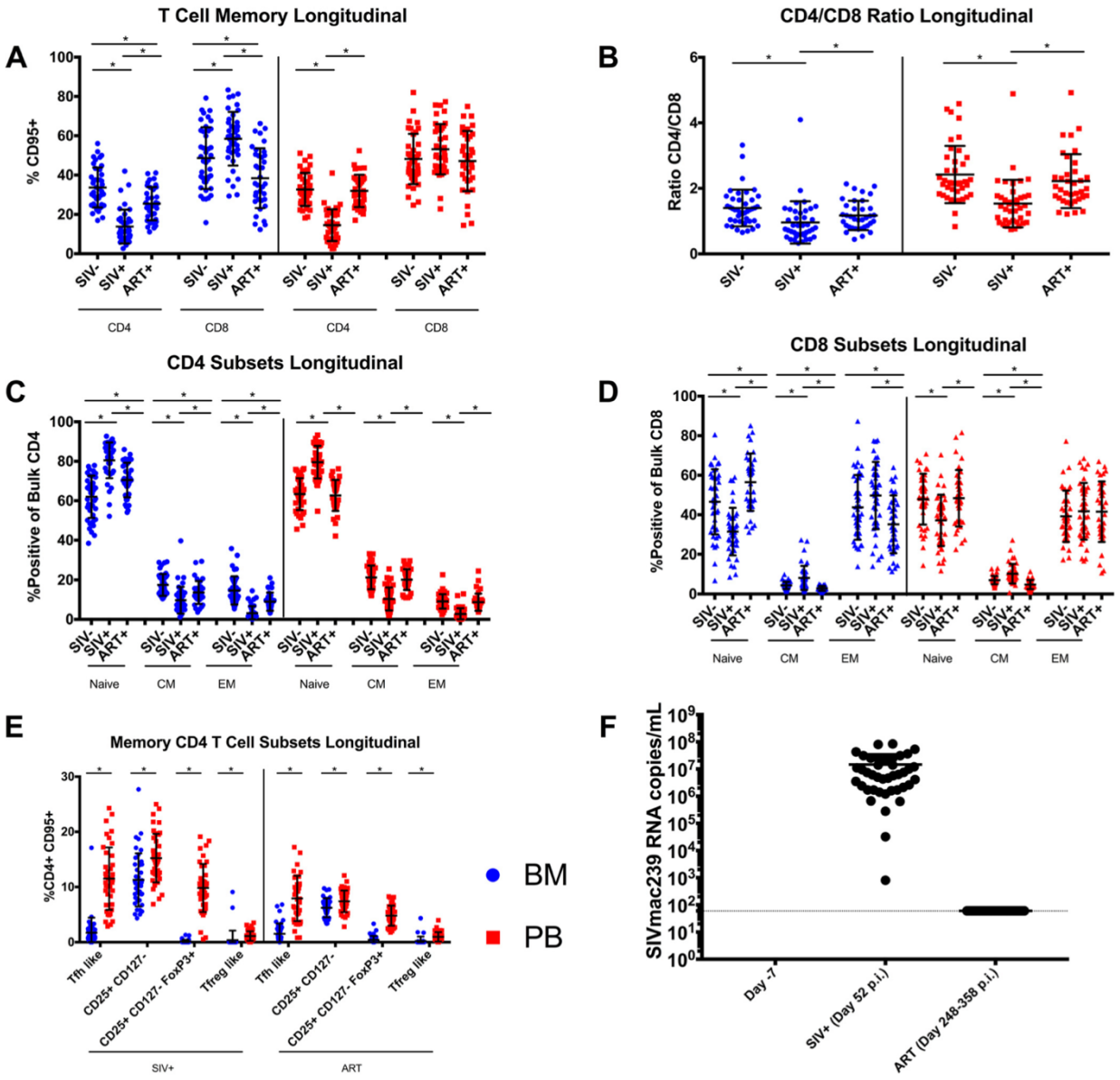

Figure 2.3 Longitudinal characterization of BM- and PB-derived T cells following SIV infection and ART treatment. (A) Frequencies of total memory $CD4^+$ and $CD8^+$ T cells before SIV infection (SIV^-), at day 52 after SIV infection (SIV^+), and following ART (ART^+) (days 248 to 358 p.i.). (B) Ratio (calculated in same manner as for Fig. 1B) of $CD4^+$ to $CD8^+$ T cells longitudinally. (C and D) Frequencies of $CD4^+$ and $CD8^+$ T cell subsets (naive, CM, and EM) longitudinally. (E) Frequencies of memory $CD4^+$ ($CD95^+$) T cell subsets: T_{FH}-like ($CXCR5^+$ $PD\text{-}1^+$), $CD25^+$ $CD127^-$, T_{Reg} ($CD25^+$ $CD127^-$ $FoxP3^+$), and T_{FReg} -like ($CXCR5^+$ $PD\text{-}1^+$ $CD25^+$ $CD127^-$ $FoxP3^+$). (F) Plasma viral loads (VL) are shown during preinfection, during early chronic infection (day 52 p.i.), and after ART (days 248 to 358 p.i.). VLs were quantified using qRT-PCR (limit of detection [LOD], 60 copies/ml of plasma; indicated by the dotted line) (n = 40 RMs). *, $P < 0.0001$.

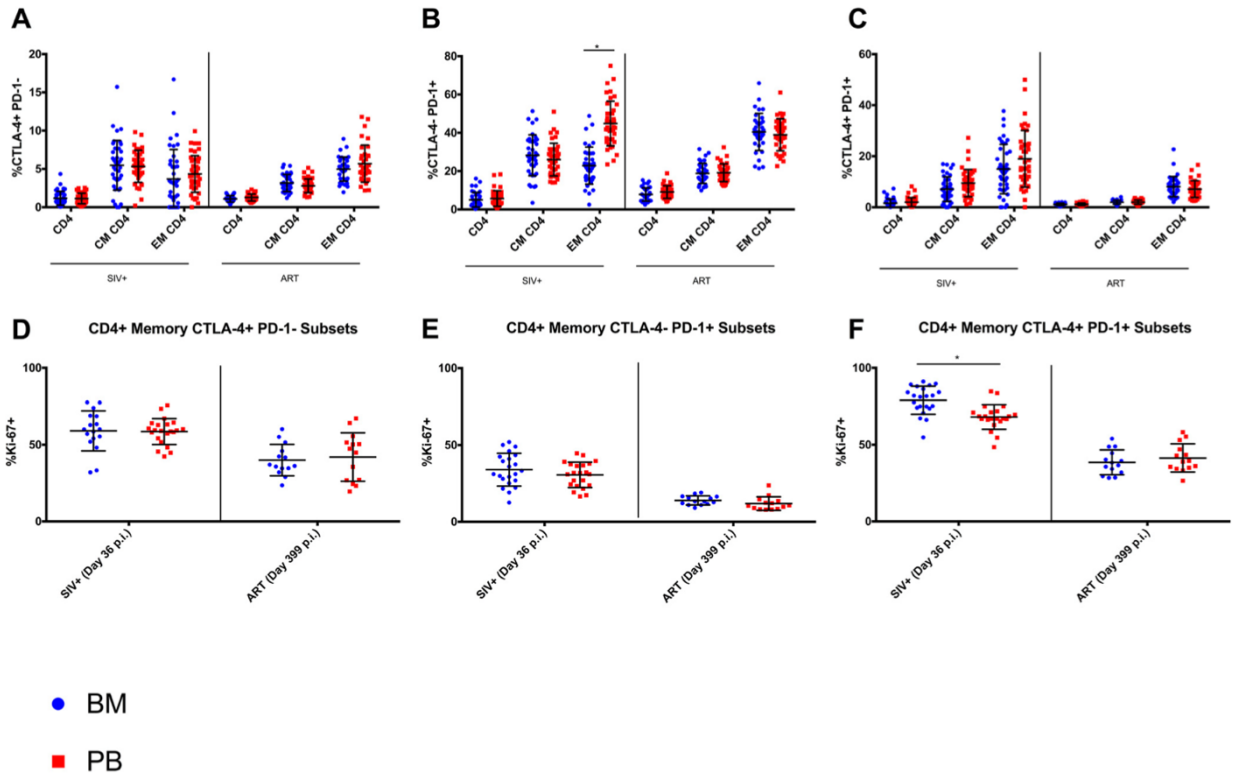

Figure 2.4 Levels of BM- and PB-derived $CD4^+$ T cells expressing co-IRs and expression of Ki-67 following SIV infection and ART. Frequencies of $CD4^+$ T cell subsets with CTLA-4^+ PD-1^- (A), CTLA-4^- PD-1^+ (B), and CTLA-4^+ PD-1^+ (C) phenotypes at day 52 postinfection (SIV^+) and following 12 months of ART (ART) (*n* = 40 RMs). Expression of Ki-67 in CTLA-4^+ PD-1^- (D), CTLA-4^- PD-1^+ (E), and CTLA-4^+ PD-1^+ (F) subsets measured in 22 RMs during SIV infection and 14 RMs during ART (see Materials and Methods). Data for 17 animals are shown in panel D due to the low numbers of CTLA-4^+ PD-1^- memory $CD4^+$ T cells in 5 of the 22 animals during SIV infection. *, $P < 0.0001$.

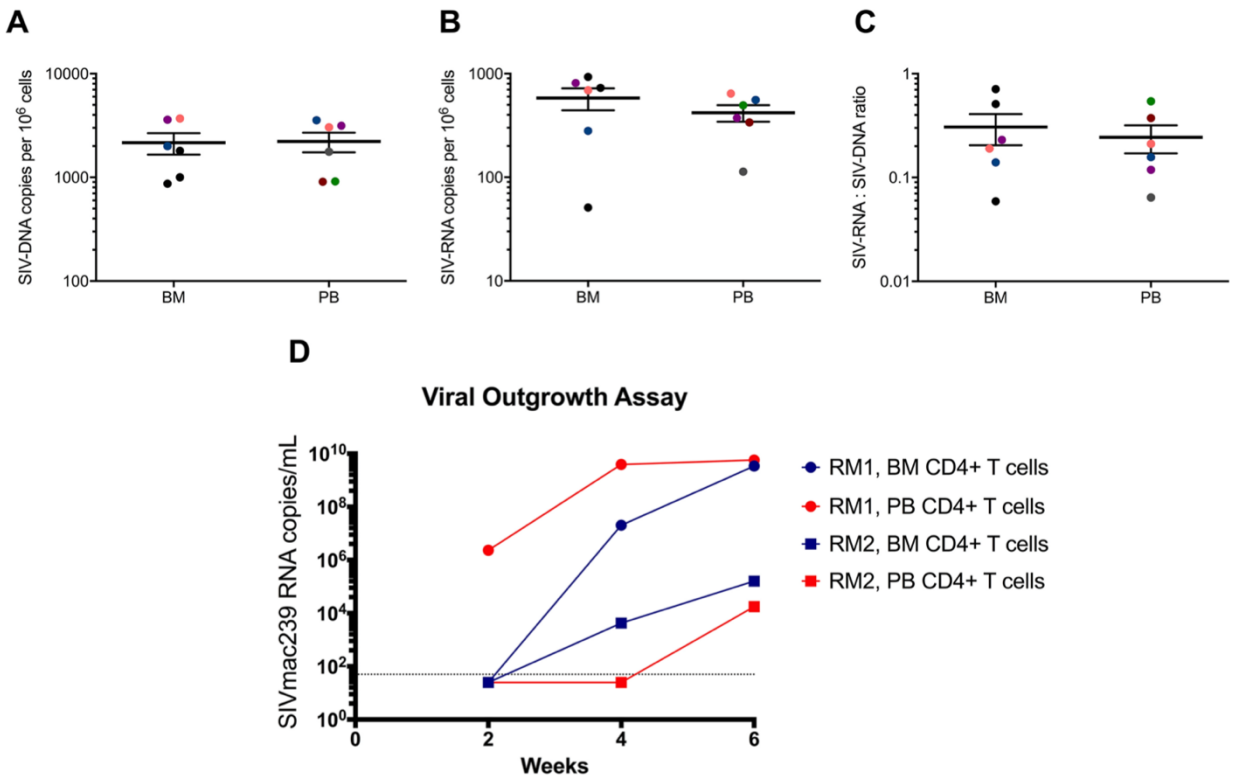

Figure 2.5 Cell-associated SIV DNA and SIV RNA and viral outgrowth assay (VOA) in BM- and PB-derived $CD4^+$ T cells of ART-treated RMs. Copies of cell-associated SIV-DNA (A) and SIV-RNA (B) per 10^6 $CD4^+$ T cells purified from BM and PB (*n* = 6 RMs). (C) Ratio of SIV RNA to SIV DNA in BM and PB. (D) $CD4^+$ T cells were isolated from BM and PB (*n* = 2 RMs) and used in the viral outgrowth assay to confirm the presence of replication-competent virus. The graph shows SIV_{mac239} RNA copies/ml of supernatant at 2, 4, and 6 weeks of the VOA.

Chapter Three: Baricitinib treatment resolves lower airway macrophage inflammation and neutrophil recruitment in SARS-CoV-2-infected rhesus macaques

Timothy N. Hoang[1,13], Maria Pino[1,13], Arun K. Boddapati[2,13], Elise G. Viox[1], Carly E. Starke[3], Amit A. Upadhyay[2], Sanjeev Gumber[4,5], Michael Nekorchuk[3], Kathleen Busman-Sahay[3], Zachary Strongin[1], Justin L. Harper[1], Gregory K. Tharp[2], Kathryn L. Pellegrini[2], Shannon Kirejczyk[5], Keivan Zandi[6], Sijia Tao[6], Tristan R. Horton[2], Elizabeth N. Beagle[2], Ernestine A. Mahar[1], Michelle YH Lee[1], Joyce Cohen[7], Sherrie M. Jean[7], Jennifer S. Wood[7], Fawn Connor-Stroud[7], Rachelle L. Stammen[7], Olivia M. Delmas[1], Shelly Wang[1], Kimberly A. Cooney[8], Michael N. Sayegh[8], Lanfang Wang[8], Peter D. Filev[9], Daniela Weiskopf[10], Guido Silvestri[1,4], Jesse Waggoner[8], Anne Piantadosi[4,8], Sudhir P. Kasturi[1], Hilmi Al-Shakhshir[11], Susan P. Ribeiro[11,†], Rafick P. Sekaly[11,†], Rebecca D. Levit[8], Jacob D. Estes[3,12], Thomas H. Vanderford[1], Raymond F. Schinazi[6,14], Steven E. Bosinger[1,2,4,14], Mirko Paiardini[*,1,4,14,15]

[1]Division of Microbiology and Immunology, Yerkes National Primate Research Center, Emory University, Atlanta, GA 30329, USA.

[2]Yerkes Genomics Core Laboratory, Yerkes National Primate Research Center, Emory University, Atlanta, GA 30329, USA.

[3]Vaccine and Gene Therapy Institute, Oregon Health & Science University, Beaverton, OR 97006, USA.

[4]Department of Pathology and Laboratory Medicine, School of Medicine, Emory University, Atlanta, GA 30322, USA.

[5]Division of Pathology, Yerkes National Primate Research Center, Emory University, Atlanta, GA 30329, USA

[6]Center for AIDS Research, Department of Pediatrics, School of Medicine, Emory University, Atlanta, GA 30322, USA.

[7]Division of Animal Resources, Yerkes National Primate Research Center, Emory University, Atlanta, GA 30329, USA.

[8]Department of Medicine, School of Medicine, Emory University, Atlanta, GA 30322, USA.

[9]Department of Radiology and Imaging Sciences, School of Medicine, Emory University, Atlanta, GA 30322, USA.

[10]Center for Infectious Disease and Vaccine Research, La Jolla Institute for Immunology, La Jolla, CA 92037, USA.

[11]Department of Pathology, Case Western Reserve University, Cleveland, OH 44106, USA.

[12]Oregon National Primate Research Center, Oregon Health & Science University, Beaverton, OR 97006, USA.

[†]Current Address: Department of Pathology and Laboratory Medicine, School of Medicine, Emory University, Atlanta, GA 30322, USA.

[13]These authors contributed equally; [14]Co-corresponding authors;

[15]Lead contact

Running title: Baricitinib mitigates inflammation in SARS-CoV-2 infected rhesus macaques

Keywords: COVID-19, SARS-CoV-2, inflammation, immune activation, baricitinib, nonhuman primate, immunology, pathogenesis

Published in *Cell* Volume 184, No. 2, January 21st, 2021, PMID: 33278358

Summary

SARS-CoV-2 induced hypercytokinemia and inflammation are critically associated with COVID-19 disease severity. Baricitinib, a clinically approved JAK1/2 inhibitor, is currently being investigated in COVID-19 clinical trials. Here, we investigated the immunologic and virologic efficacy of baricitinib in a rhesus macaque model of SARS-CoV-2 infection. Viral shedding measured from nasal and throat swabs, bronchoalveolar lavages and tissues was not reduced with baricitinib. Type-I IFN antiviral responses and SARS-CoV-2-specific T-cell responses remained similar between the two groups. Animals treated with baricitinib showed reduced inflammation, decreased lung infiltration of inflammatory cells, reduced NETosis activity, and more limited lung pathology. Importantly, baricitinib treated animals had a rapid and remarkably potent suppression of lung macrophages production of cytokines and chemokines responsible for inflammation and neutrophil recruitment. These data support a beneficial role for, and elucidate the immunological mechanisms underlying, the use of baricitinib as a frontline treatment for inflammation induced by SARS-CoV-2 infection.

Introduction

The rapid emergence and dissemination of severe acute respiratory syndrome coronavirus 2 (SARS-CoV-2) and subsequent COVID-19 pandemic has placed an excessive burden on public and private healthcare systems with over 1,000,000 deaths worldwide. Thus, therapeutic approaches aimed at mitigating disease severity are of utmost global priority. SARS-CoV-2 infection results in a wide spectrum of disease severity, ranging from asymptomatic individuals to critically-ill patients leading to death. Severe COVID-19 disease presents with high-grade fever, dry cough, pneumonia, inflammation of the lungs and infiltration of immune cells. It has been noted that individuals with co-morbidities and compromised immune systems are at higher risk for severe clinical manifestations [518].

Immunological features of COVID-19 progression includes a robust pro-inflammatory response driven by innate and adaptive immune cells, with severe cases of COVID-19 having elevated serum levels of pro-inflammatory cytokines and chemokines including: IFNγ, TNFα, IP-10, G-CSF, IL-2, IL-6 IL-8, IL-9, IL-10, and IL-17. Therefore, the use of therapeutics targeted at Janus Kinases (JAK) have the potential to ameliorate disease severity by limiting the hypercytokinemia and cytokine release syndrome (CRS) seen in COVID-19 patients [338].

Non-human primate (NHP) models have been used extensively to study pathogenesis and potential vaccine and antiviral candidates for numerous viral diseases [519]. We and others have recently used rhesus macaques (RMs) to model SARS-CoV-2 infection and pathogenesis; SARS-CoV-2 infected RMs develop transient respiratory disease and exhibit viral shedding similar to humans, recapitulating mild to moderate infection, and only in rare cases severe disease [328, 450, 520-522]. Baricitinib is an oral, selective inhibitor of JAK 1 and 2 with potent anti-inflammatory activity approved for treatment of patients with moderate to severe active rheumatoid arthritis [523]. Recently, machine learning algorithms and *in vitro* data suggested that baricitinib could also inhibit clathrin-mediated endocytosis of SARS-CoV-2 [524-527]; thus, it could provide a dual effect of dampening inflammation and viral infection. In this study, leveraging the ability to perform longitudinal collections, including bronchoalveolar lavages, and the availability of lung tissue for pathology, we tested the immunologic and virologic effects of baricitinib treatment in SARS-CoV-2 infected RMs.

Results

Baricitinib was well-tolerated and detectable in plasma and tissues, but did not limit SARS-CoV-2 replication in RMs

We inoculated 8 adult RMs (11-17 years old, mean = 14 years, **Table 3.S1**) with a total of $1.1x10^6$ PFU SARS-CoV-2 (2019-nCoV/USA-WA1/2020), administered by intranasal (IN) and intratracheal (IT) routes [522]. Two days post infection (DPI), 8 RMs were randomized to receive 4 mg of oral baricitinib, daily for 8-9 days or observed without treatment until 10-11 DPI when all RMs were euthanized (**Figure 3.1A**). At 24 hours post dose, baricitinib was readily detected in plasma of all treated animals (**Figure 3.1B**; measures performed at 6 DPI closed symbol; and 8 DPI open symbol), achieving an average level of 2.13 ng/mL. At necropsy, baricitinib was detectable at approximately 2 hours after the last dose in left/right upper and lower lung (**Figure 3.1C;** n = 4 RMs; average of 4.41 and 4.43 ng/g, respectively), brain (n = 3 RMs; 2.09 ng/g tissue) and cerebrospinal fluid (CSF; n = 2 RMs; 0.29 ng/ml) (**Figure 3.S1A**); we also detected baricitinib in CSF from 3 out of the 4 treated animals at 24 hours post dosing on 8-9 days after the final dose (**Figure 3.S1A**).

A slight reduction of peripheral monocytes, neutrophils and lymphocytes, which could be due to trafficking to the lung, as well as decreased red blood cell counts (RBC), hematocrit (HCT) and hemoglobin (HGB) were observed starting at 2 DPI in all RMs (**Figures 3.S1B-S1G**). Blood chemistries showed elevated levels of alkaline phosphatase (ALP) in one untreated animal starting at 2 DPI, and all other values were within the normal range (**Figure 3.S1H**). Body temperature remained stable in all RMs (**Figure 3.S1I**). Overall, treatment with baricitinib was well-tolerated without direct evidence of treatment-induced clinical pathology, nephrotoxicity or hepatotoxicity when compared to untreated SARS-CoV-2 infected RMs. To further monitor response to infection and baricitinib treatment, the health status of all animals was assessed daily

by veterinarians, with cage-side assessment and physical examination scored based on a standardized scoring system (modified from previous studies [338, 528] main parameters included in the scoring are listed on **Tables 3.S2 and 3.S3**). On 1 DPI, all animals exhibited changes to alertness and respiratory pattern (**Figure 3.1D**). Additional early signs of disease included: changes to pulse oximetry readings, with one untreated animal dropping below 80% (**Figure 3.1F**), reduction in appetite, hunched posture, shivering, pale appearance and agitation. Signs of disease persisted during the 10/11-day course of the study, without significant differences between treated and untreated animals (**Figure 3.1D**). Weight loss was observed in 4/4 untreated and 3/4 baricitinib treated RMs (**Figure 3.1E**), although we cannot discriminate if this is a result of the infection or related to frequent access for sample collection.

We next assessed viral RNA levels by qRT-PCR [328, 520]. We observed high levels of SARS-CoV-2 RNA in nasal and throat swabs, and bronchoalveolar lavages (BAL), with a peak between 2-4 DPI of $1.4x10^7$, $1.2x10^6$, and $1.9x10^5$ copies/mL respectively (**Figures 3.1G-1I**); viral RNA then steadily decreased until 10-11 DPI. SARS-CoV-2 RNA levels remained similar in nasal, throat, or BAL between the baricitinib treated and the untreated group. Virus was not detected in blood and transiently present in rectal swabs (**Figure 3.1J**). At necropsy (10-11 DPI), viral RNA was detected for most animals in nasopharynx, lower/upper lungs, and hilar lymph nodes; viral RNA was detected in the ileum of 4/4 untreated and 1/4 treated RMs. Viral loads (cycle threshold value) in tissue for treated and untreated RMs were overall comparable (**Figure 3.1K**). Additionally, *in situ* RNA hybridization (RNAscope) targeting both positive and negative-sense viral RNA strands identified multifocal clusters of infected cells within the lung parenchyma in both treated and untreated RMs (**Figure 3.S2A**). Thus, baricitinib treatment starting at 2 DPI was safe and well tolerated, but did not impact the kinetics of SARS-CoV-2 replication.

Baricitinib reduced lung pathology and inflammation in SARS-CoV-2 infected rhesus macaques

We then performed multiple analyses to determine the severity of SARS-CoV-2 infection in RMs and the effectiveness of baricitinib to ameliorate the pathophysiologic response. First, x-ray radiographs (RM6 x-ray; **Figure 3.2A)** were longitudinally (-5, 2, 4, 7 and 10 DPI) performed (blinded scoring by a radiologist as previously reported [450, 520]). Pulmonary infiltration and ground glass opacity were observed at multiple experimental timepoints post-infection in 2/4 untreated and 0/4 treated RMs (**Figures 3.2B and 3.2C**), with one of the untreated animals showing severe pneumonia at all post-infection time points (**Figures 3.2B and 3.2C**). Second, we measured serum levels of several systemic inflammatory markers. Among these, ferritin (4 DPI, p=0.0286; and 10 DPI, p=0.0286) and C-reactive protein (CRP; 4 DPI) were found to be elevated in the untreated when compared with the baricitinib treated RMs (**Figures 3.2D and 3.2E**). Previous reports have indicated that heightened ferritin and CRP levels are indicative of COVID-19 severity in humans [529, 530]. Finally, to assess lung damage of SARS-CoV-2 infection, all RMs were euthanized at 10 or 11 DPI. At necropsy, multiple regions of upper, middle and lower lung lobes were taken for immunologic, virologic and pathologic analyses. Lung pathologic analyses and scoring were performed by two pathologists independently in a blinded fashion. Treated RMs showed decreased type 2 pneumocyte hyperplasia, peribronchiolar hyperplasia, syncytia formation, alveolar septal thickening and inflammatory cell infiltration (**Figures 3.2F-3.2K**). Consistent with the pathology scoring, neutrophil (myeloperoxidase, MPO^+, cells) and macrophage (ionized calcium-binding adaptor molecule, $Iba\text{-}1^+$, cells) infiltration, as well as levels of cells expressing the proliferation marker Ki-67 appeared to be decreased in the lungs in baricitinib treated RMs as measured by quantitative immunohistochemistry (IHC) (**Figures 3.S2B-3.S2G**). Levels of Mx1 were similar between both groups (**Figures 3.S2H-3.S2I**). Of note, some of the SARS-CoV-2 infected animals in both groups showed cell infiltration levels similar to

uninfected RMs, indicating a resolution of the infiltration at 10-11 DPI, consistent with an earlier peak of pathogenesis in RMs, as previously published [328, 450, 520-522]. The average pathology score per lobe (measuring the average severity of abnormalities per lobe, independently of how many lobes had been effected, p=0.0286) and the total pathology score (considering severity and number of effected lobes, p=0.0857) were lower in the baricitinib treated group (0.99 and 22, respectively) as compared to untreated RMs (1.66 and 38.5, respectively) (**Figures 3.2L-3.2N**). Overall, these data support a therapeutic role of baricitinib in reducing lung pathology, infiltration of inflammatory cells in the lung, and soluble markers of inflammation associated with disease progression in humans.

Baricitinib treatment dampens gene signatures of macrophage inflammation and neutrophil degranulation in the BAL of SARS-CoV-2 infected rhesus macaques

To investigate the impact of baricitinib on the lower airway, we performed bulk RNA-Seq profiling of cells isolated from BAL prior to SARS-CoV-2 inoculation (-5 DPI; Baseline); 2 days after virus inoculation, prior to baricitinib treatment (2 DPI); and 4 days after infection, and 48 hours after beginning baricitinib (4 DPI). Relative to pre-infection, we observed a robust upregulation of differentially expressed genes (DEGs) at 2 DPI in both the treated and untreated RMs (**Figure 3.3A)**, however at 4 DPI only a handful of DEGs were detected in the baricitinib treated animals, whereas a robust transcriptional response persisted in the untreated group. To identify immunological pathways perturbed by SARS-CoV-2 infection and baricitinib treatment, we performed gene-set enrichment analysis (GSEA) [531]. To determine pathways that changed after drug administration, we directly compared gene expression profiles at 2 DPI to 4 DPI. Comparison of GSEA data from 2 DPI to 4 DPI in untreated RMs show robust, highly significant positive enrichment in pathways comprised of genes for inflammatory responses, TNFα and IL6 signaling, neutrophil and granulocyte function – indicating that, in the absence of baricitinib, expression of

these genes continues to increase (**Figure 3.3B**). In stark contrast, when a similar comparison of 2 DPI vs 4 DPI was tested in RMs receiving baricitinib, we observed negative enrichment, indicating that inflammatory genes were expressed at lower levels already after only 2 days of treatment **(Figure 3.3B)**. To confirm the robustness of our enrichment analysis in detecting downregulation of inflammatory pathways with treatment, we also conducted GSEA analyses using direct cross-sectional comparisons (i.e. 4 DPI untreated vs 4 DPI treated); these data demonstrated that inflammatory signatures were significantly lower in animals receiving baricitinib at 4 DPI, although equivalent when comparing 2 DPI samples in which neither group had received the drug (**Figures 3.S3A and 3.S3B**).

To explore the impact of baricitinib on the inflammatory responses induced by SARS-CoV-2 infection at the gene level, we examined several pathways in greater detail (**Figures 3.3C-3.3J**). One of the highest scoring pathways, neutrophil degranulation, was significantly enriched at 4 DPI relative to 2 DPI in the untreated group ($p<0.001$) (**Figure 3.3C**). Strikingly, enrichment of this pathway was completely abrogated in the treated group ($p=0.979$). When we examined individual genes that were (i) elevated by SARS-CoV-2 infection, and (ii) influenced by baricitinib treatment, we observed that several genes were those encoding degradative and bactericidal enzymes present in neutrophil granules (MMP9, MMP25, BPI, MPO), or highly expressed on polymorphonuclear neutrophils (CXCR1 and CXCR2), the alarmin S100A12, and genes for proteins that act to degrade the extracellular matrix during neutrophil extravasation: SERPINB10, ADAM8 (**Figure 3.3G**). Of note, S100A12, (EN-RAGE), for which expression was effectively reduced by baricitinib treatment, has been associated with COVID-19 severity in humans [(532)]. These genes were highly upregulated in BAL samples of untreated RMs, but substantially attenuated in treated animals, many at levels equivalent to pre-infection (**Figure 3.3G**). Collectively, these gene signatures suggest that baricitinib treatment may dampen macrophage

inflammation as well as neutrophil recruitment and activity in the lower airway during acute SARS-CoV-2 infection. We also examined the enrichment of neutrophil pathway genes in cross-sectional GSEA comparisons, as shown in **Figures 3.S3C and 3.S3D;** this analysis largely mirrored our D2 vs D4 observations. Additionally, we observed several alarmin proteins (S100A8, S100A9) had lost their induction at 4 DPI in animals receiving baricitinib, as did the MPO gene. These genes have been recently demonstrated to be highly expressed in the myeloid compartment of peripheral blood of patients exhibiting severe COVID-19 disease [533, 534].

Baricitinib treatment also rapidly induced near complete abrogation of inflammation mediators downstream of TNFα signaling and IL6 signaling (**Figures 3.3D and 3.3E, 3.3H and 3.3I).** Within these pathways, amongst the molecules suppressed by baricitinib were chemotactic factors critical for recruitment of neutrophils (CXCL6, CXCL3) and macrophages (CCL2), inflammatory serine protease factors (SERPINB2, TNFAIP6) and cytokines regulating inflammation and immune responses (IL12B). Of note, genes identified as upregulated in rheumatoid arthritis (RA) were found to be significantly enriched ($p=0.0448$) in untreated as compared to treated animals at 4 DPI, despite similar gene expression at 2 DPI (**Figures 3.S3E and 3.S3F**). In the leading-edge analysis of the RA pathway we noted lower expression of several inflammatory mediators such as CXCL8, IL1B, CCL5, CCL3, CCL20, IL18, IL6 and CXCL12 (**Figures 3.S3G and 3.S3H**). As baricitinib was developed to ameliorate inflammation in RA by inhibiting JAK1/2 signaling, and consistently with the reduction in the IL-6/JAK/STAT3 signaling pathway (**Figure 3.3I**), these data confirm the effectiveness of baricitinib in the lower airway of SARS-CoV-2 infected RMs.

Several of the significantly enriched genesets were comprised of genes in Type I interferon signaling (**Figure 3.3B**) and multiple interferon stimulated genes (ISGs) had elevated expression relative to baseline (**Figure 3.3J**). In both treated and untreated groups, we observed a slight

reduction in expression at 4 DPI relative to 2 DPI (**Figures 3.3B and 3.3F**). However, unlike genesets associated with inflammation, genes associated with Type I IFN signaling and innate antiviral responses were unperturbed by baricitinib. Thus, baricitinib treatment potently suppressed inflammatory pathways in the lower airway of RMs infected with SARS-CoV-2, but left innate antiviral signaling largely intact.

Baricitinib treatment abolishes inflammatory cytokine and neutrophil chemoattractant expression in bronchoalveolar macrophages of SAR-CoV-2 infected rhesus macaques

The bulk RNA-Seq data indicated that gene signatures consistent with macrophage activation, neutrophil infiltration and cytokine driven inflammation were evident as early as 2 DPI, and that baricitinib was capable of abrogation of these pathways. To identify the cellular component orchestrating airway inflammation, we performed single-cell RNA-Seq (sc-RNA-Seq) profiling using 10X Genomics-based droplet sequencing. Single cell suspensions of BAL samples from three untreated and two baricitinib treated RMs prior to infection, and at 4 DPI were subjected to 10X droplet capture within 3 hours of collection. After processing to remove erythrocytes and low-quality cells, the captures yielded a cumulative 45,583 cells across all samples for analysis. The cellular distribution is summarized in the UMAP shown in **Figure 3.4A**. Similar to observations reported in sc-RNA-Seq data in humans infected with SARS-CoV-2 [535-537], the vast majority of cells in BALs were predominantly macrophage/myeloid origin (80.7%), followed by lymphocytes ($CD4^+$/$CD8^+$ T cells/ NK cells) (9.8%) and approximately 3.2% were identified as epithelial. Allocation of cells from the cumulative data by treatment variables (**Figure 3.4B**) demonstrated that the cellular distribution was equivalent amongst the experimental groups and no population was enriched due to batch or technical variation associated with individual captures. We probed the macrophage population for upstream regulators associated with the inflammatory pathways identified in the bulk RNA-Seq analyses, and observed elevated expression of several

inflammatory mediators at 4 DPI: IL6, TNF□, IL1□ and IL10 (**Figures 3.4C, 3.S4 and 3.S5)**. IFN□ was also highly expressed in the macrophage cluster, however, IFN□ transcripts were detected in a virtually negligible fraction of cells (**Figures 3.4C, 3.S4 and 3.S5**). Strikingly, and consistent with the bulk RNA-Seq data, we observed that baricitinib treatment virtually dampened expression of TNF□, IL10, IFN□ and IL6 in pulmonary macrophages, and significantly reduced expression of IL1□□□**Figure 3.4C**□□ We also observed a robust induction of chemokines driving neutrophil recruitment (CXCL3/MIP2□, CXCL8/IL8), macrophage trafficking (CCL4L1/MIP1□), and CXCL10/IP10 (**Figures 3.4D and 3.4E)**, a pleiotropic chemokine upregulated in several viral infections, and long hypothesized to be associated with pathogenesis in SARS-CoV-1 viral infection and observed in SARS-CoV-1 infection of NHPs [538-540]. Notably, after 48 hours of baricitinib treatment, expression of these proinflammatory cytokines was reduced to basal levels (**Figures 3.4D and 3.4E**). Examination of the expression levels of antiviral ISGs in pulmonary macrophages yielded a much different pattern than those observed for inflammatory genes – although widespread induction of ISGs were observed after SARS-CoV-2 infection, baricitinib treatment had only a very modest impact on these pathways (**Figure 3.4F**). Collectively, these data support a model in which baricitinib administration strongly reduces airway inflammation and neutrophil accumulation, but has a minimal effect on innate antiviral immunity.

Baricitinib leads to reduced BAL levels of neutrophils and neutrophil NETosis activity

To gain insight into the immunologic effects of baricitinib treatment on cellular distribution within BAL, we applied global high-dimensional mapping of 23-parameter flow cytometry data. As shown in the UMAP representation (**Figure 3.5A**), untreated and baricitinib treated RMs had different BAL cellular distribution starting from 4 DPI, corresponding with the timepoint of peak inflammation and viremia, including in neutrophils. This was of interest considering the higher frequency of macrophages expressing neutrophil-attracting chemokines in untreated RMs

(**Figures 3.4D and 3.4E**). Thus, we focused our flow cytometry immunologic analyses in quantifying the longitudinal levels of neutrophils ($CD45^+CD3^-CD20^-CD66^+$ live granulocytes; representative staining in **Figures 3.S6A and 3.S6B**). Analyses of BAL showed an early recruitment of neutrophils in the lung at 4 DPI during the peak of viremia, particularly in the untreated RMs, which all maintained higher frequencies of neutrophils at later stages of infection (10-11 DPI) as compared to baricitinib treated RMs (**Figure 3.5B;** p=0.0286)**.** In blood, neutrophils (**Figure 3.5C**) remained relatively stable post infection as compared to pre-infection and at lower levels in untreated as compared to treated animals at the latest experimental points (p=0.0571), consistently with a higher migration to lung in untreated RMs. The levels of $CD14^+CD16^-$ (**Figure 3.5D**) and $CD14^+CD16^+$ monocytes in the BAL were, on average, slightly higher in untreated RMs at 4, 7, and 10 DPI, with the difference due to 3 of 4 untreated RMs having levels higher than the untreated animals at specific timepoints (**Figure 3.5D**). Since the flow cytometry data of BAL shows a reduced migration of neutrophils to lung in baricitinib-treated RMs, we next measured neutrophil extracellular trap (NET) activity by quantification of extracellular DNA via Sytox staining, a functional readout of NETosis activity (**Figures 3.5E and 3.5F**) and by quantification of citrullinated H3 (**Figure 3.5G**), a systemic marker indicating a post-translational modification thought to precede DNA decondensation during NETosis. NETs have been reported as an important mechanism of inflammation and microvascular thrombosis in patients with COVID-19 [(541)]. Baricitinib treated RMs showed decreased NET formation by blood neutrophils at 4 (more evident for citrullinated H3, **Figure 3.5G**; p = 0.0571) and 10 (more evident for Sytox staining, **Figure 3.5F;** p=0.0571) DPI when compared to untreated RMs. Finally, when the formation of NETs was examined directly in the lung by IHC staining for citrullinated H3, 3/4 untreated RMs showed presence of NETs whereas NETs were virtually absent in treated RMs (**Figure 3.5H)**.

Altogether, these data support baricitinib activity in reducing macrophage-derived inflammation and by decreasing pro-inflammatory neutrophilic levels, activity and NETosis.

Baricitinib reduced T cell immune activation in SARS-CoV-2 infected rhesus macaques

Our transcriptomic data indicated that baricitinib reduced macrophage expression of multiple cytokines that can induce T cell immune activation. As such, we then analyzed levels of T cells, and their frequency of activation and proliferation by flow cytometry (gating strategy shown in **Figure 3.S6C**). $CD4^+$ T cell levels in blood remained similar between treated and untreated animals, with 1/4 baricitinib treated and 2/4 untreated RMs exhibiting a pronounced reduction in $CD4^+$ T cell frequencies at 10 DPI (**Figure 3.6A**). We observed an expansion of $CD4^+$ T_{Regs} ($CD45^+CD3^+CD4^+CD95^+CD127^-CD25^+FoxP3^+$; representative staining in **Figure 3.S6C**) at 4 ($p=0.0571$) and 6 DPI in the untreated, but not in the baricitinib treated RMs (**Figure 3.6B**). Specifically, the mean fold change in $CD4^+$ T_{Regs} frequency at 4 and 6 DPI, as compared to pre-treatment baseline (2 DPI), was of 7.43 and 4.36 in untreated and of 1.22 and 1.13 in baricitinib treated RMs, respectively, suggesting higher levels of inflammation in the untreated group resulting in greater expansion of $CD4^+$ T_{Regs} **(Figure 3.6C)**. Peripheral $CD8^+$ T cells were reduced at 10 DPI in 2/4 baricitinib treated and 2/4 untreated RMs (**Figure 3.6D**). Notably, the frequency of proliferating ($Ki\text{-}67^+$) memory $CD8^+$ T cells in blood progressively and significantly increased in all 4 untreated animals at 7 and 10 DPI, while significantly decreasing in all baricitinib treated RMs already at 4 DPI. As a result, at 10 DPI the mean frequency of $CD8^+Ki\text{-}67^+$ was significantly higher in untreated RMs (24.38% vs 7.38%; $p = 0.0286$, **Figure 3.6E**).

$CD4^+$ T cells in the BAL remained relatively constant until 7 DPI, when the majority of RMs started experiencing a reduction in their frequencies (**Figure 3.6F**). Untreated RMs showed an early

(present at 4 DPI), large (mean fold change of 3.31 at 7 DPI vs 2 DPI compared to 1.14 in the treated RMs) and prolonged (up to 10 DPI) increase in the frequency of memory $CD4^+$ T cells expressing CD38 ($CD38^+HLA\text{-}DR^-$; 4 DPI, p=0.0286, **Figure 3.6G**). Remarkably, different from untreated RMs, the frequency of those activated memory $CD4^+$ T cells decreased in baricitinib treated animals starting at 4 DPI and remained lower than pre-treatment until 10 DPI (**Figure 3.6G)**. Consistent with a reduced pro-inflammatory state of $CD4^+$ T cells, baricitinib treated RMs showed a lower frequency of $CD4^+$ T cells that spontaneously (without stimulation) produced pro-inflammatory, Th17 related cytokines ($IL\text{-}17^+$; $IL\text{-}17^+IL\text{-}21^+$; $IL\text{-}17^+IL\text{-}22^+$) when compared to untreated RMs (**Figures 3.S7A-3.S7C**).

As with $CD4^+$ T cells, the reduction in $CD8^+$ T cells was more pronounced in BAL, starting at 7 DPI and maintained until necropsy (**Figure 3.6H**). Similarly, also in BAL the frequency of $CD8^+Ki\text{-}67^+$ T cells increased more extensively in untreated than baricitinib-treated RMs (30.53% vs 11.53% at 7 DPI; 39.95% vs 24.65% at 10 DPI; **Figure 3.6I**); as a result, the fold change (as compared to 2 DPI, pre-treatment) in the frequency of memory $CD8^+Ki\text{-}67^+$ T cells was higher in untreated then baricitinib treated RMs both at 7 (8.22 vs 1.02) and 10 (6.28 vs 2.48) DPI. A similar trend was measured for activated memory $CD8^+$ T cells, with higher frequency and fold change in untreated than baricitinib treated RMs at 7 (FC $CD38^+DR^-$: 23.67 vs 1.62) and 10 (FC $CD38^+DR^-$: 9.81 vs 1.43) DPI (**Figure 3.6J**). Representative staining for Ki-67 and HLA-DR by CD38 in $CD4^+$ and $CD8^+$ T cells are shown in **Figures 3.6K-3.6M**. These results corroborate the reduced frequency of $Ki\text{-}67^+$ cells observed in baricitinib treated compared with untreated animals in lung via quantitative IHC analysis (**Figures 3.S2F and 3.S2G**).

Finally, we assessed the ability of peripheral T cells to respond to *ex vivo* SARS-CoV-2 specific stimulation (with a SARS-CoV-2 S peptide pool characterized in [361]) and to non-antigen specific

stimulation (with PMA/ionomycin). Importantly, the levels of SARS-CoV-2 specific $CD4^+$ and $CD8^+$ T cells producing IFNγ, TNFα, IL-2, IL-4 and IL-17a in response to S peptide pool stimulation were similar in both groups of animals (**Figures 3.S7D-3.S7F**). Similarly, the frequency of $CD4^+$ and $CD8^+$ T cells producing IL-17a, IL-21, IL-22, IFNγ, and TNFα were similar among the two groups after PMA/Ionomycin stimulation (**Figures 3.S7G and 3.S7H**). Furthermore, levels of memory $CD4^+$ and $CD8^+$ T cells expressing granzyme B or PD-1 remained similar between untreated and treated RMs both in blood (**Figures 3.S7I and 3.S7J**) and BAL (**Figures 3.S7K and 3.S7L**).

Collectively, these findings indicate that baricitinib treatment lead to downstream reduction in T cell activation and proliferation, without an overall detrimental effect to antiviral function of T cells.

Discussion

In this study, we tested baricitinib, a JAK1/2 inhibitor clinically approved for rheumatoid arthritis, as a therapeutic candidate to reduce systemic inflammation caused by SARS-CoV-2 infection in RMs. Notably, baricitinib treated RMs displayed reduced (i) lung pathology, from moderate in untreated animals to mild; (ii) levels of inflammatory cytokines, chemokines, and signaling pathways associated with macrophage inflammation, neutrophil recruitment, and disease progression in SARS-CoV-2 infected humans; and (iii) levels of systemic inflammation that are associated with COVID-19 severity in humans while not having an impact on Type 1 IFN responses. This beneficial anti-inflammatory effect of baricitinib was confirmed by a reduced infiltration of macrophages and neutrophils into the lungs, and a reduced T cell activation in both blood and BAL as compared to untreated animals. Furthermore, we were able to observe an increased NETosis activity of neutrophils upon SARS-CoV-2 infection, previously described in serum from COVID19 patients [(541)], which was reduced in baricitinib treated RMs. Remarkably, single-cell RNA sequencing showed reduced immune activation, neutrophil recruitment, and

macrophage trafficking signatures in pulmonary macrophages from treated RMs already after two doses of baricitinib, at 4 DPI. IL-6, TNFα, IL-10, IL-1B□□□CXCL3/MIP-2□, CXCL8/IL8, CCL4L1/MIP-1□, and CXCL10/IP-10 were all expressed at higher levels in pulmonary macrophages from untreated animals compared to baricitinib treated RMs. These data confirm very recent studies that demonstrated by RNA-Seq analysis that higher levels of inflammatory cytokines in lung macrophages are associated with patients presenting with severe/critical COVID-19 cases [537]. Thus, baricitinib could have clinical benefits in reducing the inflammatory response typically seen in moderate to severe cases of COVID-19 (**Figure 3.7**). Of note, one of the advantages of baricitinib when compared with other cytokine-specific anti-inflammatory therapies is that it can inhibit production of several cytokines involved in the cytokine storm described in severe cases of COVID-19.

Clinical pathology and laboratory parameters of toxicity remained similar in the treated RMs for the 8-9-day treatment course at a dose comparable to humans [524, 527, 542]. Baricitinib was found distributed in lungs, a key tissue for SARS-CoV-2 replication, as well as in the central nervous system (CNS). Although several *in silico* modeling and *in vitro* studies suggested baricitinib as a possible treatment candidate to COVID-19 due to its potential antiviral activity [524-527], we did not observe changes in viral replication dynamics in the treated animals. One of the main concerns in using a JAK inhibitor such as baricitinib, is that its downstream anti-immune activation effects could limit immune responses necessary to combat SARS-CoV-2. Importantly, we did not identify reduction of SARS-CoV-2 specific and unspecific $CD4^+$ and $CD8^+$ T cell responses in treated animals, and baricitinib did not inhibit genes associated with Type I Interferon antiviral responses, indicating its mode of action in this context is primarily to dampen inflammatory responses while maintaining innate and adaptive antiviral immune responses. While ISGs can certainly be stimulated via the JAK/STAT pathways, ISGs have also been shown to be highly inducible via the

STING and RIG-I pathways [543-545], which are not affected by baricitinib. It is possible that these pathways could compensate for the reduced stimulation via the JAK/STAT pathway.

Several ongoing clinical trials are studying the effects of baricitinib in SARS-CoV-2 infected humans. Currently, the Adaptive COVID-19 Treatment Trial (ACTT-2; NCT04401579) is evaluating the effects of baricitinib in combination with remdesivir and the COV-BARRIER trial (NCT04421027) is studying baricitinib as a monotherapy. Participants are treated with placebo, remdesivir alone or a combination of remdesivir and baricitinib. In a retrospective cohort study, 15 patients with severe COVID-19 were administered a short-course of baricitinib in combination with hydroxychloroquine and this was associated with a complete recovery in 11/15 subjects [527]. In a separate pilot study, baricitinib was combined with lopinavir-ritonavir in 12 patients starting treatment 6 days post-symptom onset, with all individuals showing significantly improved clinical and laboratory parameters with no treated individuals requiring ICU care [524]. Being performed in an animal model, this study has some key advantages and some important limitations. Advantages include the ability to correct for parameters that may impact clinical outcome and treatment readout, including using the same virus inoculum, dose, route of infection and starting baricitinib at the same phase of infection in all subjects. Furthermore, the NHP model permits longitudinal collection of BAL and lung at necropsy, which in turn allows the in-depth characterization of the mechanism and impact of baricitinib on immune activation and immunologic responses, including single-cell RNA sequencing analyses of macrophages, at the foci of infection. The main limitation of the study is the small group size, with a total of eight RMs; furthermore, being that SARS-CoV-2 infected RMs is a model of mild to moderate COVID-19 with no untreated animals succumbing to infection, and with treatment initiated early after infection, we cannot determine if the therapeutic impact of baricitinib will be the same in severe COVID-19 patients and when started at a later phase post-infection. Mitigating that concern, in our study,

treatment started once inflammatory signatures were already up-regulated, mimicking the conditions in which baricitinib would be administered clinically. Indeed, a recent small clinical trial in 20 severe COVID-19 patients indicated that baricitinib mitigated immune dysregulation by reducing plasma levels of IL6, IL1□□and TNF□ and lowered time to recovery [542]. Our data provides rationale for baricitinib treatment in COVID-19 to be given in a window where blocking immune inflammation would prevent the formation of a cytokine storm without interfering in the initial responses necessary for preventing viral dissemination and persistence.

In conclusion, this study provides rationale and mechanisms of actions for a beneficial anti-inflammatory effect of baricitinib treatment for COVID-19.

Acknowledgments

We thank the Yerkes National Primate Research Center (YNPRC) Division of Animal Resources, especially Stephanie Ehnert, Stacey Weissman, Denise Bonenberger, John M. Wambua, Dominic M. D'Urso, Racquel Sampson-Harley, and Kalpana Patel in Research Resources for providing support in animal care. We thank Dr. Vincent Marconi for discussions and critical reading of the manuscript. Pharmaceutical-grade Baricitinib was commercially obtained, provided free of charge by Dr. Schinazi, and it was found to be > 99% pure by LC-MS-MS. This study was supported by an Emory University COVID-19 Molecules and Pathogens to Populations and Pandemics Initiative Seed Grant to M.Pa., A.P., and R.F.S.; by YNPRC Coronavirus Pilot Research Project Program grant to M.Pa. under award P51 OD11132; and by Fast Grants Award #2144 to M.Pa. This work was additionally funded by the National Institute of Allergy and Infectious Diseases (NIAID, NIH) under awards R37AI141258, R01AI116379 to M.Pa, R01MH116695 to R.F.S, R01AI143411 and R01AI149672 to J.D.E. and U24AI120134 to S.E.B.

Support for this work was also provided by award NIH Office of Research Infrastructure Programs (ORIP) P51OD11132 to YNPRC, P51OD011092 to ONPRC, 1S10OD025002-01 to the Integrated Pathology Core/ONPRC, NIAID award P30 AI050409 to the Center for AIDS Research (CFAR) at Emory University, and contract Nr. 75N9301900065 (to D.W.). Next generation sequencing services were provided by the Yerkes NHP Genomics Core which is supported in part by NIH P51OD011132. Sequencing data was acquired on an Illumina NovaSeq6000 funded by NIH S10OD026799 to S.E.B. Graphical abstract was created with BioRender.com. The content of this publication does not necessarily reflect the views or policies of the U.S. Department of Health and Human Services, nor does it imply endorsement of organizations or commercial products.

Author Contributions

Conceptualization, T.H., M.Pi., J.L.H., G.S., A.P., S.E.B., R.F.S., and M.Pa.; Methodology, T.H., M.Pi., A.K.B., E.G.V., N.K., K.B., A.A.U., Z.S., G.K.T., K.L.P., S.G., S.K., S.T., O.D., K.A.C., M.N.S., L.W., P.D.F., J.W., A.P., S.P.K., C.E.S., S.W., H.A., E.A.M., M.YH.L., K.Z., S.T., T.R.H., E.N.B., S.P.R., T.H.V.; Formal Analysis, T.H., M.Pi., Z.S., E.G.V., A.K.B., K.B., A.A.U., G.K.T., S.G., S.K., S.T., P.D.F., J.W., A.P., S.P.K., S.P.R., T.H.V; Investigation, T.H., M.Pi., E.G.V., J.C., S.J., J.S.W., F.C-S., R.L.S., R.D.L., A.P., S.P.R., R.P.S., and T.V.; Resources, D.W., R.F.S., S.B., and M.Pa.; Writing – Original Draft, T.H., M.Pi., J.L.H. and M.Pa.; Writing – Review & Editing, T.H., M.Pi., J.L.H., S.E.B. and M.Pa.; Visualization, T.H., M.Pi., A.K.B., A.A.U., G.K.T., Z.S. and E.V.; Supervision, R.F.S., S.E.B., and M.Pa.; Funding Acquisition, T.V., A.P.,S.E.B. R.F.S., and M.Pa.

Declaration of Interests

Dr. Raymond Schinazi served as an unpaid consultant for Eli Lilly whose drugs are being evaluated in the research described in this paper. In addition, Dr. Schinazi owns shares in Eli Lilly. The terms of this arrangement have been reviewed and approved by Emory University in accordance with its conflict of interest policies. Eli Lilly had no role in the design of this study and did not have any role during its execution, analyses, interpretation of the data, or decision to submit results. All other authors do not have any conflicts to declare.

Materials and Methods

RESOURCE AVAILABILITY

Lead Contact

Further information and requests for resources and reagents should be directed to and will be fulfilled by the Lead Contact, Dr. Mirko Paiardini (mirko.paiardini@emory.edu).

Materials Availability

This study did not generate new unique reagents.

Data and Code Availability

The datasets generated during this study are available at Gene Expression Omnibus (GEO) accession GSE159214 and code can be made available upon requests.

Data Availability Statement

Source data supporting this work are available from the corresponding author upon reasonable request. The following sequencing data have been deposited in GenBank: SARS-CoV-2 viral

stock. Data tables for expression counts for bulk and single-cell RNA-Seq for BAL are deposited in NCBI's Gene Expression Omnibus and are accessible through GEO accession GSE159214. Custom scripts and supporting documentation on the RNA-Seq analyses will be made available at https://github.com/BosingerLab/.

EXPERIMENTAL MODEL AND SUBJECT DETAILS

Study Approval

YNPRC's animal care facilities are accredited by both the U.S. Department of Agriculture (USDA) and by the Association for Assessment and Accreditation of Laboratory Animal Care (AAALAC). All animal procedures were performed in line with institutional regulations and guidelines set forth by the NIH's Guide for the Care and Use of Laboratory Animals, 8th edition, and were conducted under anesthesia with appropriate follow-up pain management to minimize animal suffering. All animal experimentation was reviewed and approved by Emory University's Institutional Animal Care and Use Committee (IACUC) under permit PROTO202000035.

Animal models

Eight (4 female and 4 male) specific-pathogen-free (SPF) Indian-origin rhesus macaques (RM; *Macaca mulatta;* **Table 3.S1**) were housed at Yerkes National Primate Research Center (YNPRC) as previously described [(129)] in the ABSL3 facility. Animals for study assignment were requested to be greater than 11 years old without preference for gender or MHC haplotype. RMs were infected with 1.1x10^6 plaque forming units (PFU) SARS-CoV-2 via both the intranasal (1 mL) and intratracheal (1 mL) routes concurrently. Absent further stratification criteria, four RMs were administered 4 mg Baricitinib (Olumiant®, Eli Lilly) starting at day 2 post-infection (DPI) for 8-9 consecutive days. Baricitinib was supplied as a powder that was folded into food items (i.e. honey, yogurt, etc.) or distilled water, which was delivered either orally or as a gavage when animals

were being anesthetically accessed, respectively. At each anesthetic access pulse oximetry was recorded and RMs were clinically scored for responsiveness and recumbency; discharges; skin condition; respiration, dyspnea, and cough; food consumption; and fecal consistency (**Tables 3.S2 and 3.S3**). At 10-11 DPI, RMs were administered Baricitinib and subjected to necropsy after 2 hours with blood and cerebrospinal fluid (CSF) collected perimortem to assess pharmacokinetics of baricitinib. Longitudinal tissue collections of peripheral blood (PB); axillary or inguinal lymph node (LN) biopsies; bronchoalveolar lavage (BAL); and nasal, and pharyngeal mucosal swabs in addition to thoracic X-rays (ventrodorsal and right lateral views) were performed immediately prior to Baricitinib administration as annotated (**Figure 3.1A**). In addition to the tissues listed above, at necropsy the following tissues were processed for mononuclear cells: hilar LN, lower lung, and upper lung. Additional necropsy tissues harvested for histology included nasopharynx.

METHOD DETAILS

Viral Stocks

Vero E6 cell line (African Green Monkey Kidney cell line; CRL-1586, ATCC) was used in this study. Vero cells were cultured and maintained in MEM (Sigma) supplemented with 10% heat inactivated fetal bovine serum (FBS) (Gibco) and 1 mM L-glutamine (Gibco), 50 U/ml penicillin and 50 µg/ml streptomycin (Gibco). The cells were kept at 37°C in the presence 5% CO_2. At the time of virus inoculation and propagation, the concentration of FBS was reduced to 2%. SARS-CoV-2 (NR-52281: BEI Resources, Manassas, VA; USA-WA/2020, Lot no. 70033175) was passaged on Vero E6 cells at a MOI of 0.01 to produce the infectious viral stock. SARS-CoV-2 has been propagated and titrated by $TCID_{50}$ method followed by storage of aliquots at -80°C until further use in the experiments.

Back titration of viral stocks via plaque assay was used to determine the infectious dose delivered to the RMs. The virus stock was also directly sequenced via metagenomic methods prior to inoculation to confirm the presence of the furin cleavage motif, which has been shown to be lost upon sequential passage of SARS-CoV-2 in culture [546]). Our stock contained fewer than 6% of viral genomes with a mutation that could potentially abrogate furin-mediated cleavage of S.

Determination of viral load RNA

SARS-CoV-2 genomic RNA was quantified in nasopharyngeal (NP) swabs, throat swabs, plasma, and bronchoalveolar lavages (BAL). Swabs were placed in 1mL of Viral Transport Medium (VTM-1L, Labscoop, LLC). Viral RNA was extracted from NP swabs, throat swabs, and BAL on fresh specimens, while plasma was frozen for future analysis. Viral RNA was extracted manually using the QiaAmp Viral RNA mini kit according to the manufacturer's protocol. Quantitative PCR (qPCR) was performed on viral RNA samples using the N2 primer and probe set designed by the CDC for their diagnostic algorithm: CoV2-N2-F: 5'-TTACAAACATTGGCCGCAAA-3', CoV2-N2-R: 5'-GCGCGACATTCCGAAGAA-3', and CoV2-N2-Pr: 5'-FAM-ACAATTTGCCCCCAGCGCTTCAG-BHQ-3'. qPCR reactions were performed in duplicate with the TaqMan Fast Virus 1-step Master Mix using the manufacturer's cycling conditions, 200nM of each primer, and 125nM of the probe. The limit of detection in this assay was 257 copies per mL of VTM/plasma/BAL. To verify sample quality the CDC RNase P p30 subunit qPCR was modified to account for rhesus macaque specific polymorphisms. The primer and probe sequences are RM-RPP30-F 5'-AGACTTGGACGTGCGAGCG-3', RM-RPP30-R 5'-GAGCCGCTGTCTCCACAAGT-3', and RPP30-Pr 5'-FAM-TTCTGACCTGAAGGCTCTGCGCG-BHQ1-3'. A single well from each extraction was run as above to verify RNA integrity and sample quality via detectable and consistent cycle threshold values.

SARS-CoV-2 quantification from necropsy samples

An approximately 0.5 cm^3 sample of each tissue was collected at necropsy, placed in 500µL Nuclisens lysis buffer (Biomerieux), and stored at -80℃. Thawed samples were homogenized with a sterile pestle, treated with 50µL proteinase K (Qiagen) for 30 minutes at 55℃, and pelleted. Total nucleic acid was extracted from 250µL of supernatant using eMAG (Biomerieux) and eluted into 50µL. RT-PCR for SARS-CoV-2 N2 was performed as previously described, and singleplex RT-PCR for RNase P was performed using primers and probes optimized for quantitation, each using 5µL of eluate [547]. To allow for comparison of SARS-CoV-2 levels between samples that may have had subtle differences in starting material, the SARS-CoV-2 N2 Ct was normalized to the RNase P control by: 1) calculating the difference between N2 Ct and RNase P Ct for each sample, and 2) adding this to the median RNase P Ct value for the sample type. For the purposes of data visualization, samples in which SARS-CoV-2 N2 was undetected were assigned a Ct value of 40 (the assay limit of detection).

Quantification of baricitinib by LC-MS/MS in plasma, CSF and tissue.

One hundred µL of plasma or CSF samples were extracted with 500 µL of methanol. For tissues like brain and lung, 0.2 to 0.5 g of tissue were homogenized and extracted with 2 mL of methanol. [$^2H_9$]-ruxolitinib dissolved in 50% methanol at 500 nM was spiked in plasma/CSF (10 µL) or tissue samples (40 µL) as internal standard before extraction. The supernatant of each extraction (50 µL) was mixed with equal amount of 0.1% formic acid and then subjected to LC-MS/MS analysis after filtration through 0.22 µm membrane with Costar Spin-X centrifuge tube filters (Corning, NY). A Vanquish Flex HPLC system (Thermo Scientific, Waltham, MA) coupled with a TSQ Quantiva triple quadrupole mass spectrometer (Thermo Scientific, Waltham, MA) with an ESI interface was

used for LC-MS analysis. Analytes were separated by a Kinetex EVO-C18 column (100 x 2.1 mm, 2.6 μm; Phenomenex, Torrance, CA) at a flow rate of 300 μL/min, 35°C. Gradient elution was used for the separation with mobile phase A (0.1% formic acid) and mobile phase B (acetonitrile). The LC gradient started with 10% of mobile phase B for 0.5 min, then increased from 10% to 90% in 4 min and kept at 90% for 0.5 min before returning to the initial condition. Selected reaction monitoring in positive mode (spray voltage: 3,200 V; sheath gas: 40 Arb; auxiliary gas: 20 Arb; ion transfer tube temperature: 350°C; vaporizer temperature: 350°C) was used to detect baricitinib (372.1 → 251.1) and the internal standard [$^2H_9$]-ruxolitinib (316.2 → 186.1). Data were collected and processed by Thermo Xcalibur 3.0 software. Calibration curves were generated from standard baricitinib by serial dilutions in blank biometric samples using the same extraction method described above. For CSF, 0.5% plasma was used as surrogate to make calibration curve. The calibration curves had r^2 value greater than 0.99.

All the chemicals are analytical grade or higher and were obtained commercially from Sigma-Aldrich (St. Louis, MO). [$^2H_9$]-ruxolitinib was purchased from ALSACHIM (Illkirch, Alsace, France) with purity greater than 98%.

Quantification of ferritin and CRP

Serum ferritin (Beckman Coulter; Cat# 33020) and C-Reactive protein (Beckman Coulter; Cat# OSR6147) levels were quantified by Emory Medical Laboratory using manufacturer protocols.

Histopathology and immunohistochemistry

Due to study end point, the animals were euthanized, and a complete necropsy was performed. For histopathologic examination, various tissue samples including lung, nasal turbinates, trachea,

or brain, were fixed in 4% neutral-buffered paraformaldehyde for 24h at room temperature, routinely processed, paraffin-embedded, sectioned at 4µm, and stained with hematoxylin and eosin (H& E). The H&E slides from all tissues were examined by two board certified veterinary pathologists. For each animal, all the lung lobes were used for analysis and affected microscopic fields were scored semi-quantitatively as Grade 0 (None); Grade 1 (Mild); Grade 2 (Moderate) and Grade 3 (Severe). Scoring was performed based on these criteria: number of lung lobes affected, type 2 pneumocyte hyperplasia, alveolar septal thickening, fibrosis, perivascular cuffing, peribronchiolar hyperplasia, inflammatory infiltrates, hyaline membrane formation. An average lung lobe score was calculated by combining scores from each criterion. Digital images of H&E stained slides were captured at 40× and 200× magnification with an Olympus BX43 microscope equipped with a digital camera (DP27, Olympus) using Cellsens® Standard 2.3 digital imaging software (Olympus).

Immunohistochemical (IHC) staining of sections of lung was performed using a biotin-free polymer system. The paraffin-embedded sections were subjected to deparaffinization in xylene, rehydration in graded series of ethanol, and rinsed with double distilled water. Antigen retrieval was performed by immersing sections in DIVA Decloaker (Biocare Medical) at 125℃ for 30 seconds in a steam pressure decloaking chamber (Biocare Medical) followed by blocking with Background Sniper Reagent (Biocare Medical) for 10 minutes. The sections were incubated with Thyroid Transcription Factor-1 (Clone 8G7G3/1) for overnight at 4°C followed by a detection polymer system (MACH 2™; Biocare Medical). Labeled antibody was visualized by development of the chromogen (DAB Chromogen Kits; Biocare Medical).

Tissues were fixed in freshly prepared 4% paraformaldehyde for 24 h, transferred to 70% ethanol, paraffin embedded within 7-10 days, and blocks sectioned at 5 µm. Slides were baked for 30-60

min at 65°C then deparaffinized in xylene and rehydrated through a series of graded ethanol to distilled water. Heat induced epitope retrieval (HIER) was performed with the antigen retrieval buffers citraconic anhydride (0.01% with 0.05% Tween; Mx1, Iba-1, and Ki-67) or citrate buffer (pH 6.0; MPO) in a Biocare NxGen Decloaking Chamber that was set to 110°C for 15 min. The slides were cooled, rinsed twice in distilled water and 1X TBS with 0.05% Tween-20 (TBS-T), blocked (TBS-T + 0.25% casein) for 30 minutes at room temperature, then incubated at room temperature with antibodies against Mx1 (EMD; Cat. No. MABF938 at 1:1000 for 1 hour), MPO (Dako; Cat. No. A0398 at 1:1000 for 1 hour), Iba-1 (BioCare; Cat. No. CP290A at 1:500 for 1 hour), and Ki67 (BD Pharmingen; Cat. No. 550609 at 1:200 for 1 hour). Endogenous peroxidases were blocked with 1.5% H_2O_2 in TBS-T for 10 minutes. Slides were then incubated with Rabbit Polink-1 HRP (GBI Labs; Cat. No. D13-110 for MPO and Iba-1) and Mouse Polink-2 HRP (GBI Labs; Cat. No. D37-110 for Mx1 and Ki67). Slides were developed using Impact™ DAB (3,3′-diaminobenzidine; Vector Laboratories), washed in ddH_2O, counterstained with hematoxylin, mounted in Permount (Fisher Scientific), and scanned at 20x magnification on an Aperio AT2 (Leica Biosystems). Staining for MPO, Mx1, Iba-1, and Ki67 IHC was performed as previously described using a Biocare intelliPATH autostainer.

Quantitative image analysis

Quantitative image analysis was performed using HALO software (v3.0.311.405; Indica Labs) on at least one lung lobe cross section from each animal. For MPO (neutrophil) and Iba-1 (macrophage) quantification, blood vessels (>5mm^2), bronchi, bronchioles, cartilage, and connective tissue were manually excluded; subsequently, the Multiplex IHC v2.3.4 module was used to detect MPO+ or Iba-1+ cells and is presented as a proportion of total alveolar tissue (cells/mm^2). For Mx1, the Area Quantification v2 module was used to determine the percentage of Mx1 as a proportion of the total tissue area. For Ki67, the Multiplex IHC v2.3.4 module was

used to quantitative the percentage of positive cells. In all instances, manual curation was performed on each sample to ensure the annotations were accurate and to correct false positives/false negatives.

RNAscope in situ hybridization

RNAscope in situ hybridization was performed as previously described [328] using SARS-CoV2 anti-sense specific probe v-nCoV2019-S (ACD Cat. No. 848561) targeting the positive-sense viral RNA and SARS-CoV2 sense specific probe v-nCoV2019-orf1ab-sense (ACD Cat. No. 859151) targeting the negative-sense genomic viral RNA. In brief, after slides were deparaffinized in xylene and rehydrated through a series of graded ethanol to distilled water, retrieval was performed for 30 min in ACD P2 retrieval buffer (ACD Cat. No. 322000) at 95-98 °C, followed by treatment with protease III (ACD Cat. No. 322337) diluted 1:10 in PBS for 20 min at 40 °C. Slides were then incubated with 3% H_2O_2 in PBS for 10 min at room temperature. Prior to hybridization, probes stocks were centrifuged at 13,000 rpm using a microcentrifuge for 10 min, then for the antisense probe diluted 1:2 in probe diluent (ACD Cat. No. 300041) to reduce probe aggregation tissue artifacts. Slides were developed using the RNAscope® 2.5 HD Detection Reagents-RED (ACD Cat. No.322360).

Tissue Processing

PB was collected from the femoral vein in sodium citrate, serum separation, and EDTA tubes from which plasma was separated by centrifugation within 1 hour of phlebotomy. PB was used for complete blood counts, comprehensive serum chemistry panels, and measurement of neutrophil extracellular traps (NET) activity. From EDTA PB, peripheral blood mononuclear cells (PBMCs) were isolated using a Ficoll-Paque Premium density gradient (GE Healthcare), and washed with

R-10 media. R-10 media was composed of RPMI 1640 (Corning) supplemented with 10% heat-inactivated fetal bovine serum (FBS), 100 IU/mL penicillin, 100 μg/mL streptomycin, and 200 mM L-glutamine (GeminiBio). CSF was collected by inserting a 0.75-1.5-inch, 22-25-gauge needle below the external occipital protuberance into the cisterna magna and was separated by centrifugation.

Nasopharyngeal swabs were collected under anesthesia by using a clean rayon-tipped swab (ThermoFischer Scientific, BactiSwab NPG, R12300) placed approximately 2-3cm into the nares. Oropharyneal swabs were collected under anesthesia using polyester tipped swabs (Puritan Standard Polyester Tipped applicator, polystyrene handle, 25-806 2PD, VWR International) to streak the tonsils and back of throat bilaterally (throat/pharyngeal). The swabs were dipped in 1 mL viral transport media (Viral transport Media, VTM-1L, Labscoop, LLC) and vortexed for 30 sec, and the eluate was collected.

To collect BAL, a fiberoptic bronchoscope (Olympus BF-XP190 EVIS EXERA III ULTRA SLM BRNCH and BF-P190 EVIS EXERA 4.1mm) was manipulated into the trachea, directed into the primary bronchus, and secured into a distal subsegmental bronchus upon which 35-50 mL of normal saline (0.9% NaCl) was administered into the bronchus and re-aspirated to obtain a minimum of 20ml of lavage fluid. BAL was filtered through a 70μm cell strainer.

Lung tissue was cut into small pieces, using blunt end scissors, then digested using 1.5 U/mL DNase I (Roche) and 1 mg/mL of Type I collagenase (Sigma-Aldrich) using gentleMACS C tubes and gentleMACS Dissociator (miltenyi Biotec).

Hilar LN biopsies were collected at necropsy, sectioned using blunt, micro-dissection scissors and mechanically disrupted through a 70µm cell strainer and washed with R-10 media.

Mononuclear cells were counted for viability using a Countess II Automated Cell Counter (Thermo Fisher) with trypan blue stain and were cryo-preserved in aliquots of up to $2x10^7$ cells in 10% DMSO in heat-inactivated FBS. Whole tissue segments (0.5 cm^3) were snap frozen dry, or stored in RNAlater (Qiagen), or Nuclisens lysis buffer (Biomerieux) for analyses of compound distribution, RNA-seq, and tissue viral quantification, respectively.

Bulk and single-cell RNA-Seq Library and sequencing from NHP BALs

Single cell suspensions from BAL were prepared in BSL3 as described above for flow cytometry; for bulk RNA-Seq, 50,000 cells were lysed directly into 700 ul of QIAzol reagent. RNA was isolated using RNeasy Mini or Micro kits (Qiagen) with on-column DNase digestion. RNA quality was assessed using an Agilent Bioanalyzer and total RNA was used as input for cDNA synthesis using the Clontech SMART-Seq v4 Ultra Low Input RNA kit (Takara Bio) according to the manufacturer's instructions. Amplified cDNA was fragmented and appended with dual-indexed bar codes using the NexteraXT DNA Library Preparation kit (Illumina). Libraries were validated by capillary electrophoresis on an Agilent 4200 TapeStation, pooled at equimolar concentrations, and sequenced on an Illumina NovaSeq6000 at 100SR, yielding 20-25 million reads per sample. For single-cell RNA-Seq, single-cell suspensions of 100,000 BAL-derived cells, and approximately 30,000 cells were loaded onto 10X Chromium Controller in the BSL3. Single cells were partitioned into droplets (Gel Beads in Emulsion: GEMs) using Chromium NextGEM Single Cell 5' Library & Gel Bead kits on the 10X Chromium Controller [548]. The resulting cDNA was amplified and libraries were prepared for transcriptomic analysis according to manufacturer instructions. Gene expression libraries were sequenced as paired-end 26x91 reads on an Illumina

NovaSeq6000 targeting a depth of 50,000 reads per cell in the Yerkes Genomics Core Laboratory(http://www.yerkes.emory.edu/nhp_genomics_core/). Cell Ranger software was used to perform demultiplexing of cellular transcript data, and mapping and annotation of UMIs and transcripts for downstream data analysis.

Bulk RNA-Seq analysis

The quality of reads was evaluated using FastQC (https://www.bioinformatics.babraham.ac.uk/projects/fastqc/). Reads were aligned using STAR v2.7.3.[549]. The STAR index was built by combining genome sequences for Macaca mulatta (Mmul10 Ensembl release 100), SARS-CoV2 (strain MN985325.1 - NCBI) and ERCC sequences. The gffread utility (https://github.com/gpertea/gffread) was used to convert gff3 file for SARS-CoV2 and the resulting gtf file for SARS-CoV2 was edited to include exon entries which had the same coordinates as CDS to get counts with STAR. The combined genomic and gtf files were used for generating the STAR index. Transcript abundance estimates were calculated internal to the STAR aligner using the algorithm of htseq-count [82]. The ReadsPerGene files were used to generate counts in the htseq format using a custom script that also converted the Ensembl ID to gene names using the gtf file. These files were imported in DESeq2 using the DESeqDataSetFromHTSeqCount function. DESeq2 was used for normalization [550], producing both a normalized read count table and a regularized log expression table. Only the protein coding genes defined in the gtf file were used for analysis. The design used was: ~ Subject + Group where Group was a combination of Timepoint (baseline/2dpi/4dpi) and Condition (Untreated/Treated) factors. The regularized log expression values were obtained using the rlog function with the parameters blind =FALSE and filtType = “parametric”. The thresholds of padj < 0.05, fold-change > 1.5 and lfcSE < 1 were used to obtain significant differentially expressed genes. The VennDiagram R library was used to create the venn diagrams. GSEA 4.1.0 (https://www.gsea-msigdb.org/) was used for gene set enrichment analysis with the following

gene sets: Hallmark and Canonical pathways (MsigDB), NHP ISGs [82] and Rheumatoid arthritis (KEGG map05323). GSEA was run with default parameters with the permutation type set to gene_set. The input for GSEA was the regularized log expression values obtained from DESeq2 which was filtered to remove genes with mean expression <=0. The regularized log expression values were also used to generate heatmaps using the Complex Heatmap R library [551].

Single-cell RNA-Seq Bioinformatic Analysis

Bronchoalveolar lavage (BAL) samples from five Rhesus Macaque's were run on 2 Nova Seq 1000 lanes and the resultant bcl files were converted to counts matrices using Cell Ranger v3.1 (10X Genomics). Further, the count matrices for each sample were processed using an inhouse single-cell RNA-seq pipeline that uses Seurat v3.0 [552] to initially integrate data from SARS-CoV-2 infected and Baricitinib treated samples. The batch corrected samples were filtered for cells expressing <250 genes, >10% Mitochondria genes, HBB, RPS and RPL genes and any doublets were removed using DoubletFinder [553]. After filtration, the data were normalized using scTransform normalization followed by Principal Component analysis. PCs 1-30 were chosen for clustering analysis, as there was very little additional variance observed beyond PC 30. Cells were then clustered based on PC scores using the Louvian-Jaccard method. Uniform Manifold Approximation and Projection (UMAP) [554] method was used to visualize the single cells in 2D embedding. We used Blueprint Encode database from SingleR [555] to classify cells into different cell subtypes. Differential gene expression between the clusters was assessed by MAST [556]. Heatmaps, Dot plots and Violin plots were generated using ggplot2 [557] package in R.

Immunophenotyping

23-parameter flow cytometric analysis was perform on fresh PBMCs and mononuclear cells (10^6 cells) derived from LN biopsies, BAL, and lung. Immunophenotyping was performed using anti-human monoclonal antibodies (mAbs), which we [111, 129, 288, 558] and others, including databases maintained by the NHP Reagent Resource (MassBiologics), have shown as being cross-reactive in RMs. A panel of the following mAbs was used for longitudinal T-cell phenotyping in PBMCs: anti-CCR7-BB700 (clone 3D12; 2.5 μL; cat. # 566437), anti-CD103-BV421 (clone Ber-ACT8; 5 μL; cat. # 563882), anti-Ki-67-BV480 (clone B56; 5 μL; cat. # 566109), anti-CXCR6-BV750 (clone 13B 1E5; 2.5 μL; cat. # 747052), anti-CD3-BUV395 (clone SP34-2; 2.5 μL; cat. # 564117), anti-CD8-BUV496 (clone RPA-T8; 2.5 μL; cat. # 612942), anti-CD45-BUV563 (clone D058-1283; 2.5 μL; cat. # 741414), anti-CD49a-BUV661 (clone SR84; 2.5 μL; cat. # 750628), anti-CD28-BUV737 (clone CD28.2; 5 μL; cat. # 612815), anti-CD69-BUV805 (clone FN50; 2.5 μL; cat. # 748763), and Fixable Viability Stain 700 (2 μL; cat. # 564997) all from BD Biosciences; anti-CD95-BV605 (clone DX2; 5 μL; cat. # 305628), anti-HLA-DR-BV650 (clone L243; 5 μL; cat. # 307650), anti-CD25-BV711 (clone BC96; 5 μL; cat. # 302636), anti-PD-1-BV785 (clone EH12.2H7; 5 μL; cat. # 329930), anti-CD101-PE-Cy7 (clone BB27; 2.5 μL; cat. # 331014), anti-FoxP3-AF647 (clone 150D; 5 μL; cat. # 320014), and anti-CD4-APC-Cy7 (clone OKT4; 2.5 μL; cat. # 317418) all from Biolegend; anti-CD38-FITC (clone AT1; 5 μL; cat. # 60131FI) from STEMCELL Technologies; and anti-CXCR5-PE (clone MU5UBEE; 5 μL; cat. # 12-9185-42), anti-GranzymeB-PE-TexasRed (clone GB11; 2.5 μL; cat. # GRB17), and anti-CD127-PE-Cy5 (clone eBioRDR5; 5 μL; cat. # 15-1278-42) all from Thermo Fisher (**Figure 3.S6**). mAbs for chemokine receptors (i.e. CCR7) were incubate at 37°C for 15 min, and cells were fixed and permeabilized for 30 min at room temperature using a FoxP3 / Transcription Factor Staining Buffer Kit (Tonbo Biosciences; cat. # TNB-0607-KIT). A panel of the following mAbs was used for the longitudinal phenotyping of innate immune cells in whole blood (500 μL), as described in [339], and mononuclear cells (10^6 cells) derived from LN biopsies, BAL, and lung: anti-CD20-BB700 (clone 2H7; 2.5 μL; cat. # 745889),

anti-Ki-67-BV480 (clone B56; 5 μL; cat. # 566109), anti-CD14-BV605 (clone M5E2; 2.5 μL; cat. # 564054), anti-CD56-BV711 (clone B159; 2.5 μL; cat. # 740781), anti-CD115-BV750 (clone 9-4D2-1E4; 2.5 μL; cat. # 747093), anti-CD3-BUV395 (clone SP34-2; 2.5 μL; cat. # 564117), anti-CD8-BUV496 (clone RPA-T8; 2.5 μL; cat. # 612942), anti-CD45-BUV563 (clone D058-1283; 2.5 μL; cat. # 741414), anti-CCR2-BUV661 (clone LS132.1D9; 2.5 μL; cat. # 750472), anti-CD16-BUV737 (clone 3G8; 2.5 μL; cat. # 564434), anti-CD69-BUV805 (clone FN50; 2.5 μL; cat. # 748763), and Fixable Viability Stain 700 (2 μL; cat. # 564997) all from BD Biosciences; anti-CD38-FITC (clone AT1; 2.5 μL; cat. # 60131FI) from STEMCELL Technologies; anti-CD161-BV421 (clone HP-3G10; 5 μL; cat. # 339914), anti-HLA-DR-BV650 (clone L243; 5 μL; cat. # 307650), anti-CD11c-BV785 (clone 3.9; 5 μL; cat. # 301644), anti-CD11b-PE (clone ICRF44; 2.5 μL; cat. # 301306), and anti-CD123-APC-Fire750 (clone 315; 2.5 μL; cat. # 306042) all from Biolegend; anti-GranzymeB-PE-TexasRed (clone GB11; 2.5 μL; cat. # GRB17) from Thermo Fisher; anti-CD66abce-PE-Vio770 (clone TET2; 1 μL; cat. # 130-119-849) from Miltenyi Biotec; and anti-CD27-PE-Cy5 (clone 1A4CD27; 2.5 μL; cat. # 6607107) and anti-NKG2A-APC (clone Z199; 5 μL; cat. # A60797) from Beckman Coulter (**Figure 3.S6**). mAbs for chemokine receptors (i.e. CCR2) were incubated at 37°C for 15 min, and cells were fixed and permeabilized at room temperature for 15 min with Fixation/Permeabilization Solution Kit (BD Biosciences; cat. #554714). For each sample a minimum of $1.2x10^5$ stopping gate events (live $CD3^+$ T-cells) were recorded except for RB in which a minimum of $5x10^4$ stopping gate events were recorded. All samples were fixed with 4% paraformaldehyde and acquired within 24 hours of fixation. Acquisition of data was performed on a FACSymphony A5 (BD Biosciences) driven by FACS DiVa software and analyzed with FlowJo (version 10.7; Becton, Dickinson, and Company).

Single cells were then selected using FSC-A x FCS-H gate. A lymphocyte and granulocyte gate based on FSC-A and SSC-A was defined. Live cells were gated followed by $CD45^+$ cells. UMAP analysis (Uniform Manifold Approximation and Projection for Dimension Reduction) was performed in live $CD45^+$for unbiased evaluation of the distribution of the key markers. Projection of the density of cells expressing markers of interest were visualized/plotted on a 2-dimensional UMAP (https://arxiv.org/abs/1802.03426, https://github.com/lmcinnes/umap). We used the Phenograph clustering approach (https://github.com/jacoblevine/PhenoGraph)

Determination of intracellular cytokine induction following SARS-CoV-2 S peptide pool and PMA/Ionomycin stimulation

Cryo-preserved PBMCs were thawed, resuspended in RPMI medium supplemented to contain a final concentration of 10% Fetal Bovine Serum (FBS) (Corning Life Sciences/Media Tech Inc, Manassas, VA), 10mM HEPES, 1x MEM nonessential amino acids (Corning Life Sciences/Media Tech Inc, Manassas, VA), 1mM Sodium Pyruvate (Lonza, Walkersville, MD, U.S.A), 1mM Penicillin/Streptomycin containing Amphothericin B (Sigma Life Sciences, St Louis, MO, U.S.A) and 1x 2-Mercaptoethanol (GIBCO, Invitrogen, Carlsbad, CA, U.S.A). PBMCs were rested overnight at 37°C in a cell culture incubator. Cells were then stimulated for detection of cytokine production by T cells as described before [559]. Briefly, 2 x 10^6 cells were cultured in 200µL final volume in 5mL polypropylene tubes (BD Biosciences, San Diego, CA, U.S.A) in the presence of anti-CD28 (1µg/mL) and anti-CD49d (1µg/mL) [BD Biosciences] and the following conditions; a) negative control with DMSO only, b) S peptide pool [361] and c) PMA/Ionomycin in the presence of Golgi transport inhibitors - 10 µg/mL of Brefeldin A (Sigma-Aldrich). After stimulation, cells were washed and stained for cell surface antigens with two panels. Panel 1: anti-CD3 BUV395 (clone SP34-2; 2.5 µL; cat. # 564117), anti-CD8-BUV496 (clone RPA-T8; 2.5 µL; cat. # 612942), and Fixable Viability Stain 700 (2 µL; cat. # 564997) all from BD Bioscience; anti-CD4 APC/Cy7 (clone

OKT4; 2.5 μL; cat. # 317418) from Biolegend; To detect intracellular expression of cytokines, mononuclear cells were fixed and permeabilized with a Cytofix/Cytoperm kit (BD Biosciences) and stained as follows: anti-IL-21 BV421 (clone 3A3-N2.1; 5 μL; cat# 564755) from BD Bioscience; anti-IL-2 BV650 (clone MQ1-17H12; 5 μL; cat# 500334) and anti-IFNγ PE/Dazzle 594 (clone B27; 5 μL; cat# 506530) both from Biolegend; anti-IL-17a Alexa Fluor 488 (clone eBio64DEC17; 5 μL; cat# 53-7179-42), anti-IL-22 APC (clone IL22JOP; 5 μL; cat# 17-7222-82), and anti-TNFα PE-Cyanine7 (clone Mab11; 0.5 μL; cat# 25-7349-82) all from Thermo Fisher Scientific; and anti-IL-4 PE (clone 7A3-3; 5 μL; cat# 130-091-647) from Miltenyl Biotech. Panel 2: anti-IL-2 Alexa Fluor 488 (clone MQ1-17H12; 3 μL; cat# 500314), anti-CD8a PerCP Cy5.5 (clone RPA-T8; 3 μL; cat# 301032), anti-CD4 BV421 (clone OKT4; 2.5 μL; cat# 317434), and anti-IFNγ Alexa 647 (clone 4S.B3; 3 μL; cat# 502516) from Biolegend; anti-CD3 BV605 (clone SP34-2; 2 μL; cat# 562994) from BD Biosciences; anti-IL-4 PE (clone 7A3-3; 5 μL; cat# 130-091-647) from Miltenyl Biotech; anti-IL-17a PE-efluor 610 (clone eBio64DEC17; 3 μL; cat# 61-7179-42), anti-TNFα PE-Cyanine7 (clone Mab11; 0.5 μL; cat# 25-7349-82), and Live Dead APC-Cy7 (1:1000; cat# 65086514) from Thermo Fisher Scientific. The frequency of SARS-CoV-2 specific $CD4^+$ and $CD8^+$ T-cells producing single or multiple cytokines was determined after background subtraction. All samples were fixed with 4% paraformaldehyde and acquired within 24 hours of fixation. Acquisition of data was performed on a FACSymphony A5 (BD Biosciences) driven by FACS DiVa software and analyzed with FlowJo (version 10.7; Becton, Dickinson, and Company).

Isolation of Non-human Primate Neutrophils

Neutrophils were obtained from peripheral blood of SARS-Cov-2 infected Rhesus Macaques 5 days pre-infection and at days 4, 7, and 10 post-infection. Peripheral blood (0.5-1 ml) was

collected using a citrate containing Vacutainer and the upper serum layer was removed. The red blood cell layer was lysed with 2 mL of Red Blood Cell Lysis Buffer (Cat# 11814389001, Roche) in a 15 mL tube. The tube was gently inverted for 10 minutes at room temperature and centrifuged at 500 x *g* for 7 minutes at room temperature. This step was repeated gently inverting for 5 minutes. Following centrifugation, the cell pellet was re-suspended in a final volume of 2 mL of 1x PBS/EDTA buffer gently. Cells were centrifuged at 500 x *g* for 7 mins a room temperature and the leukocyte pellet was re-suspended in 1 mL 1x PBS/EDTA buffer and carefully overlaid onto 3 mL of 65% Percoll/EDTA solution. The Percoll cell gradient was centrifuged at 400 x g for 20 mins at room temperature with the brake turned off. The neutrophil cell layer was collected, re-suspended/washed with 5 mL of 1x PBS/EDTA buffer and centrifuged at 500 x g for 10 minutes at room temperature. The neutrophil cellular pellet was re-suspended in RPMI 1640 media. Purification of the cell fragment was confirmed using flow cytometry and Wright Giemsa staining.

Quantification of extracellular DNA using SYTOX green Assay

Abundance of extracellular DNA, a surrogate of NETs, was quantified using the SYTOX green assay. Freshly, isolated non-human primate neutrophils were plated onto a 96-well plate at a density of 10^5 cells per well in 100 µL RPMI 1640 media then stimulated with 50 µg/mL LPS to induce NET formation. SYTOX green dye (5 µM, #S7020; Invitrogen, Carlsbad, CA) was added to each well and the fluorescence intensity was read with a filter setting at 485-nm excitation/525-nm emission using a Synergy H1 Microplate Reader and Gene5 software (Biotek, Winooski, VT). A fluorescence reading was collected every 15 mins for a total of 2 hours at 37°C. Images of the fluorescent cells were immediately taken using a fluorescent microscope (Olympus).

Staining of citH3

Paraffin-embedded lung sections were subjected to deparaffinization followed by heat induced antigen retrieval in 10 mM sodium citrate buffer (pH 6.0). Sections were blocked with 10% goat serum in 1x PBS for 1 hour. Primary antibody staining was performed for citrullinated H3 (Cayman Chemical, Cat. No. 17939, 1:50) overnight at 4°C. Slides were then incubated with Alexa Fluor 633 anti-mouse IgG secondary antibody (Thermo Fisher Scientific, Cat. No. A21052, 1:1000) for 90 mins at room temperature. Images were taken at 20x objective using a Zeiss LSM 800 Airyscan laser scanning confocal microscope.

Quantification of citrullinated H3

We quantified citrullinated histone 3 using an ELISA kit (Cayman Cat # 501620) with the antibody clone 11D3 per the manufacturer's instructions. In short, 100 uL sample or standard was added in duplicate to a pre-coated 96-well plate and incubated for 2 hrs on an orbital shaker. All steps were performed at room temperature. After 4 washes with the kit's wash buffer, 100 uL per well horseradish peroxidase (HRP) conjugate working solution was added and the plate incubated for 1 hour on an orbital shaker. Then the plate was washed 4 times again and 100uL 3,3′,5,5′-Tetramethylbenzidine (TMB) solution was added per well then incubated for 30 minutes on an orbital shaker, followed by addition of 100 uL HRP stop solution. The plate was read at 450 nm absorbance using a microplate reader and the amount of citrullinated H3 quantified using the standards.

QUANTIFICATION AND STATISTICAL ANALYSIS

All statistical analyses were performed two-sided with p-values ≤0.05 deemed significant. Ranges of significance were graphically annotated as follows: *, $p<0.05$; **, $p<0.01$; ***, $p<0.001$; ****,

$p<0.0001$. Due to the low number of animals included in our study, p values ≤ 0.1 have been indicated in the graphs. Analyses, unless otherwise noted, were performed with Prism version 8 (GraphPad).

Chapter Three Figures

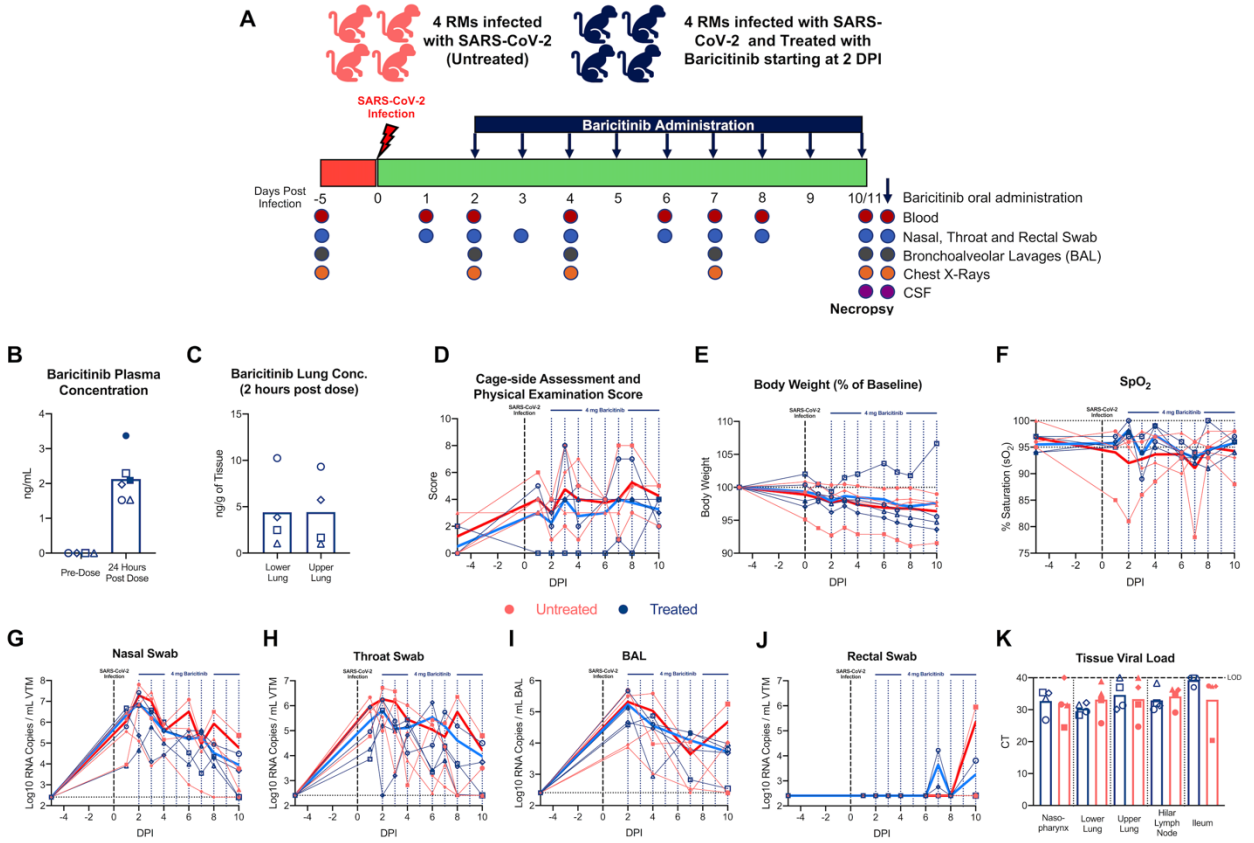

Figure 3.1 Baricitinib is detectable in plasma and tissues from SARS-CoV-2-infected RMs but has no impact on viral kinetics. (A) Study design; 8 RMs were infected intranasally and intratracheally with SARS-CoV-2, and at 2 days after infection, 4 RMs began daily baricitinib administration (4 mg). Longitudinal collections performed are indicated in circles. (B and C) Concentration of baricitinib 24 h after dosing in plasma (6 days after infection closed symbol; 8 days after infection open symbol) (B) and at necropsy in upper and lower lungs of baricitinib-treated SARS-CoV-2-infected RMs (C). (D and E) Daily cage-side assessment and physical examination scores (D) and changes in body weight from baseline (E) in baricitinib-treated (blue symbols; n = 4) and untreated (red symbols; n = 4) SARS-CoV-2-infected RMs. (F) Longitudinal pulse oximetry readings. (G–J) After SARS-CoV-2 inoculation, nasal, throat, bronchoalveolar lavages (BALs), and rectal swabs were collected, and viral loads were quantified by qRT-PCR. (K) Viral loads in tissues measured at necropsy (10–11 days after infection). Abbreviation is as follows: Ct, cycle threshold. Different symbols represent individual RMs. Thick lines represent the average of the baricitinib-treated (blue lines) and untreated (red lines) groups. Bars in (B), (C), and (K) represent the average of the treated and untreated groups. Statistical analysis was performed using a non-parametric Mann-Whitney test. See also Figures 3.S1 and 3.S2A and Tables 3.S1, 3.S2, and 3.S3.

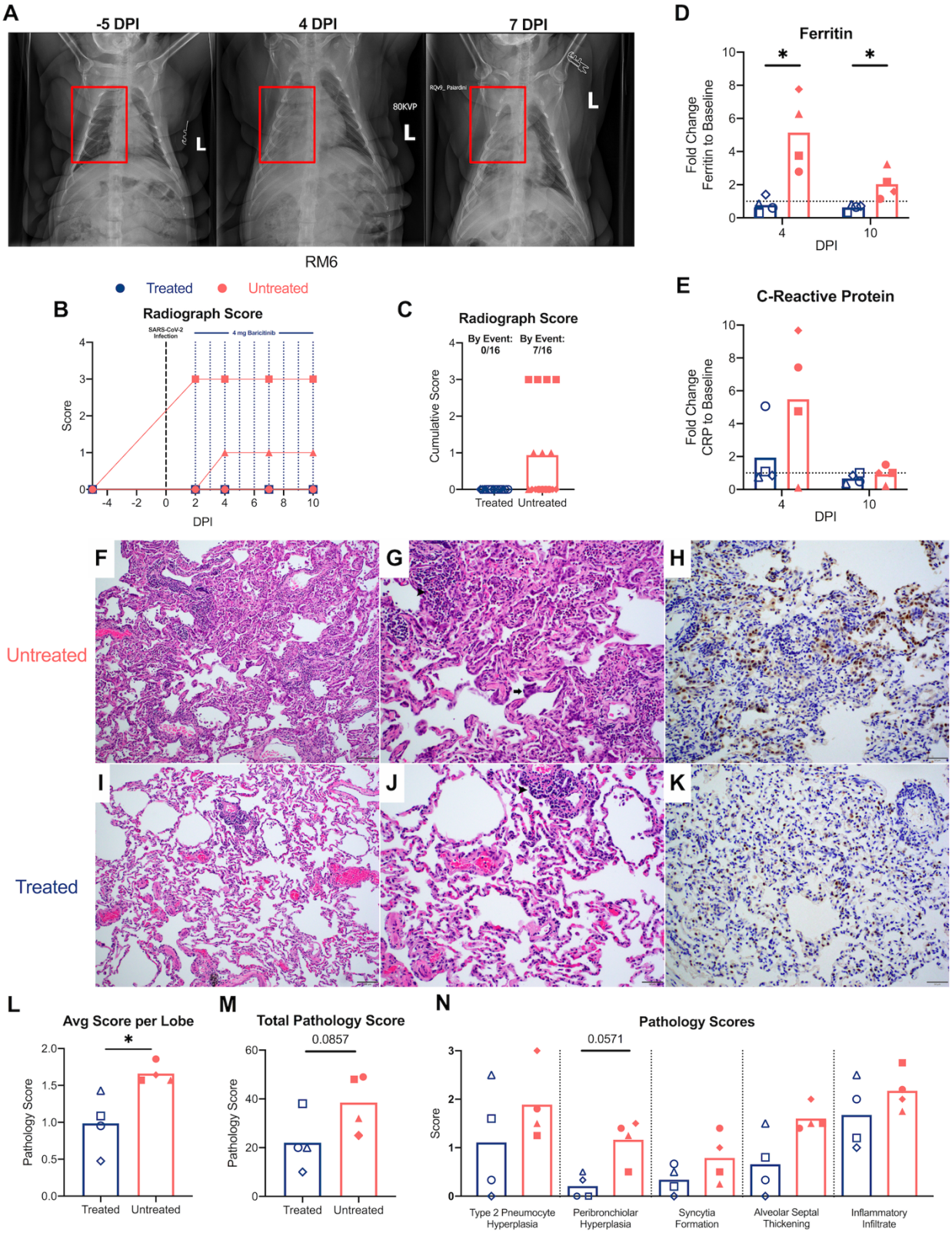
A
-5 DPI
4 DPI
7 DPI
80KVP
L
RM6
D
Ferritin
Fold Change Ferritin to Baseline
DPI
Treated
Untreated
B
Radiograph Score
SARS-CoV-2 Infection
4 mg Baricitinib
Score
DPI
C
Radiograph Score
By Event: 0/16
By Event: 7/16
Cumulative Score
Treated
Untreated
E
C-Reactive Protein
Fold Change CRP to Baseline
DPI
F
G
H
I
J
K
Untreated
Treated
L
Avg Score per Lobe
Pathology Score
Treated
Untreated
M
Total Pathology Score
0.0857
Pathology Score
Treated
Untreated
N
Pathology Scores
0.0571
Score
Type 2 Pneumocyte Hyperplasia
Peribronchiolar Hyperplasia
Syncytia Formation
Alveolar Septal Thickening
Inflammatory Infiltrate

Figure 3.2. Reduced respiratory disease and lower levels of lung pathology in baricitinib-treated RMs. (A) Representative ventrodorsal radiograph of an untreated RM before SARS-CoV-2 infection (5 days before infection), and at 4, and 7 days after infection. Red squares indicate regions of pulmonary infiltrates and opacity. (B and C) Daily (B) and cumulative (C) radiograph scores; ventrodorsal and lateral radiographs were scored for the presence of pulmonary infiltration by a clinical radiologist according to a standard scoring system (0: normal; 1: mild interstitial pulmonary infiltrates; 2: moderate pulmonary infiltrates with partial cardiac border effacement and small areas of pulmonary consolidation; 3: severe interstitial infiltrates, large areas of pulmonary consolidation, alveolar patterns, and air bronchograms). (D and E) Fold change to 2 days after infection for ferritin (D) and C-reactive protein (CRP) levels (E). (F and G) Panel (F) shows 100x magnification, and (G) shows 200x magnification (zoomed in from F), representative lung lesions in an untreated SARS-Cov-2- infected RM with focally extensive interstitial pneumonia, type 2 pneumocytes hyperplasia, alveolar septal thickening, syncytia formation (arrow), neutrophils, and macrophages infiltrations (arrowhead). (H) 200x magnification, Thyroid Transcription Factor-1 (TTF-1) staining with prominent type 2 pneumocyte hyperplasia (brown) in a control SARS-CoV-2-in- fected RM. (I and J) Panel (I) shows 100x magnification, and (J) shows 200x magnification (zoomed in from I), treatment effects of baricitinib in SARS-CoV-2-infected RMs with a reduction in pulmonary lesions, lesser inflammatory infiltrates (arrowhead), and reduced type 2 pneumocyte hyperplasia. (K) 200x magnification, TTF-1 staining with lesser type 2 pneumocyte hyperplasia (brown) after baricitinib treatment. (L) Average pathology score per lobe. (M) Total pathology score. (N) Pathology scores for individual parameters. Scale bar, (F) and (I): 100 mM; (G), (H), (J), and (K): 50 mM. Bars in (D), (E), (L), (M), and (N) indicate mean values for baricitinib-treated (blue) and untreated (red) SARS-CoV-2-infected RMs. Each symbol represents individual animals. Statistical analysis in (D), (E), and (L)–(N) were performed using non-parametric Mann-Whitney test. Statistical analyses were performed two-sided with p % 0.05 deemed significant. Ranges of significance were graphically annotated as follows: *$p < 0.05$. See also Figures 3.S2B–3.S2I.

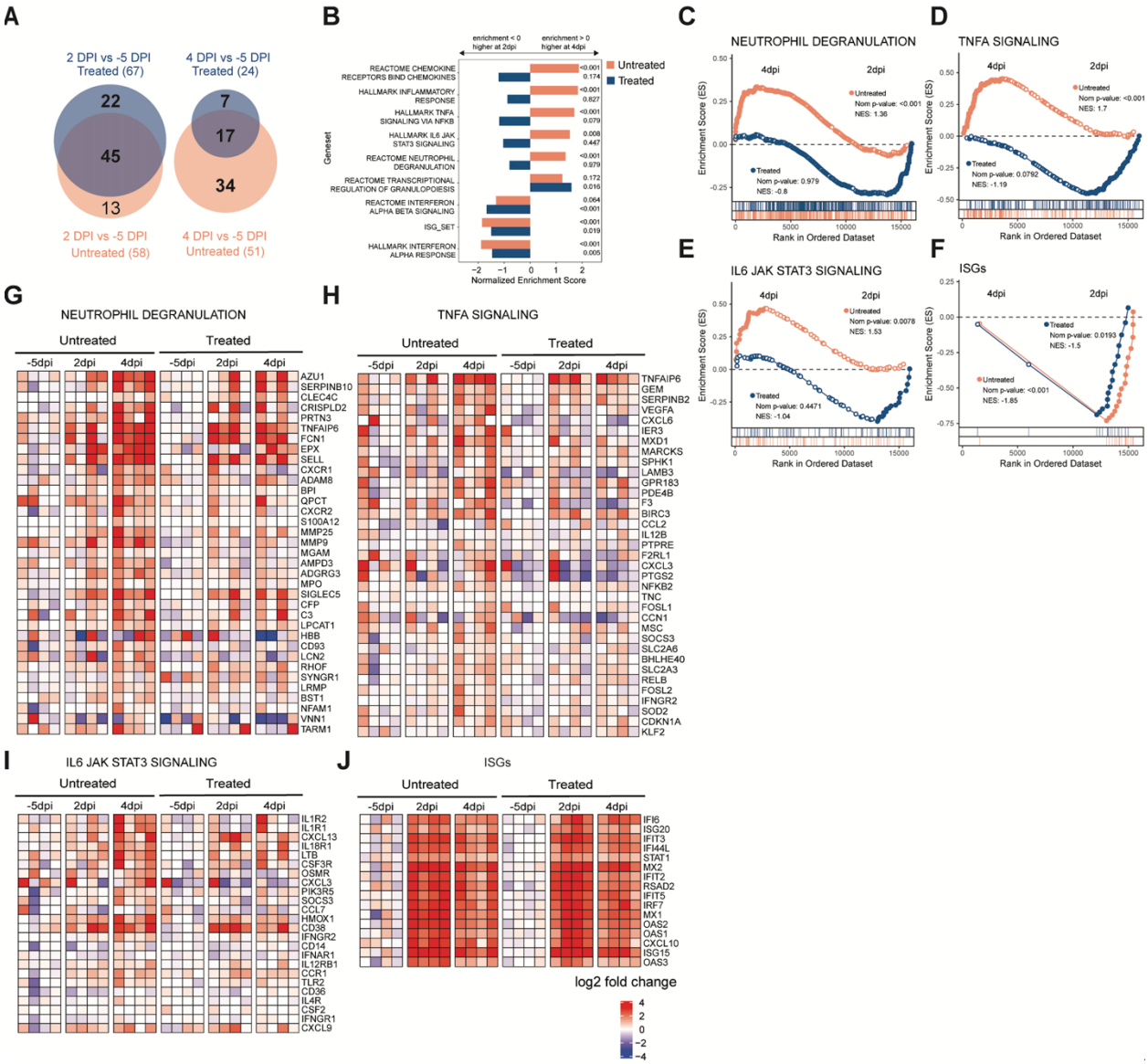

Figure 3.3. **Baricitinib treatment suppresses gene expression of inflammation and neutrophil degranulation in the BALs of SARS-CoV-2-infected RMs.** Bulk RNA-seq profiles of BAL cell suspensions from RMs obtained at day 5 prior to SARS-CoV-2 inoculation (baseline), at 2 days after infection, prior to baricitinib treatment, and at 4 days after infection, 2 days after initiation of baricitinib. (A) Venn diagrams indicating the number of differential expression genes (DEGs) detected at 2 or 4 days after infection relative to 5 days after infection in the untreated (red) and baricitinib-treated (blue) groups. The total DEGs for each comparison are shown in parentheses. (B) Bar plots showing enrichment of top scoring inflammatory and immunological gene signatures from the MSIGDB (Hallmark and Canonical Pathways) and databases, and custom gene sets (interferon-stimulated genes [ISGs]; see below) ranked by GSEA comparisons of gene expression in the 4 days after infection versus 2 days after infection samples from the untreated (red bars) and baricitinib-treated (blue bars) groups. The x axis depicts the normalized enrichment score (NES); a positive enrichment score indicated higher expression at 4 days after infection relative to 2 days after infection (bars facing right); conversely, negative scores of a

pathway indicate cumulatively higher expression in 2 days after infection samples relative to 4 days after infection (bars facing left). Nominal p values are indicated. (C–F) GSEA enrichment plots depicting pairwise comparison of gene expression of 2 days after infection versus 4 days after infection samples for the untreated group and for the baricitinib-treated group. The top-scoring (i.e., leading edge) genes are indicated by solid dots. The hash plot under GSEA curves indicates individual genes and their rank in the dataset. Left-leaning curves (i.e., positive enrichment scores) indicate higher expression of pathways at 4 days after infection; right-leaning curves (negative enrichment scores) indicate higher expression at 2 days after infection. Sigmoidal curves indicate equivalent expression between the groups being compared. The NES and nominal p values testing the significance of each comparison are indicated. (C) REACTOME_ NEU- TROPHIL_DEGRANULATION (MSIDB #M27620). (D) GSEA line plot of HALLMARK_TNFA_SIGNALING_VIA_NFKB pathway (MSIGDB #M5890). (E) GSEA line plot of HALLMARK_IL6_JAK_STAT3_SIGNALING (MSIGDB #M5897). (F) A custom gene set of ISGs from prior NHP studies [79, 81, 82]. (G–J) Heatmaps of top-scoring (i.e., leading edge) from the untreated 4 days after infection versus 2 days after infection GSEA analyses. The color scale indicates the log2 expression relative to the median of all baseline samples. See also Figure 3.S3.

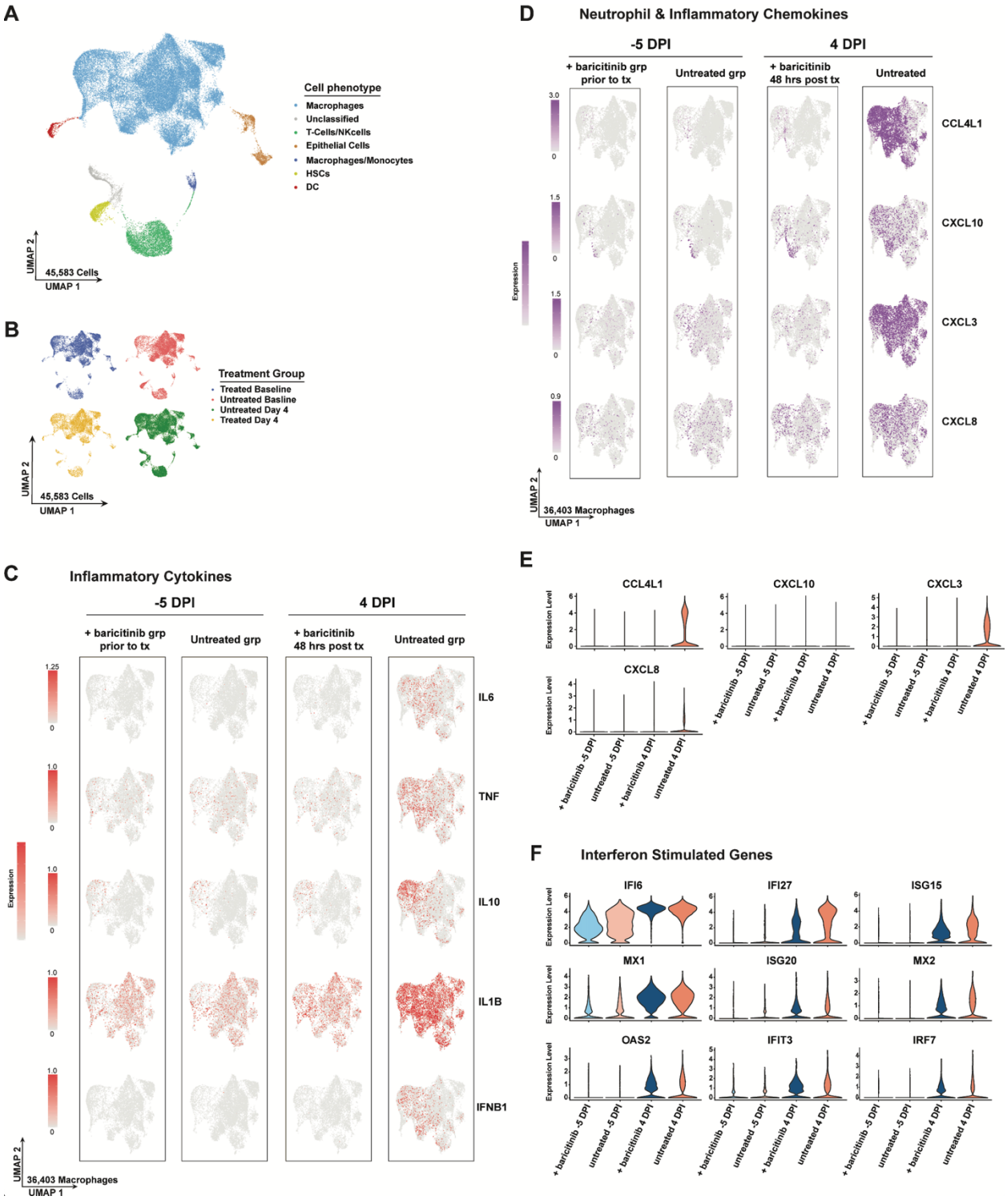

Figure 3.4. Baricitinib treatment abolishes inflammatory cytokine and neutrophil chemoattractant expression in bronchoalveolar macrophages. Single-cell suspensions from BALs of SARS-CoV-2-infected RMs were subject to 10x Genomics capture and sequencing. (A) UMAP showing major cell types in BAL samples (n = 10 samples; untreated, baseline n = 3; untreated, 4 days after infection n = 3; treated, baseline n = 2; treated, 4 days after infection n=2), (B) UMAP showing clusters in BAL samples by treatment days (n = 10). (C) UMAP projection of

pro-inflammatory cytokines in macrophages. (D) UMAP projection of neutrophil chemoattractant and pro-inflammatory chemokines. (E and F) Expression of chemokines and interferon-stimulated genes (ISGs) in treated and untreated samples at baseline and 4 days after infection. The colored expression scale of expression in UMAPs is depicted on a per gene basis: the scale represents the per cell reads for each gene divided by the total reads for of that cell, scaled to the factor shown and natural log-transformed. See also Figures 3.S4 and 3.S5.

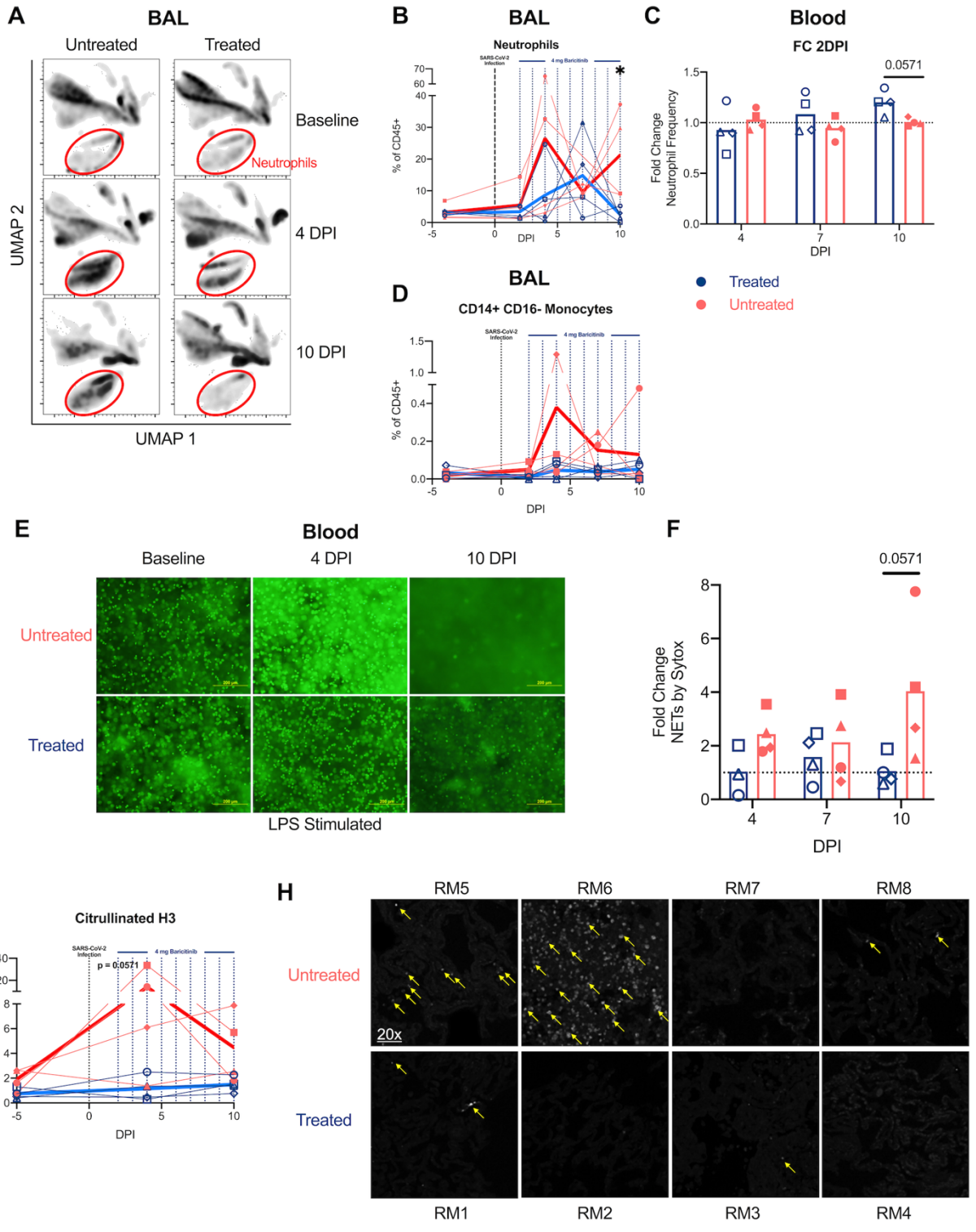
A
BAL
Untreated
Treated
Baseline
Neutrophils
4 DPI
10 DPI
UMAP 2
UMAP 1
B
BAL
Neutrophils
SARS-CoV-2 Infection
4 mg Baricitinib
% of CD45+
DPI
C
Blood
FC 2DPI
0.0571
Fold Change Neutrophil Frequency
DPI
Treated
Untreated
D
BAL
CD14+ CD16- Monocytes
SARS-CoV-2 Infection
4 mg Baricitinib
% of CD45+
DPI
E
Blood
Baseline
4 DPI
10 DPI
Untreated
Treated
LPS Stimulated
F
0.0571
Fold Change NETs by Sytox
DPI
G
Citrullinated H3
SARS-CoV-2 Infection
4 mg Baricitinib
p = 0.0571
ng/mL
DPI
H
RM5
RM6
RM7
RM8
Untreated
20x
Treated
RM1
RM2
RM3
RM4

Figure 3.5. **Baricitinib-treated RMs have decreased infiltration of innate immune cells and lowered neutrophil NETosis**. (A) UMAP analysis of BALs in baricitinib-treated (n = 4) and untreated (n = 4) SARS-CoV-2-infected RMs before infection (D 5 PI; baseline), and at 4 and 10 days after infection. (B) Longitudinal levels of neutrophils within BAL samples depicted as a percentage of $CD45^+$ cells. (C) Fold change to 2 days after infection of neutrophils in blood of baricitinib-treated and untreated SARS-CoV-2-infected RMs. (D) Longitudinal levels of $CD14^+CD16^-$ monocytes within BAL samples depicted as a percentage of $CD45^+$ cells. (E) Representative microscopy images of NETS by Sytox green assay in baricitinib-treated and untreated SARS-CoV-2-infected RMs. Scale bar, 200 mm. (F) Quantification of NETosis activity upon staining extracellular DNA with Sytox in isolated stimulated neutrophils from blood. Fold change of Sytox levels to 5 days after infection. (G) Quantification of citrullinated H3 in plasma. (H) Staining of citrullinated H3 in lungs at 10–11 days after infection. In (B)–(D), (F), and (G), each symbol represents individual animals. Thick lines represent the average of the baricitinib-treated (blue line) and untreated groups (red line). Bars in (C) and (F) represent the average of the treated and untreated groups. Statistical analysis in (B), (C), (F), and (G) was performed using a non-parametric Mann-Whitney test. Statistical analyses were performed two-sided with p % 0.05 deemed significant. Ranges of significance were graphically annotated as follows: *p < 0.05. See also Figures 3.S6A and 3.S6B.

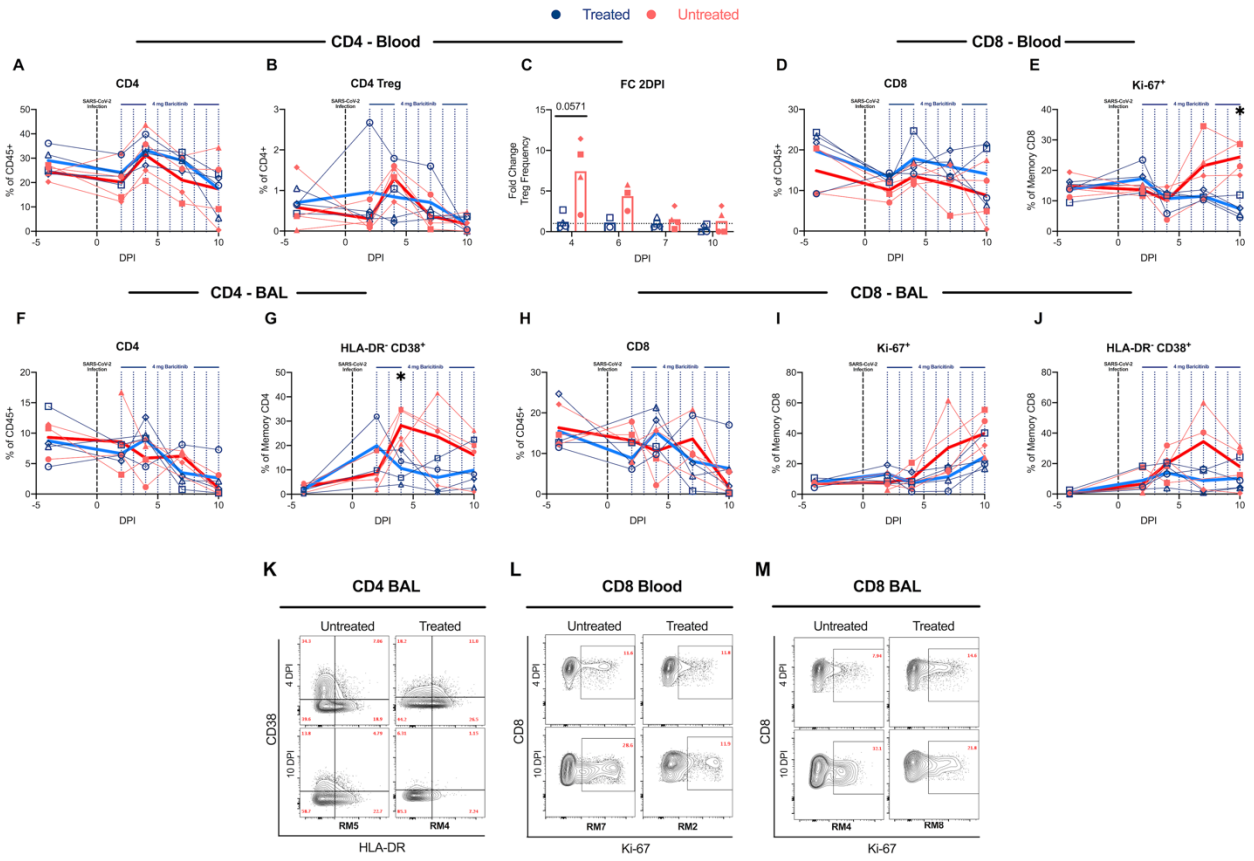

Figure 3.6. **Decreased levels of T cell proliferation and activation in baricitinib-treated RMs.** (A and B) Longitudinal levels of (A) circulating $CD4^+$ T cells and (B) $CD4^+$ TReg ($CD45^+CD3^+CD4^+$ $CD95^+$ $CD127^-$ $CD25^+$ $FoxP3^+$; representative staining in Figure 3.S6C) cells measured by flow cytometry of baricitinib-treated (blue) and untreated (red) SARS-CoV-2-infected RMs. (C) Fold changes to 2 days after infection of circulating $CD4^+$ T_{Reg} cells. (D and E) Levels of circulating $CD8^+$ T cells (D) and proliferating ($Ki\text{-}67^+$) memory $CD8^+$ T cells (E). (F and G) Levels of $CD4^+$ T cells (F) and $HLA\text{-}DR^-CD38^+$ memory $CD4^+$ T cells (G) in bronchoalveolar lavages (BALs) measured by flow cytometry. (H–J) Levels of $CD8^+$ T cells (H), proliferating ($Ki\text{-}67^+$) memory $CD8^+$ T cells (I), and $HLA\text{-}DR^-CD38^+$ memory $CD8^+$ T cells (J) in BALs. Each symbol represents individual animals. Thick lines represent the average of the baricitinib-treated (blue line) and untreated groups (red line). (K–M) Representative staining of Ki-67 and CD38 by HLA-DR. Bars in (C) represent the average of the treated and untreated groups. Statistical analysis in (C), (E), and (G) was performed using non-parametric Mann-Whitney test. Statistical analyses were performed two-sided with $p \leq 0.05$ deemed significant. Ranges of significance were graphically annotated as follows: *$p < 0.05$. See also Figures 3.S6C and 3.S7.

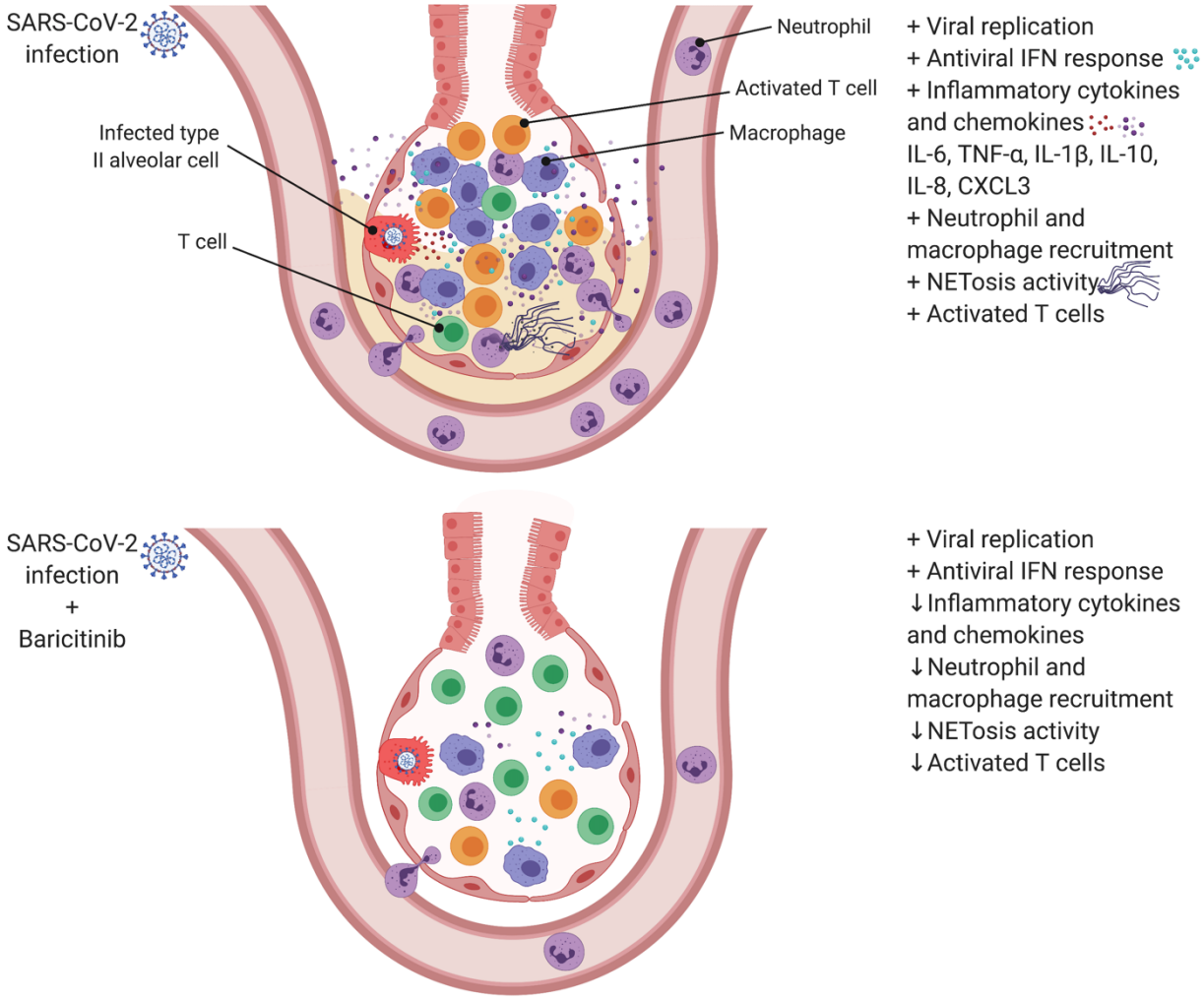

Figure 3.7. **Effect of baricitinib treatment on the lower airway of SARS-CoV-2-infected RMs.** (A) SARS-Cov-2 infection in RMs results in an accumulation of inflammatory macrophages and neutrophils in the lower airway. These airway macrophages produce high amounts of inflammatory cytokines and neutrophil-attracting chemokines and show upregulated type I interferon signaling. Neutrophil NETs and the inflammation induced by SARS-CoV-2 infection both contribute to lung pathology. (B) Baricitinib treatment reduced the levels of macrophages producing inflammatory cytokines and neutrophil-attracting chemokines, decreased the infiltration of neutrophils into the lung, and reduced T cell activation. The Netosis activity of neutrophils was also reduced. In treated animals, the antiviral interferon response was maintained, viral replication was not impacted, and lung pathology was mild.

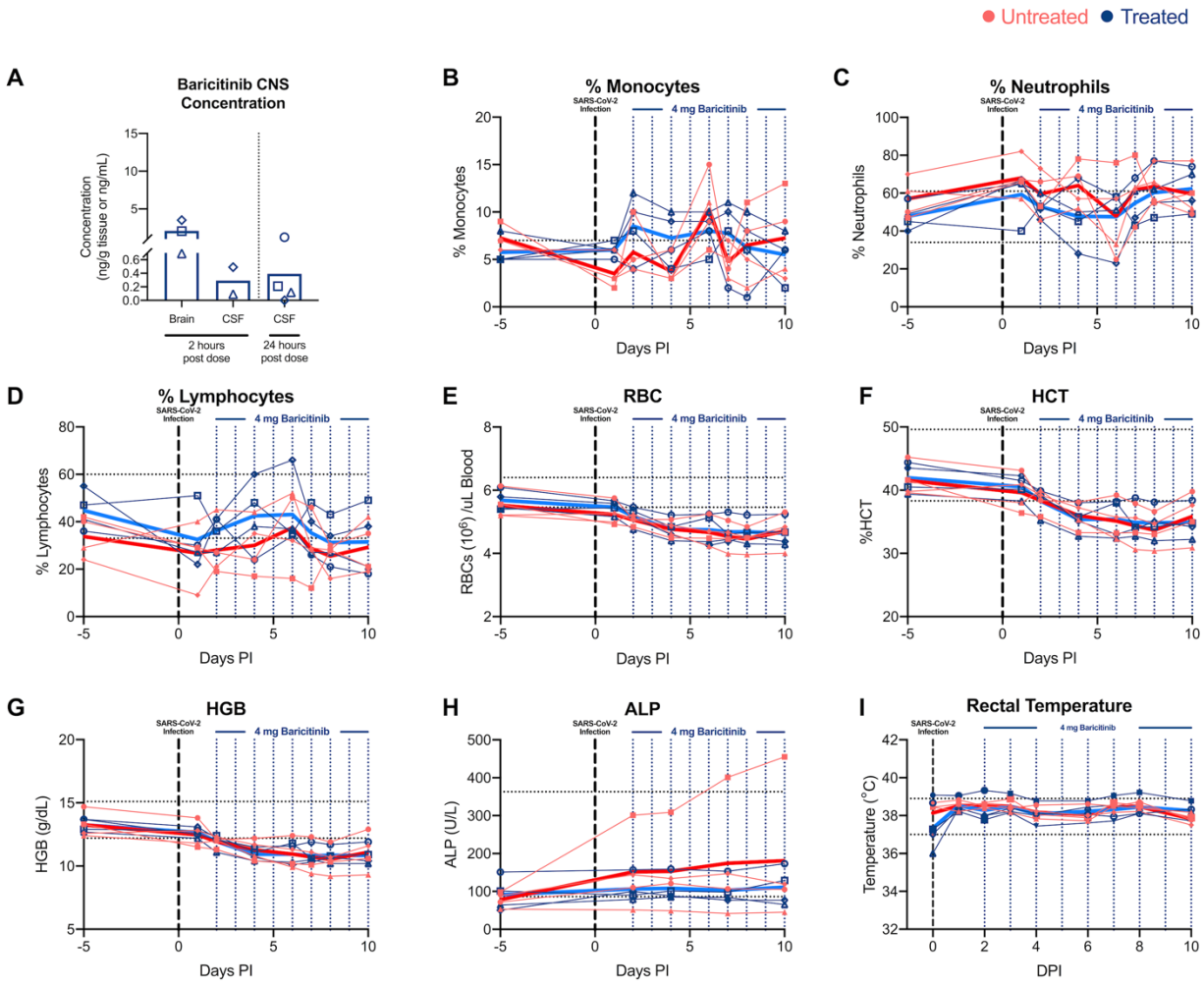

Figure 3.S1. **Baricitinib was well-tolerated and detectable in the central nervous system in SARS-CoV-2-infected RMs, related to Figure 3.1** (A) Left, concentration of baricitinib 2 hours after dosing in brain and CSF and, right, 24 hours after dosing in CSF. (B–D) Longitudinal frequency of (B) monocytes, (C) neutrophils, and (D) lymphocytes in blood of SARS-CoV-2 infected RMs. (E–H) In (E), red blood cell counts (RBC), (F) hematocrit (HCT), (G) hemoglobin (HGB) and (H) alkaline phosphatase (ALP) levels were analyzed throughout the study. (I) Longitudinal rectal temperatures. Different symbols represent individual animals. Bold lines represent the average of the baricitinib treated group (blue), and the untreated group (red).

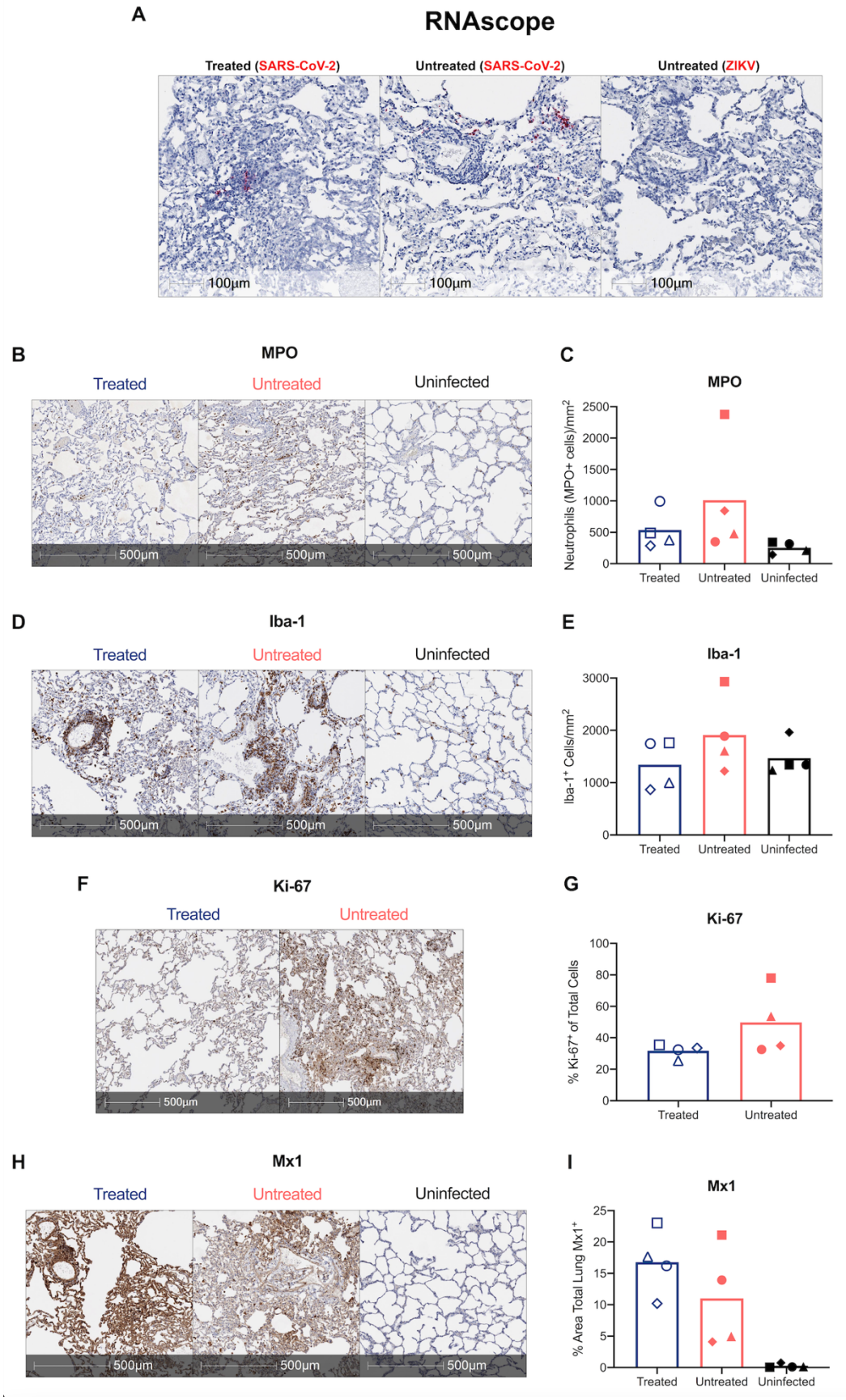
A
RNAscope
Treated (SARS-CoV-2)
Untreated (SARS-CoV-2)
Untreated (ZIKV)
100µm
B
MPO
Treated
Untreated
Uninfected
500µm
C
MPO
Neutrophils (MPO+ cells)/mm2
2500
2000
1500
1000
500
0
Treated
Untreated
Uninfected
D
Iba-1
E
Iba-1
Iba-1+ Cells/mm2
3000
2000
1000
F
Ki-67
G
Ki-67
% Ki-67+ of Total Cells
100
80
60
40
20
H
Mx1
I
Mx1
% Area Total Lung Mx1+
25
20
15
10
5

Figure 3.S2. **Baricitinib reduced lung neutrophil and macrophage infiltration, preserved IFN responses but did not reduce SARS-CoV-2 replication in RMs, related to Figures 3.1 and 3.2.** (A–I) In (A), representative images of *in situ* RNA hybridization (RNAscope) targeting viral RNA strands identifying clusters of infected cells within the lung pa- renchyma in both treated and untreated SARS-CoV-2 infected RMs. Scale bars: 100 um. Representative immunohistochemistry (IHC) images of (B) neutrophils (myeloperoxidase+, MPO, cells) (D) macrophages (ionized calcium-binding adaptor molecule 1+, Iba 1, cells), (F) proliferating (Ki-67), and (H) Interferon-induced GTP-binding protein+ (Mx1), cells in lungs of baricitinib treated and untreated SARS-CoV-2 infected RMs, and uninfected RMs. Scale bars 500 mm. Quantification of (C) neutrophils (MPO+ positive cells/mm^2), (E) macrophages (Iba-1+ cells/mm^2), (G) proliferating ($Ki\text{-}67^+$), and (I) Interferon-induced protein Mx1 (% area total lung Mx1+) in IHC lung images of baricitinib treated, and untreated controls of SARS-CoV-2 infected RMs, and uninfected RMs.

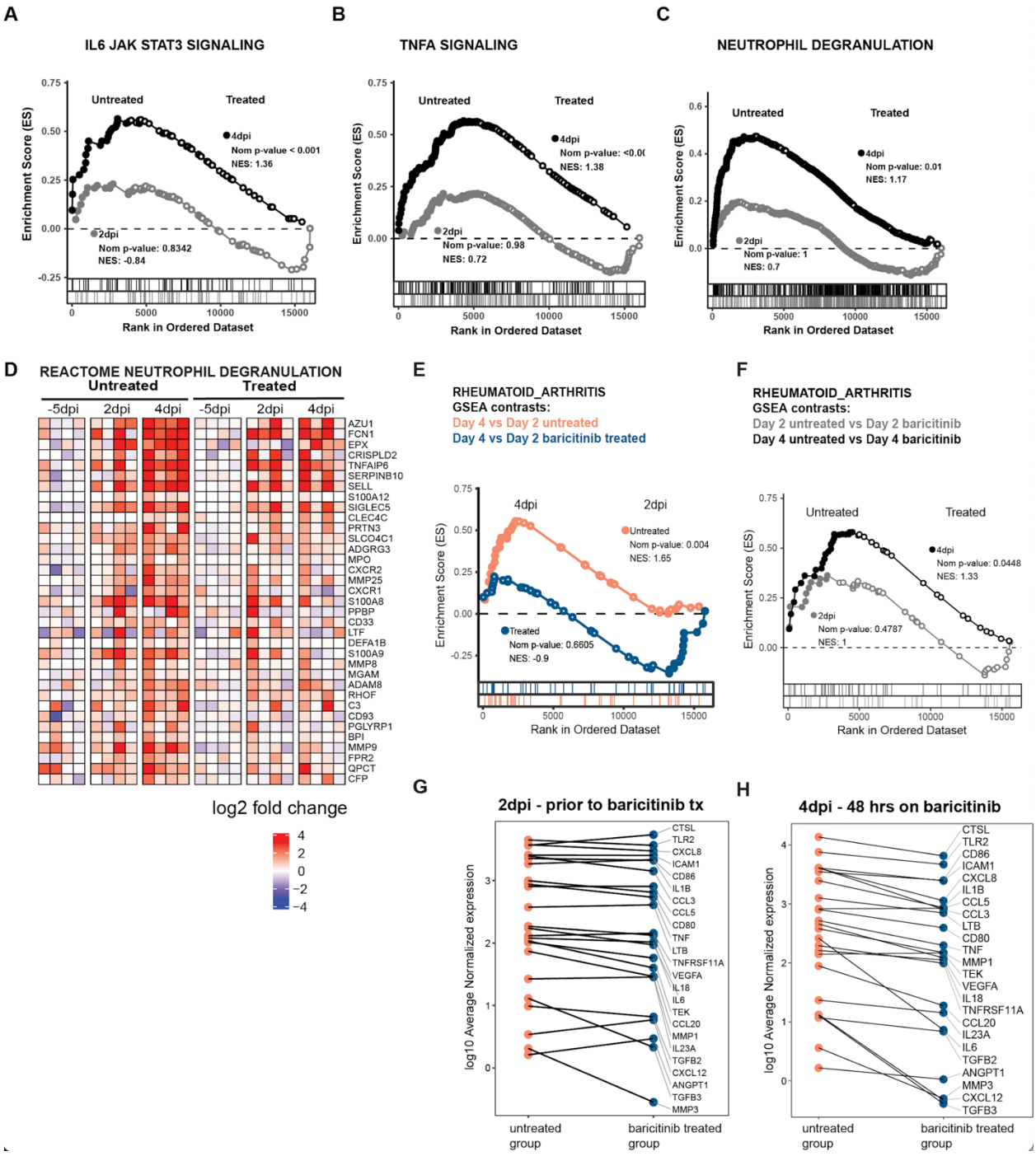

Figure 3.S3. Baricitinib Suppressed the expression of inflammatory mediators and neutrophil degranulation genes in BALs from SARS-CoV-2-infected RMs, related to Figure 3.3. Cross-sectional GSEA analysis comparing 4 days after infection untreated versus 4 days after infection baricitinib treated, or 2 days after infection untreated versus 2 days after infection baricitinib treated in bulk BAL from SARS-CoV-2 infected RMs. (A–C) GSEA comparisons of 4

days after infection untreated versus 4 days after infection baricitinib treated are shown as black symbols, and comparisons of or 2 days after infection untreated versus 2 days after infection baricitinib treated are shown as gray symbols. (A) GSEA enrichment plots for the GSEA line plot of HALLMARK_IL6_JAK_STAT3_SIGNALING pathway (MSIGDB #M5897). (B) GSEA line plot of HALLMARK_TNFA_SIGNALING_VIA_NFKB pathway (MSIGDB #M5890). (C) GSEA line plot of REACTOME NEUTROPHIL DEGRANULATION gene set (REACTOME #M27620). (D) Heatmap of leading edge genes for REACTOME NEUTROPHIL DEGRANULATION gene set based on untreated 4 days after infection versus baseline contrast. The log2 expression and the reference is the median of all baseline samples as indicated at right. The top 35 genes are shown in order of GSEA analysis of the cross-sectional 4 days after infection comparison. (E and F) GSEA analysis for KEGG Rheumatoid Arthritis gene set (E) GSEA contrasting 4 days after infection versus 2 days after infection for untreated and treated arms. GSEA curves are colored by experimental arm. Leading edge genes are indicated by solid dots. The hash plot under GSEA curves indicate individual genes and their rank in the dataset. Left-leaning curves (i.e., positive enrichment scores) indicate enrichment at 4 days after infection, right-leaning curves (negative enrichment scores) indicate higher enrichment at 2 days after infection, and sigmoidal curves indicate a lack of enrichment, i.e., equivalent expression between the groups being compared. The normalized enrichment scores and nominal p values testing the significance of each comparison are indicated. (F) GSEA comparisons of 4 days after infection untreated versus 4 days after infection baricitinib treated samples (black symbols); comparisons of 2 days after infection untreated versus 2 days after infection baricitinib treated samples (gray symbols). (G) plot showing log10 average normalized counts obtained from DESeq2 for leading edge genes at 2 days after infection in untreated and treated samples, and (H) at 4 days after infection.

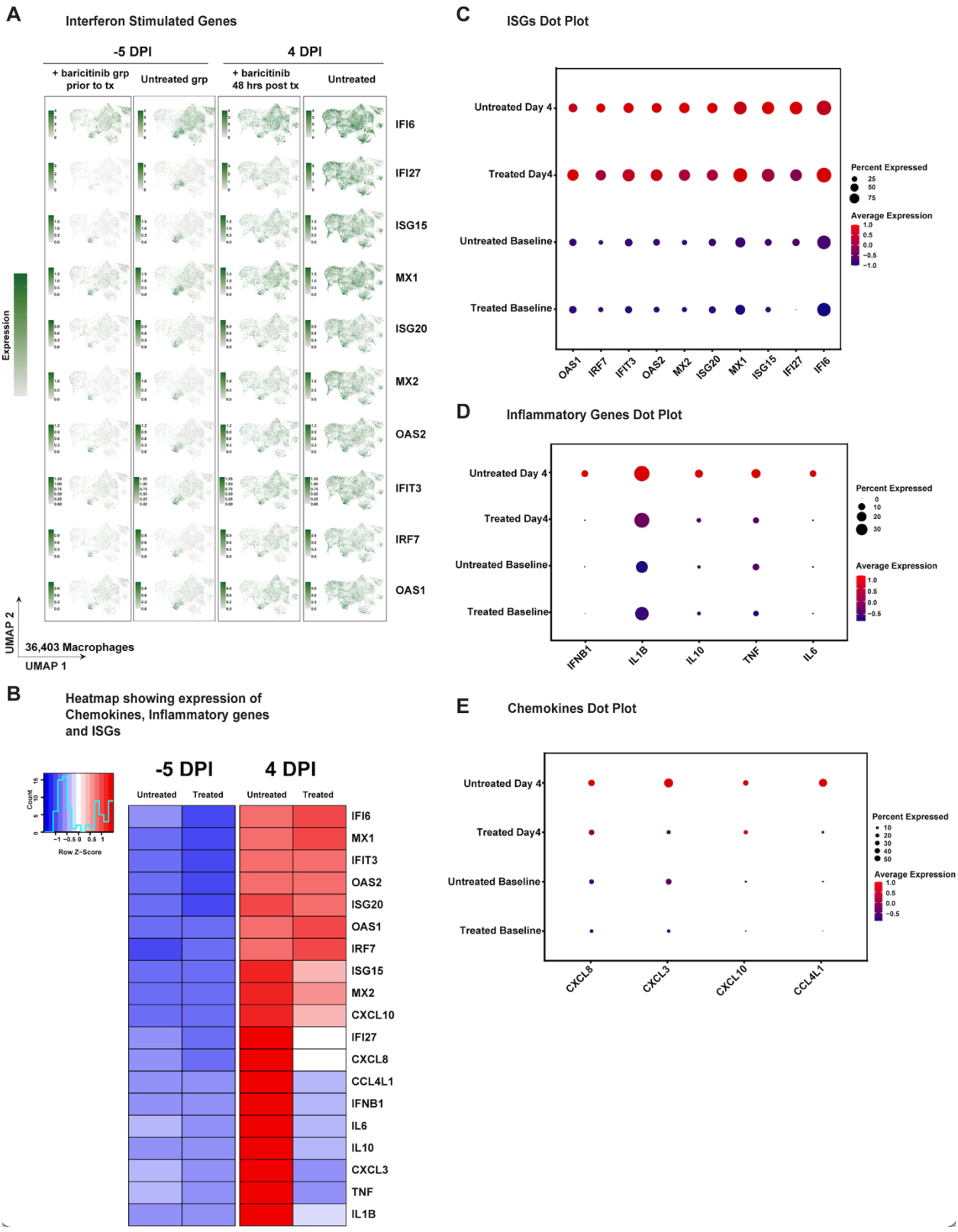
A
Interferon Stimulated Genes
-5 DPI
4 DPI
+ baricitinib grp prior to tx
Untreated grp
+ baricitinib 48 hrs post tx
Untreated
IFI6
IFI27
ISG15
MX1
ISG20
MX2
OAS2
IFIT3
IRF7
OAS1
Expression
UMAP 2
36,403 Macrophages
UMAP 1
B
Heatmap showing expression of Chemokines, Inflammatory genes and ISGs
Count
Row Z-Score
-5 DPI
4 DPI
Untreated
Treated
Untreated
Treated
IFI6
MX1
IFIT3
OAS2
ISG20
OAS1
IRF7
ISG15
MX2
CXCL10
IFI27
CXCL8
CCL4L1
IFNB1
IL6
IL10
CXCL3
TNF
IL1B
C
ISGs Dot Plot
Untreated Day 4
Treated Day4
Untreated Baseline
Treated Baseline
OAS1
IRF7
IFIT3
OAS2
MX2
ISG20
MX1
ISG15
IFI27
IFI6
Percent Expressed
Average Expression
D
Inflammatory Genes Dot Plot
Untreated Day 4
Treated Day4
Untreated Baseline
Treated Baseline
IFNB1
IL1B
IL10
TNF
IL6
Percent Expressed
Average Expression
E
Chemokines Dot Plot
Untreated Day 4
Treated Day4
Untreated Baseline
Treated Baseline
CXCL8
CXCL3
CXCL10
CCL4L1
Percent Expressed
Average Expression

Figure 3.S4. **Baricitinib inhibited the expression of inflammatory and macrophage/neutrophil chemokine genes while preserving ISGs in lung macrophages from SARS-CoV-2-infected RMs, related to Figure 3.4.** (A) Expression as UMAP projection of interferon stimulated genes (ISGs) in macrophages for treated and untreated samples at baseline and 4 days after infection. (B) Heatmap showing average expression of genes of interest in macrophages for treated and untreated samples at baseline and 4 days after infection. (C–E) Dot plots representing gene expression levels and percentage of cells expressing genes associated with inflammation, chemokine response and interferon stimulation

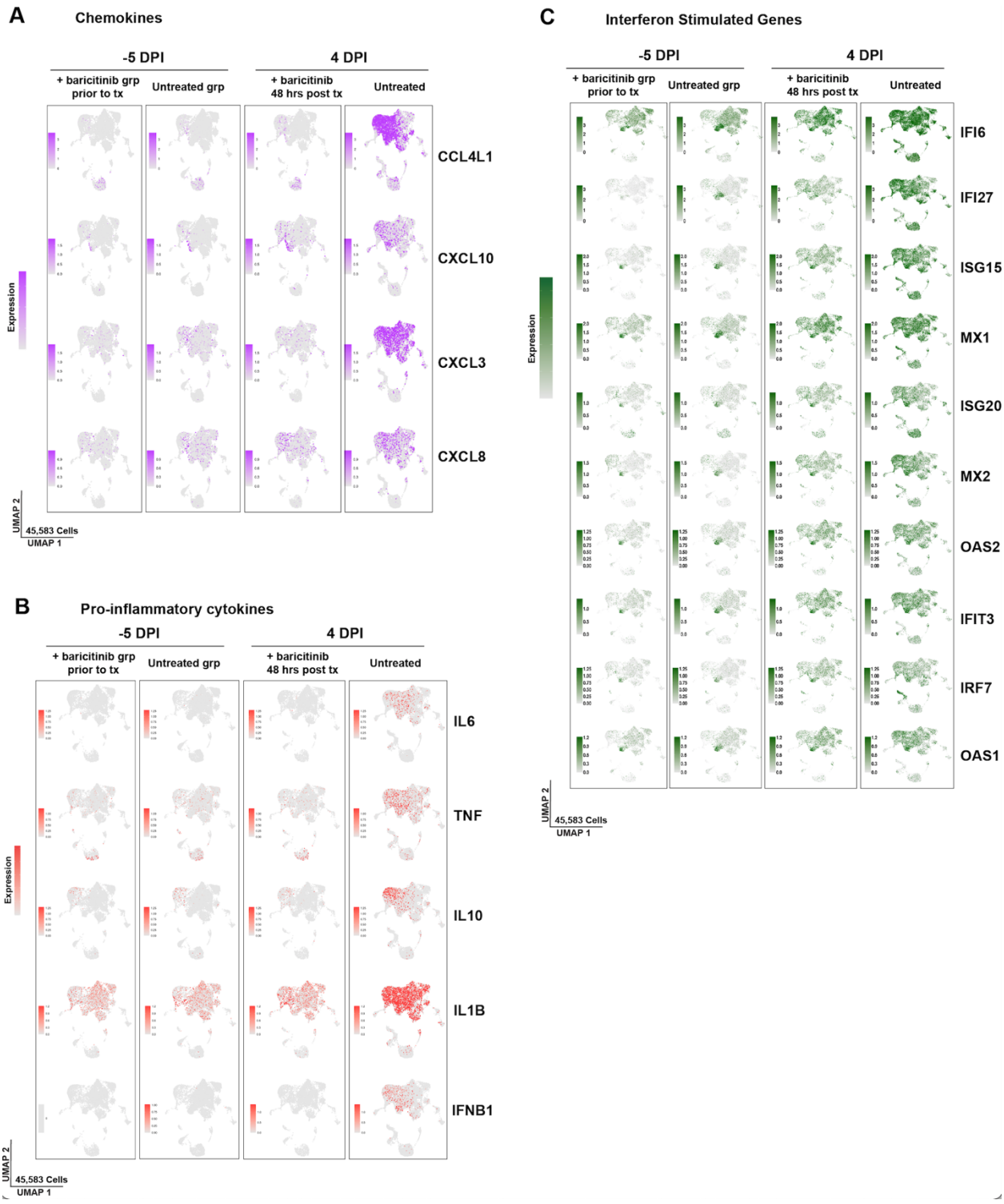
A
Chemokines
-5 DPI
4 DPI
+ baricitinib grp prior to tx
Untreated grp
+ baricitinib 48 hrs post tx
Untreated
CCL4L1
CXCL10
CXCL3
CXCL8
Expression
UMAP 2
45,583 Cells
UMAP 1
B
Pro-inflammatory cytokines
IL6
TNF
IL10
IL1B
IFNB1
C
Interferon Stimulated Genes
IFI6
IFI27
ISG15
MX1
ISG20
MX2
OAS2
IFIT3
IRF7
OAS1

Figure 3.S5. **Baricitinib reduced the expression of inflammatory and chemokine genes while maintaining ISGs in BALs from SARS-CoV-2- infected RMs, related to Figure 3.4.** (A–C) Expression as UMAP projection of inflammation, chemokine and interferon stimulated genes (ISGs) across major cell types in BAL for treated and untreated samples at baseline and 4 days after infection.

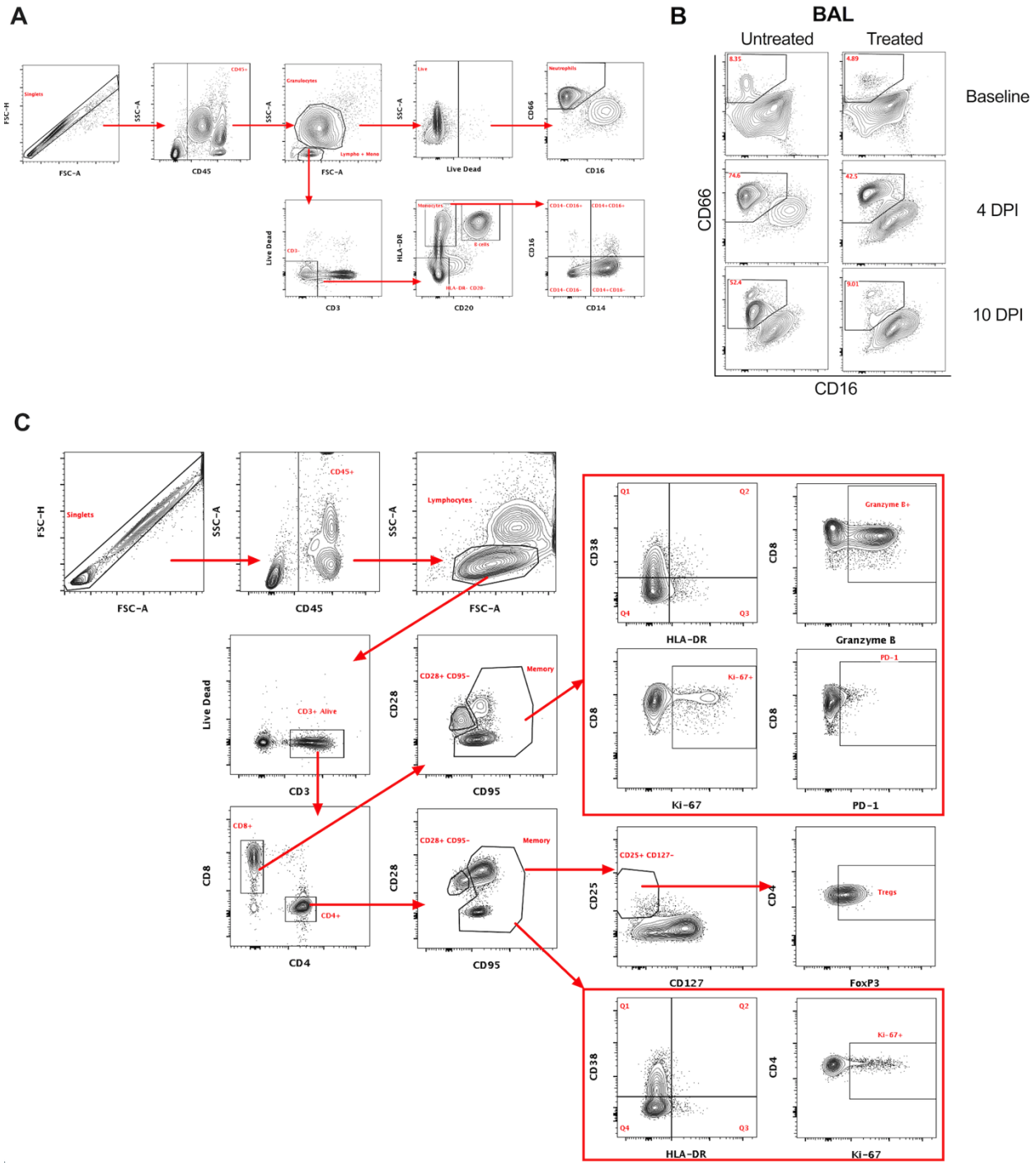

Figure 3.S6. Flow cytometry gating strategy for innate and adaptive cells, related to Figures 3.5 and 3.6. Representative gating strategy of (A) neutrophils, (B) neutrophil infiltration in BAL at baseline, and 4 and 10 days after infection, and (C) T cell populations analyzed in the study.

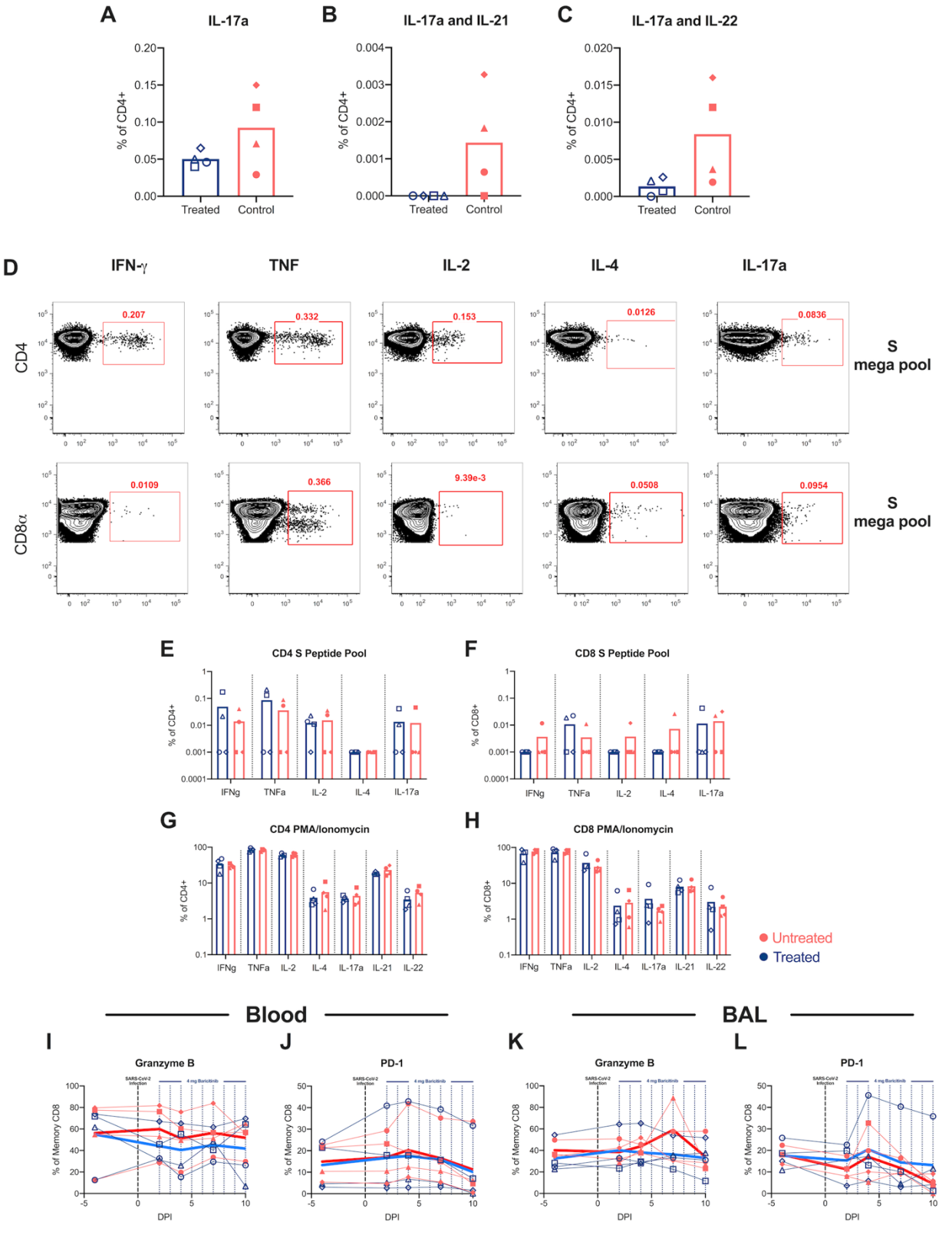
A
IL-17a
% of CD4+
Treated
Control
B
IL-17a and IL-21
% of CD4+
Treated
Control
C
IL-17a and IL-22
% of CD4+
Treated
Control
D
IFN-γ
TNF
IL-2
IL-4
IL-17a
CD4
CD8α
S mega pool
S mega pool
E
CD4 S Peptide Pool
% of CD4+
IFNg
TNFa
IL-2
IL-4
IL-17a
F
CD8 S Peptide Pool
% of CD8+
IFNg
TNFa
IL-2
IL-4
IL-17a
G
CD4 PMA/Ionomycin
% of CD4+
IFNg
TNFa
IL-2
IL-4
IL-17a
IL-21
IL-22
H
CD8 PMA/Ionomycin
% of CD8+
IFNg
TNFa
IL-2
IL-4
IL-17a
IL-21
IL-22
Untreated
Treated
Blood
BAL
I
Granzyme B
% of Memory CD8
DPI
J
PD-1
% of Memory CD8
DPI
K
Granzyme B
% of Memory CD8
DPI
L
PD-1
% of Memory CD8
DPI

Figure 3.S7. **Baricitinib treatment did not affect the immune T cell responses in SARS-CoV-2-infected RMs, related to Figure 3.6.** (A–C) Frequency of circulating CD4+ T cells spontaneously (without stimulation) producing pro-inflammatory Th17 related cytokines (A) IL-17$^+$, (B) IL-17$^+$IL-21$^+$, (C) IL-17$^+$IL- 22$^+$ at necropsy (days 10–11 after infection) in baricitinib (blue) and untreated (red) SARS-CoV-2 infected RMs. (D) Representative flow cytometry staining of IFNg, TNFa, IL-2, IL-4 and IL-17a in CD4$^+$ and CD8$^+$ T cells of a SARS-CoV-2 infected RM following stimulation with SARS-CoV-2 S peptide pool. IFNg, Unstimulated background values were subtracted from S peptide stimulated values to determine T cell cytokine. (E and F) IFNg, TNFa, IL-2, IL-4 and IL-17a frequency levels in (E) CD4$^+$ and (F) CD8$^+$T cells following stimulation with SARS-CoV-2 S peptide pool. (G–L) IFNg, TNFa, IL-2, IL-4 and IL-17a frequency levels in (G) CD4$^+$ and (H) CD8$^+$T cells following stimulation with PMA/Ionomycin. Values from unstimulated controls were subtracted in all cases. Granzyme B and PD-1 levels in (I and J) blood and (K and L) BAL memory CD8$^+$T cells measured by flow cytometry. Each symbol represents individual animals. Thick lines represent the average of the baricitinib treated (blue line), and untreated groups (red line). Bars represent the average of the treated and untreated groups. Statistical analysis was performed using a non-parametric Mann-Whitney Test.

Table 3.S1. Macaque characteristics and treatment group, Related to Figure 3.1. Animal ID in manuscript and assignment. Age in months and weight at time of infection. Treatment group assignment. The four uninfected control animals were historical samples that were only used for IHC staining in **Figure 3.S2.** Annotated symbol in figures.

Animal ID	Animal Name	Sex	Age (months) at Infection	Weight (kgs) at Infection	Treatment	Annotated Symbol
RM1	RAt11	M	166	10.98	Baricitinib	○
RM2	RLf10	M	201	12.96	Baricitinib	□
RM3	RVf12	F	155	9.63	Baricitinib	△
RM4	7_141	F	155	9.51	Baricitinib	◇
RM5	06_112	F	167	8.71	Untreated	●
RM6	RQv9	M	204	14.86	Untreated	■
RM7	5_215	F	176	8.44	Untreated	▲
RM8	RHz12	M	141	11.77	Untreated	◆
	P378	F	36-60	8.71	Uninfected	●
	P377	F	36-60	14.86	Uninfected	■
	P376	F	36-60	8.44	Uninfected	▲
	P375	M	36-60	11.77	Uninfected	◆

Table 3.S2, Cage-side assessment scoring sheet, Related to Figure 3.1. The table was modified from a previous NHP influenza A virus study to include cage-side assessments relevant to COVID-19 and respiratory rates for cynomolgus macaques. The highest sum of scores for an animal determined the severity of disease. Disease severity was classified as no illness (0-4), mild (5-9), moderate (10-15), severe (>16). BPM = breaths per minute.

Cage-Side Assessment			
Parameter	**Description**	**Score**	
Responsiveness and recumbency	Normal - bright, alert, responsive	0	
	Mild - slightly depressed, acts disinterested when personnel in room, lying down in cage but gets up when approached	2	
	Moderate/obtunded - non-responsive, very disinterested in personnel, hunched or lying down, will get up when prodded, pinched, or similarly stimulated	4	
	Severe/comatose - lying down completely unresponsive to stimuli	6	
Discharges	Nasal or ocular	2	
	Nasal and ocular	4	
Skin	Rash	1	

Respiration, dyspnea, and cough	Normal - no apparent changes in breathing, 30-54 BPM, and no cough	0	
	Mild - slightly increased effort breathing, 55-65 BPM, or mild cough	2	
	Moderate - obvious difficulty breathing, 66-80 BPM, or apparent cough	4	
	Severe - respirations labored, open mouth breathing, abdominal breathing, >80 BPM, cyanosis, or haemoptysis	6	
Food consumption	100% of chow and enrichment food consumed	0	
	10-25% of chow remaining	1	
	25-50% of chow remaining, possibly some enrichment food remaining	2	
	>50% of chow remaining, some or all enrichment food remaining	3	
Fecal consistency	Normal	0	
	Soft	1	
	Fluid	2	
	Fluid and profuse amount	3	
		Total	
Notes *(any observed sneezing, vomit, conjunctival erythema, or other abnormalities*)			

Table 3.S3. Physical examination under anesthesia scoring criteria, **Related to Figure 3.1**. Physical examinations were performed whenever an animal was anesthetized. The highest sum of scores for an animal determined the severity of disease. Disease severity was classified as no illness (0-2), mild (3-7), moderate (8-13), severe (>13). BPM = breaths per minute.

Physical Examination Under Anesthesia			
Parameter	**Description**	**Score**	
Rectal temperature *(taken immediately after sedation)*	Normal (37.0-38.9C)	0	
	Low grade fever (39-39.5C)	2	
	Fever (>39.5C)	4	
Heart rate and blood pressure	Normal (*** BPM, ***/***)	0	
	Mild tachycardia (*** BPM), normotensive	1	
	Moderate tachycardia (*** BPM), normotensive	2	
	Severe tachycardia (*** BPM), hypotensive (***/***)	3	
	Normal - 30-54 BPM	0	
	Mild tachypnea- 55-65 BPM	2	

Respiratory rate	Moderate tachypnea - 66-80 BPM	4	
	Severe tachypnea - >80 BPM	6	
SpO_2	Normal (95-100%)	0	
	Mildly decreased (90-94%)	1	
	Moderately decreased (87-89)	2	
	Severely decreased (<87)	3	
Body weight	Normal (0-3% loss)	0	
	Mild (4-9% loss)	1	
	Moderate (10-16% loss)	2	
	Severe (>16% loss)	3	
Dehydration	Normal skin turgor, moist mucous membranes	0	
	Skin tenting or dry mucous membranes	1	
	Skin tenting and dry mucous membranes	2	
	Skin tenting, dry mucous membranes, and sunken eyes	3	
		Total	

Notes *(auscultation findings if applicable, conjunctival erythema, palpable masses, or any other abnormalities)*

Chapter Four: TREM2+ and interstitial macrophages orchestrate airway inflammation in SARS-CoV-2 infection in rhesus macaques

Amit A. Upadhyay[1,9], Timothy N. Hoang[1,9], Maria Pino[1,9], Arun K. Boddapati[2], Elise G. Viox[1,] Michelle Y.H. Lee[1], Jacqueline Corry[3], Zachary Strongin[1], David A. Cowan[2], Elizabeth N. Beagle[2], Tristan R. Horton[2], Sydney Hamilton[2], Hadj Aoued[2], Justin L. Harper[1], Kevin Nguyen[1], Kathryn L. Pellegrini[2], Gregory K. Tharp[2], Anne Piantadosi[4], Rebecca D. Levit[5], Rama R. Amara[1,6], Simon M. Barratt-Boyes[3,7], Susan P. Ribeiro[4], Rafick P. Sekaly[4], Thomas H. Vanderford[1], Raymond F. Schinazi[8], Mirko Paiardini[,1,4*], Steven E. Bosinger[1,4*].

Affiliations:

[1]Division of Microbiology and Immunology, Yerkes National Primate Research Center, Emory University, Atlanta, Georgia, USA.

[2]Yerkes Genomics Core Laboratory, Yerkes National Primate Research Center, Emory University, Atlanta, Georgia, USA

[3]Department of Infectious Diseases and Microbiology, University of Pittsburgh, Pittsburgh, Pennsylvania, USA.

[4]Department of Pathology and Laboratory Medicine, School of Medicine, Emory University, Atlanta, Georgia, USA.

[5]Department of Medicine, School of Medicine, Emory University, Atlanta, Georgia, USA.

[6]Department of Microbiology and Immunology, Emory School of Medicine, Emory University, Atlanta, Georgia, USA

[7]Department of Immunology, University of Pittsburgh, Pittsburgh, Pennsylvania, USA.

[8]Department of Pediatrics, School of Medicine, Emory University and Children's Healthcare of Atlanta, Atlanta, Georgia, USA.

[9]These authors contributed equally

[*]Correspondence to

Steven E. Bosinger: steven.bosinger@emory.edu;

Mirko Paiardini: mirko.paiardini@emory.edu

One sentence summary: Multi-omic analyses of hyperacute SARS-CoV-2 infection in rhesus macaques identified two population of infiltrating macrophages, as the primary orchestrators of inflammation in the lower airway that can be successfully treated with baricitinib

Main Text:

Introduction

The COVID-19 pandemic began with a series of reports of localized outbreaks of pneumonia caused by a novel coronavirus, SARS-CoV-2, in Wuhan, China in December 2019 [320, 323]. As of late 2021, there have been over 200,000,000 documented infections, and over 4,500,000 fatalities attributed to sequelae of COVID-19. The rapid development and availability of effective vaccines [461, 462, 560] against SARS-CoV-2 infection has provided much needed optimism that infection rates will decline and that the containment of the virus at the population level is possible. Despite these landmark achievements, continued research efforts are essential to safeguard against potential breakthrough variants, to develop therapies for those afflicted while the vaccine rollout continues, and to prevent or minimize the impact of future viral outbreaks. In this light, basic research into the innate and adaptive immune responses to SARS-CoV-2 continues to be critical for informing vaccine and therapeutic approaches directed at ending the COVID-19 pandemic or at decreasing mortality.

Since the emergence of the COVID-19 pandemic, research into the virology, immune responses and pathogenesis of SARS-CoV-2 infection has amassed at an unprecedented rate, and numerous hypotheses have arisen to explain the underlying mechanisms of severe COVID-19. Of these, the concepts that have accumulated the most supporting evidence are: (i) evasion or impairment of early Type I interferon (IFN) responses [561], (ii) vascular complications arising from hypercoagulability syndromes [562], and (iii) perturbations of the granulocyte and myeloid compartments in the lower airway and blood manifesting in inflammatory cytokine production [534,

[537]. Immunologically, severe disease in COVID-19 patients has been associated with a widespread increase in levels of inflammatory mediators (e.g. CXCL10, IL-6, and TNFa) in plasma and bronchoalveolar lavage (BAL) fluid in what is commonly referred to as a "cytokine storm" [563], and an expansion of macrophages, neutrophils and lymphocytes in the lower airway [537]. Despite this impressive accruement of data, the precise early immunological events and immune cell infiltration that drive inflammation in the lower airway remain uncharacterized.

Non-human primate (NHP) models of SARS-CoV-2 infection (primarily macaque species and African green monkeys (AGMs)) have proven to be critical tools, primarily due to the ability to examine early events after infection longitudinally and in tissues not available in most human studies [564]. NHPs support high levels of viral replication in the upper and lower airway [328, 520, 521], share tissue distribution of ACE2 and TMPRSS2 with humans [333], and have been invaluable pre-clinical models of vaccines [565-567] and therapeutics [329, 450]. Additionally, mild to moderate COVID-19 has been shown to be recapitulated in SARS-CoV-2-infected NHPs [564] that typically resolve by 10-15 days post infection (dpi) [329, 564, 568]. Mechanistic studies of SARS-CoV-2 infection in NHPs have utilized a variety of high-throughput techniques and have reported (i) Type I IFN responses are robustly induced in blood and the lower airway very early after infection [329, 569], (ii) elevated pro-inflammatory cytokines consistent with the "cytokine storm" seen in humans are detectable in plasma and BAL [570], (iii) vascular pathology and gene expression consistent with hypercoagulability are evident in the lower airways [569], and (iv) increased production of inflammatory cytokines by myeloid origin cells [329, 571].

In the current study, we used SARS-CoV-2 infected rhesus macaque (RM) to investigate the early inflammatory events occurring in the blood and lower airway using high dimensional flow cytometry, multi-analyte cytokine detection, and bulk and single-cell RNA-Seq (sc-RNA-Seq). To

dissect the role of discrete immune subsets within the myeloid fraction in SARS-CoV-2-driven inflammation, we used two different strategies, employing scRNA-Seq and bulk-RNA-Seq reference datasets to classify the macrophage/monocyte population. With this approach, we identified the main subsets of pro-inflammatory macrophages that expand after SARS-CoV2 infection and are the predominant source of inflammatory cytokines in the airway. We also observed an early induction of plasmacytoid dendritic cells (pDCs) in blood and the lower airway that coincided with the peak of the IFN signaling. Finally, we described that treatment of SARS-CoV-2 infected RMs with baricitinib, a JAK1/2 inhibitor recently demonstrated to reduce hospitalization time and mortality for severe COVID-19 patients [(453)], suppressed airway inflammation by abrogating the infiltration of pro-inflammatory macrophages to the alveolar space. Collectively, this study defines the early kinetics of pDC recruitment and Type I IFN responses, and identifies discrete subsets of infiltrating macrophages as the predominant source of pro-inflammatory cytokine production in SARS-CoV-2 infection.

Results

Study Overview

An overview of the study design is shown in **Fig. 4.1a**. Eight RMs (mean age 14 years old; range 11-17 years old) were inoculated intranasally and intratracheally with 1.1 x 10^6 plaque-forming units (PFU) of SARS-CoV-2 (2019-nCoV/USA-WA1/202). These animals were previously reported in a study evaluating the therapeutic efficacy of baricitinib in SARS-CoV-2 infection [329]. At 2dpi, four of the eight animals started receiving baricitinib [329]. For this study, pre-infection baseline and hyperacute time points (1-2dpi) include n = 8 RMs, all untreated, and the remaining longitudinal time-points assessed to determine the pathogenesis of SARS-CoV-2 infection are comprised of n = 4 of the RMs that remained untreated. Inoculation with SARS-CoV-2 led to reproducibly high viral titers detectable in the upper and lower airways by genomic and sub-genomic qPCR assays (**Fig. 4.1b**). The peak of viremia in the nasal passage, throat and BAL was at 2-4dpi (**Fig. 4.1b**).

SARS-CoV-2 induces a robust, but transient, expansion of pDCs during hyperacute infection

To characterize the innate immune response following SARS-CoV-2 infection, we analyzed changes in innate populations using multi-parametric flow cytometry in blood and BAL samples in the first 2dpi, or "hyperacute" phase of infection (**Fig. 4.1c-e, Fig. 4.S1**), and over the full course of infection (**Fig. 4.S2**). In blood, we did not observe a significant increase in the proportion of classical monocytes (CD14+CD16-) at 2dpi (**Fig. 4.1c**) nor at extended time-points (**Fig. 4.S2a)**. Similar to reports in humans [534], we observed a rapid, but transient, increase in blood CD14-CD16+ and CD14+CD16+ monocytes (**Fig. 4.1c**, **Fig. 4.S2c)**. Using these conventional markers for blood monocyte subsets, we did not observe any significant changes in CD14-CD16+, CD14+CD16+, nor CD14-CD16+ within the BAL (**Fig. 4.1c, Fig. 4.S2c)**.

We observed a significantly elevated level of pDCs in blood at 2dpi and similarly, a trend of elevated pDCs in BAL samples (**Fig. 4.1d, Fig. 4.S2c**). This expansion was transient, as pDC numbers returned to baseline by 4dpi. While the overall frequencies of natural killer cells (NK) were not changed in blood or BAL (**Fig. 4.S2b)**, the fraction of Granzyme B+ NK cells increased significantly at 2dpi in blood, from 4% to 25% **(Fig. 4.1e)** and remained elevated throughout the course of infection (**Fig. 4.S2**). Similarly, increases in NK cell activation were also observed in the BAL, rising from 12% to 33% at 2dpi **(Fig. 4.1e)**, and persisting at this level until the study termination at 10/11dpi (**Fig. 4.S2b**). Collectively, these data indicate that during the hyperacute phase of SARS-CoV-2 infection, there is a significant mobilization of innate immune cells capable of initiating and orchestrating effector responses of the Type I IFN system.

SARS-CoV-2 infection drives robust, but transient, upregulation of IFN responses in blood and lower airway

To understand the extent of immunological perturbations induced by SARS-CoV-2 infection, we performed extensive gene expression profiling of PBMC and BAL samples. During the hyperacute phase, the BAL had widespread induction of pathways associated with innate immunity and inflammation (**Fig. 4.2a**). Notably, we observed a rapid and robust induction of interferon-stimulated genes (ISGs) in the PBMC and BAL compartments starting at 1 or 2dpi (**Fig. 4.2b, Fig. 4.S3a**). The ISG response, although widespread, had largely returned to baseline by 10/11dpi (**Fig 4.2b, Fig. 4.S3a**). We also detected a trend of elevated IFNa2 protein in 4/6 and 5/8 animals in BAL and plasma, respectively (**Fig. 4.2c,d)** and a significant increase in RNA-Seq read counts mapping to IFNA genes at 2dpi in BAL (**Fig. 4.2e)**, which coincided with the expansion of pDCs in the airway and blood (**Fig. 4.1d**). A significant enrichment of genes representing NK cell cytotoxicity (**Fig. 4.2a**) was observed at 2dpi in BAL, consistent with our observation of elevated Granzyme B+ NK cells by flow cytometry (**Fig. 4.1e**). Taken together, these data demonstrate the presence of primary cells able to produce Type I IFNs (i.e., pDCs), coincident with detectable IFNA transcripts and protein, and with downstream IFN-induced effector functions (ISGs, NK cell activation) following SAR-CoV-2 infection, and that these responses were transient, having largely subsided by 10/11dpi.

SARS-CoV-2 infection drives a shift in airway macrophage populations

We observed that SARS-CoV-2 infection induced significant enrichment of several inflammatory cytokine signaling pathways, namely IFNA, IL4, IL6, IL10, IL12, IL23 and TNF, and the chemokine pathways CXCR4 and CXCR3, in both PBMCs and BAL of RMs, with higher magnitude in the BAL (**Fig. 4.2a, Supplementary Files 4.1&4.2**). For many of these pathways, we were able to quantify significant increases in the upstream regulator at either the protein, or mRNA level, or

both: IL6 protein levels were significantly increased in the BAL fluid (BALF) (**Fig. 4.2c**), as were RNA transcripts in BAL (**Fig. 4.S3b)**. Similarly, the induction of CXCR3 pathways signaling was consistent with detection of increased IP10/CXCL10 protein in BALF and RNA at 2dpi in BAL **(Fig. 4.2c, Fig. 4.S3b)**. The appearance of inflammatory pathways in the blood and airway have been reported in a multitude of human studies (reviewed in [572]). However, we noted that SARS-CoV-2 infection also drove early expression of several immunoregulatory/immunosuppressive pathways in the BAL, namely: PD1 and CTLA4 signaling, and negative regulators of MAP kinase and DDX58/RIG-I signaling (**Fig. 4.2a)**. Previously, we reported that the myeloid fraction in BAL was primarily responsible for the production of pro-inflammatory mediators, however the specific immunophenotypes were not defined. To further investigate the presence of different macrophage subsets within the lower airway after SARS-CoV-2 infection, we performed GSEA on bulk BAL data using AM gene signature (obtained from SingleR [555]) specific for RM pulmonary macrophages. We observed that genes specific for alveolar macrophages (AMs) were significantly enriched at baseline (-5dpi) relative to 4dpi, indicating a downregulation of this gene set after SARS-CoV-2 infection (**Fig. 4.2f**). Collectively, these bulk RNA-Seq data indicate a rapid and significant shift in the balance of macrophage populations in the lower airway following SARS-CoV-2 infection.

SARS-CoV-2 infection induces an influx of two subsets of infiltrating macrophages into the alveolar space

In our prior work in RMs, we demonstrated that cells of myeloid origin were the predominant subset responsible for production of inflammatory cytokines in the lower airway following SARS-CoV-2 infection [329]. While our prior sc-RNA-seq analyses determined the majority of cells in the BAL after infection to be of monocyte/macrophage origin, with relatively few neutrophils or

granulocytes, the precise immunophenotypes of the myeloid cells driving inflammation in the lower airway have not been precisely delineated.

Cell classification based on cell-surface marker genes is typically problematic in sc-RNA-seq data due to gene dropouts inherent to the technology. Accurate classification is further complicated in the rhesus model system, in which genomic references have incomplete annotation, and markers from other model species may not phenocopy. Several significant advances have been made recently elucidating the resident tissue macrophage subsets in the lung and their function during viral infection and inflammation [573-576]. However, analysis of sc-RNA-Seq data from RM lung suspensions and BAL during steady state condition indicated that several key markers used to differentiate macrophages in the murine lung (e.g. Lyve1) were not expressed at levels sufficient to distinguish populations in the rhesus pulmonary myeloid populations (**Fig. 4.S4**). Therefore, we used two overlapping alternative strategies to accurately classify tissue macrophages and monocyte-derived/infiltrating macrophages in the RM airway after SARS-Cov-2 infection in our sc-RNA-Seq data. The first strategy was based on using existing lung scRNA-Seq data from uninfected RMs as a reference to map and annotate the BAL cells. We processed lung 10X data from three uninfected RMs (NCBI GEO: GSE149758) [577] through Seurat pipeline [578] and reproduced the four reported macrophage/monocyte subsets: CD163+MRC1+, resembling alveolar macrophages; CD163+MRC1+TREM2+ macrophages, similar to infiltrating monocytes; CD163+MRC1-, similar to interstitial macrophages; and CD16+ non-classical monocytes (**Fig 4.S4 a-d**). We used Seurat to map BAL macrophages/monocytes from SARS-CoV2 infected RMs and transfer annotations from the lung reference. The second strategy involved using bulk RNA-Seq on sorted AM and IM from the lungs of three uninfected RMs, according to the phenotype defined by Cai et al [579], based on expression of CD206/MRC1 and CD163, to annotate cells using SingleR [555] **Fig. 4.S4e**). 2069 genes were found to be differentially expressed between IMs

and AMs (FDR< 0.05, fold-change>2) (**Fig. 4.S4f**). Of note, CX3CR1 was highly expressed in the IMs, consistent with both murine and human definitions of this subset (**Fig. 4.S4g**). APOBEC3A, an RNA-editing cytidine deaminase, was also highly expressed in IMs along with PTGS2, a pro-inflammatory COX-2 cyclooxygenase enzyme, TIMP1, which enables migration of cells via the breakdown of connective tissue, VCAN, an immunosuppressive regulator, and PDE4B, which regulates expression of TNFa (**Fig. 4.S4g**). We annotated the lung macrophage/monocyte subsets using the bulk sorted AM and IM datasets and found that almost all of CD163+MRC1+ cluster and some CD163+MRC1+TREM2+ cells were annotated as AM and the remaining as IM (**Fig 4.S4h**). Thus, benchmarking our lung sc-RNA-seq based reference against rudimentary bulk transcriptomic signatures demonstrated their accuracy in resolving the AM phenotype from non-AM in steady state conditions.

We next analyzed changes in the myeloid populations within the BAL of RMs after SARS-CoV-2 infection. Using our lung/sc-RNA-seq reference, we found that most of the BAL macrophages/monocytes belonged to the AM-like CD163+MRC1+ macrophage subset at -5dpi along with some cells from the CD163+MRC1+TREM2+ macrophage subset (**Fig. 4.3a,b**). At 4dpi, there was an influx of both CD163+MRC1+TREM2+ macrophages and the IM-like CD163+MRC1- macrophages with few cells annotated as CD16+ non-classical monocytes. The expression of gene markers such as MARCO, FABP4 and CHIT1 further supported the cell subset annotations (**Fig 4.3c**). We also observed a similar increase in APOBEC3A and decreases in MARCO and CHIT1 expression in bulk BAL samples (**Fig 4.3d**). The percentage of CD163+MRC1+ macrophages reduced overall from 70% to 29% of all macrophages/monocytes in BAL (**Fig 4.3e**). Similarly, we saw an overall increase in the percentage of CD163+MRC1+TREM2+ macrophages from 5% to 21% and the IM-like CD163+MRC1- macrophages from 0.1% to 4%. Thus, COVID-19 infection resulted in an influx of monocyte-

derived and IM-like macrophages in BAL at 4dpi. We also found that these infiltrating macrophages expressed higher levels of several pro-inflammatory cytokines and chemokines compared to the CD163+MRC1+ AM-like macrophages (**Fig 4.3f-h, Supplementary File 4.4**).

To further validate our cell classification and support the observation that it is the infiltrating cells that increase in numbers and predominantly producing inflammatory mediators, we used the second strategy of using gene expression of bulk sorted AM and IM cells to classify the BAL macrophages/monocytes. Using this definition, we confirmed that there is an increase in the percentage of non-AM population with a corresponding decrease in the AM population (**Fig 4.S5b, d**). The non-AM population was also found to show higher expression of pro-inflammatory cytokines (**Fig 4.S5e, Supplementary File 4.4**).

Differential expression analysis of 4dpi and -5dpi BAL macrophages/monocytes showed that CHIT1, MARCO and MRC1 were among the top-ranking genes exhibiting downregulation in the BAL, while genes such as ADAMDEC1 [(580)] and S100A8 [(581)] that are associated with monocyte-derived macrophages were among the most upregulated (**Supplementary File 4.4**). These data demonstrate that our observation of an influx of infiltrating macrophages into the BAL at 4dpi was consistent across multiple definitions of this phenotype.

Infiltrating macrophages produce the majority of lower airway inflammatory cytokines during acute SARS-CoV-2 infection

Given our observation of the dynamics of pulmonary macrophages within the alveolar space during early SARS-CoV-2 infection, we characterized the transcriptional changes in each macrophage/monocyte population. Several chemokines (CCL4L1, CCL3, CXCL3, CCL2), multiple ISGs, NFKB1A, S100A8, and GZMB were among the most upregulated genes at 4dpi in

BAL populations (**Supplementary File 4.4**). Elevated expression of multiple inflammatory genes, including IL6, TNF, IL10, IFNB1 and IL1B, were observed in the CD163+MRC1+TREM2 Mac and CD163+MRC1- subsets (**Fig. 4.3f, Fig. 4.S6**) after infection. The infiltrating macrophages were also observed to upregulate multiple chemokines, including those specific for recruiting neutrophils (CXCL3, CXCL8), macrophages (CCL2, CCL3, CCL5, CCL4L1), and activated T cells (CXCL10) as well as multiple ISGs (**Fig. 4.3g-h, Fig. 4.S6)**. When we examined CD163+ MRC1+ macrophages, many of the same inflammatory cytokines and gene sets seen in the infiltrating macrophages were elevated at 4dpi, albeit at much lower magnitude (**Fig. 4.3f-h, Fig. 4.S6**). Having observed a significantly higher average expression of inflammatory cytokines in infiltrating macrophages compared to CD163+MRC1+ macrophages, we compared the fractions of sequencing reads detected from each of the subsets to assess the overall contribution to inflammatory cytokine production (**Fig. 4.3i**). At 4dpi, we observed that the CD163+MRC1+TREM2+ macrophages accounted for 55% of IL6, 57% of TNF, 86% of IL10 and 66% of IFNB1 expression while the CD163+MRC1- macrophages accounted for 20% of IL6, 21% of TNF, 6% of IL10 and 19% of IFNB1 expression. We also found that CD163+MRC1- macrophages expressed higher levels of several of these genes (**Fig. 4.S6**). Thus, infiltrating macrophages are responsible for the majority of lower airway inflammatory cytokine production during acute SARS-CoV-2 infection.

Baricitinib treatment prevents the influx of inflammatory IM into the lower airway

Baricitinib is a JAK1/2 inhibitor approved for the treatment of active rheumatoid arthritis that was recently granted emergency use authorization for the treatment of hospitalized COVID-19 patients, and reported to reduce mortality when administered as monotherapy [(542)] or in combination with remdesivir [(453)]. In our earlier study, we found that baricitinib was able to suppress the expression of pro-inflammatory cytokines in BAL of RMs infected with SARS-CoV-

2 [329]. Here, we extended this study to further characterize the impact of baricitinib on the myeloid populations in the airway from five RMs before infection (-5) and at 4dpi, with three RMs that remained untreated and two that received baricitinib). We found that two days of baricitinib administration virtually abrogated the influx of infiltrating macrophages into the alveolar space at 4dpi (**Fig. 4.4a-c**). This observation was consistent using classifications of macrophages either based on mapping to 10X lung reference or using bulk sorted AM/IM cells (**Fig. 4.4a-c, Fig. 4.S5a-d**). In addition to preventing the influx of infiltrating macrophages, baricitinib treatment also resulted in significantly lower expression of inflammatory cytokines and chemokines, but the ISG expression remained comparable to untreated animals (**Fig. 4.4d-f, Fig. 4.S5e**). In summary, these data further elucidate the mechanism of action by which baricitinib treatment abrogates airway inflammation in SARS-CoV-2 infection [329], by demonstrating its ability to block infiltration of discrete pro-inflammatory macrophage populations into the alveolar compartment.

Discussion

The mechanisms by which SARS-CoV-2 infection establishes severe disease remain largely unknown, but remain a key priority for reducing the toll of the COVID-19 pandemic. As the appearance of symptoms range from 2-14 days after SARS-CoV-2 infection, characterization of the early immunological events using clinical samples is challenging. Here, we utilized the RM model of SARS-CoV-2 infection and an integrated systems analysis to dissect the immune response during hyper-acute infection. Our findings were: (i) SARS-CoV-2 infection initiated a robust Type I IFN response in the blood and lower airway apparent at 1-2dpi; (ii) SARS-CoV-2 induced a rapid influx of two infiltrating macrophage populations, into the bronchoalveolar space, which produced the majority of inflammatory cytokine production; and (iii) the mechanism of action of baricitinib, a drug recently authorized for emergency use in the treatment of severe COVID-19, is to abrogate infiltration of these inflammatory cells into the airway. Our data present, to date, the

most comprehensive analysis of the immunopathological events occurring during hyperacute SARS-CoV-2 infection.

Using our reference datasets of RM lung macrophages, we identified two myeloid cell subsets, both clearly distinct from alveolar macrophages, infiltrating the airway after SARS-CoV-2 infection, that were the main producers of lower airway inflammatory cytokines and chemokines. One population, defined as CD163+MRC+TREM2+ cells, were highly similar to murine definitions of infiltrating CCR2+ monocytes. The second, CD163+MRC-, largely resembled interstitial macrophages. Our data are consistent with a recent observation of a rapid (3dpi) increase of IMs in the BAL of RMs using flow cytometry [568]. Similarly, an accumulation of non-AMs (defined as CD16+CD206-HLA-DR+/CD11b+), and reciprocal reduction of AMs, has been observed in the BAL and lungs of infected RMs and AGMs [570]. Lastly, our data are consistent with our recent findings in the murine model, in which SARS-CoV-2 elicited recruitment of circulating monocytes to the lung parenchyma, but was significantly abrogated in CCR2-deficient mice [582]. The CD163+MRC1+ Mac/AM-like subset also contributed to the inflammatory milieu, producing IL6, TNF, and IL10, albeit in significantly lower quantities.

It is important to note that our observations were during hyperacute infection, and that our animals did not develop severe disease, so although our data indicate that these infiltrating populations orchestrate early inflammation and may contribute to airway pathogenesis, we cannot formally make this link. However, this model is consistent with recent data by Ren et al. [583], who observed a significant loss of MARCO expression in BAL-resident myeloid populations of patients with severe COVID-19 relative to those with moderate disease, similar to our observations, in which the appearance of infiltrating macrophages diluted the population of MARCO+ macrophages [583]. Those observations, taken together with our data, suggest that the inflammatory macrophage

phenotype we identify here may be preferentially retained in the lower airway of patients with severe COVID-19. Additionally, we demonstrated that *in vivo* treatment with the JAK1/2 inhibitor baricitinib, which has demonstrated efficacy in reducing severe disease, was able to virtually abrogate the recruitment of these inflammatory macrophages into the airway, providing an additional mechanistic link with the development of COVID-19-related pathogenesis.

In addition to inflammatory cytokines, we observed that the infiltrating macrophage subsets produced high levels of IL10, and were enriched in IL10 signaling pathways. Lung IM's are considered to be a "professional IL10-producing cell" producing IL10 at both a steady state and in response to innate stimuli (LPS, unmethylated CpGs) [(584)]. The majority of data to date has demonstrated an immunoregulatory, protective role for IMs in murine models of asthma, lung fibrosis, and allergen induced inflammation [(573)]. However, while the pro-inflammatory potential of IMs has been relatively understudied, they have been demonstrated to be efficient at producing IL6 and TNF in response to TLR ligands [(585)]. Given our observations of high IL10 production in infiltrating macrophages, we cannot exclude a potential immunoregulatory role for this subset, and indeed, it presents an interesting hypothesis in which the balance of infiltrating IM vs TREM2+ macrophages into the bronchoalveolar space determines the pathogenic outcome of SARS-CoV-2 infection. Lastly, recent publications have reported that lung IMs may be comprised of two, or even three, functionally distinct populations, defined by an axis of expression of Lyve1, MHC, CD169, and CD11c [(573-576)]. We did not observe separate clustering amongst BAL IMs, nor differential expression amongst these markers, and further work is needed to understand the congruency of macaque macrophage subsets with those identified in the murine model.

We observed a very rapid and robust induction of the Type I IFN pathway at 1-2dpi, characterized by elevated pDCs in the airway and blood, IFNA and IFNB transcripts and protein, upregulated

ISGs, and increased granzyme B in NK cells. The Type I IFN response in SARS-CoV-2 infection has been intensely studied: in vitro infection of airway epithelial cells have consistently resulted in a muted ISG response [430], and patients developing severe COVID-19 have been reported to have higher incidence of mutations in IFN response genes, or elevated levels of autoantibodies against IFN-response genes (reviewed in [424, 425, 561, 586-591]). Our data, in which the IFN response peaked at 2dpi and had largely abated by 10/11dpi, provides well defined kinetics of the ISG response, and similar observations have been reported in other NHP studies [568, 569]. The rapid and short-lived nature of the IFN response underscores the difficulty in interpreting the IFN response in clinical samples.

Our multiparametric analyses demonstrated an increase of pDCs at 2dpi that coincided with the peak of ISG production, IFNA/B detection, and NK cell activation, thus implicating pDCs as the primary cell orchestrating the IFN response in the lower airway. We had previously observed a reduction in peripheral blood pDCs frequencies and activity in human SARS-CoV-2 infection [532], and other have reported signatures of pDCs apoptosis that predicted lower IFN-I responses [592]. Taken in the context of these clinical findings, our observation of pDC accumulation in the BAL indicates that they undergo rapid mobilization from the blood to the lower airway, and this suggests they likely drive early protective innate immune responses. However, pDCs may also contribute to pathological inflammation; and future interventional studies targeting the pDC/IFN axis in animal models will be necessary to test these hypotheses.

In our prior study, we demonstrated the ability of baricitinib to block airway pro-inflammatory cytokine production in SARS-CoV-2-infected RMs while preserving Type I IFN responses [329]. Here, we extended these findings to demonstrate that baricitinib blocked the influx of inflammatory macrophages into the bronchoalveolar space. These data adds to our mechanistic understanding

of the action of baricitinib, and provide a potential explanation for the disparity of baricitinib's impact on IFN vs IL6/TNF signaling when considering the timing of the drug administration. We administered baricitinib at 2dpi, after the peak influx of pDCs, but before the likely appearance of the APOBEC3A+ inflammatory macrophages at 3-4dpi. The ongoing ISG response, and suppressed TNF/IL6 response, suggest that the primary mechanism by which baricitinib protects the airway is by blocking recruitment of inflammatory cells to the bronchoalveolar space. In regards to guiding future clinical application of baricitinib, our data suggest that timing is critical, and would favor earlier drug administration.

Our study had some limitations; first, while the RM/SARS-CoV-2 model has rapidly been adopted by several groups for pre-clinical testing of anti-COVID drugs and vaccines, no group has demonstrated overt, reproducible symptomatic disease [564]. Thus, linking early immunological events to the development of severe COVID-19 requires validation in human studies, such as the observations of reduced MARCO expression in the airway myeloid populations of severe COVID-19 patients noted above [583]. Another drawback was the relatively low power of our study. While our observations at 0, 1, and 2dpi were n = 8, we were limited to n = 4 for day 4-10 observations. However, it should be noted that there was no lack of statistical power for our key observations.

While the global vaccine rollout has made great strides to reduce the transmission and severity of SARS-CoV-2 infection, millions of people remain vulnerable. Understanding the early events of SARS-CoV-2 infection, and the mechanisms by which clinically approved drugs afford protection, remains a global priority. In this study, we have identified a novel population of inflammatory myeloid cells that are responsible for the preponderance of airway inflammation in acute SARS-CoV-2 infection. We also demonstrated that treatment with the emergency authorized JAK1/2 inhibitor baricitinib in combination with remdesivir, blocked infiltration of these

inflammatory cells into the alveolar space. These data identify both a key druggable target (airway infiltrating macrophages), and an efficacious mechanism by which to lower airway inflammation, and should prove useful for identifying additional drugs to reduce the incidence and mortality of severe COVID-19 disease.

Materials and Methods

Animal and SARS-CoV-2 infections

The animal care facilities at YNPRC are accredited by the Association for Assessment and Accreditation of Laboratory Animal Care (AAALAC) as well as the U.S. Department of Agriculture (USDA). Emory University's Institutional Animal Care and Use Committee (IACUC) reviewed and approved all animal experiments under permit PROTO202000035. All procedures were performed as per the institutional regulations and guidelines set forth by the NIH's Guide for the Care and Use of Laboratory Animals (8^{th} edition) and were conducted under anesthesia and appropriate follow-up pain management to minimize animal suffering. Eight (4 female, 4 males, aged >11 yrs) specific-pathogen-free Indian-origin rhesus macaques were infected via intranasal and intratracheal routes with 1.1×10^6 plaque forming units (PFU) SARS-CoV-2 (see SI for details), as previously described [329] and were maintained in the ABSL3 at YNPRC. The processing of nasopharyngeal swabs, BAL and mononuclear cells was performed as described previously [329].

Immunophenotyping and flow cytometric purification of RM pulmonary macrophages

23-parameter flow cytometric analysis was perform on fresh PBMCs and BAL mononuclear cells from SARS-CoV-2 infected RMs as described previously [329]. For purification of

$CD163^{+}CD206^{+}$ (AM), $CD163^{+}CD206^{-}$ (IM) cells, cryopreserved single-cell lung suspensions from RMs were stained with BD CD163(GHI/61), CD206(19.2)(BD Biosciences), and purified using BD FACSAria in the Regional Biocontainment Laboratory at the University of Pittsburgh.

Bulk and sc-RNA-Seq Library and sequencing

The data for -5dpi, 2dpi and 4dpi for bulk BAL samples was obtained from our previous study [329]. Here we expanded our study to include 7dpi and 10dpi/11dpi samples for BAL and -5dpi, 1dpi, 2dpi, 4dpi, 6dpi, 7dpi, 8dpi and 10/11dpi for PBMC. Cell suspensions were prepared in BSL3, for bulk RNA-Seq, 250,000 cells (PBMCs) or 100,000 cells (BAL) were lysed directly into 700 ul of QIAzol reagent. Libraries were prepared as described previously [329] and sequenced on an Illumina NovaSeq6000 at 100SR, yielding 20-25 million reads per sample. For sc-RNA-Seq, approximately 30,000 cells were loaded onto a 10X Chromium Controller in a BSL3 and single cells were partitioned into droplets using Chromium NextGEM Single Cell 50 Library & Gel Bead kits(10X Genomics, Pleasanton, CA). cDNA was amplified and libraries were prepared for sequencing according to manufacturer instructions. Gene expression libraries were sequenced as paired-end 26x91 reads targeting 50,000 reads per cell.

scRNA-Seq and bulk RNA-Seq analysis

The filtered count matrices for BAL were obtained from [329]. The Seurat library v4.0.4 [578] was used to perform the analysis (see SI for details). The macrophages/monocytes from BAL samples were annotated into subsets using two approaches – (i) mapping to macrophages/monocytes from lung reference using Seurat and (ii) using bulk sorted cells as reference with SingleR [555]. The 10X lung scRNA-seq data from three uninfected macaque was obtained from a published study (NCBI GEO: GSE149758) [577]. The SingleR library was used for cell classification with the

BluePrintEncodeData reference. Regularized log counts obtained from DESeq2 for bulk sorted IM and AM were used as reference to annotate the cells from BAL samples using SingleR with default parameters. Bulk RNA-Seq analysis was performed as previously described [329].

Mesoscale cytokine analysis.

U-PLEX assays (Meso Scale MULTI-ARRAY Technology) were used for plasma and BALF cytokine detection according to manufacturer's instructions, using 25 microliters as input.

Data and materials availability:

Source data supporting this work are available from the corresponding author upon reasonable request.

Code availability:

The scripts used for analysis are available at https://github.com/BosingerLab/NHP_COVID-19_2.

Viral Stocks

The viral stocks used for infecting RM were previously described[329]. SARS-CoV-2 (NR-52281: BEI Resources, Manassas, VA; USA-WA/2020, Lot no. 70033175) was passaged on Vero E6 cell line (African Green Monkey Kidney cell line; CRL-1586, ATCC) at a MOI of 0.01. SARS-CoV-2 was propagated and titrated by $TCID_{50}$ method followed by storage of aliquots at -80°C until further use. The infectious dose delivered was determined by back titration of viral stocks via plaque assay. The virus stock was sequenced to confirm the presence of furin cleavage motif. The viral stocks used had less than 6% of genomes with a mutation that may abrogate furin cleavage.

Determination of viral load RNA

The swabs were kept in 1mL of Viral Transport Medium (VTM-1L, Labscoop, LLC). The viral RNA was extracted from fresh specimens of nasopharyngeal (NP) swabs, throat swabs, and BAL manually using the QiaAmp Viral RNA mini kit as per the manufacturer's protocol. For genomic RNA, N2 primer and probe set designed by the CDC for their diagnostic algorithm: CoV2-N2-F: 5'-TTACAAACATTGGCCGCAAA-3', CoV2-N2-R: 5'-GCGCGACATTCCGAAGAA-3', and CoV2-N2-Pr: 5'-FAM-ACAATTTGCCCCCAGCGCTTCAG-BHQ-3'[547] were used for quantitative PCR (qPCR). For sub-genomic RNA, the primer and probe sequences for E gene subgenomic mRNA transcript[593] were used: SGMRNA-E-F: 5'-CGATCTCTTGTAGATCTGTTCTC-3', SGMRNA-E-R: 5'-ATATTGCAGCAGTACGCACACA-3', and SGMRNA-E-Pr: 5'-FAM-ACACTAGCCATCCTTACTGCGCTTCG-3'. The qPCR reactions were performed with the TaqMan Fast Virus 1-step Master Mix using the manufacturer's cycling conditions, 200nM of each primer, and 125nM of the probe in duplicate. The limit of detection in this assay was 257 copies per mL of VTM/plasma/BAL. The CDC RNase P p30 subunit qPCR, modified for rhesus macaque specific polymorphisms, was used to verify sample quality using the following primer and probe sequences: RM-RPP30-F 5'-AGACTTGGACGTGCGAGCG-3', RM-RPP30-R 5'-GAGCCGCTGTCTCCACAAGT-3', and RPP30-Pr 5'-FAM-TTCTGACCTGAAGGCTCTGCGCG-BHQ1-3'. The RNA integrity and sample quality was verified by running a single well from each extraction.

Tissue processing

NP swabs were collected under anesthesia by using a clean rayon-tipped swab (ThermoFischer Scientific, BactiSwab NPG, R12300) placed approximately 2-3cm into the nares. Oropharyneal swabs were collected under anesthesia using polyester tipped swabs (Puritan Standard Polyester Tipped applicator, polystyrene handle, 25-806 2PD, VWR International) to streak the tonsils and back of throat bilaterally (throat/pharyngeal). The swabs were dipped in 1 mL viral transport media

(Viral transport Media, VTM-1L, Labscoop, LLC) and vortexed for 30 sec, and the eluate was collected.

To collect BAL, a fiberoptic bronchoscope (Olympus BF-XP190 EVIS EXERA III ULTRA SLM BRNCH and BF-P190 EVIS EXERA 4.1mm) was manipulated into the trachea, directed into the primary bronchus, and secured into a distal subsegmental bronchus upon which 35-50 mL of normal saline (0.9% NaCl) was administered into the bronchus and re-aspirated to obtain a minimum of 20ml of lavage fluid. BAL was filtered through a 70μm cell strainer.

Mononuclear cells were counted for viability using a Countess II Automated Cell Counter (Thermo Fisher) with trypan blue stain and were cryo-preserved in aliquots of up to $2x10^7$ cells in 10% DMSO in heat-inactivated FBS. Whole tissue segments (0.5 cm^3) were snap frozen dry, or stored in RNAlater (Qiagen), or Nuclisens lysis buffer (Biomerieux) for analyses of compound distribution, RNA-seq, and tissue viral quantification, respectively.

Immunophenotyping

The following mAbs were used for the phenotyping of innate immune cells in whole blood (500 μL), as described in[339], and mononuclear cells (10^6 cells) derived from BAL: anti-CD20-BB700 (clone 2H7; 2.5 μL; cat. # 745889), anti-Ki-67-BV480 (clone B56; 5 μL; cat. # 566109), anti-CD14-BV605 (clone M5E2; 2.5 μL; cat. # 564054), anti-CD56-BV711 (clone B159; 2.5 μL; cat. # 740781), anti-CD115-BV750 (clone 9-4D2-1E4; 2.5 μL; cat. # 747093), anti-CD3-BUV395 (clone SP34-2; 2.5 μL; cat. # 564117), anti-CD8-BUV496 (clone RPA-T8; 2.5 μL; cat. # 612942), anti-CD45-BUV563 (clone D058-1283; 2.5 μL; cat. # 741414), anti-CCR2-BUV661 (clone LS132.1D9; 2.5 μL; cat. # 750472), anti-CD16-BUV737 (clone 3G8; 2.5 μL; cat. # 564434), anti-CD69-BUV805 (clone FN50; 2.5 μL; cat. # 748763), and Fixable Viability Stain 700 (2 μL; cat. # 564997) all from BD Biosciences; anti-CD38-FITC (clone AT1; 2.5 μL; cat. # 60131FI) from STEMCELL Technologies; anti-CD161-BV421 (clone HP-3G10; 5 μL; cat. # 339914), anti-HLA-DR-BV650

(clone L243; 5 μL; cat. # 307650), anti-CD11c-BV785 (clone 3.9; 5 μL; cat. # 301644), anti-CD11b-PE (clone ICRF44; 2.5 μL; cat. # 301306), and anti-CD123-APC-Fire750 (clone 315; 2.5 μL; cat. # 306042) all from Biolegend; anti-GranzymeB-PE-TexasRed (clone GB11; 2.5 μL; cat. # GRB17) from Thermo Fisher; anti-CD66abce-PE-Vio770 (clone TET2; 1 μL; cat. # 130-119-849) from Miltenyi Biotec; and anti-CD27-PE-Cy5 (clone 1A4CD27; 2.5 μL; cat. # 6607107) and anti-NKG2A-APC (clone Z199; 5 μL; cat. # A60797) from Beckman Coulter. The sorting strategy is show in **Fig. S1**.

Bulk RNA-Seq library & sequencing

RNA was isolated using RNeasy Mini or Micro kits (QIAGEN) with on-column DNase digestion. The quality of RNA was determined using an Agilent Bioanalyzer and the cDNA synthesis was carried out using the total RNA with Clontech SMARTSeq v4 Ultra Low Input RNA kit (Takara Bio) as per the manufacturer's instructions. Dual-indexed bar codes were appended to the amplified cDNA after fragmenting using the NexteraXT DNA Library Preparation kit (Illumina). Agilent 4200 TapeStation was used to validate the libraries by capillary electrophoresis and the libraries were pooled at equimolar concentrations,

Bulk RNA-Seq analysis

The STAR index was built by combining genome sequences for Macaca mulatta (Mmul10 Ensembl release 100), SARS-CoV2 (strain MN985325.1 - NCBI) and ERCC sequences as described previously[329]. The ReadsPerGene files were used to generate counts in the htseq format and were imported in DESeq2[550] using the DESeqDataSetFromHTSeqCount function.

The PBMC and BAL samples were analyzed separately and the design used was: ~ Group + Subject + Timepoint where Group distinguished between samples that were untreated or treated with baricitinib during the time course. Differentially expressed genes for BAL and PBMC were

determined using a threshold of padj < 0.05, fold-change > 2 and filtering out lowly expressed genes where all of the samples at a particular timepoint were required to have detectable expression by normalized reads > 0 for that gene.

In order to obtain references for assigning cell types in single-cell data, bulk RNA-Seq data of interstitial (IM) and alveolar macrophages (AM) from three uninfected rhesus macaques was analyzed using DESeq2. The regularized log expression values were obtained using the rlog function with the parameters blind = FALSE and filtType = "parametric." The significant genes were filtered based on following criteria: padj < 0.05; fold-change > 2 and normalized mean expression > 5000 for either IM or AM samples.

The input for GSEA was the regularized log expression values obtained from DESeq2. The following gene sets were used for GSEA[531] analysis: Hallmark and Canonical pathways (MsigDB), NHP ISGs[82] and Rheumatoid arthritis (KEGG map05323). GSEA was run with default parameters with the permutation type set to gene_set. Volcano plots of differential expression at each timepoint were generated with Enhanced Volcano R library[594]. The regularized log expression values from DESeq2 were used to generate heatmaps using the Complex Heatmap R library[551].

scRNA-Seq analysis

For each BAL sample from SARS-CoV2 infected rhesus macaque, the count matrix was filtered to include only the protein coding genes. Genes encoded on Y chromosome, mitochondrial genes, RPS and RPL genes, B-cell receptor and T-cell receptor genes, and HBB were filtered out. The following parameters were used to filter cells: (i) nFeature_RNA >=200 & <=4000, (ii) % of HBB gene < 10, (iii) % of mitochondrial genes < 20, (iv) % of RPS/RPL genes < 30 and (v) log10(nFeature_RNA) / log10(nCount_RNA) >= 0.8. The number of cells from each sample that passed QC metrics are included in Supplementary File 3. All the BAL samples from each animal at -5dpi and 4dpi were then integrated as per the Seurat integration pipeline[595] after normalizing

the samples using SCTransform method. The first 30 dimensions were used with RunUMAP and FindNeighbors functions. For getting the subset of macrophages/monocytes, the largest cluster primarily comprised of macrophages/monocytes annotated by SingleR (BluePrintEncode database) was selected. Cells that were annotated as another cell type in this cluster were filtered out. The macrophages/monocytes from all BAL samples were then split into individual samples, normalized using SCTransform method and then integrated again using 30 dimensions.

The three lung samples from uninfected rhesus macaques were processed similarly. The following parameters were used to filter cells: (i) nFeature_RNA >=200 & <=4000, (iii) % of mitochondrial genes < 20, (iv) % of RPS/RPL genes < 50 and (v) log10(nFeature_RNA) / log10(nCount_RNA) >= 0.8. The samples were normalized using SCTransform and integrated. The first 40 dimensions were used for the initial clustering. The macrophage/monocyte cells as annotated by SingleR were then selected, split into individual samples and integrated again using 30 dimensions. Louvain clustering resulted in four clusters which were annotates based on the expression of marker genes. This integrated dataset served as the reference to map the macrophages/monocytes from SARS-CoV2 infected BAL using the FindTransferAnchors and MapQuery with reference.reduction set to pca and umap as the reduction.model. The BAL samples were also annotated using SingleR library with the IM and AM bulk sorted cells as reference.

Chapter Four Figures

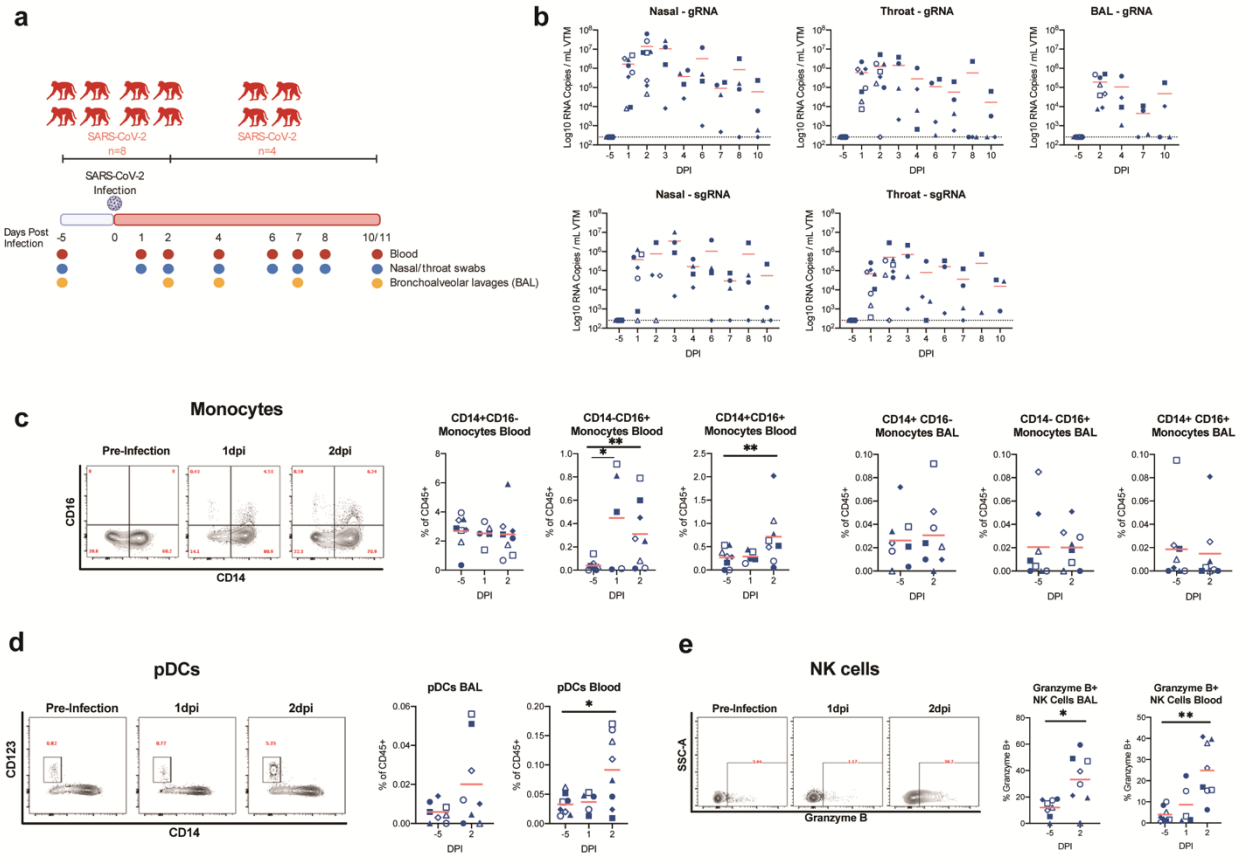

Figure 4.1. Early expansion of inflammatory cells in the blood following infection with SARS-CoV-2. (**a**) Study design; 8 RMs were infected intranasally and intratracheally with SARS-CoV-2 and tracked longitudinally. Baricitinib was administered daily to 4 RMs starting at 2dpi and the remaining 4 RMs were untreated. (**b**) After SARS-CoV-2 inoculation, nasal, throat, and bronchoalveolar lavages (BAL) were collected and viral loads were quantified by qRT-PCR for total gRNA and sgRNA. (**c**) Longitudinal levels of monocytes within BAL and blood depicted as a % of CD45+ cells. (d) Longitudinal levels of plasmacytoid dendritic cells (pDCs) within BAL and blood depicted as a % of CD45+ cells. (**e**) Longitudinal levels of NK cells expressing Granzyme B in BAL and blood. Open symbols represent RMs that received baricitinib treatment starting 2dpi and filled symbols represent untreated RMs. The red bars represent the mean. Statistical analysis

was performed using one-tailed Wilcoxon signed-rank test comparing each timepoint to -5dpi. * p-value < 0.05, ** p-value < 0.01.

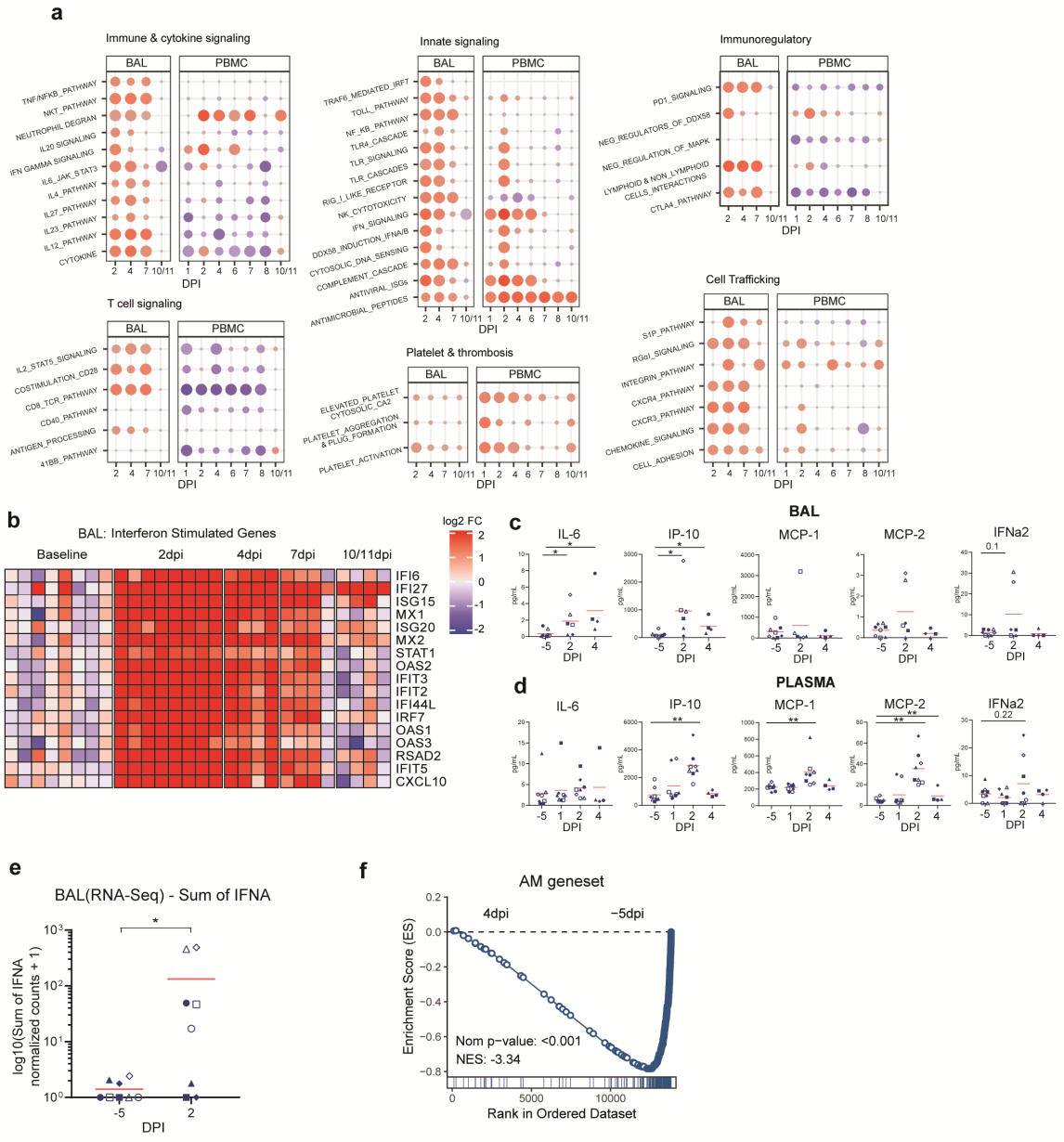

Figure 4.2. Early pro-inflammatory and ISG response observed in airways and peripheral blood by bulk transcriptomics. (a) Dot plots showing normalized enrichment scores and nominal p-values for gene sets. Enrichment is indicated by dot color (red: positively enriched vs -5dpi; blue: negatively enriched), dot size indicates significance. **(b)** Heatmap of longitudinal responses for the ISG gene set. The color scale indicates log2 expression relative to the median

of the -5dpi samples. **(c)** Cytokines evaluation (Mesoscale) in BALF and **(d)** Plasma; only significant cytokines are shown. **(e)** Sum of normalized expression of all IFNA genes in BAL. **(f)** GSEA enrichment plot showing negative enrichment for AM gene signature (derived from SingleR) when comparing bulk BAL RNA-Seq samples from 4dpi to -5dpi. The red bar represents the mean. Statistical analysis was performed using one-tailed Wilcoxon signed-rank test comparing each timepoint to -5dpi. * p-value < 0.05, ** p-value < 0.01.

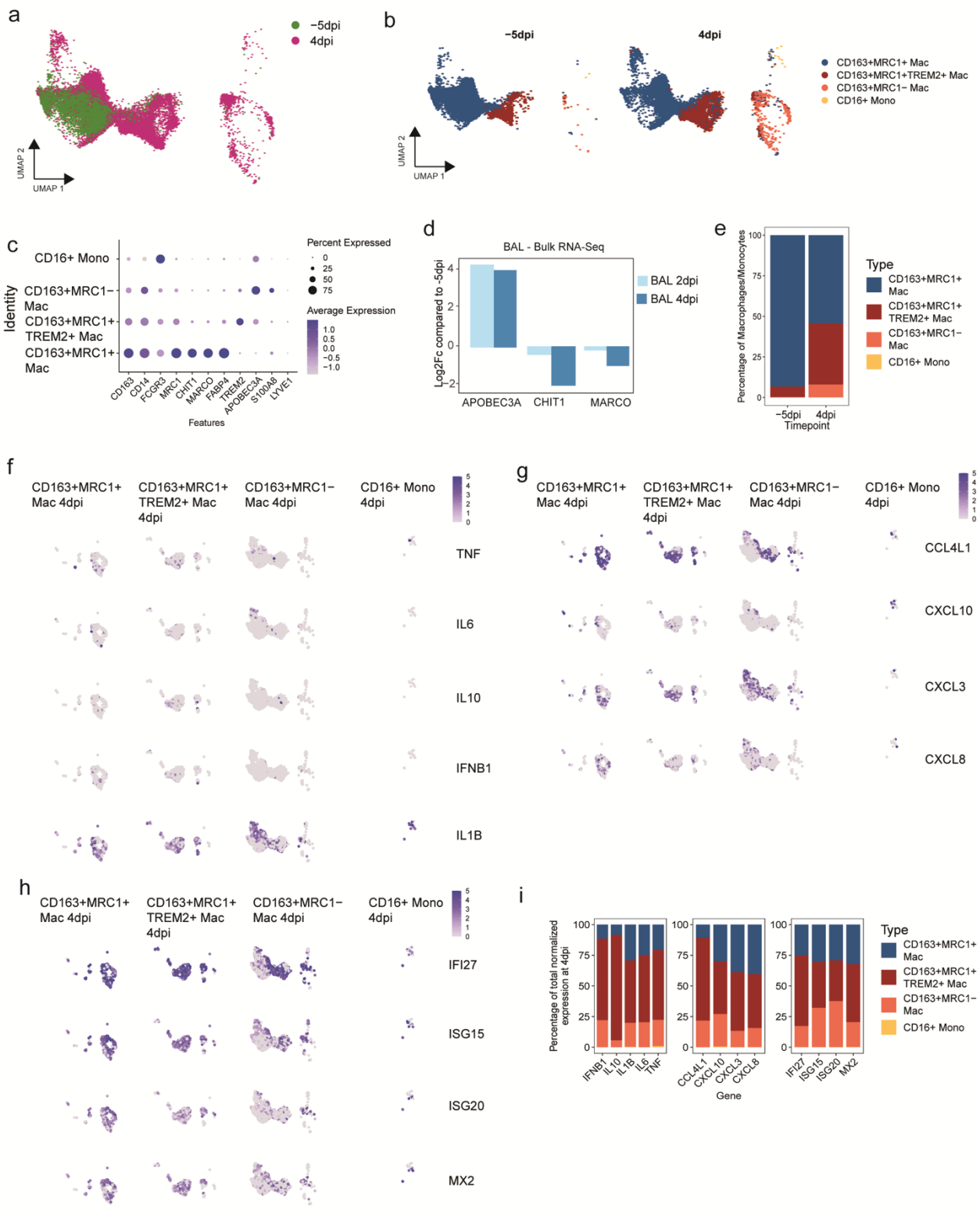
a
−5dpi
4dpi
UMAP 2
UMAP 1
b
−5dpi
4dpi
CD163+MRC1+ Mac
CD163+MRC1+TREM2+ Mac
CD163+MRC1− Mac
CD16+ Mono
c
Identity
CD16+ Mono
CD163+MRC1− Mac
CD163+MRC1+ TREM2+ Mac
CD163+MRC1+ Mac
CD163 CD14 FCGR3 MRC1 CHIT1 MARCO FABP4 TREM2 APOBEC3A S100A8 LYVE1
Features
Percent Expressed
Average Expression
d
BAL - Bulk RNA-Seq
Log2Fc compared to -5dpi
BAL 2dpi
BAL 4dpi
APOBEC3A CHIT1 MARCO
e
Percentage of Macrophages/Monocytes
−5dpi 4dpi
Timepoint
Type
CD163+MRC1+ Mac
CD163+MRC1+ TREM2+ Mac
CD163+MRC1− Mac
CD16+ Mono
f
CD163+MRC1+ Mac 4dpi
CD163+MRC1+ TREM2+ Mac 4dpi
CD163+MRC1− Mac 4dpi
CD16+ Mono 4dpi
TNF
IL6
IL10
IFNB1
IL1B
g
CCL4L1
CXCL10
CXCL3
CXCL8
h
IFI27
ISG15
ISG20
MX2
i
Percentage of total normalized expression at 4dpi
IFNB1 IL10 IL1B IL6 TNF
CCL4L1 CXCL10 CXCL3 CXCL8
IFI27 ISG15 ISG20 MX2
Gene
Type
CD163+MRC1+ Mac
CD163+MRC1+ TREM2+ Mac
CD163+MRC1− Mac
CD16+ Mono

Figure 4.3. Influx of pro-inflammatory macrophages in BAL (a) Projection of single-cell macrophages/monocytes from -5dpi (green) and 4dpi (magenta) 10X BAL samples obtained from three SARS-CoV2 infected rhesus macaques onto the reference UMAP of lung macrophage/monocytes from uninfected rhesus macaques (NCBI GEO : GSE149758). **(b)** UMAP projections showing the predicted cell type annotations from the uninfected lung reference split by time of sample collection. **(c)** DotPlots showing the expression of marker genes for the different macrophage/monocyte subsets in SARS-CoV2 infected BAL samples **(d)** Log2 fold-changes compared to -5dpi for APOBEC3A, CHIT1 and MARCO in bulk BAL RNA-Seq data. **(e)** Percentage of a given subset out of all macrophage/monocyte subsets at -5dpi and 4dpi from all three animals **(f,g,h)** FeaturePlots showing the expression of selected pro-inflammatory cytokines (f), chemokines (g) and ISG (h) in different macrophage/monocyte subsets at 4 dpi. **(i)** Contribution of each macrophage/monocyte subset towards the production of the pro-inflammatory genes and ISG. The percentage contribution was calculated by dividing the sum of normalized expression of a given gene in a macrophage/monocyte subset by the sum of the normalized expression of the gene in all macrophage/monocyte subsets.

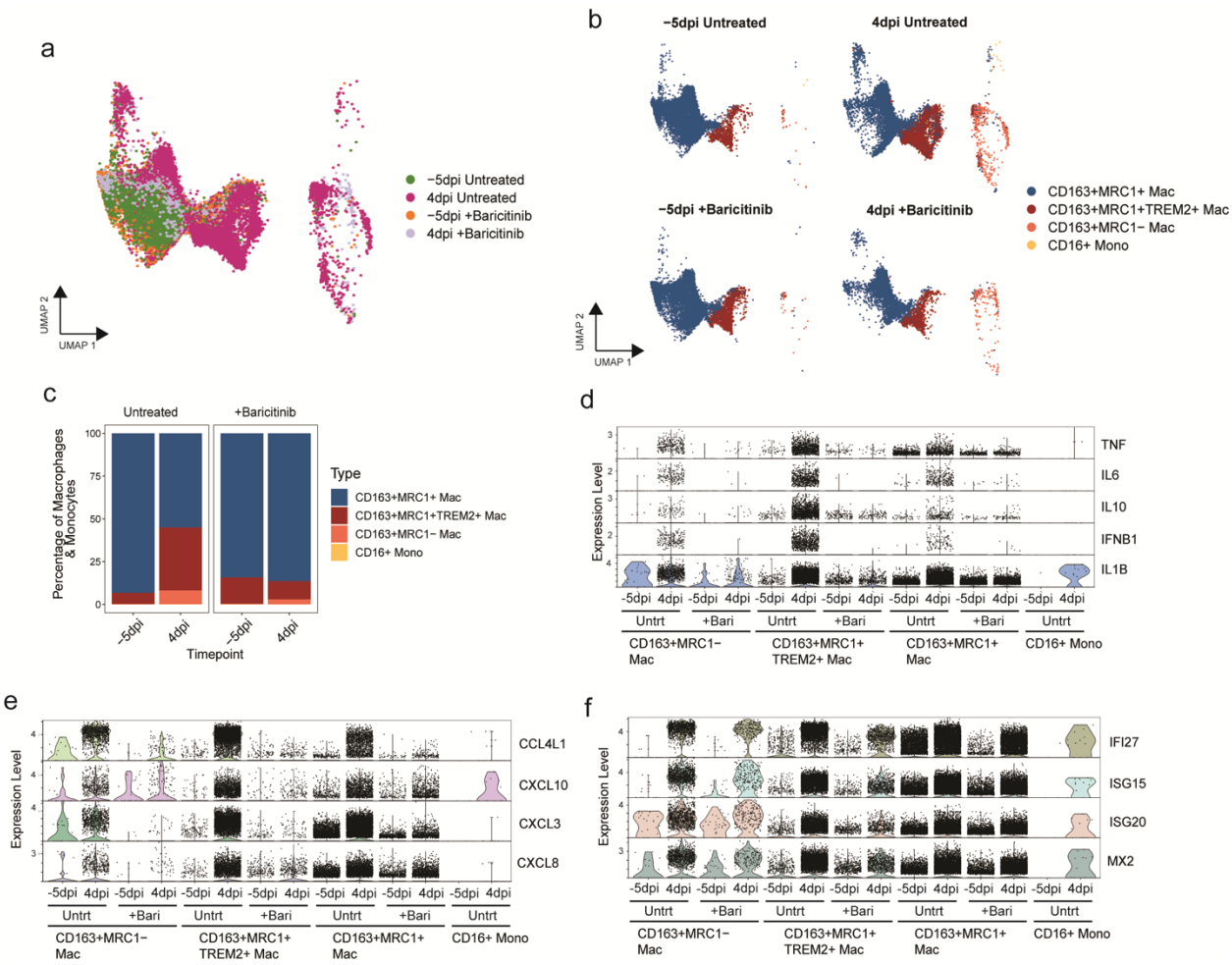

Figure 4.4. Baricitinib reduced the influx of pro-inflammatory macrophages in addition to the pro-inflammatory gene expression profile. **(a)** Projection of macrophages/monocytes from -5dpi and 4dpi 10X BAL samples from three untreated and two baricitinib treated rhesus macaques on the reference UMAP of uninfected lung macrophages/monocytes (NCBI GEO: GSE149758) **(b)** UMAP split by treatment and timepoint showing predicted cells annotations based on mapping to the reference lung macrophages/monocytes **(c)** Percentage of a given macrophage/monocyte subset of all the macrophages/monocytes in the BAL samples. **(d)** Violin plots showing expression of pro-inflammatory cytokines, chemokines and ISG in the different macrophage/monocyte subsets in BAL 10X samples from baricitinib treated and untreated samples.

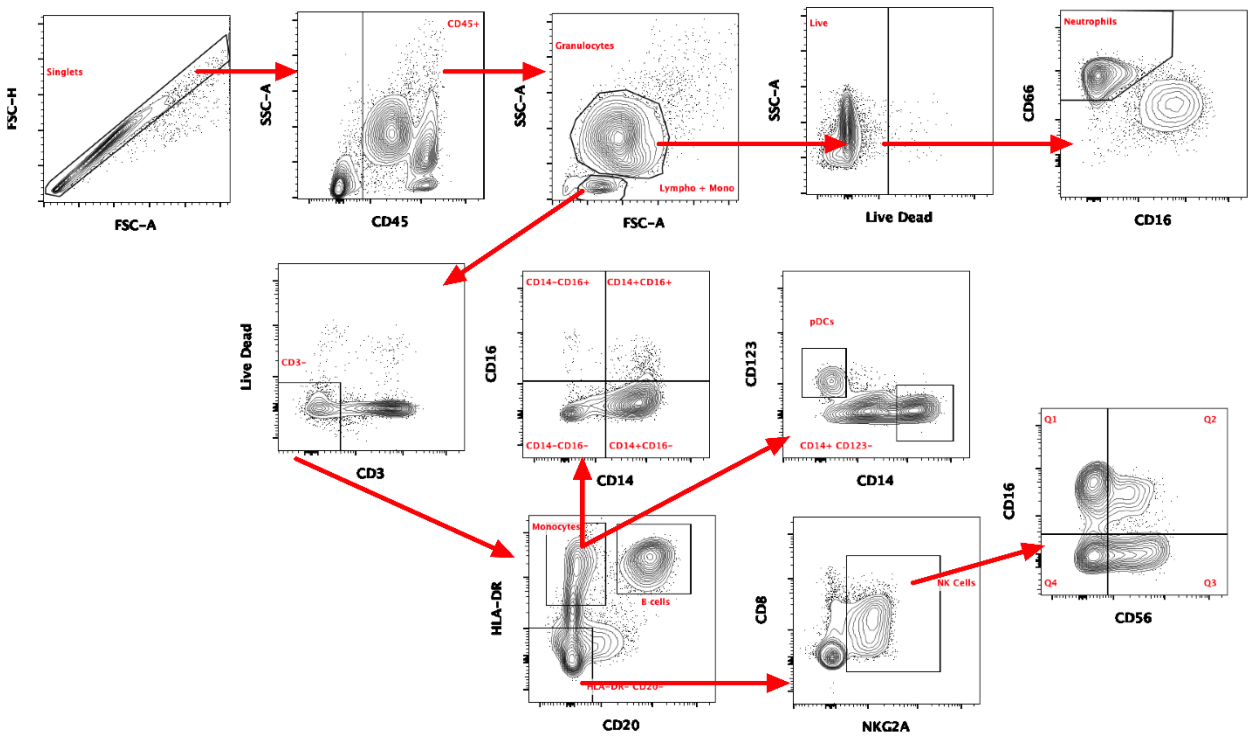

Figure 4.S1. Flow sorting strategy for different immune cell populations.

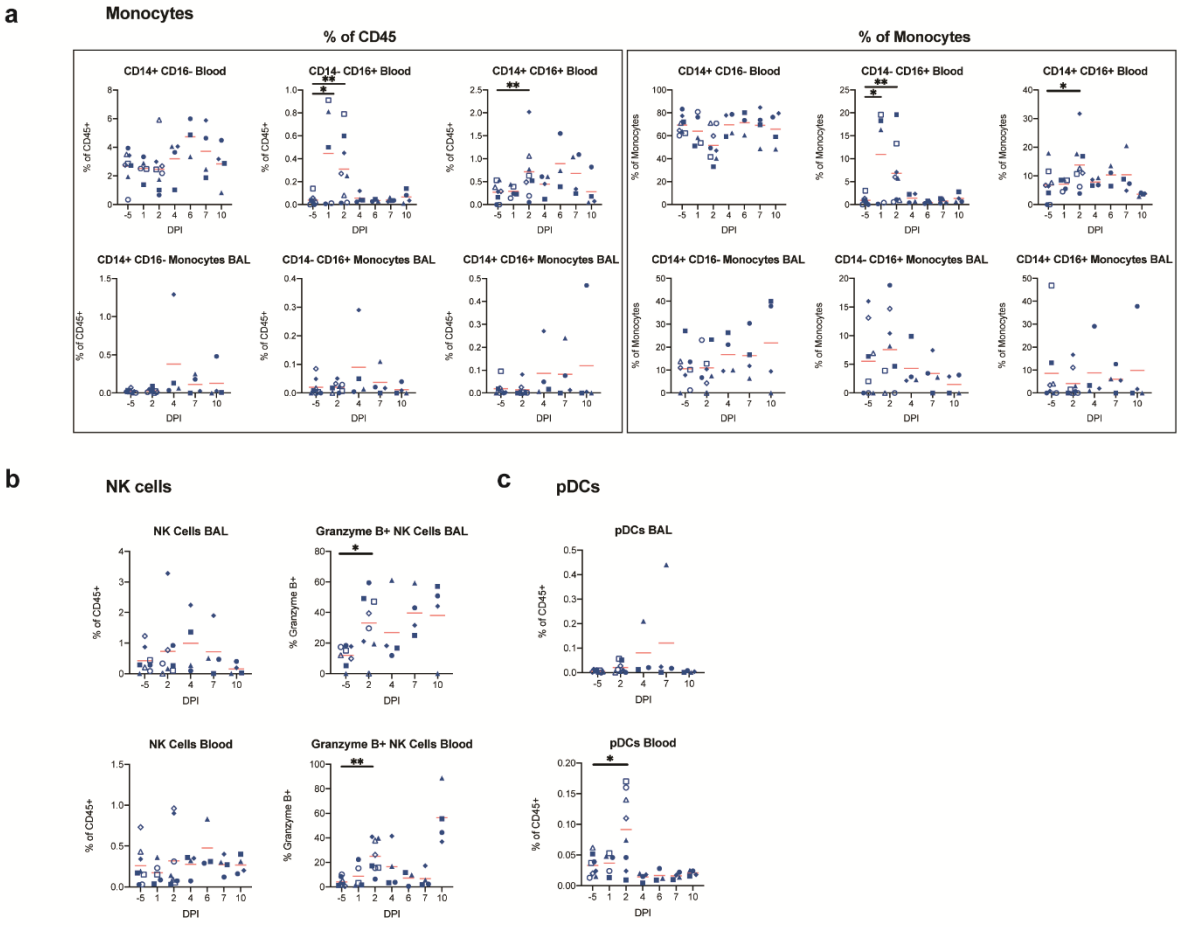

Figure 4.S2. Longitudinal flow cytometric analysis in BAL and blood following SARS-CoV-2 infection. (**A**) Longitudinal levels of monocytes within BAL and blood depicted as the percentage of CD45+ cells and % of monocytes ($CD3^-$ $CD20^-$ $HLA\text{-}DR^+$). (**B**) Longitudinal levels of NK cells as a percentage of CD45+ cells and frequency of NK cells expressing Granzyme B in BAL and blood. (**C**) Longitudinal levels of plasmacytoid dendritic cells (pDCs) within BAL and blood depicted as a % of CD45+ cells. The red bars represent the mean. Statistical analysis was performed using one-tailed Wilcoxon signed-rank test comparing each timepoint to -5dpi. * p-value < 0.05, ** p-value < 0.01.

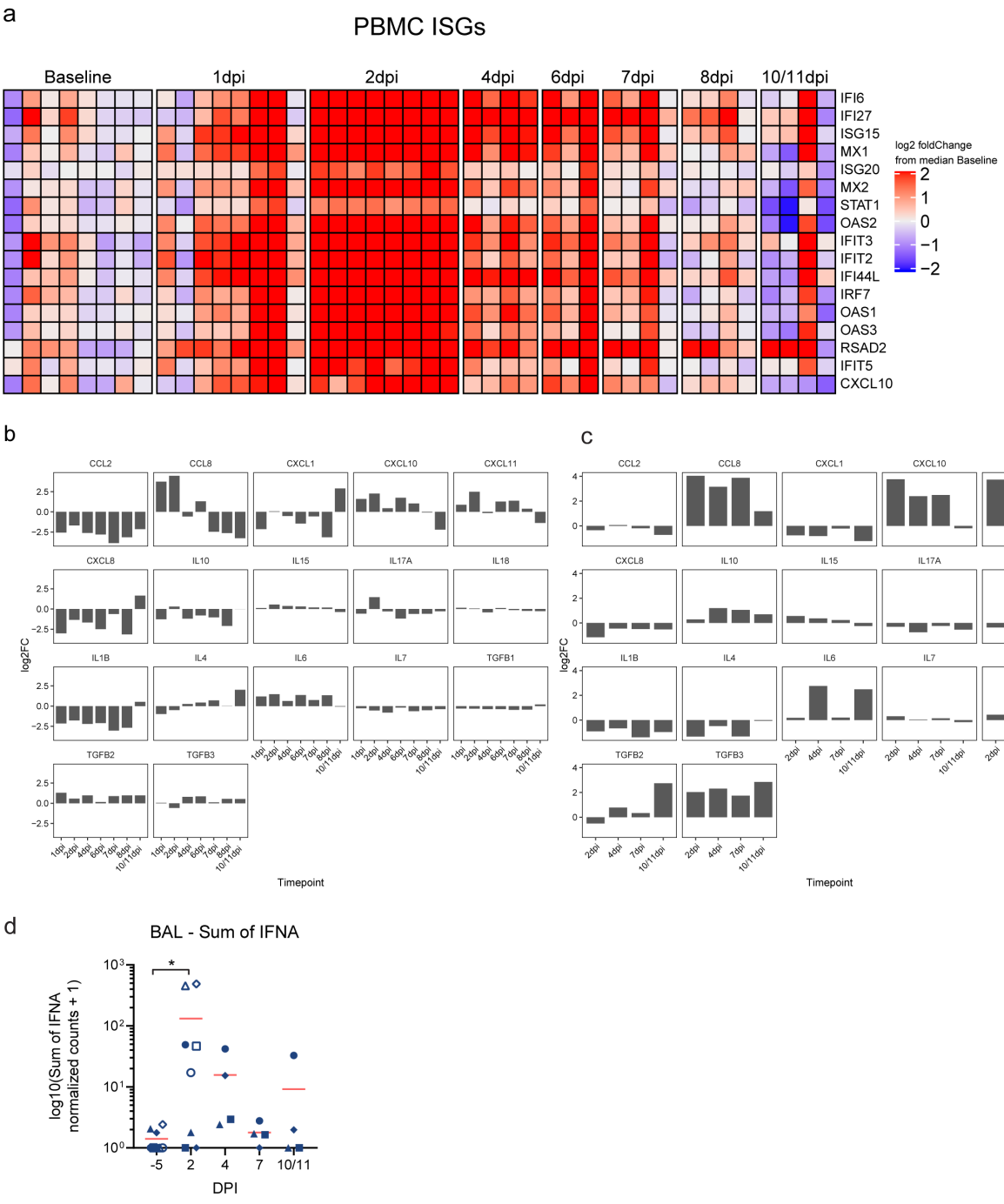

Figure 4.S3. Bulk transcriptomic analysis of airways and peripheral blood. (A) Heatmap showing expression of ISG in PBMC over all sampled time points. The color scale indicates log2 expression relative to the median of -5dpi samples. **(B & C)** Normalized expression of cytokines and chemokines in bulk RNA-Seq in BAL (B) and PBMC (C). **(D)** Sum of normalized expression

of IFNA in longitudinal BAL samples. The red bars represent the mean. Statistical analysis was performed using one-tailed Wilcoxon signed-rank test comparing each timepoint to -5dpi. * p-value < 0.05.

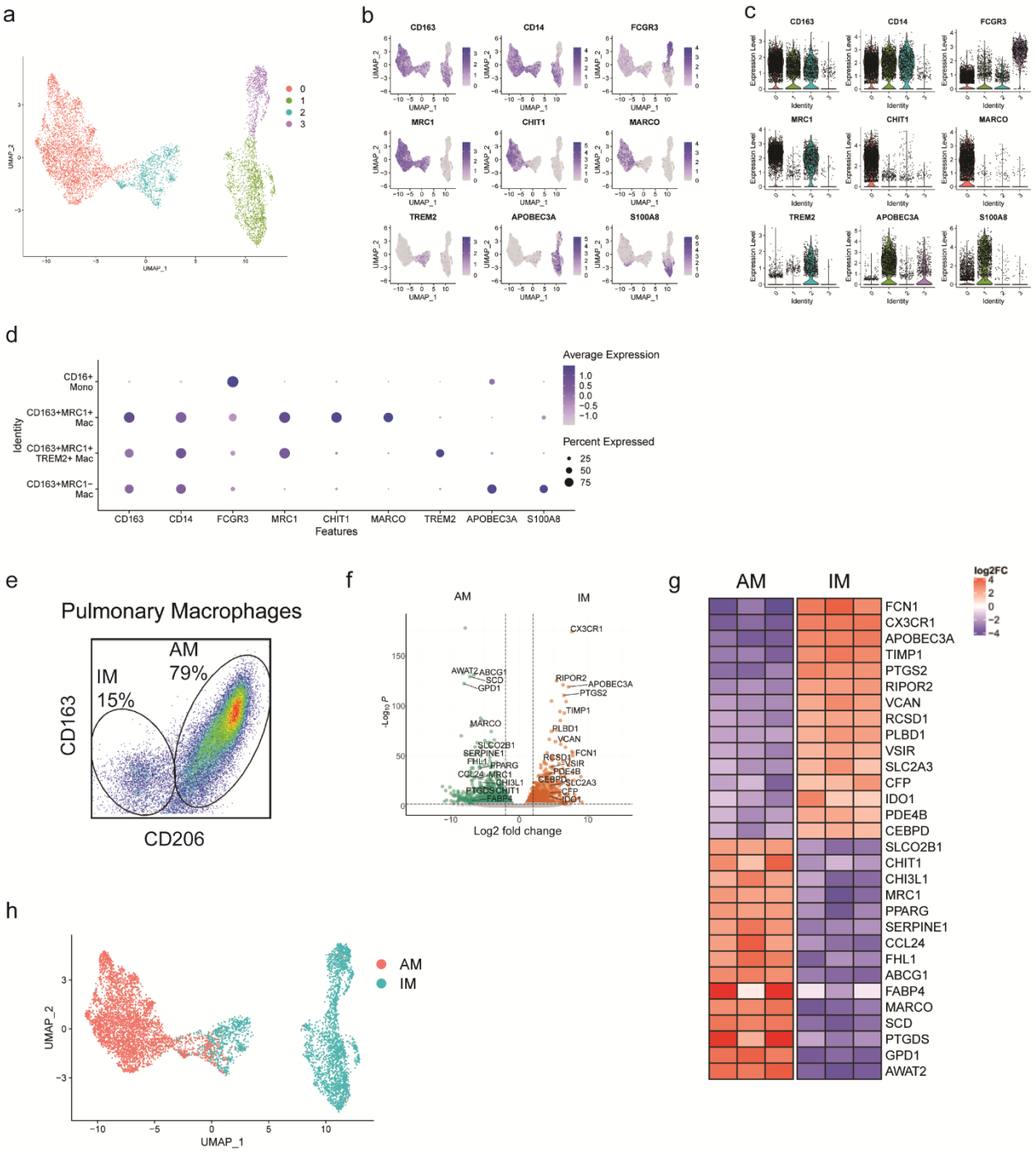
a
b
c
d
e
f
g
h
Pulmonary Macrophages
AM
IM
79%
15%
CD163
CD206
Average Expression
Percent Expressed
Features
Log2 fold change
log2FC
AM
IM
FCN1
CX3CR1
APOBEC3A
TIMP1
PTGS2
RIPOR2
VCAN
RCSD1
PLBD1
VSIR
SLC2A3
CFP
IDO1
PDE4B
CEBPD
SLCO2B1
CHIT1
CHI3L1
MRC1
PPARG
SERPINE1
CCL24
FHL1
ABCG1
FABP4
MARCO
SCD
PTGDS
GPD1
AWAT2

Figure 4.S4. Reference used for annotating macrophage/monocyte subsets. (a) UMAP of macrophages/monocytes from 10X lung samples of three uninfected rhesus macaques (NCBI GEO: GSE149758) showing Louvain clustering. (**b & c**) FeaturePlot (b) and Violin Plots (c) showing the expression of marker genes in the macrophage/monocyte clusters. **(d)** DotPlot showing expression of marker genes for the different monocyte/macrophage subsets as defined previously [577, 579] **(e)** Sorting strategy for interstitial and alveolar macrophages from lungs of three uninfected rhesus macaques **(f)** Volcano plots showing differentially expressed genes for pairwise comparison of alveolar and interstitial macrophages. The thresholds used are an adjusted p-value < 0.05 and a fold change of 2 for alveolar vs interstitial macrophage. Top 15 genes that have a mean normalized expression of at least 5000 for either type have been indicated. **(g)** Heatmap showing the top 15 genes for each subset. The color scale indicates log2 expression relative to the median of all samples. (**h**) UMAP of single-cell 10X lung samples showing SingleR annotations using the bulk sorted cells as reference.

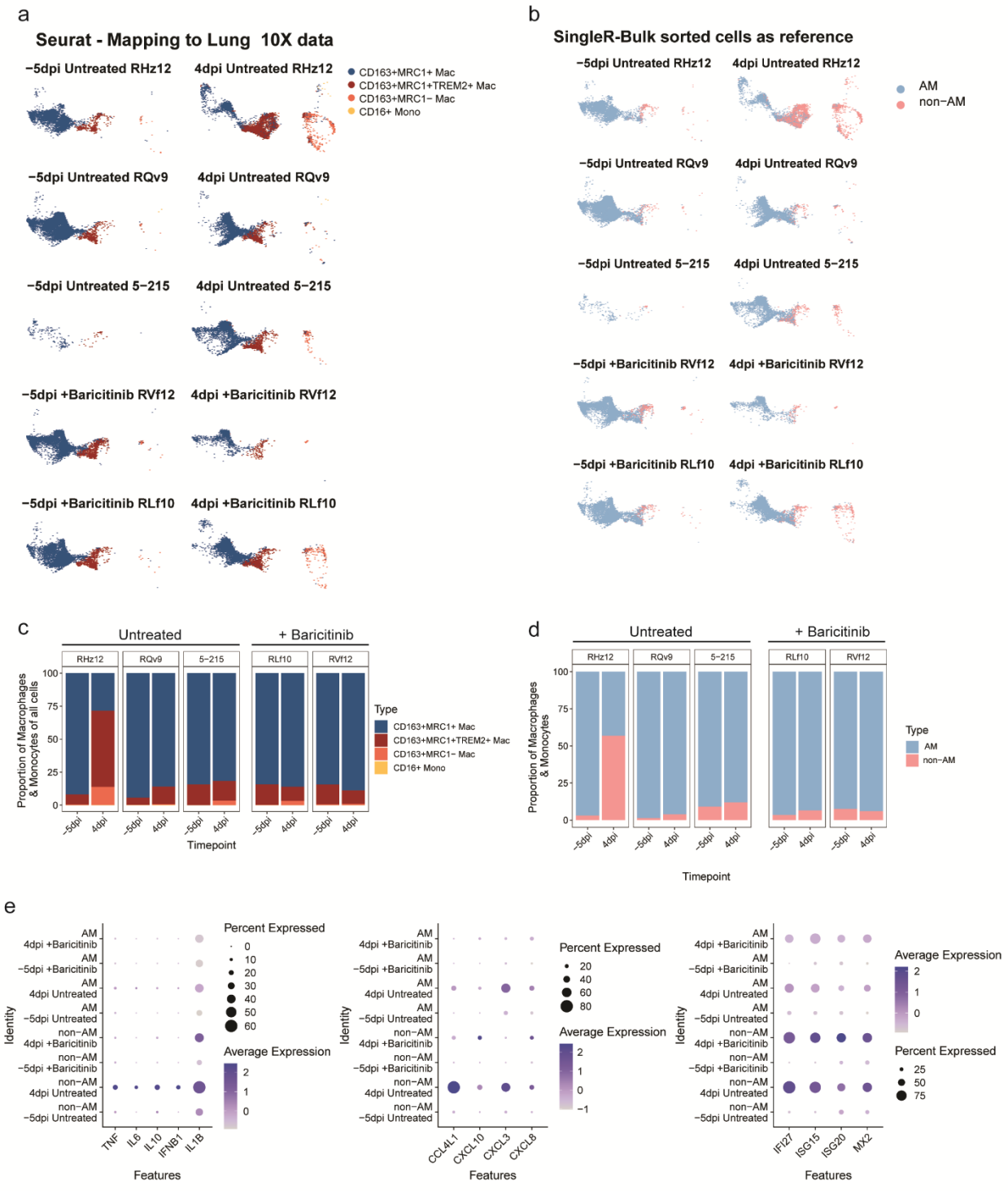

Figure 4.S5. Cell annotation using bulk sorted cells as reference. (a & b) The BAL macrophage/monocytes from SARS-CoV2 infected rhesus macaques (three untreated and two

baricitinib treated) projected on the 10X lung reference macrophages/monocytes UMAP split by each animal and timepoint. (a) Annotations predicted from mapping to 10X lung samples using Seurat (b) Annotations predicted by SingleR using the bulk sorted AM and IM cells as reference.**(c & d)** Percentage of a macrophage/monocytes subset out of all the macrophage/monocyte cells in a given sample based on 10X lung reference (c) and the bulk sorted cells as reference (d). **(e)** DotPlots showing expression of pro-inflammatory cytokines, chemokines and ISG in macrophage/monocyte subsets based on the bulk sorted cells reference at -5dpi and 4dpi in BAL samples from untreated and baricitinib treated rhesus macaques.

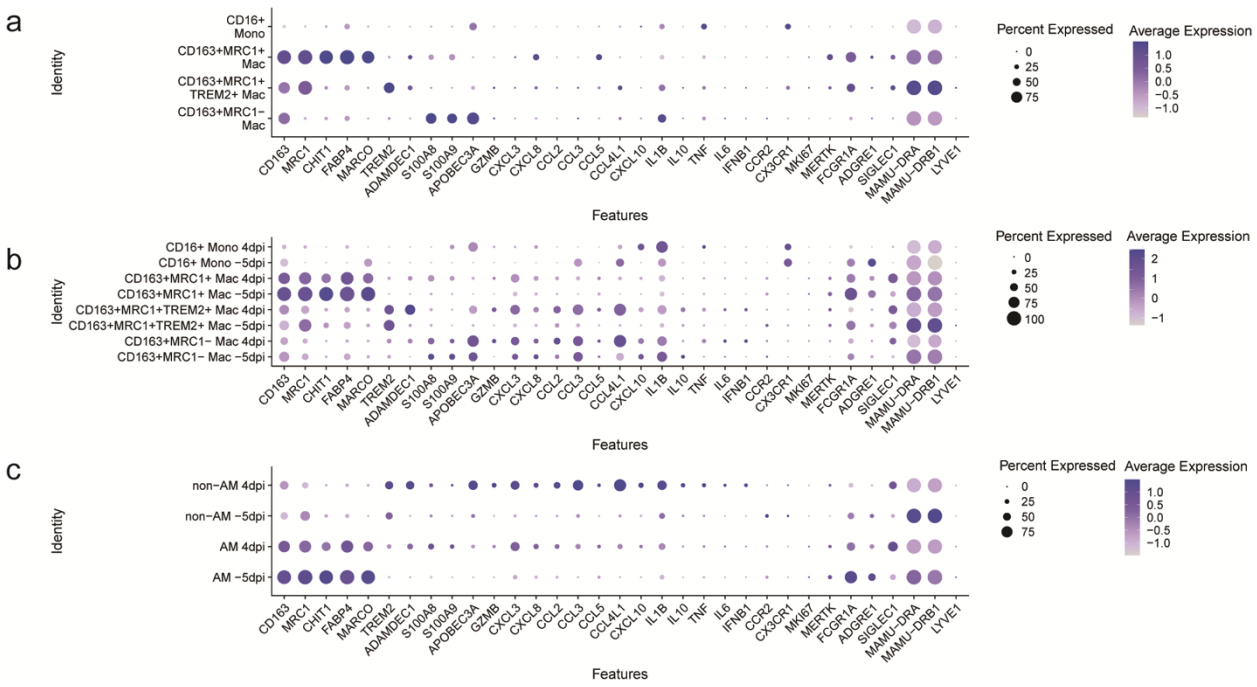

Figure 4.S6. Expression of DE genes in different macrophage/monocyte subsets in **(a)** 10X lung control samples from three uninfected RM. **(b & c)** BAL samples from three SARS-CoV2 infected RM annotated using the 10X lung reference (b) or the bulk sorted cells as reference (c).

Chapter Five: Modulation of type-I interferon responses results in decreased inflammation and enhanced virologic control in SARS-CoV-2-infected rhesus macaques

Timothy N. Hoang[1,14], Elise G. Viox[1,14], Amit A. Upadhyay[2], Maria Pino[1], Arun K. Boddapati[2], Zachary Strongin[1], Justin L. Harper[1], Kevin Nguyen[1], Gregory K. Tharp[2], Kathryn L. Pellegrini[2], Shannon Kirejczyk[3], Joyce Cohen[4], Chelsea Wallace[4], Sherrie M. Jean[4], Jennifer S. Wood[4], Fawn Connor-Stroud[4], Rachelle L. Stammen[4], Sanjeev Gumber[3], Matthew Gagne[5], Shelly Wang[1], Lanfang Wang[6], Peter D. Filev[7], Rebecca D. Levit[6], Monica Vaccari[8], Michael Gale[9], Daniel C. Douek[5], Thomas H. Vanderford[1], R. Paul Johnson[1], Jacob Estes[10,11], Gideon Schreiber[12], Steven E. Bosinger[1,2], Mirko Paiardini[1,13]

[1] Division of Microbiology and Immunology, Yerkes National Primate Research Center, Emory University, Atlanta, GA 30329, USA.

[2] Yerkes Genomics Core Laboratory, Yerkes National Primate Research Center, Emory University, Atlanta, GA 30329, USA.

[3] Division of Pathology, Yerkes National Primate Research Center, Emory University, Atlanta, GA 30329, USA

[4] Division of Animal Resources, Yerkes National Primate Research Center, Emory University, Atlanta, GA 30329, USA.

[5] Vaccine Research Center, National Institutes of Health, Bethesda, MD 20892, USA.

[6] Department of Medicine, School of Medicine, Emory University, Atlanta, GA 30322, USA.

[7] Department of Radiology and Imaging Sciences, School of Medicine, Emory University, Atlanta, GA 30322, USA.

[8] Tulane National Primate Research Center, School of Medicine, Tulane University, Covington, LA 70433, USA.

[9] Department of Immunology, School of Medicine, University of Washington, Seattle, WA 98109, USA.

[10] Vaccine and Gene Therapy Institute, Oregon Health & Science University, Beaverton, OR 97006, USA.

[11] Oregon National Primate Research Center, Oregon Health & Science University, Beaverton, OR 97006, USA.

[12] Department of Biological Chemistry, Weizmann Institute of Science, Rehovat 76100, Israel

[13] Department of Pathology and Laboratory Medicine, School of Medicine, Emory University, Atlanta, GA 30322, USA.

[14]These authors contributed equally

[*] **Main corresponding Author**: mirko.paiardini@emory.edu

Summary

Inflammation following SARS-CoV-2 infection is a hallmark of COVID-19 and predictive of morbidity and death, however, the inflammatory pathways contributing to host-defense vs immune-mediated pathology have not been fully elucidated. This duality is clearly seen with type-I interferons (IFN-I) which are a critical mediator of innate control of viral infections, but also drives recruitment of inflammatory cells to site of infection, a key feature of severe COVID-19. Here, we modulated IFN-I signaling in rhesus macaques (*Macaca mulatta*) prior to and during acute SARS-CoV-2 infection (from day -1 through day 2 post infection) using an IFN-I antagonist (IFNant) which blocks binding to its receptors and signaling of endogenous IFN-I. IFNant treatment resulted in a highly significant and consistent reduction in SARS-CoV-2 viral load in the lower airways (>3-log difference; 2dpi BAL) and upper airways (nasal and throat swabs), with viral loads remaining at low levels when treatment was halted. IFNant also potently reduced soluble markers of inflammation in BAL, expansion of inflammatory monocytes ($CD14^+CD16^+$), and pathogenesis in the lung. Furthermore, Siglec-1 expression, which has been shown to enhance SARS-CoV-2 infection, was rapidly downregulated in the lung and on monocytes of IFNant-treated SARS-CoV-2 infected RMs. In conclusion, IFN-I plays a vital and early role in regulating COVID-19 progression. A better understanding of the role of IFN-I pathways is absolutely needed to design therapies targeting these pathways and aimed at limiting COVID-19 pathogenesis.

Introduction

Coronavirus disease 2019 (COVID-19) is caused by severe acute respiratory syndrome coronavirus 2 (SARS-CoV-2) and is an ongoing and rapidly developing pandemic [319, 320]. Due to the rapid rise and subsequent transmission of SARS-CoV-2 and the emerging variants of concern [414-420], it is imperative to fully characterize the viral pathogenesis and early immune responses that may inform the treatment of infected individuals, identify correlates of protection, and design

therapeutics targeted at SARS-CoV-2 infection. While vaccines are highly effective, the emergence of SARS-CoV-2 variants resulting in breakthrough infections remains worrisome, necessitating the need for therapeutics that can mitigate disease severity and viral replication.

Following SARS-CoV-2 infection, there is a rapid induction of systemic inflammation and infiltration of immune cells, including macrophages and neutrophils, into the lung [338-341]. Although the majority or cases are mild to moderate disease, 5-10% of patients will progress to severe/critical disease, including bilateral interstitial pneumonia or acute respiratory distress syndrome (ARDS) [335, 342]. Severe cases of COVID-19 are associated with elevated levels of pro-inflammatory cytokines and chemokines, and hampered innate antiviral responses. Therefore, it is imperative to understand the mechanisms driving inflammation and infection, and to design therapies targeted at these pathways.

Type-I interferons (IFN-I), first described in the late 1950s by Alick Isaacs and Jean Lindenmann, are ubiquitously expressed cytokines that play a pivotal role in innate antiviral immunity and cell-intrinsic immunity against viral pathogens [596-600]. Receptors for IFN-I are universally expressed and trigger the induction of interferon stimulated genes (ISGs), leading to downstream signaling of antiviral mechanisms and recruitment of inflammatory cells. Recent work has shown that individuals with severe COVID-19 were more likely to have deficiencies to IFN-I responses, either by the presence of inborn errors (*TLR3*, *IRF7*, *TICAM1*, *TBK1*, or *IFNAR1*), neutralizing auto-antibodies against IFN-I, or the lack of production of IFN-I [424, 425, 429-432]. Typically, patients with auto-antibodies against IFN-I do not tend to suffer from severe viral diseases, although some inborn errors to IFN-I can underlie severe viral infection, suggesting that the immune system has compensatory mechanisms for individuals with deficiencies to IFN-I. Notably, and in contrast to the above mentioned studies, additional work by Povysil et al. have shown that there were no

associations with rare-of-functions variants in IFN-I with severe COVID-19 [601]. Lee et al. show that patients with severe COVID-19 exhibit hyper-inflammatory signatures, and in particular an IFN-I response in conjunction with TNF/IL-1β driven inflammation, suggesting that IFN-I responses may result in severe disease by exacerbating inflammation [602]. Recent work [435, 436] show that prolonged IFN signaling can also interfere with lung repair following viral infection, and can increase disease severity and susceptibility to subsequent bacterial infections. Interestingly, ACE2 the entry receptor for SARS-CoV-2, has also been linked as an interferon stimulated gene [333]. Additionally, interferon-induced transmembrane proteins (IFITM1-3), which are ISGs can be commandeered by SARS-CoV-2 to increase efficiency of viral infection [603]. The C-type lectin receptors DC-SIGN, L-SIGN, and sialic acid-binding Ig-like lectin 1 (Siglec-1/CD169) were also shown to function as attachment receptors through enhancement of ACE2-mediated infection and inducing trans-infection [437]. Thus, it is critical to better understand the roles of IFN-I signaling in regulating SARS-CoV-2 replication and pathogenesis, including for implementing therapeutic strategies targeting those pathways.

Non-human primate (NHP) models, specifically rhesus macaques (RMs), have been used extensively to study pathogenesis and potential vaccine and antiviral candidates for numerous viral diseases, including HIV and, more recently, SARS-CoV-2 [519]. RMs infected with SARS-CoV-2 develop mild to moderate disease, mimic patterns of viral shedding, and, in similar fashion to humans, rarely progress to severe disease. Previously, we and others [329, 568, 569], have shown the RMs generate a rapid and robust IFN-I response following SARS-CoV-2 infection, with numerous ISGs upregulated as early as 1dpi. Here, we sought to understand the roles of IFN-I following SARS-CoV-2 infection by modulating IFN-I responses prior to and during the first two days of infection using a mutated IFNa2 that, by binding IFNAR1/2, block binding and signaling of all forms of endogenous IFNalpha and IFNbeta (IFN-I antagonist; IFNant) [82, 604-606].

Results

IFNant treatment resulted in decreased SARS-CoV-2 viral loads in upper and lower airways of treated RMs

20 adult RMs (6-20 years old, mean = 10 years) were randomized (age and sex matched) to receive (IFNant treated group), or not (untreated; control group), IFNant (intramuscularly, 1 mg/day) starting from one day prior to infection (d-1) and continued until 2 days post-infection (dpi) (**Figure 5.1A**). On day 0, all 20 RMs were inoculated with a total of $1.1x10^6$ PFU SARS-CoV-2 (2019-nCoV/USA-WA1/2020), administered by intranasal (IN) and intratracheal (IT) routes. 8 RMs (4 IFNant and 4 untreated) were euthanized at 2 dpi, 6 RMs (3 IFNant and 3 untreated) were euthanized at 4 dpi, and 6 RMs (3 IFNant and 3 untreated) at 7 dpi.

There were slight reductions in all RMs to absolute counts of peripheral monocytes, neutrophils and lymphocytes, which could be due to trafficking to the lung as a result of infection, and decreased red blood cell counts (RBC), hematocrit (HCT) and hemoglobin (HGB) were observed starting at 1 dpi in all RMs. Overall, IFNant was well tolerated without evidence of treatment induced clinical-pathology, nephrotoxicity, or hepatotoxicity when compared to untreated SARS-CoV-2 infected RMs. Weight loss was observed in both untreated and IFNant treated RMs, however, this could be attributed to the daily access of the animals.

Viral RNA levels were measured, blinding to the treatment group, using genomic (gRNA) and sub-genomic (sgRNA) qRT-PCR as previously described [329, 569]. At 2dpi, during the treatment phase of the study, we observed a drastic reduction in the levels of gRNA and sgRNA E in the BAL

(gRNA – 2 dpi: $3.22x10^7$ vs $6.63x10^4$ $p < 0.0001$; sgRNA – 2 dpi: $1.03x10^7$ vs $9.39x10^3$ $p < 0.0001$; **Fig. 5.1B-M**), nasal swabs (gRNA – 1 dpi: $1.86x10^7$ vs $3.40x10^5$ $p = 0.0089$; sgRNA – 1 dpi: $1.02x10^6$ vs $2.69x10^4$ $p = 0.0162$; **Fig. 5.1B-M**), and throat swabs (gRNA – 1 dpi: $2.48x10^6$ vs $7.52x10^3$ $p = 0.0065$; gRNA – 2 dpi: $6.56x10^5$ vs $3.44x10^5$ $p = 0.028$; **Fig. 5.1B-M**) of IFNant treated RMs during the treatment phase of the study (Fig). Specifically, IFNant treatment resulted in a ~500-fold reduction in gRNA (**Fig. 5.1B and H**) and a >1000-fold reduction in sgRNA E (**Fig. 5.1E and K**) in the BAL at 2 dpi. Additionally, in the nasal swabs at 1 dpi, there was a 50-fold reduction in gRNA copies and ~40-fold reduction in sgRNA E copies in IFNant treated RMs (**Fig. 5.1C and I**). The gRNA at 1 and 2 dpi in the throat also followed the same trend, with 330-fold and 2-fold less virus in IFNant treated RMs than untreated RMs, respectively. The BAL and nasal swab viral loads were confirmed with sgRNA targeting the N gene. Of note, due to limited space and resources in BSL-3, we have divided the 20 animals into 7 groups of 2-4 animals each; each group included age and sex matched controls and IFNant treated RMs. As a result, infection has been performed in 7 different experiments, with IFNant treated animals in each of the 7 experiments consistently showing lower viral loads as compared to the controls. Once treatment was stopped, viral loads remained stable, without any increase, in the treated group up till 7 dpi, the latest accessed time point. As consistently shown in many studies, viral loads decreased in control RMs after the early peak, thus values were no longer statistically different between IFNant treated and untreated RMs starting from 4 dpi. In summation, treatment with IFNant was safe and well tolerated, and resulted in a consistent and drastic (between 1 to 3.5 logs) decreased viremia in the upper and lower airways.

IFNant treatment reduced lung pathology and soluble markers of inflammation in SARS-CoV-2 infected rhesus macaques

To assess lung damage following SARS-CoV-2 infection, all RMs were euthanized at either 2, 4 or 7 dpi. At necropsy, multiple sections of upper, middle, and lower lung lobes were taken for

immunologic, virologic and pathologic analyses. Pathological analysis was performed as previously described by two pathologists, independently and blinded to the experimental arms. Treated RMs showed decreased type 2 pneumocyte hyperplasia, alveolar septal thickening, and perivascular cuffing **(Fig. 5.2A**). The average pathology score per lobe (measuring the average severity of abnormalities per lobe, independently of how many lobes had been affected, p=0.0913) and the total pathology score (considering severity and number of effected lobes, p=0.0331) were lower in the IFNant treated group (2.07 and 3.6, respectively) as compared to untreated RMs (5 and 10.2, respectively) (**Fig. 5.2B and C**). Consistent with the ability of IFNant to reduce BAL viral loads, treated RMs displayed decreased expression of nucleocapsid in the lung, including at 7 dpi (**Fig. 5.2D**) when the differences in viremias are no longer significant in BAL, thus suggesting a longer impact when analyses are performed directly in lung tissue. Notably, the nucleocapsid was staining was more diffuse in the untreated RMs, whereas IFNant treated RMs had small foci of infected cells, suggesting that treatment restrained infection to fewer cells in the lung. Levels of Mx1 were lower in IFNant treated RMs, with all 6 untreated RMs having between 25%-75% of lung area positive for Mx1 as compared to 2 out of 6 IFNant RMs with between 25%-50% positive for Mx1 and the majority having less than 25% of the area positive for Mx1.

SARS-Cov-2 infection has been shown to induce the production of multiple mediators of inflammation and chemotaxis of inflammatory cells. Accordingly, multiple chemokines and cytokines were shown to be upregulated in the BAL of untreated RMs already at 2 days post SARS-CoV-2 infection as measured by fold change (FC) to baseline (-7 dpi), whereas they remained remarkably stable in IFNant treated RMs (**Fig. 5.2 L-S**). Molecules showing the most significant differences at 2dpi include IL-1β (FC: 8.1 vs 0.81), IL-6 (FC: 196.9 vs 2.92), TNFβ (FC: 1.77 vs 0.99), IFNg (FC: 2.15 vs 0.86), MIP1a (FC: 16.93 vs 2.49), MIP1b (FC: 105.2 vs 1.57), MCP4 (FC: 3.14 vs 1.02) and Eotaxin 3 (FC: 8.51 vs 2.32).

Overall, these data suggest that treatment with IFN-ant reduced pathology, inflammation, and tissue viral load.

IFNant treated RMs displayed decreased expansion of inflammatory monocytes and rapid downregulation of Siglec-1

To monitor the immunological effects of IFNant on cellular distribution within BAL and blood, we performed high-dimensional flow cytometry to assess cellular populations longitudinally during infection. We measured the frequencies of classical ($CD14^+CD16^-$), non-classical ($CD14^-CD16^+$), and inflammatory ($CD14^+CD16^+$) monocytes. Recent reports have shown that patients with mild to severe COVID-19 have an expansion of inflammatory monocytes. Here, we observed that, when compared to controls, IFNant treated RMs had a significantly lower expansion of inflammatory monocytes as early as 2 dpi, which was maintained until RMs were euthanized at 4 and 7 dpi (**Fig 5.3 A-E**). The difference was specific for blood, with no difference observed within the BAL. Thus, reduced levels of IFN-I genes resulted in a decrease in expansion of inflammatory monocytes and neutrophils, thus reducing systemic and lung inflammation.

Recently, it was shown that sialic acid-binding Ig-like lectin 1 (Siglec-1/CD169) can function as attachment receptors through enhancement of ACE2-mediated infection and inducing trans-infection [(437)]. Additional work by Perez-Zsolt et al. have shown that Siglec-1, which is present on antigen presenting cells and interacts with retrovirus and filoviruses, can bind to SARS-CoV-2 [(607)]. This interaction of Siglec-1 can mediate trans-infection and induce a rapid proinflammatory response. Furthermore, upregulation of Siglec-1 on circulating human monocytes has been identified as an early marker identifying SARS-CoV-2 infection and been associated with disease

severity [608]. In our study, we found a rapid upregulation of Siglec-1 on classical and inflammatory monocytes following SARS-CoV-2 infection in all untreated animals, both in term of frequency of CD14+ monocytes (**Fig 5.3 F and G**), MFI on CD14+ monocytes (**Fig 5.3 H**), and on CD14+CD16+ monocytes (**Fig 5.3 I**). The increased expression of Siglec-1 was significantly lower in the IFNant treated RMs, both as frequency of CD14+ monocytes and as MFI, at both 2 and 4 dpi, suggesting that blockade of IFN-I signaling had a dramatic effect on overall expression of Siglec-1. This is complimentary to the viral load data, where IFNant treated RMs had significantly lower levels of genomic and sub-genomic levels of viral RNA in the BAL and nasal swabs.

Discussion

The mechanisms by which SARS-CoV-2 drives systemic inflammation remains largely unknown, but remains a key to understanding disease pathogenesis and the development of therapeutics. Here we utilized nonhuman primates as a model of SARS-CoV-2 to understand the roles of IFN-I following infection using an integrated systems approach to characterize IFN-I pathways. Notably, modulation of IFN-I with an antagonist starting prior to infection resulted in decreased: i) viral loads in the BAL, nasal, and throat swabs during treatment, ii) lung pathology and expression of Mx1, iii) expansion of inflammatory monocytes and frequency of Siglec-1, and iv) signatures of systemic inflammation. This suggests that treatments targeted at modulating IFN-I responses could be promising in mitigating disease severity if administered early during infection. This beneficial, but unexpected outcome, was confirmed with viral loads in the BAL, nasal swabs, and tissue at necropsy and an overall decrease to signatures of systemic inflammation that has been associated with severe disease in human cohorts.

These data are contrary to data that has been recently published regarding deficiencies to IFN-I, whereby a lack of IFN-I response was associated was increased disease severity. Based on

conventional ideas, the lack of a robust IFN-I response would likely lead to a hampered antiviral response and increased dissemination of infection. However, patients with auto-antibodies against IFN-I typically do not suffer unusually severe viral infections when compared to patients without neutralizing antibodies against IFN-I. However, patients with inborn errors of *TLR3* and *IRF7* have been linked to increased disease severity following respiratory infections. This suggests that the immune system has compensatory mechanisms that can counteract the lack of IFN-I response and induce an antiviral response. However, recent work by Major et el. has shown that Type I and III IFNs can hinder lung tissue repair following viral infection and rendering the host susceptible to opportunistic bacterial infections. Thus, therapies targeting IFN pathways warrant further research to obtain the optimal balance of stimulation of antiviral response, while maintaining tissue repair pathways.

Several ongoing and recently competed clinical trials administering IFN- α/β have shown little to no positive effects of therapy during acute infection. The Solidarity Trial evaluated 4 treatments: remdesivir, hydroxychloroquine, lopinavir/ritonavir, and interferon and found that all 4 treatments had little or no effect on the overall patient mortality, ventilation requirements, and duration of hospital stay. However, therapeutics targeted at dampening inflammation, such as dexamethasone and baricitinib, have shown promise. As a result, there are continued efforts to understand inflammatory pathways triggered following SARS-CoV-2 infection to develop better targeted approaches to treat COVID-19.

In conclusion, our study provides insight to IFN-I derived inflammation and transient upregulation of antiviral genes are beneficial following SARS-CoV-2 infection.

Acknowledgments

We thank the Yerkes National Primate Research Center (YNPRC) Division of Animal Resources, especially Stephanie Ehnert, Stacey Weissman, Denise Bonenberger, John M. Wambua, and Racquel Sampson-Harley Research Resources for providing support in animal care. This work was additionally funded by the National Institute of Allergy and Infectious Diseases (NIAID, NIH) under awards R37AI141258, R01AI116379 to M.Pa, and U24AI120134 to S.E.B. Support for this work was also provided by award NIH Office of Research Infrastructure Programs (ORIP) P51OD11132 to YNPRC, and NIAID award P30 AI050409 to the Center for AIDS Research (CFAR) at Emory University. Next generation sequencing services were provided by the Yerkes NHP Genomics Core which is supported in part by NIH P51OD011132. Sequencing data was acquired on an Illumina NovaSeq6000 funded by NIH S10OD026799 to S.E.B. The content of this publication does not necessarily reflect the views or policies of the U.S. Department of Health and Human Services, nor does it imply endorsement of organizations or commercial products.

Author Contributions

Conceptualization, T.H., and M.Pa.; Methodology, T.H., E.G.V., A.A.U., M.Pi., A.K.B., Z.S., G.K.T., K.L.P., S.G., S.K., S.W., T.R.H., E.N.B., T.H.V.; Formal Analysis, T.H., A.K.B., A.A.U., G.K.T., S.G., S.K., T.H.V; Investigation, T.H., M.Pi., E.G.V., J.C., S.J., J.S.W., F.C-S., R.L.S., R.D.L., and T.V.; Resources, S.B. and M.Pa.; Writing – Original Draft, T.H., and M.Pa.; Writing – Review & Editing, T.H., E.G.V., S.E.B. and M.Pa.; Visualization, T.H., A.K.B., A.A.U., and G.K.T; Supervision, M.Pa.; Funding Acquisition, M.Pa.

Materials and Methods

Declaration of Interests

The authors have nothing to disclose.

RESOURCE AVAILABILITY

Lead Contact

Further information and requests for resources and reagents should be directed to and will be fulfilled by the Lead Contact, Dr. Mirko Paiardini (mirko.paiardini@emory.edu).

Materials Availability

This study did not generate new unique reagents.

Data and Code Availability

The datasets generated during this study are available at Gene Expression Omnibus (GEO) accession PENDING and code can be made available upon requests.

Data Availability Statement

Source data supporting this work are available from the corresponding author upon reasonable request. The following sequencing data have been deposited in GenBank: SARS-CoV-2 viral stock (accession # PENDING). Data tables for expression counts for bulk and single-cell RNA-Seq for BAL are deposited in NCBI's Gene Expression Omnibus and are accessible through GEO accession PENDING. Custom scripts and supporting documentation on the RNA-Seq analyses will be made available at https://github.com/BosingerLab/.

EXPERIMENTAL MODEL AND SUBJECT DETAILS

Study Approval

YNPRC's animal care facilities are accredited by both the U.S. Department of Agriculture (USDA) and by the Association for Assessment and Accreditation of Laboratory Animal Care (AAALAC). All animal procedures were performed in line with institutional regulations and guidelines set forth by the NIH's Guide for the Care and Use of Laboratory Animals, 8th edition, and were conducted under anesthesia with appropriate follow-up pain management to minimize animal suffering. All animal experimentation was reviewed and approved by Emory University's Institutional Animal Care and Use Committee (IACUC) under permit PROTO202000035.

Animal models

Twenty (10 female and 10 male) specific-pathogen-free (SPF) Indian-origin rhesus macaques (RM; *Macaca mulatta;* **Table S1**) were housed at Yerkes National Primate Research Center (YNPRC) as previously described [129] in the ABSL3 facility. Animals for study assignment were requested to be greater than 6 years old without preference for gender or MHC haplotype. RMs were infected with $1.1x10^6$ plaque forming units (PFU) SARS-CoV-2 via both the intranasal (1 mL) and intratracheal (1 mL) routes concurrently. Absent further stratification criteria, 10 RMs were administered 1 mg/day of IFN-I antagonist (IFNant) starting one day prior to infection (-1 dpi) until 2 dpi. IFNant was supplied in solution and diluted with PBS and administered intramuscularly in the thigh. At each anesthetic access pulse oximetry was recorded and RMs were clinically scored for responsiveness and recumbency; discharges; skin condition; respiration, dyspnea, and cough; food consumption; and fecal consistency. Longitudinal tissue collections of peripheral blood (PB); bronchoalveolar lavage (BAL); and nasal, and pharyngeal mucosal swabs in addition to thoracic X-rays (ventrodorsal and right lateral views) were performed immediately prior to IFNant administration as annotated (**Figure 5.1A**). In addition to the tissues

listed above, at necropsy the following tissues were processed for mononuclear cells: hilar LN, lower lung, and upper lung. Additional necropsy tissues harvested for histology included nasopharynx.

METHOD DETAILS

Vero E6 cell line (African Green Monkey Kidney cell line; CRL-1586, ATCC) was used in this study. Vero cells were cultured and maintained in MEM (Sigma) supplemented with 10% heat inactivated fetal bovine serum (FBS) (Gibco) and 1 mM L-glutamine (Gibco), 50 U/ml penicillin and 50 µg/ml streptomycin (Gibco). The cells were kept at 37°C in the presence 5% CO_2. At the time of virus inoculation and propagation, the concentration of FBS was reduced to 2%. SARS-CoV-2 (NR-52281: BEI Resources, Manassas, VA; USA-WA/2020, Lot no. 70033175) was passaged on Vero E6 cells at a MOI of 0.01 to produce the infectious viral stock. SARS-CoV-2 has been propagated and titrated by $TCID_{50}$ method followed by storage of aliquots at -80°C until further use in the experiments.

Determination of viral load RNA

SARS-CoV-2 genomic RNA was quantified in nasopharyngeal (NP) swabs, throat swabs, rectal swabs, and bronchoalveolar lavages (BAL). Swabs were placed in 2mL of PBS (CORNING). Viral RNA was extracted from NP swabs, throat swabs, rectal swabs, and BAL on fresh specimens. Viral RNA was extracted manually using the QiaAmp Viral RNA mini kit according to the manufacturer's protocol. Quantitative PCR (qPCR) was performed on viral RNA samples using the N2 primer and probe set designed by the CDC for their diagnostic algorithm: CoV2-N2-F: 5'-TTACAAACATTGGCCGCAAA-3', CoV2-N2-R: 5'-GCGCGACATTCCGAAGAA-3', and CoV2-N2-Pr: 5'-FAM-ACAATTTGCCCCCAGCGCTTCAG-BHQ-3'. qPCR reactions were performed in duplicate with the TaqMan Fast Virus 1-step Master Mix using the manufacturer's cycling

conditions, 200nM of each primer, and 125nM of the probe. The limit of detection in this assay was 70 copies per mL of PBS or BAL. To verify sample quality the CDC RNase P p30 subunit qPCR was modified to account for rhesus macaque specific polymorphisms. The primer and probe sequences are RM-RPP30-F 5'-AGACTTGGACGTGCGAGCG-3', RM-RPP30-R 5'-GAGCCGCTGTCTCCACAAGT-3', and RPP30-Pr 5'-FAM-TTCTGACCTGAAGGCTCTGCGCG-BHQ1-3'. A single well from each extraction was run as above to verify RNA integrity and sample quality via detectable and consistent cycle threshold values.

Histopathology and immunohistochemistry

Due to study end point, the animals were euthanized, and a complete necropsy was performed. For histopathologic examination, various tissue samples including lung, nasal turbinates, trachea, or brain, were fixed in 4% neutral-buffered paraformaldehyde for 24h at room temperature, routinely processed, paraffin-embedded, sectioned at 4µm, and stained with hematoxylin and eosin (H& E). The H&E slides from all tissues were examined by two board certified veterinary pathologists. For each animal, all the lung lobes were used for analysis and affected microscopic fields were scored semi-quantitatively as Grade 0 (None); Grade 1 (Mild); Grade 2 (Moderate) and Grade 3 (Severe). Scoring was performed based on these criteria: number of lung lobes affected, type 2 pneumocyte hyperplasia, alveolar septal thickening, fibrosis, perivascular cuffing, peribronchiolar hyperplasia, inflammatory infiltrates, hyaline membrane formation. An average lung lobe score was calculated by combining scores from each criterion. Digital images of H&E stained slides were captured at 40× and 200× magnification with an Olympus BX43 microscope equipped with a digital camera (DP27, Olympus) using Cellsens® Standard 2.3 digital imaging software (Olympus).

Immunohistochemical (IHC) staining of sections of lung was performed using a biotin-free polymer system. The paraffin-embedded sections were subjected to deparaffinization in xylene,

rehydration in graded series of ethanol, and rinsed with double distilled water. Antigen retrieval was performed by immersing sections in DIVA Decloaker (Biocare Medical) at 125℃ for 30 seconds in a steam pressure decloaking chamber (Biocare Medical) followed by blocking with Background Sniper Reagent (Biocare Medical) for 10 minutes. The sections were incubated with Thyroid Transcription Factor-1 (Clone 8G7G3/1) for overnight at 4°C followed by a detection polymer system (MACH 2™; Biocare Medical). Labeled antibody was visualized by development of the chromogen (DAB Chromogen Kits; Biocare Medical).

Tissues were fixed in freshly prepared 4% paraformaldehyde for 24 h, transferred to 70% ethanol, paraffin embedded within 7-10 days, and blocks sectioned at 5 µm. Slides were baked for 30-60 min at 65°C then deparaffinized in xylene and rehydrated through a series of graded ethanol to distilled water. Heat induced epitope retrieval (HIER) was performed with the antigen retrieval buffers citraconic anhydride (0.01% with 0.05% Tween; Mx1, Iba-1, and Ki-67) or citrate buffer (pH 6.0; MPO) in a Biocare NxGen Decloaking Chamber that was set to 110°C for 15 min. The slides were cooled, rinsed twice in distilled water and 1X TBS with 0.05% Tween-20 (TBS-T), blocked (TBS-T + 0.25% casein) for 30 minutes at room temperature, then incubated at room temperature with antibodies against Mx1 (EMD; Cat. No. MABF938 at 1:1000 for 1 hour), MPO (Dako; Cat. No. A0398 at 1:1000 for 1 hour), Iba-1 (BioCare; Cat. No. CP290A at 1:500 for 1 hour), and Ki67 (BD Pharmingen; Cat. No. 550609 at 1:200 for 1 hour). Endogenous peroxidases were blocked with 1.5% H_2O_2 in TBS-T for 10 minutes. Slides were then incubated with Rabbit Polink-1 HRP (GBI Labs; Cat. No. D13-110 for MPO and Iba-1) and Mouse Polink-2 HRP (GBI Labs; Cat. No. D37-110 for Mx1 and Ki67). Slides were developed using Impact™ DAB (3,3′-diaminobenzidine; Vector Laboratories), washed in ddH_2O, counterstained with hematoxylin, mounted in Permount (Fisher Scientific), and scanned at 20x magnification on an Aperio AT2

(Leica Biosystems). Staining for MPO, Mx1, Iba-1, and Ki67 IHC was performed as previously described using a Biocare intelliPATH autostainer.

Tissue Processing

PB was collected from the femoral vein in sodium citrate, serum separation, and EDTA tubes from which plasma was separated by centrifugation within 1 hour of phlebotomy. PB was used for complete blood counts, comprehensive serum chemistry panels, and measurement of neutrophil extracellular traps (NET) activity. From EDTA PB, peripheral blood mononuclear cells (PBMCs) were isolated using a Ficoll-Paque Premium density gradient (GE Healthcare), and washed with R-10 media. R-10 media was composed of RPMI 1640 (Corning) supplemented with 10% heat-inactivated fetal bovine serum (FBS), 100 IU/mL penicillin, 100 μg/mL streptomycin, and 200 mM L-glutamine (GeminiBio).

Nasopharyngeal swabs were collected under anesthesia by using a clean rayon-tipped swab (ThermoFischer Scientific, BactiSwab NPG, R12300) placed approximately 2-3cm into the nares. Oropharyneal swabs were collected under anesthesia using polyester tipped swabs (Puritan Standard Polyester Tipped applicator, polystyrene handle, 25-806 2PD, VWR International) to streak the tonsils and back of throat bilaterally (throat/pharyngeal). The swabs were dipped in 2 mL PBS (CORNING) and vortexed for 30 sec, and the eluate was collected.

To collect BAL, a fiberoptic bronchoscope (Olympus BF-XP190 EVIS EXERA III ULTRA SLM BRNCH and BF-P190 EVIS EXERA 4.1mm) was manipulated into the trachea, directed into the primary bronchus, and secured into a distal subsegmental bronchus upon which 35-50 mL of normal saline (0.9% NaCl) was administered into the bronchus and re-aspirated to obtain a minimum of 20ml of lavage fluid. BAL was filtered through a 70μm cell strainer.

Hilar LN biopsies were collected at necropsy, sectioned using blunt, micro-dissection scissors and mechanically disrupted through a 70μm cell strainer and washed with R-10 media.

Mononuclear cells were counted for viability using a Countess II Automated Cell Counter (Thermo Fisher) with trypan blue stain and were cryo-preserved in aliquots of up to $2x10^7$ cells in 10% DMSO in heat-inactivated FBS. Whole tissue segments (0.5 cm^3) were snap frozen dry, or stored in RNAlater (Qiagen), or Nuclisens lysis buffer (Biomerieux) for analyses of compound distribution, RNA-seq, and tissue viral quantification, respectively.

Immunophenotyping

23-parameter flow cytometric analysis was perform on fresh PBMCs and mononuclear cells (10^6 cells) derived from LN biopsies, BAL, and lung. Immunophenotyping was performed using anti-human monoclonal antibodies (mAbs), which we [111, 129, 288, 558] and others, including databases maintained by the NHP Reagent Resource (MassBiologics), have shown as being cross-reactive in RMs. A panel of the following mAbs was used for longitudinal T-cell phenotyping in PBMCs: anti-CCR7-BB700 (clone 3D12; 2.5 μL; cat. # 566437), anti-CXCR3-BV421 (clone IC6; 2.5 μL; cat. # 562558), anti-Ki-67-BV480 (clone B56; 5 μL; cat. # 566109), anti-CCR4-BV750 (clone 1G1 1E5; 2.5 μL; cat. # 746980), anti-CD3-BUV395 (clone SP34-2; 2.5 μL; cat. # 564117), anti-CD8-BUV496 (clone RPA-T8; 2.5 μL; cat. # 612942), anti-CD45-BUV563 (clone D058-1283; 2.5 μL; cat. # 741414), anti-CD49a-BUV661 (clone SR84; 2.5 μL; cat. # 750628), anti-CD28-BUV737 (clone CD28.2; 5 μL; cat. # 612815), anti-CD69-BUV805 (clone FN50; 2.5 μL; cat. # 748763), and Fixable Viability Stain 700 (2 μL; cat. # 564997) all from BD Biosciences; anti-CD95-BV605 (clone DX2; 5 μL; cat. # 305628), anti-HLA-DR-BV650 (clone L243; 5 μL; cat. # 307650), anti-

CD25-BV711 (clone BC96; 5 μL; cat. # 302636), anti-PD-1-BV785 (clone EH12.2H7; 5 μL; cat. # 329930), anti-CD101-PE-Cy7 (clone BB27; 2.5 μL; cat. # 331014), anti-FoxP3-AF647 (clone 150D; 5 μL; cat. # 320014), and anti-CD4-APC-Cy7 (clone OKT4; 2.5 μL; cat. # 317418) all from Biolegend; anti-CD38-FITC (clone AT1; 5 μL; cat. # 60131FI) from STEMCELL Technologies; and anti-CXCR5-PE (clone MU5UBEE; 5 μL; cat. # 12-9185-42), anti-GranzymeB-PE-TexasRed (clone GB11; 2.5 μL; cat. # GRB17), and anti-CD127-PE-Cy5 (clone eBioRDR5; 5 μL; cat. # 15-1278-42) all from Thermo Fisher (**Figure S6**). mAbs for chemokine receptors (i.e. CCR7) were incubate at 37°C for 15 min, and cells were fixed and permeabilized for 30 min at room temperature using a FoxP3 / Transcription Factor Staining Buffer Kit (Tonbo Biosciences; cat. # TNB-0607-KIT). A panel of the following mAbs was used for the longitudinal phenotyping of innate immune cells in whole blood (500 μL), as described in [339], and mononuclear cells (10^6 cells) derived from LN biopsies, BAL, and lung: anti-CD20-BB700 (clone 2H7; 2.5 μL; cat. # 745889), anti-CD11b-BV421 (clone ICRFF44; 2.5 μL; cat. # 562632), anti-Ki-67-BV480 (clone B56; 5 μL; cat. # 566109), anti-CD14-BV605 (clone M5E2; 2.5 μL; cat. # 564054), anti-CD56-BV711 (clone B159; 2.5 μL; cat. # 740781), anti-CD163-BV750 (clone GHI/61; 2.5 μL; cat. # 747185), anti-CD3-BUV395 (clone SP34-2; 2.5 μL; cat. # 564117), anti-CD8-BUV496 (clone RPA-T8; 2.5 μL; cat. # 612942), anti-CD45-BUV563 (clone D058-1283; 2.5 μL; cat. # 741414), anti-CCR2-BUV661 (clone LS132.1D9; 2.5 μL; cat. # 750472), anti-CD16-BUV737 (clone 3G8; 2.5 μL; cat. # 564434), anti-CD101-BUV805 (clone V7.1; 2.5 μL; cat. # 749163), anti-CD169-PE (clone 7-239; 2.5 μL; cat. # 565248), and anti-CD206-PE-Cy5 (clone 19.2; 20 μL; cat. # 551136) and Fixable Viability Stain 700 (2 μL; cat. # 564997) all from BD Biosciences; anti-ACE2-AF488 (clone Polyclonal; 5 μL; cat. # FAB9332G-100UG) from R & D; anti-HLA-DR-BV650 (clone L243; 5 μL; cat. # 307650), anti-CD11c-BV785 (clone 3.9; 5 μL; cat. # 301644), and anti-CD123-APC-Fire750 (clone 315; 2.5 μL; cat. # 306042) all from Biolegend; anti-GranzymeB-PE-TexasRed (clone GB11; 2.5 μL; cat.

GRB17) from Thermo Fisher; anti-CD66abce-PE-Vio770 (clone TET2; 1 μL; cat. # 130-119-849) from Miltenyi Biotec; anti-NKG2A-APC (clone Z199; 5 μL; cat. # A60797) from Beckman Coulter (**Figure S6**). mAbs for chemokine receptors (i.e. CCR2) were incubated at 37°C for 15 min, and cells were fixed and permeabilized at room temperature for 15 min with Fixation/Permeabilization Solution Kit (BD Biosciences; cat. #554714). For each sample a minimum of $1.2x10^5$ stopping gate events (live $CD3^+$ T-cells) were recorded except for RB in which a minimum of $5x10^4$ stopping gate events were recorded. All samples were fixed with 4% paraformaldehyde and acquired within 24 hours of fixation. Acquisition of data was performed on a FACSymphony A5 (BD Biosciences) driven by FACS DiVa software and analyzed with FlowJo (version 10.7; Becton, Dickinson, and Company).

QUANTIFICATION AND STATISTICAL ANALYSIS

All statistical analyses were performed two-sided with p-values ≤0.05 deemed significant. Ranges of significance were graphically annotated as follows: *, p<0.05; **, p<0.01; ***, p<0.001; ****, p<0.0001. Due to the low number of animals included in our study, p values ≤0.1 have been indicated in the graphs. Analyses, unless otherwise noted, were performed with Prism version 8 (GraphPad).

Chapter Five Figures

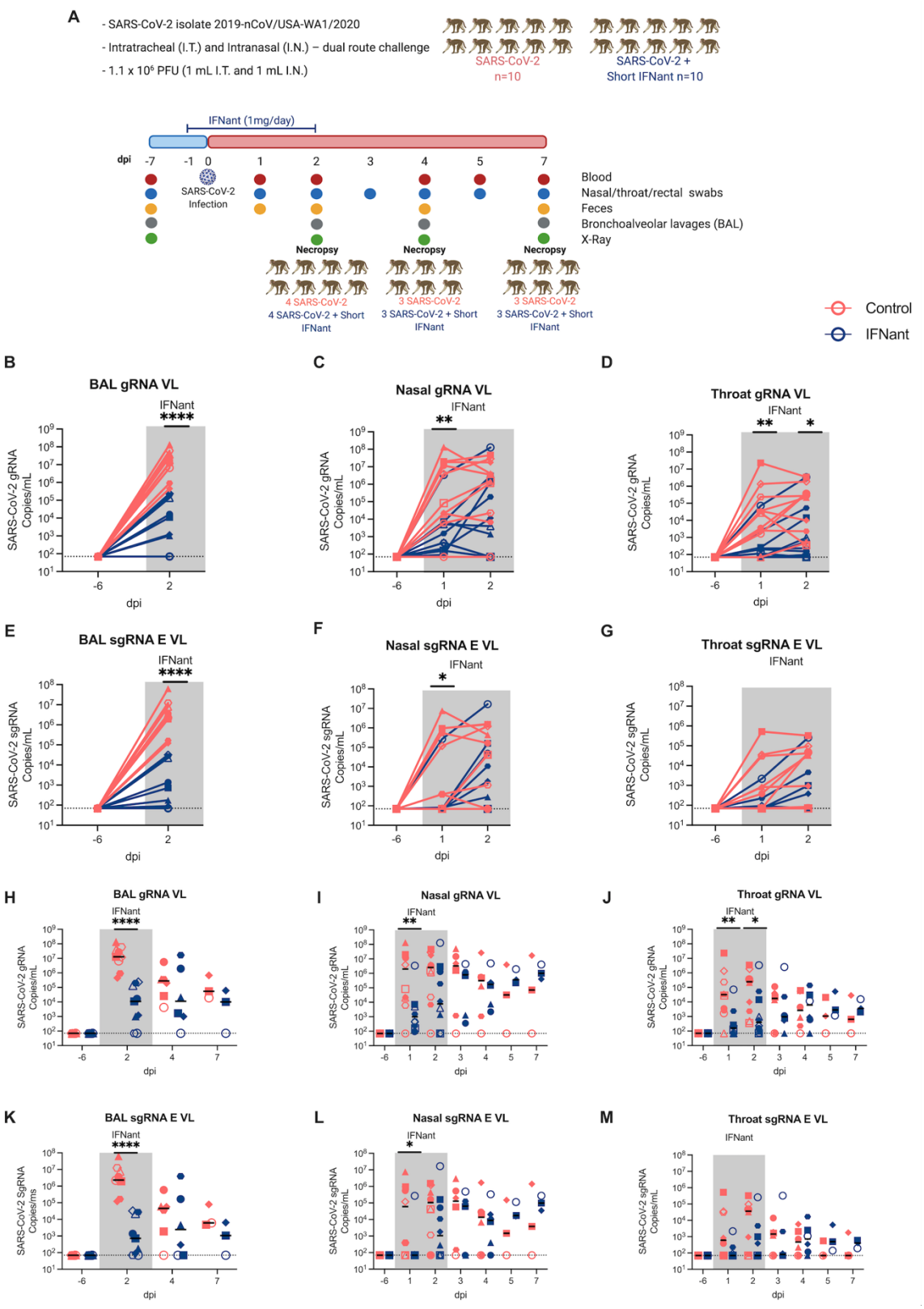

Figure 5.1 IFNant treated RMs have lower levels of viremia during treatment phase. (A) Study design; 20 RMs were infected intranasally and intratracheally with SARS-CoV-2, with 10 RMs receiving IFNant 1 day prior to infection (1 mg/day IM). Longitudinal collections performed are indicated in circles. (B-M) After SARS-CoV-2 inoculation, bronchoalveolar lavages (BALs), nasal, and throat swabs were collected, and viral loads were quantified for gRNA (N2) and sgRNA (E). Different symbols represent individual RMs. Lines represent the median of each group. Statistical analysis was performed using a non-parametric Mann-Whitney test.

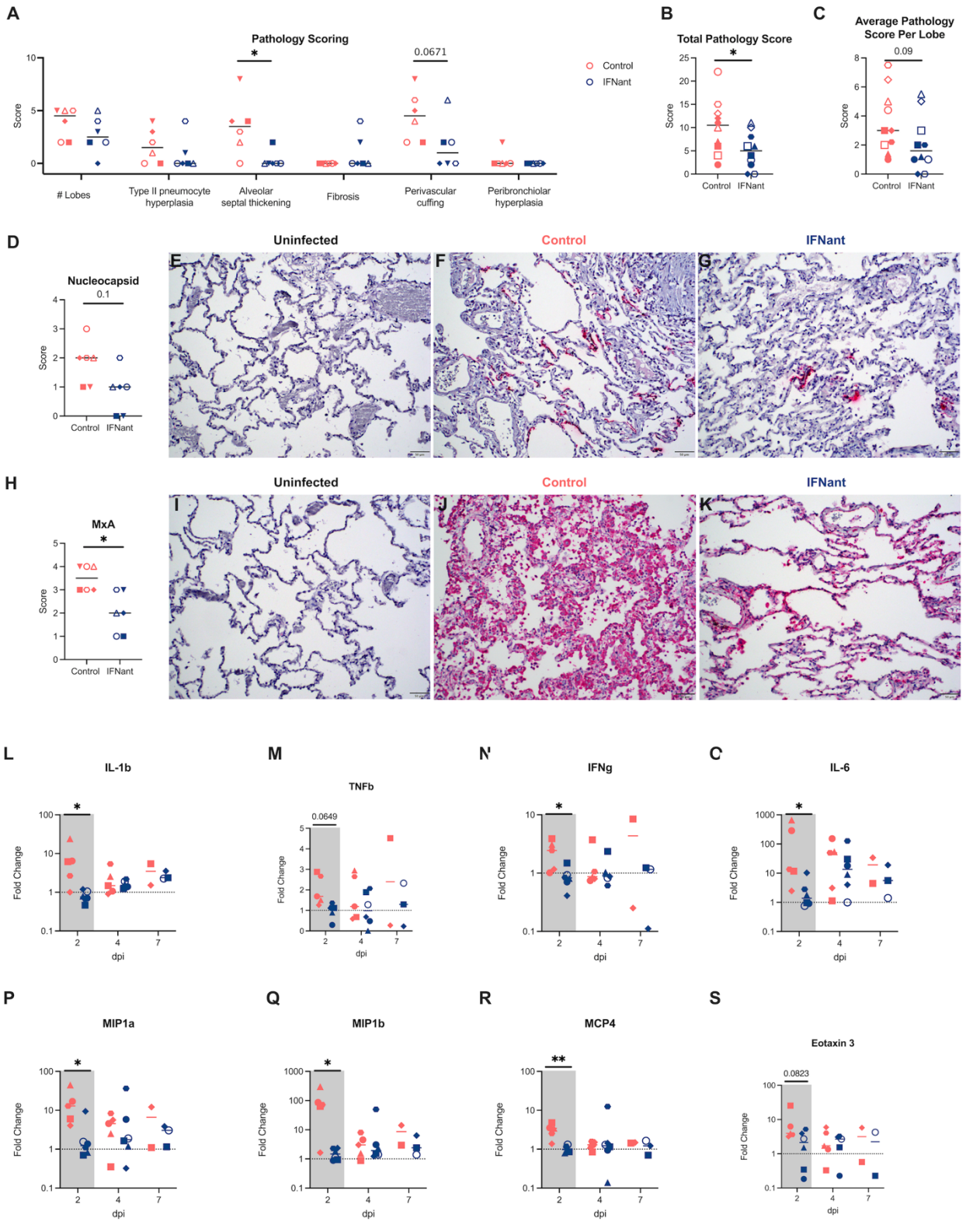

Figure 5.2. Reduced disease pathogenesis and lower levels of lung pathology in IFNant-treated RMs. (A) Pathology scoring for animals at necropsy. (B and C) (B) Total pathology score

per lobe. (C) Average pathology score. (D) Scoring for nucleocapsid staining. (E-G) Nucleocapsid staining in uninfected (E), control (F), and IFNant treated (G) RMs. (H-K) (H) Scoring for MxA staining. MxA staining in uninfected (I), control (J), and IFNant treated (K) RMs. (L-S) Fold change to baseline of soluble cytokines and chemokines in BALs of control and IFNant treated RMs. Each symbol represents individual animals. Statistical analysis in were performed using non-parametric Mann- Whitney test. Statistical analyses were performed two-sided with $p < 0.05$ deemed significant. Ranges of significance were graphically annotated as follows: $*p < 0.05$.

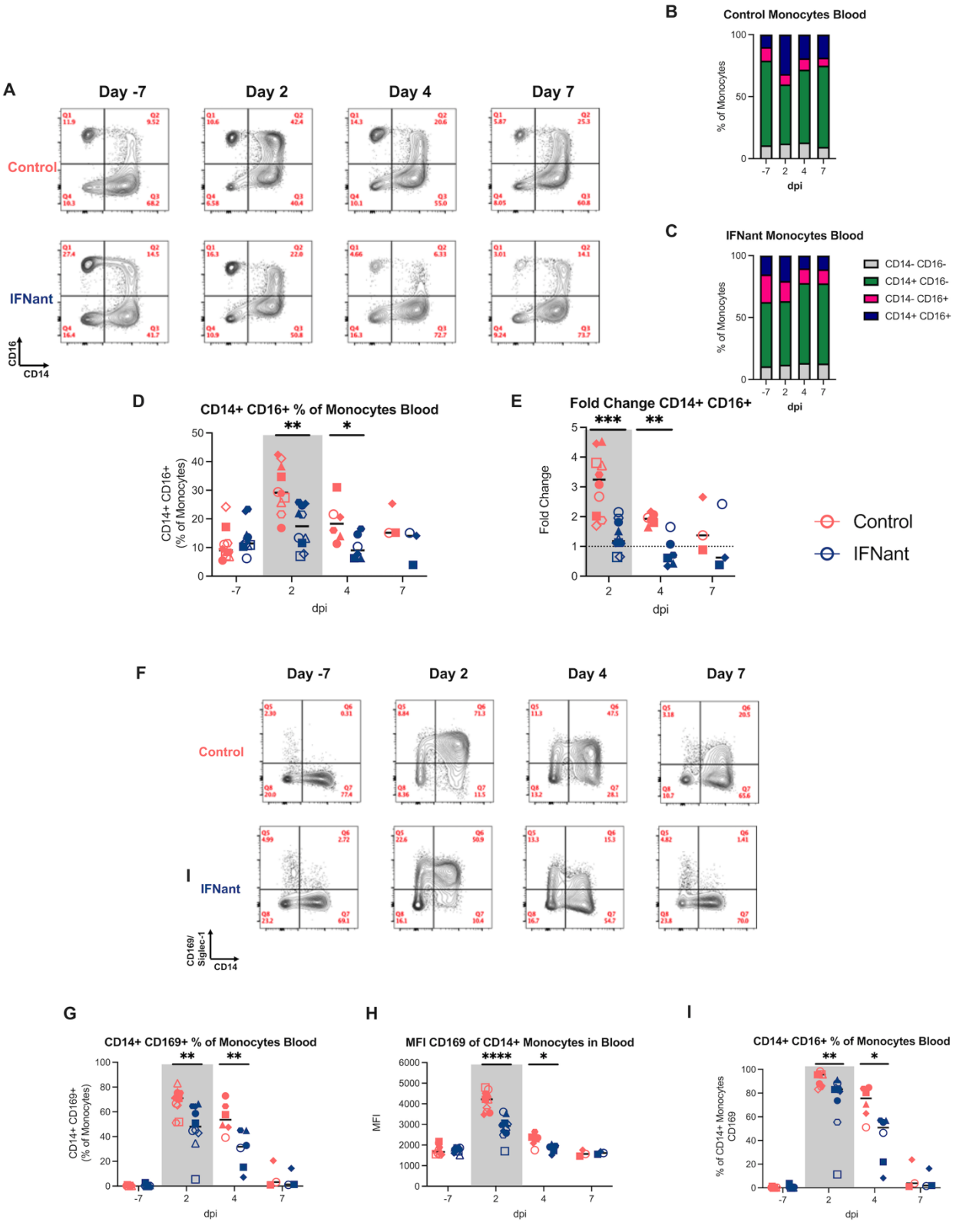
A
Day -7
Day 2
Day 4
Day 7
Control
IFNant
CD16
CD14
B
Control Monocytes Blood
% of Monocytes
dpi
C
IFNant Monocytes Blood
CD14- CD16-
CD14+ CD16-
CD14- CD16+
CD14+ CD16+
D
CD14+ CD16+ % of Monocytes Blood
CD14+ CD16+ (% of Monocytes)
E
Fold Change CD14+ CD16+
Fold Change
Control
IFNant
F
Day -7
Day 2
Day 4
Day 7
Control
IFNant
CD169/ Siglec-1
CD14
G
CD14+ CD169+ % of Monocytes Blood
CD14+ CD169+ (% of Monocytes)
H
MFI CD169 of CD14+ Monocytes in Blood
MFI
I
CD14+ CD16+ % of Monocytes Blood
% of CD14+ Monocytes CD169

Figure 5.3. Decreased expansion of pro-inflammaotry monocytes and Siglec-1 expression in IFNant-treated RMs. (A) Representative staining of blood monocytes for CD14 and CD16. (B and C) Frequency of monocyte populations of (B) Control RMs. (C) IFNant RMs. (D) Frequency and (E) fold change of $CD14^{+}CD16^{+}$ (pro-inflammatory) monocytes following SARS-CoV-2 infection. (F) Representative staining of blood monocytes for CD169/Siglec-1. (D) Frequency and (H) MFI of Siglec-1 expression within blood monocytes. (I) Frequency Siglec-1 expression within pro-inflammatory monocytes. Each symbol represents individual animals. Statistical analysis in were performed using non-parametric Mann- Whitney test. Statistical analyses were performed two-sided with $p < 0.05$ deemed significant. Ranges of significance were graphically annotated as follows: $*p < 0.05$.

References

1. Barre-Sinoussi F, Chermann JC, Rey F, Nugeyre MT, Chamaret S, Gruest J, Dauguet C, Axler-Blin C, Vezinet-Brun F, Rouzioux C, Rozenbaum W, Montagnier L. Isolation of a T-lymphotropic retrovirus from a patient at risk for acquired immune deficiency syndrome (AIDS). Science. 1983;220(4599):868-71. Epub 1983/05/20. doi: 10.1126/science.6189183. PubMed PMID: 6189183.

2. Barre-Sinoussi F, Ross AL, Delfraissy JF. Past, present and future: 30 years of HIV research. Nat Rev Microbiol. 2013;11(12):877-83. Epub 2013/10/29. doi: 10.1038/nrmicro3132. PubMed PMID: 24162027.

3. Centers for Disease C. Kaposi's sarcoma and Pneumocystis pneumonia among homosexual men--New York City and California. MMWR Morb Mortal Wkly Rep. 1981;30(25):305-8. Epub 1981/07/03. PubMed PMID: 6789108.

4. Gilbert PB, McKeague IW, Eisen G, Mullins C, Gueye NA, Mboup S, Kanki PJ. Comparison of HIV-1 and HIV-2 infectivity from a prospective cohort study in Senegal. Stat Med. 2003;22(4):573-93. Epub 2003/02/19. doi: 10.1002/sim.1342. PubMed PMID: 12590415.

5. Gao F, Bailes E, Robertson DL, Chen Y, Rodenburg CM, Michael SF, Cummins LB, Arthur LO, Peeters M, Shaw GM, Sharp PM, Hahn BH. Origin of HIV-1 in the chimpanzee Pan troglodytes troglodytes. Nature. 1999;397(6718):436-41. Epub 1999/02/16. doi: 10.1038/17130. PubMed PMID: 9989410.

6. Hahn BH, Shaw GM, De Cock KM, Sharp PM. AIDS as a zoonosis: scientific and public health implications. Science. 2000;287(5453):607-14. Epub 2000/01/29. doi: 10.1126/science.287.5453.607. PubMed PMID: 10649986.

7. Huet T, Cheynier R, Meyerhans A, Roelants G, Wain-Hobson S. Genetic organization of a chimpanzee lentivirus related to HIV-1. Nature. 1990;345(6273):356-9. Epub 1990/05/24. doi: 10.1038/345356a0. PubMed PMID: 2188136.

8. De Leys R, Vanderborght B, Vanden Haesevelde M, Heyndrickx L, van Geel A, Wauters C, Bernaerts R, Saman E, Nijs P, Willems B, et al. Isolation and partial characterization of an unusual human immunodeficiency retrovirus from two persons of west-central African origin. J Virol. 1990;64(3):1207-16. Epub 1990/03/01. doi: 10.1128/JVI.64.3.1207-1216.1990. PubMed PMID: 2304140; PMCID: PMC249235.

9. Gurtler LG, Hauser PH, Eberle J, von Brunn A, Knapp S, Zekeng L, Tsague JM, Kaptue L. A new subtype of human immunodeficiency virus type 1 (MVP-5180) from Cameroon. J Virol. 1994;68(3):1581-5. Epub 1994/03/01. doi: 10.1128/JVI.68.3.1581-1585.1994. PubMed PMID: 8107219; PMCID: PMC236615.

10. Sharp PM, Bailes E, Chaudhuri RR, Rodenburg CM, Santiago MO, Hahn BH. The origins of acquired immune deficiency syndrome viruses: where and when? Philos Trans R Soc Lond B Biol Sci. 2001;356(1410):867-76. Epub 2001/06/19. doi: 10.1098/rstb.2001.0863. PubMed PMID: 11405934; PMCID: PMC1088480.

11. Taylor BS, Sobieszczyk ME, McCutchan FE, Hammer SM. The challenge of HIV-1 subtype diversity. N Engl J Med. 2008;358(15):1590-602. Epub 2008/04/12. doi: 10.1056/NEJMra0706737. PubMed PMID: 18403767; PMCID: PMC2614444.

12. Abecasis AB, Wensing AM, Paraskevis D, Vercauteren J, Theys K, Van de Vijver DA, Albert J, Asjo B, Balotta C, Beshkov D, Camacho RJ, Clotet B, De Gascun C, Griskevicius A, Grossman Z, Hamouda O, Horban A, Kolupajeva T, Korn K, Kostrikis LG, Kucherer C, Liitsola K, Linka M, Nielsen C, Otelea D, Paredes R, Poljak M, Puchhammer-Stockl E, Schmit JC, Sonnerborg A, Stanekova D, Stanojevic M, Struck D, Boucher CA, Vandamme AM. HIV-1 subtype distribution and its demographic determinants in newly diagnosed patients in Europe suggest highly compartmentalized epidemics. Retrovirology. 2013;10:7. Epub 2013/01/16. doi: 10.1186/1742-4690-10-7. PubMed PMID: 23317093; PMCID: PMC3564855.

13. Bobkov AF, Kazennova EV, Selimova LM, Khanina TA, Ryabov GS, Bobkova MR, Sukhanova AL, Kravchenko AV, Ladnaya NN, Weber JN, Pokrovsky VV. Temporal trends in the

HIV-1 epidemic in Russia: predominance of subtype A. J Med Virol. 2004;74(2):191-6. Epub 2004/08/28. doi: 10.1002/jmv.20177. PubMed PMID: 15332265.

14. Engelman A, Cherepanov P. The structural biology of HIV-1: mechanistic and therapeutic insights. Nat Rev Microbiol. 2012;10(4):279-90. Epub 2012/03/17. doi: 10.1038/nrmicro2747. PubMed PMID: 22421880; PMCID: PMC3588166.

15. Deeks SG, Overbaugh J, Phillips A, Buchbinder S. HIV infection. Nat Rev Dis Primers. 2015;1:15035. Epub 2015/01/01. doi: 10.1038/nrdp.2015.35. PubMed PMID: 27188527.

16. Frankel AD, Young JA. HIV-1: fifteen proteins and an RNA. Annu Rev Biochem. 1998;67:1-25. Epub 1998/10/06. doi: 10.1146/annurev.biochem.67.1.1. PubMed PMID: 9759480.

17. Dragic T, Litwin V, Allaway GP, Martin SR, Huang Y, Nagashima KA, Cayanan C, Maddon PJ, Koup RA, Moore JP, Paxton WA. HIV-1 entry into CD4+ cells is mediated by the chemokine receptor CC-CKR-5. Nature. 1996;381(6584):667-73. Epub 1996/06/20. doi: 10.1038/381667a0. PubMed PMID: 8649512.

18. Huang Y, Paxton WA, Wolinsky SM, Neumann AU, Zhang L, He T, Kang S, Ceradini D, Jin Z, Yazdanbakhsh K, Kunstman K, Erickson D, Dragon E, Landau NR, Phair J, Ho DD, Koup RA. The role of a mutant CCR5 allele in HIV-1 transmission and disease progression. Nat Med. 1996;2(11):1240-3. Epub 1996/11/01. doi: 10.1038/nm1196-1240. PubMed PMID: 8898752.

19. Liu J, Bartesaghi A, Borgnia MJ, Sapiro G, Subramaniam S. Molecular architecture of native HIV-1 gp120 trimers. Nature. 2008;455(7209):109-13. Epub 2008/08/01. doi: 10.1038/nature07159. PubMed PMID: 18668044; PMCID: PMC2610422.

20. Liu R, Paxton WA, Choe S, Ceradini D, Martin SR, Horuk R, MacDonald ME, Stuhlmann H, Koup RA, Landau NR. Homozygous defect in HIV-1 coreceptor accounts for resistance of some multiply-exposed individuals to HIV-1 infection. Cell. 1996;86(3):367-77. Epub 1996/08/09. doi: 10.1016/s0092-8674(00)80110-5. PubMed PMID: 8756719.

21. Mosier DE. How HIV changes its tropism: evolution and adaptation? Curr Opin HIV AIDS. 2009;4(2):125-30. Epub 2009/04/03. doi: 10.1097/COH.0b013e3283223d61. PubMed PMID: 19339951; PMCID: PMC2697388.

22. Zanetti G, Briggs JA, Grunewald K, Sattentau QJ, Fuller SD. Cryo-electron tomographic structure of an immunodeficiency virus envelope complex in situ. PLoS Pathog. 2006;2(8):e83. Epub 2006/08/29. doi: 10.1371/journal.ppat.0020083. PubMed PMID: 16933990; PMCID: PMC1557830.

23. Zhu P, Liu J, Bess J, Jr., Chertova E, Lifson JD, Grise H, Ofek GA, Taylor KA, Roux KH. Distribution and three-dimensional structure of AIDS virus envelope spikes. Nature. 2006;441(7095):847-52. Epub 2006/05/27. doi: 10.1038/nature04817. PubMed PMID: 16728975.

24. Kong R, Duan H, Sheng Z, Xu K, Acharya P, Chen X, Cheng C, Dingens AS, Gorman J, Sastry M, Shen CH, Zhang B, Zhou T, Chuang GY, Chao CW, Gu Y, Jafari AJ, Louder MK, O'Dell S, Rowshan AP, Viox EG, Wang Y, Choi CW, Corcoran MM, Corrigan AR, Dandey VP, Eng ET, Geng H, Foulds KE, Guo Y, Kwon YD, Lin B, Liu K, Mason RD, Nason MC, Ohr TY, Ou L, Rawi R, Sarfo EK, Schon A, Todd JP, Wang S, Wei H, Wu W, Program NCS, Mullikin JC, Bailer RT, Doria-Rose NA, Karlsson Hedestam GB, Scorpio DG, Overbaugh J, Bloom JD, Carragher B, Potter CS, Shapiro L, Kwong PD, Mascola JR. Antibody Lineages with Vaccine-Induced Antigen-Binding Hotspots Develop Broad HIV Neutralization. Cell. 2019;178(3):567-84 e19. Epub 2019/07/28. doi: 10.1016/j.cell.2019.06.030. PubMed PMID: 31348886; PMCID: PMC6755680.

25. Xu K, Acharya P, Kong R, Cheng C, Chuang GY, Liu K, Louder MK, O'Dell S, Rawi R, Sastry M, Shen CH, Zhang B, Zhou T, Asokan M, Bailer RT, Chambers M, Chen X, Choi CW, Dandey VP, Doria-Rose NA, Druz A, Eng ET, Farney SK, Foulds KE, Geng H, Georgiev IS, Gorman J, Hill KR, Jafari AJ, Kwon YD, Lai YT, Lemmin T, McKee K, Ohr TY, Ou L, Peng D, Rowshan AP, Sheng Z, Todd JP, Tsybovsky Y, Viox EG, Wang Y, Wei H, Yang Y, Zhou AF, Chen R, Yang L, Scorpio DG, McDermott AB, Shapiro L, Carragher B, Potter CS, Mascola JR, Kwong PD. Epitope-based vaccine design yields fusion peptide-directed antibodies that neutralize

diverse strains of HIV-1. Nat Med. 2018;24(6):857-67. Epub 2018/06/06. doi: 10.1038/s41591-018-0042-6. PubMed PMID: 29867235; PMCID: PMC6358635.

26. Bebenek K, Abbotts J, Wilson SH, Kunkel TA. Error-prone polymerization by HIV-1 reverse transcriptase. Contribution of template-primer misalignment, miscoding, and termination probability to mutational hot spots. J Biol Chem. 1993;268(14):10324-34. Epub 1993/05/15. PubMed PMID: 7683675.

27. Li WH, Tanimura M, Sharp PM. Rates and dates of divergence between AIDS virus nucleotide sequences. Mol Biol Evol. 1988;5(4):313-30. Epub 1988/07/01. doi: 10.1093/oxfordjournals.molbev.a040503. PubMed PMID: 3405075.

28. Roberts JD, Bebenek K, Kunkel TA. The accuracy of reverse transcriptase from HIV-1. Science. 1988;242(4882):1171-3. Epub 1988/11/25. doi: 10.1126/science.2460925. PubMed PMID: 2460925.

29. Cohen MS, Hellmann N, Levy JA, DeCock K, Lange J. The spread, treatment, and prevention of HIV-1: evolution of a global pandemic. J Clin Invest. 2008;118(4):1244-54. Epub 2008/04/03. doi: 10.1172/JCI34706. PubMed PMID: 18382737; PMCID: PMC2276790.

30. Shaw GM, Hunter E. HIV transmission. Cold Spring Harb Perspect Med. 2012;2(11). Epub 2012/10/09. doi: 10.1101/cshperspect.a006965. PubMed PMID: 23043157; PMCID: PMC3543106.

31. Simon V, Ho DD, Abdool Karim Q. HIV/AIDS epidemiology, pathogenesis, prevention, and treatment. Lancet. 2006;368(9534):489-504. Epub 2006/08/08. doi: 10.1016/S0140-6736(06)69157-5. PubMed PMID: 16890836; PMCID: PMC2913538.

32. Chi BH, Bolton-Moore C, Holmes CB. Prevention of mother-to-child HIV transmission within the continuum of maternal, newborn, and child health services. Curr Opin HIV AIDS. 2013;8(5):498-503. Epub 2013/07/23. doi: 10.1097/COH.0b013e3283637f7a. PubMed PMID: 23872611; PMCID: PMC4049298.

33. Jin F, Jansson J, Law M, Prestage GP, Zablotska I, Imrie JC, Kippax SC, Kaldor JM, Grulich AE, Wilson DP. Per-contact probability of HIV transmission in homosexual men in Sydney in the era of HAART. AIDS. 2010;24(6):907-13. Epub 2010/02/09. doi: 10.1097/QAD.0b013e3283372d90. PubMed PMID: 20139750; PMCID: PMC2852627.

34. Patel P, Borkowf CB, Brooks JT, Lasry A, Lansky A, Mermin J. Estimating per-act HIV transmission risk: a systematic review. AIDS. 2014;28(10):1509-19. Epub 2014/05/09. doi: 10.1097/QAD.0000000000000298. PubMed PMID: 24809629; PMCID: PMC6195215.

35. Bracq L, Xie M, Benichou S, Bouchet J. Mechanisms for Cell-to-Cell Transmission of HIV-1. Front Immunol. 2018;9:260. Epub 2018/03/09. doi: 10.3389/fimmu.2018.00260. PubMed PMID: 29515578; PMCID: PMC5825902.

36. Derdeyn CA, Decker JM, Bibollet-Ruche F, Mokili JL, Muldoon M, Denham SA, Heil ML, Kasolo F, Musonda R, Hahn BH, Shaw GM, Korber BT, Allen S, Hunter E. Envelope-constrained neutralization-sensitive HIV-1 after heterosexual transmission. Science. 2004;303(5666):2019-22. Epub 2004/03/27. doi: 10.1126/science.1093137. PubMed PMID: 15044802.

37. Joseph SB, Swanstrom R, Kashuba AD, Cohen MS. Bottlenecks in HIV-1 transmission: insights from the study of founder viruses. Nat Rev Microbiol. 2015;13(7):414-25. Epub 2015/06/09. doi: 10.1038/nrmicro3471. PubMed PMID: 26052661; PMCID: PMC4793885.

38. Borrow P, Lewicki H, Wei X, Horwitz MS, Peffer N, Meyers H, Nelson JA, Gairin JE, Hahn BH, Oldstone MB, Shaw GM. Antiviral pressure exerted by HIV-1-specific cytotoxic T lymphocytes (CTLs) during primary infection demonstrated by rapid selection of CTL escape virus. Nat Med. 1997;3(2):205-11. Epub 1997/02/01. doi: 10.1038/nm0297-205. PubMed PMID: 9018240.

39. Kwong PD, Doyle ML, Casper DJ, Cicala C, Leavitt SA, Majeed S, Steenbeke TD, Venturi M, Chaiken I, Fung M, Katinger H, Parren PW, Robinson J, Van Ryk D, Wang L, Burton DR, Freire E, Wyatt R, Sodroski J, Hendrickson WA, Arthos J. HIV-1 evades antibody-mediated neutralization through conformational masking of receptor-binding sites. Nature. 2002;420(6916):678-82. Epub 2002/12/13. doi: 10.1038/nature01188. PubMed PMID: 12478295.

40. Piatak M, Jr., Saag MS, Yang LC, Clark SJ, Kappes JC, Luk KC, Hahn BH, Shaw GM, Lifson JD. High levels of HIV-1 in plasma during all stages of infection determined by competitive PCR. Science. 1993;259(5102):1749-54. Epub 1993/03/19. doi: 10.1126/science.8096089. PubMed PMID: 8096089.

41. Price DA, Goulder PJ, Klenerman P, Sewell AK, Easterbrook PJ, Troop M, Bangham CR, Phillips RE. Positive selection of HIV-1 cytotoxic T lymphocyte escape variants during primary infection. Proc Natl Acad Sci U S A. 1997;94(5):1890-5. Epub 1997/03/04. doi: 10.1073/pnas.94.5.1890. PubMed PMID: 9050875; PMCID: PMC20013.

42. Douek DC, Picker LJ, Koup RA. T cell dynamics in HIV-1 infection. Annu Rev Immunol. 2003;21:265-304. Epub 2003/01/14. doi: 10.1146/annurev.immunol.21.120601.141053. PubMed PMID: 12524385.

43. Brenchley JM, Schacker TW, Ruff LE, Price DA, Taylor JH, Beilman GJ, Nguyen PL, Khoruts A, Larson M, Haase AT, Douek DC. CD4+ T cell depletion during all stages of HIV disease occurs predominantly in the gastrointestinal tract. J Exp Med. 2004;200(6):749-59. Epub 2004/09/15. doi: 10.1084/jem.20040874. PubMed PMID: 15365096; PMCID: PMC2211962.

44. Mattapallil JJ, Douek DC, Hill B, Nishimura Y, Martin M, Roederer M. Massive infection and loss of memory CD4+ T cells in multiple tissues during acute SIV infection. Nature. 2005;434(7037):1093-7. Epub 2005/03/29. doi: 10.1038/nature03501. PubMed PMID: 15793563.

45. Veazey RS, Mansfield KG, Tham IC, Carville AC, Shvetz DE, Forand AE, Lackner AA. Dynamics of CCR5 expression by CD4(+) T cells in lymphoid tissues during simian immunodeficiency virus infection. J Virol. 2000;74(23):11001-7. Epub 2000/11/09. doi: 10.1128/jvi.74.23.11001-11007.2000. PubMed PMID: 11069995; PMCID: PMC113180.

46. Veazey RS, Tham IC, Mansfield KG, DeMaria M, Forand AE, Shvetz DE, Chalifoux LV, Sehgal PK, Lackner AA. Identifying the target cell in primary simian immunodeficiency virus (SIV) infection: highly activated memory CD4(+) T cells are rapidly eliminated in early SIV infection in

vivo. J Virol. 2000;74(1):57-64. Epub 1999/12/10. doi: 10.1128/jvi.74.1.57-64.2000. PubMed PMID: 10590091; PMCID: PMC111513.

47. Reimann KA, Tenner-Racz K, Racz P, Montefiori DC, Yasutomi Y, Lin W, Ransil BJ, Letvin NL. Immunopathogenic events in acute infection of rhesus monkeys with simian immunodeficiency virus of macaques. J Virol. 1994;68(4):2362-70. Epub 1994/04/01. doi: 10.1128/JVI.68.4.2362-2370.1994. PubMed PMID: 8139022; PMCID: PMC236713.

48. Vajdy M, Veazey RS, Knight HK, Lackner AA, Neutra MR. Differential effects of simian immunodeficiency virus infection on immune inductive and effector sites in the rectal mucosa of rhesus macaques. Am J Pathol. 2000;157(2):485-95. Epub 2000/08/10. doi: 10.1016/S0002-9440(10)64560-9. PubMed PMID: 10934152; PMCID: PMC1850137.

49. Veazey RS, DeMaria M, Chalifoux LV, Shvetz DE, Pauley DR, Knight HL, Rosenzweig M, Johnson RP, Desrosiers RC, Lackner AA. Gastrointestinal tract as a major site of CD4+ T cell depletion and viral replication in SIV infection. Science. 1998;280(5362):427-31. Epub 1998/05/09. doi: 10.1126/science.280.5362.427. PubMed PMID: 9545219.

50. Zhang Z, Schuler T, Zupancic M, Wietgrefe S, Staskus KA, Reimann KA, Reinhart TA, Rogan M, Cavert W, Miller CJ, Veazey RS, Notermans D, Little S, Danner SA, Richman DD, Havlir D, Wong J, Jordan HL, Schacker TW, Racz P, Tenner-Racz K, Letvin NL, Wolinsky S, Haase AT. Sexual transmission and propagation of SIV and HIV in resting and activated CD4+ T cells. Science. 1999;286(5443):1353-7. Epub 1999/11/13. doi: 10.1126/science.286.5443.1353. PubMed PMID: 10558989.

51. Haase AT. Population biology of HIV-1 infection: viral and CD4+ T cell demographics and dynamics in lymphatic tissues. Annu Rev Immunol. 1999;17:625-56. Epub 1999/06/08. doi: 10.1146/annurev.immunol.17.1.625. PubMed PMID: 10358770.

52. Schacker T, Little S, Connick E, Gebhard K, Zhang ZQ, Krieger J, Pryor J, Havlir D, Wong JK, Schooley RT, Richman D, Corey L, Haase AT. Productive infection of T cells in lymphoid

tissues during primary and early human immunodeficiency virus infection. J Infect Dis. 2001;183(4):555-62. Epub 2001/02/15. doi: 10.1086/318524. PubMed PMID: 11170980.

53. Stahl-Hennig C, Steinman RM, Tenner-Racz K, Pope M, Stolte N, Matz-Rensing K, Grobschupff G, Raschdorff B, Hunsmann G, Racz P. Rapid infection of oral mucosal-associated lymphoid tissue with simian immunodeficiency virus. Science. 1999;285(5431):1261-5. Epub 1999/08/24. doi: 10.1126/science.285.5431.1261. PubMed PMID: 10455052.

54. Borrow P, Lewicki H, Hahn BH, Shaw GM, Oldstone MB. Virus-specific CD8+ cytotoxic T-lymphocyte activity associated with control of viremia in primary human immunodeficiency virus type 1 infection. J Virol. 1994;68(9):6103-10. Epub 1994/09/01. doi: 10.1128/JVI.68.9.6103-6110.1994. PubMed PMID: 8057491; PMCID: PMC237022.

55. Chun TW, Carruth L, Finzi D, Shen X, DiGiuseppe JA, Taylor H, Hermankova M, Chadwick K, Margolick J, Quinn TC, Kuo YH, Brookmeyer R, Zeiger MA, Barditch-Crovo P, Siliciano RF. Quantification of latent tissue reservoirs and total body viral load in HIV-1 infection. Nature. 1997;387(6629):183-8. Epub 1997/05/08. doi: 10.1038/387183a0. PubMed PMID: 9144289.

56. Chun TW, Engel D, Berrey MM, Shea T, Corey L, Fauci AS. Early establishment of a pool of latently infected, resting CD4(+) T cells during primary HIV-1 infection. Proc Natl Acad Sci U S A. 1998;95(15):8869-73. Epub 1998/07/22. doi: 10.1073/pnas.95.15.8869. PubMed PMID: 9671771; PMCID: PMC21169.

57. Clark SJ, Saag MS, Decker WD, Campbell-Hill S, Roberson JL, Veldkamp PJ, Kappes JC, Hahn BH, Shaw GM. High titers of cytopathic virus in plasma of patients with symptomatic primary HIV-1 infection. N Engl J Med. 1991;324(14):954-60. Epub 1991/04/04. doi: 10.1056/NEJM199104043241404. PubMed PMID: 1900576.

58. Cooper DA, Gold J, Maclean P, Donovan B, Finlayson R, Barnes TG, Michelmore HM, Brooke P, Penny R. Acute AIDS retrovirus infection. Definition of a clinical illness associated with seroconversion. Lancet. 1985;1(8428):537-40. Epub 1985/03/09. doi: 10.1016/s0140-6736(85)91205-x. PubMed PMID: 2857899.

59. Finzi D, Blankson J, Siliciano JD, Margolick JB, Chadwick K, Pierson T, Smith K, Lisziewicz J, Lori F, Flexner C, Quinn TC, Chaisson RE, Rosenberg E, Walker B, Gange S, Gallant J, Siliciano RF. Latent infection of CD4+ T cells provides a mechanism for lifelong persistence of HIV-1, even in patients on effective combination therapy. Nat Med. 1999;5(5):512-7. Epub 1999/05/06. doi: 10.1038/8394. PubMed PMID: 10229227.

60. Finzi D, Hermankova M, Pierson T, Carruth LM, Buck C, Chaisson RE, Quinn TC, Chadwick K, Margolick J, Brookmeyer R, Gallant J, Markowitz M, Ho DD, Richman DD, Siliciano RF. Identification of a reservoir for HIV-1 in patients on highly active antiretroviral therapy. Science. 1997;278(5341):1295-300. Epub 1997/11/21. doi: 10.1126/science.278.5341.1295. PubMed PMID: 9360927.

61. Henrard DR, Daar E, Farzadegan H, Clark SJ, Phillips J, Shaw GM, Busch MP. Virologic and immunologic characterization of symptomatic and asymptomatic primary HIV-1 infection. J Acquir Immune Defic Syndr Hum Retrovirol. 1995;9(3):305-10. Epub 1995/07/01. PubMed PMID: 7788430.

62. Ho DD, Sarngadharan MG, Resnick L, Dimarzoveronese F, Rota TR, Hirsch MS. Primary human T-lymphotropic virus type III infection. Ann Intern Med. 1985;103(6 (Pt 1)):880-3. Epub 1985/12/01. doi: 10.7326/0003-4819-103-6-880. PubMed PMID: 2998251.

63. Koup RA, Safrit JT, Cao Y, Andrews CA, McLeod G, Borkowsky W, Farthing C, Ho DD. Temporal association of cellular immune responses with the initial control of viremia in primary human immunodeficiency virus type 1 syndrome. J Virol. 1994;68(7):4650-5. Epub 1994/07/01. doi: 10.1128/JVI.68.7.4650-4655.1994. PubMed PMID: 8207839; PMCID: PMC236393.

64. Lyles RH, Munoz A, Yamashita TE, Bazmi H, Detels R, Rinaldo CR, Margolick JB, Phair JP, Mellors JW. Natural history of human immunodeficiency virus type 1 viremia after seroconversion and proximal to AIDS in a large cohort of homosexual men. Multicenter AIDS Cohort Study. J Infect Dis. 2000;181(3):872-80. Epub 2000/03/18. doi: 10.1086/315339. PubMed PMID: 10720507.

65. Pitcher CJ, Quittner C, Peterson DM, Connors M, Koup RA, Maino VC, Picker LJ. HIV-1-specific CD4+ T cells are detectable in most individuals with active HIV-1 infection, but decline with prolonged viral suppression. Nat Med. 1999;5(5):518-25. Epub 1999/05/06. doi: 10.1038/8400. PubMed PMID: 10229228.

66. Rosenberg ES, Billingsley JM, Caliendo AM, Boswell SL, Sax PE, Kalams SA, Walker BD. Vigorous HIV-1-specific CD4+ T cell responses associated with control of viremia. Science. 1997;278(5342):1447-50. Epub 1997/12/31. doi: 10.1126/science.278.5342.1447. PubMed PMID: 9367954.

67. Schacker TW, Hughes JP, Shea T, Coombs RW, Corey L. Biological and virologic characteristics of primary HIV infection. Ann Intern Med. 1998;128(8):613-20. Epub 1998/12/16. doi: 10.7326/0003-4819-128-8-199804150-00001. PubMed PMID: 9537934.

68. Sebastian S, Luban J. TRIM5alpha selectively binds a restriction-sensitive retroviral capsid. Retrovirology. 2005;2:40. Epub 2005/06/22. doi: 10.1186/1742-4690-2-40. PubMed PMID: 15967037; PMCID: PMC1166576.

69. Stremlau M, Perron M, Lee M, Li Y, Song B, Javanbakht H, Diaz-Griffero F, Anderson DJ, Sundquist WI, Sodroski J. Specific recognition and accelerated uncoating of retroviral capsids by the TRIM5alpha restriction factor. Proc Natl Acad Sci U S A. 2006;103(14):5514-9. Epub 2006/03/17. doi: 10.1073/pnas.0509996103. PubMed PMID: 16540544; PMCID: PMC1459386.

70. Wu X, Anderson JL, Campbell EM, Joseph AM, Hope TJ. Proteasome inhibitors uncouple rhesus TRIM5alpha restriction of HIV-1 reverse transcription and infection. Proc Natl Acad Sci U S A. 2006;103(19):7465-70. Epub 2006/05/02. doi: 10.1073/pnas.0510483103. PubMed PMID: 16648264; PMCID: PMC1464362.

71. Galao RP, Pickering S, Curnock R, Neil SJ. Retroviral retention activates a Syk-dependent HemITAM in human tetherin. Cell Host Microbe. 2014;16(3):291-303. Epub 2014/09/12. doi: 10.1016/j.chom.2014.08.005. PubMed PMID: 25211072; PMCID: PMC4161388.

72. Donahue JP, Vetter ML, Mukhtar NA, D'Aquila RT. The HIV-1 Vif PPLP motif is necessary for human APOBEC3G binding and degradation. Virology. 2008;377(1):49-53. Epub 2008/05/24. doi: 10.1016/j.virol.2008.04.017. PubMed PMID: 18499212; PMCID: PMC2474554.

73. Harris RS, Liddament MT. Retroviral restriction by APOBEC proteins. Nat Rev Immunol. 2004;4(11):868-77. Epub 2004/11/02. doi: 10.1038/nri1489. PubMed PMID: 15516966.

74. Mbisa JL, Barr R, Thomas JA, Vandegraaff N, Dorweiler IJ, Svarovskaia ES, Brown WL, Mansky LM, Gorelick RJ, Harris RS, Engelman A, Pathak VK. Human immunodeficiency virus type 1 cDNAs produced in the presence of APOBEC3G exhibit defects in plus-strand DNA transfer and integration. J Virol. 2007;81(13):7099-110. Epub 2007/04/13. doi: 10.1128/JVI.00272-07. PubMed PMID: 17428871; PMCID: PMC1933301.

75. Kwa S, Kannanganat S, Nigam P, Siddiqui M, Shetty RD, Armstrong W, Ansari A, Bosinger SE, Silvestri G, Amara RR. Plasmacytoid dendritic cells are recruited to the colorectum and contribute to immune activation during pathogenic SIV infection in rhesus macaques. Blood. 2011;118(10):2763-73. Epub 2011/06/23. doi: 10.1182/blood-2011-02-339515. PubMed PMID: 21693759; PMCID: PMC3172794.

76. Li Q, Estes JD, Schlievert PM, Duan L, Brosnahan AJ, Southern PJ, Reilly CS, Peterson ML, Schultz-Darken N, Brunner KG, Nephew KR, Pambuccian S, Lifson JD, Carlis JV, Haase AT. Glycerol monolaurate prevents mucosal SIV transmission. Nature. 2009;458(7241):1034-8. Epub 2009/03/06. doi: 10.1038/nature07831. PubMed PMID: 19262509; PMCID: PMC2785041.

77. Malleret B, Maneglier B, Karlsson I, Lebon P, Nascimbeni M, Perie L, Brochard P, Delache B, Calvo J, Andrieu T, Spreux-Varoquaux O, Hosmalin A, Le Grand R, Vaslin B. Primary infection with simian immunodeficiency virus: plasmacytoid dendritic cell homing to lymph nodes, type I interferon, and immune suppression. Blood. 2008;112(12):4598-608. Epub 2008/09/13. doi: 10.1182/blood-2008-06-162651. PubMed PMID: 18787223.

78. Bosinger SE, Johnson ZP, Folkner KA, Patel N, Hashempour T, Jochems SP, Del Rio Estrada PM, Paiardini M, Lin R, Vanderford TH, Hiscott J, Silvestri G. Intact type I Interferon

production and IRF7 function in sooty mangabeys. PLoS Pathog. 2013;9(8):e1003597. Epub 2013/09/07. doi: 10.1371/journal.ppat.1003597. PubMed PMID: 24009514; PMCID: PMC3757038.

79. Nganou-Makamdop K, Billingsley JM, Yaffe Z, O'Connor G, Tharp GK, Ransier A, Laboune F, Matus-Nicodemos R, Lerner A, Gharu L, Robertson JM, Ford ML, Schlapschy M, Kuhn N, Lensch A, Lifson J, Nason M, Skerra A, Schreiber G, Bosinger SE, Douek DC. Type I IFN signaling blockade by a PASylated antagonist during chronic SIV infection suppresses specific inflammatory pathways but does not alter T cell activation or virus replication. PLoS Pathog. 2018;14(8):e1007246. Epub 2018/08/25. doi: 10.1371/journal.ppat.1007246. PubMed PMID: 30142226; PMCID: PMC6126880 conflict of interest.

80. Nganou-Makamdop K, Douek DC. Manipulating the Interferon Signaling Pathway: Implications for HIV Infection. Virol Sin. 2019;34(2):192-6. Epub 2019/02/15. doi: 10.1007/s12250-019-00085-5. PubMed PMID: 30762199; PMCID: PMC6513936.

81. Palesch D, Bosinger SE, Mavigner M, Billingsley JM, Mattingly C, Carnathan DG, Paiardini M, Chahroudi A, Vanderford TH, Silvestri G. Short-Term Pegylated Interferon alpha2a Treatment Does Not Significantly Reduce the Viral Reservoir of Simian Immunodeficiency Virus-Infected, Antiretroviral Therapy-Treated Rhesus Macaques. J Virol. 2018;92(14). Epub 2018/05/04. doi: 10.1128/JVI.00279-18. PubMed PMID: 29720521; PMCID: PMC6026735.

82. Sandler NG, Bosinger SE, Estes JD, Zhu RT, Tharp GK, Boritz E, Levin D, Wijeyesinghe S, Makamdop KN, del Prete GQ, Hill BJ, Timmer JK, Reiss E, Yarden G, Darko S, Contijoch E, Todd JP, Silvestri G, Nason M, Norgren RB, Jr., Keele BF, Rao S, Langer JA, Lifson JD, Schreiber G, Douek DC. Type I interferon responses in rhesus macaques prevent SIV infection and slow disease progression. Nature. 2014;511(7511):601-5. Epub 2014/07/22. doi: 10.1038/nature13554. PubMed PMID: 25043006; PMCID: PMC4418221.

83. Utay NS, Douek DC. Interferons and HIV Infection: The Good, the Bad, and the Ugly. Pathog Immun. 2016;1(1):107-16. Epub 2016/08/09. doi: 10.20411/pai.v1i1.125. PubMed PMID: 27500281; PMCID: PMC4972494.

84. Heil F, Hemmi H, Hochrein H, Ampenberger F, Kirschning C, Akira S, Lipford G, Wagner H, Bauer S. Species-specific recognition of single-stranded RNA via toll-like receptor 7 and 8. Science. 2004;303(5663):1526-9. Epub 2004/02/21. doi: 10.1126/science.1093620. PubMed PMID: 14976262.

85. Brenchley JM, Price DA, Schacker TW, Asher TE, Silvestri G, Rao S, Kazzaz Z, Bornstein E, Lambotte O, Altmann D, Blazar BR, Rodriguez B, Teixeira-Johnson L, Landay A, Martin JN, Hecht FM, Picker LJ, Lederman MM, Deeks SG, Douek DC. Microbial translocation is a cause of systemic immune activation in chronic HIV infection. Nat Med. 2006;12(12):1365-71. Epub 2006/11/23. doi: 10.1038/nm1511. PubMed PMID: 17115046.

86. Brenchley JM, Paiardini M, Knox KS, Asher AI, Cervasi B, Asher TE, Scheinberg P, Price DA, Hage CA, Kholi LM, Khoruts A, Frank I, Else J, Schacker T, Silvestri G, Douek DC. Differential Th17 CD4 T-cell depletion in pathogenic and nonpathogenic lentiviral infections. Blood. 2008;112(7):2826-35. Epub 2008/07/31. doi: 10.1182/blood-2008-05-159301. PubMed PMID: 18664624; PMCID: PMC2556618.

87. Cecchinato V, Trindade CJ, Laurence A, Heraud JM, Brenchley JM, Ferrari MG, Zaffiri L, Tryniszewska E, Tsai WP, Vaccari M, Parks RW, Venzon D, Douek DC, O'Shea JJ, Franchini G. Altered balance between Th17 and Th1 cells at mucosal sites predicts AIDS progression in simian immunodeficiency virus-infected macaques. Mucosal Immunol. 2008;1(4):279-88. Epub 2008/12/17. doi: 10.1038/mi.2008.14. PubMed PMID: 19079189; PMCID: PMC2997489.

88. Jacquelin B, Mayau V, Targat B, Liovat AS, Kunkel D, Petitjean G, Dillies MA, Roques P, Butor C, Silvestri G, Giavedoni LD, Lebon P, Barre-Sinoussi F, Benecke A, Muller-Trutwin MC. Nonpathogenic SIV infection of African green monkeys induces a strong but rapidly controlled

type I IFN response. J Clin Invest. 2009;119(12):3544-55. Epub 2009/12/05. doi: 10.1172/JCI40093. PubMed PMID: 19959873; PMCID: PMC2786805.

89. Lederer S, Favre D, Walters KA, Proll S, Kanwar B, Kasakow Z, Baskin CR, Palermo R, McCune JM, Katze MG. Transcriptional profiling in pathogenic and non-pathogenic SIV infections reveals significant distinctions in kinetics and tissue compartmentalization. PLoS Pathog. 2009;5(2):e1000296. Epub 2009/02/14. doi: 10.1371/journal.ppat.1000296. PubMed PMID: 19214219; PMCID: PMC2633618.

90. Huot N, Jacquelin B, Garcia-Tellez T, Rascle P, Ploquin MJ, Madec Y, Reeves RK, Derreudre-Bosquet N, Muller-Trutwin M. Natural killer cells migrate into and control simian immunodeficiency virus replication in lymph node follicles in African green monkeys. Nat Med. 2017;23(11):1277-86. Epub 2017/10/17. doi: 10.1038/nm.4421. PubMed PMID: 29035370; PMCID: PMC6362838.

91. Appay V, Papagno L, Spina CA, Hansasuta P, King A, Jones L, Ogg GS, Little S, McMichael AJ, Richman DD, Rowland-Jones SL. Dynamics of T cell responses in HIV infection. J Immunol. 2002;168(7):3660-6. Epub 2002/03/22. doi: 10.4049/jimmunol.168.7.3660. PubMed PMID: 11907132.

92. Doisne JM, Urrutia A, Lacabaratz-Porret C, Goujard C, Meyer L, Chaix ML, Sinet M, Venet A. CD8+ T cells specific for EBV, cytomegalovirus, and influenza virus are activated during primary HIV infection. J Immunol. 2004;173(4):2410-8. Epub 2004/08/06. doi: 10.4049/jimmunol.173.4.2410. PubMed PMID: 15294954.

93. Ndhlovu ZM, Kamya P, Mewalal N, Kloverpris HN, Nkosi T, Pretorius K, Laher F, Ogunshola F, Chopera D, Shekhar K, Ghebremichael M, Ismail N, Moodley A, Malik A, Leslie A, Goulder PJ, Buus S, Chakraborty A, Dong K, Ndung'u T, Walker BD. Magnitude and Kinetics of CD8+ T Cell Activation during Hyperacute HIV Infection Impact Viral Set Point. Immunity. 2015;43(3):591-604. Epub 2015/09/13. doi: 10.1016/j.immuni.2015.08.012. PubMed PMID: 26362266; PMCID: PMC4575777.

94. Papagno L, Spina CA, Marchant A, Salio M, Rufer N, Little S, Dong T, Chesney G, Waters A, Easterbrook P, Dunbar PR, Shepherd D, Cerundolo V, Emery V, Griffiths P, Conlon C, McMichael AJ, Richman DD, Rowland-Jones SL, Appay V. Immune activation and CD8+ T-cell differentiation towards senescence in HIV-1 infection. PLoS Biol. 2004;2(2):E20. Epub 2004/02/18. doi: 10.1371/journal.pbio.0020020. PubMed PMID: 14966528; PMCID: PMC340937.

95. Takata H, Buranapraditkun S, Kessing C, Fletcher JL, Muir R, Tardif V, Cartwright P, Vandergeeten C, Bakeman W, Nichols CN, Pinyakorn S, Hansasuta P, Kroon E, Chalermchai T, O'Connell R, Kim J, Phanuphak N, Robb ML, Michael NL, Chomont N, Haddad EK, Ananworanich J, Trautmann L, Rv254/Search, the RVSSG. Delayed differentiation of potent effector CD8(+) T cells reducing viremia and reservoir seeding in acute HIV infection. Sci Transl Med. 2017;9(377). Epub 2017/02/17. doi: 10.1126/scitranslmed.aag1809. PubMed PMID: 28202771; PMCID: PMC5678930.

96. Walker B, McMichael A. The T-cell response to HIV. Cold Spring Harb Perspect Med. 2012;2(11). Epub 2012/09/25. doi: 10.1101/cshperspect.a007054. PubMed PMID: 23002014; PMCID: PMC3543107.

97. Okoye A, Park H, Rohankhedkar M, Coyne-Johnson L, Lum R, Walker JM, Planer SL, Legasse AW, Sylwester AW, Piatak M, Jr., Lifson JD, Sodora DL, Villinger F, Axthelm MK, Schmitz JE, Picker LJ. Profound CD4+/CCR5+ T cell expansion is induced by CD8+ lymphocyte depletion but does not account for accelerated SIV pathogenesis. J Exp Med. 2009;206(7):1575-88. Epub 2009/06/24. doi: 10.1084/jem.20090356. PubMed PMID: 19546246; PMCID: PMC2715089.

98. Addo MM, Draenert R, Rathod A, Verrill CL, Davis BT, Gandhi RT, Robbins GK, Basgoz NO, Stone DR, Cohen DE, Johnston MN, Flynn T, Wurcel AG, Rosenberg ES, Altfeld M, Walker BD. Fully differentiated HIV-1 specific CD8+ T effector cells are more frequently detectable in controlled than in progressive HIV-1 infection. PLoS One. 2007;2(3):e321. Epub 2007/03/29. doi: 10.1371/journal.pone.0000321. PubMed PMID: 17389912; PMCID: PMC1824710.

99. Angin M, Wong G, Papagno L, Versmisse P, David A, Bayard C, Charmeteau-De Muylder B, Besseghir A, Thiebaut R, Boufassa F, Pancino G, Sauce D, Lambotte O, Brun-Vezinet F, Matheron S, Rowland-Jones SL, Cheynier R, Saez-Cirion A, Appay V, Group ACI-S. Preservation of Lymphopoietic Potential and Virus Suppressive Capacity by CD8+ T Cells in HIV-2-Infected Controllers. J Immunol. 2016;197(7):2787-95. Epub 2016/08/28. doi: 10.4049/jimmunol.1600693. PubMed PMID: 27566819.

100. Hersperger AR, Pereyra F, Nason M, Demers K, Sheth P, Shin LY, Kovacs CM, Rodriguez B, Sieg SF, Teixeira-Johnson L, Gudonis D, Goepfert PA, Lederman MM, Frank I, Makedonas G, Kaul R, Walker BD, Betts MR. Perforin expression directly ex vivo by HIV-specific CD8 T-cells is a correlate of HIV elite control. PLoS Pathog. 2010;6(5):e1000917. Epub 2010/06/05. doi: 10.1371/journal.ppat.1000917. PubMed PMID: 20523897; PMCID: PMC2877741.

101. Migueles SA, Osborne CM, Royce C, Compton AA, Joshi RP, Weeks KA, Rood JE, Berkley AM, Sacha JB, Cogliano-Shutta NA, Lloyd M, Roby G, Kwan R, McLaughlin M, Stallings S, Rehm C, O'Shea MA, Mican J, Packard BZ, Komoriya A, Palmer S, Wiegand AP, Maldarelli F, Coffin JM, Mellors JW, Hallahan CW, Follman DA, Connors M. Lytic granule loading of CD8+ T cells is required for HIV-infected cell elimination associated with immune control. Immunity. 2008;29(6):1009-21. Epub 2008/12/09. doi: 10.1016/j.immuni.2008.10.010. PubMed PMID: 19062316; PMCID: PMC2622434.

102. Saez-Cirion A, Jacquelin B, Barre-Sinoussi F, Muller-Trutwin M. Immune responses during spontaneous control of HIV and AIDS: what is the hope for a cure? Philos Trans R Soc Lond B Biol Sci. 2014;369(1645):20130436. Epub 2014/05/14. doi: 10.1098/rstb.2013.0436. PubMed PMID: 24821922; PMCID: PMC4024229.

103. Saez-Cirion A, Lacabaratz C, Lambotte O, Versmisse P, Urrutia A, Boufassa F, Barre-Sinoussi F, Delfraissy JF, Sinet M, Pancino G, Venet A, Agence Nationale de Recherches sur le Sida EPHIVCSG. HIV controllers exhibit potent CD8 T cell capacity to suppress HIV infection ex vivo and peculiar cytotoxic T lymphocyte activation phenotype. Proc Natl Acad Sci U S A.

2007;104(16):6776-81. Epub 2007/04/13. doi: 10.1073/pnas.0611244104. PubMed PMID: 17428922; PMCID: PMC1851664.

104. Shasha D, Karel D, Angiuli O, Greenblatt A, Ghebremichael M, Yu X, Porichis F, Walker BD. Elite controller CD8+ T cells exhibit comparable viral inhibition capacity, but better sustained effector properties compared to chronic progressors. J Leukoc Biol. 2016;100(6):1425-33. Epub 2016/07/14. doi: 10.1189/jlb.4A0915-422R. PubMed PMID: 27406996; PMCID: PMC5109996.

105. Buggert M, Nguyen S, Salgado-Montes de Oca G, Bengsch B, Darko S, Ransier A, Roberts ER, Del Alcazar D, Brody IB, Vella LA, Beura L, Wijeyesinghe S, Herati RS, Del Rio Estrada PM, Ablanedo-Terrazas Y, Kuri-Cervantes L, Sada Japp A, Manne S, Vartanian S, Huffman A, Sandberg JK, Gostick E, Nadolski G, Silvestri G, Canaday DH, Price DA, Petrovas C, Su LF, Vahedi G, Dori Y, Frank I, Itkin MG, Wherry EJ, Deeks SG, Naji A, Reyes-Teran G, Masopust D, Douek DC, Betts MR. Identification and characterization of HIV-specific resident memory CD8(+) T cells in human lymphoid tissue. Sci Immunol. 2018;3(24). Epub 2018/06/03. doi: 10.1126/sciimmunol.aar4526. PubMed PMID: 29858286; PMCID: PMC6357781.

106. Bailey JR, Williams TM, Siliciano RF, Blankson JN. Maintenance of viral suppression in HIV-1-infected HLA-B*57+ elite suppressors despite CTL escape mutations. J Exp Med. 2006;203(5):1357-69. Epub 2006/05/10. doi: 10.1084/jem.20052319. PubMed PMID: 16682496; PMCID: PMC2121215.

107. Henn MR, Boutwell CL, Charlebois P, Lennon NJ, Power KA, Macalalad AR, Berlin AM, Malboeuf CM, Ryan EM, Gnerre S, Zody MC, Erlich RL, Green LM, Berical A, Wang Y, Casali M, Streeck H, Bloom AK, Dudek T, Tully D, Newman R, Axten KL, Gladden AD, Battis L, Kemper M, Zeng Q, Shea TP, Gujja S, Zedlack C, Gasser O, Brander C, Hess C, Gunthard HF, Brumme ZL, Brumme CJ, Bazner S, Rychert J, Tinsley JP, Mayer KH, Rosenberg E, Pereyra F, Levin JZ, Young SK, Jessen H, Altfeld M, Birren BW, Walker BD, Allen TM. Whole genome deep sequencing of HIV-1 reveals the impact of early minor variants upon immune recognition during

acute infection. PLoS Pathog. 2012;8(3):e1002529. Epub 2012/03/14. doi: 10.1371/journal.ppat.1002529. PubMed PMID: 22412369; PMCID: PMC3297584.

108. Soghoian DZ, Jessen H, Flanders M, Sierra-Davidson K, Cutler S, Pertel T, Ranasinghe S, Lindqvist M, Davis I, Lane K, Rychert J, Rosenberg ES, Piechocka-Trocha A, Brass AL, Brenchley JM, Walker BD, Streeck H. HIV-specific cytolytic CD4 T cell responses during acute HIV infection predict disease outcome. Sci Transl Med. 2012;4(123):123ra25. Epub 2012/03/02. doi: 10.1126/scitranslmed.3003165. PubMed PMID: 22378925; PMCID: PMC3918726.

109. Douek DC, Brenchley JM, Betts MR, Ambrozak DR, Hill BJ, Okamoto Y, Casazza JP, Kuruppu J, Kunstman K, Wolinsky S, Grossman Z, Dybul M, Oxenius A, Price DA, Connors M, Koup RA. HIV preferentially infects HIV-specific CD4+ T cells. Nature. 2002;417(6884):95-8. Epub 2002/05/03. doi: 10.1038/417095a. PubMed PMID: 11986671.

110. Ryan ES, Micci L, Fromentin R, Paganini S, McGary CS, Easley K, Chomont N, Paiardini M. Loss of Function of Intestinal IL-17 and IL-22 Producing Cells Contributes to Inflammation and Viral Persistence in SIV-Infected Rhesus Macaques. PLoS Pathog. 2016;12(2):e1005412. Epub 2016/02/02. doi: 10.1371/journal.ppat.1005412. PubMed PMID: 26829644; PMCID: PMC4735119.

111. Micci L, Ryan ES, Fromentin R, Bosinger SE, Harper JL, He T, Paganini S, Easley KA, Chahroudi A, Benne C, Gumber S, McGary CS, Rogers KA, Deleage C, Lucero C, Byrareddy SN, Apetrei C, Estes JD, Lifson JD, Piatak M, Jr., Chomont N, Villinger F, Silvestri G, Brenchley JM, Paiardini M. Interleukin-21 combined with ART reduces inflammation and viral reservoir in SIV-infected macaques. J Clin Invest. 2015;125(12):4497-513. Epub 2015/11/10. doi: 10.1172/JCI81400. PubMed PMID: 26551680; PMCID: PMC4665780.

112. Tomaras GD, Haynes BF. HIV-1-specific antibody responses during acute and chronic HIV-1 infection. Curr Opin HIV AIDS. 2009;4(5):373-9. Epub 2010/01/06. doi: 10.1097/COH.0b013e32832f00c0. PubMed PMID: 20048700; PMCID: PMC3133462.

113. Victora GD, Mouquet H. What Are the Primary Limitations in B-Cell Affinity Maturation, and How Much Affinity Maturation Can We Drive with Vaccination? Lessons from the Antibody Response to HIV-1. Cold Spring Harb Perspect Biol. 2018;10(5). Epub 2017/06/21. doi: 10.1101/cshperspect.a029389. PubMed PMID: 28630079; PMCID: PMC5932586.

114. Mouquet H. Antibody B cell responses in HIV-1 infection. Trends Immunol. 2014;35(11):549-61. Epub 2014/09/23. doi: 10.1016/j.it.2014.08.007. PubMed PMID: 25240985.

115. Mouquet H, Scharf L, Euler Z, Liu Y, Eden C, Scheid JF, Halper-Stromberg A, Gnanapragasam PN, Spencer DI, Seaman MS, Schuitemaker H, Feizi T, Nussenzweig MC, Bjorkman PJ. Complex-type N-glycan recognition by potent broadly neutralizing HIV antibodies. Proc Natl Acad Sci U S A. 2012;109(47):E3268-77. Epub 2012/11/02. doi: 10.1073/pnas.1217207109. PubMed PMID: 23115339; PMCID: PMC3511153.

116. Rusert P, Kouyos RD, Kadelka C, Ebner H, Schanz M, Huber M, Braun DL, Hoze N, Scherrer A, Magnus C, Weber J, Uhr T, Cippa V, Thorball CW, Kuster H, Cavassini M, Bernasconi E, Hoffmann M, Calmy A, Battegay M, Rauch A, Yerly S, Aubert V, Klimkait T, Boni J, Fellay J, Regoes RR, Gunthard HF, Trkola A, Swiss HIVCS. Determinants of HIV-1 broadly neutralizing antibody induction. Nat Med. 2016;22(11):1260-7. Epub 2016/11/01. doi: 10.1038/nm.4187. PubMed PMID: 27668936.

117. Kelsoe G, Haynes BF. What Are the Primary Limitations in B-Cell Affinity Maturation, and How Much Affinity Maturation Can We Drive with Vaccination? Breaking through Immunity's Glass Ceiling. Cold Spring Harb Perspect Biol. 2018;10(5). Epub 2017/06/21. doi: 10.1101/cshperspect.a029397. PubMed PMID: 28630077; PMCID: PMC5736460.

118. Klein F, Diskin R, Scheid JF, Gaebler C, Mouquet H, Georgiev IS, Pancera M, Zhou T, Incesu RB, Fu BZ, Gnanapragasam PN, Oliveira TY, Seaman MS, Kwong PD, Bjorkman PJ, Nussenzweig MC. Somatic mutations of the immunoglobulin framework are generally required for broad and potent HIV-1 neutralization. Cell. 2013;153(1):126-38. Epub 2013/04/02. doi: 10.1016/j.cell.2013.03.018. PubMed PMID: 23540694; PMCID: PMC3792590.

119. Kardava L, Moir S, Shah N, Wang W, Wilson R, Buckner CM, Santich BH, Kim LJ, Spurlin EE, Nelson AK, Wheatley AK, Harvey CJ, McDermott AB, Wucherpfennig KW, Chun TW, Tsang JS, Li Y, Fauci AS. Abnormal B cell memory subsets dominate HIV-specific responses in infected individuals. J Clin Invest. 2014;124(7):3252-62. Epub 2014/06/04. doi: 10.1172/JCI74351. PubMed PMID: 24892810; PMCID: PMC4071400.

120. Moir S, Fauci AS. Pathogenic mechanisms of B-lymphocyte dysfunction in HIV disease. J Allergy Clin Immunol. 2008;122(1):12-9; quiz 20-1. Epub 2008/06/13. doi: 10.1016/j.jaci.2008.04.034. PubMed PMID: 18547629; PMCID: PMC2708937.

121. Moir S, Ho J, Malaspina A, Wang W, DiPoto AC, O'Shea MA, Roby G, Kottilil S, Arthos J, Proschan MA, Chun TW, Fauci AS. Evidence for HIV-associated B cell exhaustion in a dysfunctional memory B cell compartment in HIV-infected viremic individuals. J Exp Med. 2008;205(8):1797-805. Epub 2008/07/16. doi: 10.1084/jem.20072683. PubMed PMID: 18625747; PMCID: PMC2525604.

122. Moir S, Malaspina A, Ogwaro KM, Donoghue ET, Hallahan CW, Ehler LA, Liu S, Adelsberger J, Lapointe R, Hwu P, Baseler M, Orenstein JM, Chun TW, Mican JA, Fauci AS. HIV-1 induces phenotypic and functional perturbations of B cells in chronically infected individuals. Proc Natl Acad Sci U S A. 2001;98(18):10362-7. Epub 2001/08/16. doi: 10.1073/pnas.181347898. PubMed PMID: 11504927; PMCID: PMC56966.

123. Banga R, Procopio FA, Noto A, Pollakis G, Cavassini M, Ohmiti K, Corpataux JM, de Leval L, Pantaleo G, Perreau M. PD-1(+) and follicular helper T cells are responsible for persistent HIV-1 transcription in treated aviremic individuals. Nat Med. 2016;22(7):754-61. Epub 2016/05/31. doi: 10.1038/nm.4113. PubMed PMID: 27239760.

124. Boritz EA, Darko S, Swaszek L, Wolf G, Wells D, Wu X, Henry AR, Laboune F, Hu J, Ambrozak D, Hughes MS, Hoh R, Casazza JP, Vostal A, Bunis D, Nganou-Makamdop K, Lee JS, Migueles SA, Koup RA, Connors M, Moir S, Schacker T, Maldarelli F, Hughes SH, Deeks SG, Douek DC. Multiple Origins of Virus Persistence during Natural Control of HIV Infection. Cell.

2016;166(4):1004-15. Epub 2016/07/28. doi: 10.1016/j.cell.2016.06.039. PubMed PMID: 27453467; PMCID: PMC4983216.

125. Deeks SG, Lewin SR, Ross AL, Ananworanich J, Benkirane M, Cannon P, Chomont N, Douek D, Lifson JD, Lo YR, Kuritzkes D, Margolis D, Mellors J, Persaud D, Tucker JD, Barre-Sinoussi F, International ASTaCWG, Alter G, Auerbach J, Autran B, Barouch DH, Behrens G, Cavazzana M, Chen Z, Cohen EA, Corbelli GM, Eholie S, Eyal N, Fidler S, Garcia L, Grossman C, Henderson G, Henrich TJ, Jefferys R, Kiem HP, McCune J, Moodley K, Newman PA, Nijhuis M, Nsubuga MS, Ott M, Palmer S, Richman D, Saez-Cirion A, Sharp M, Siliciano J, Silvestri G, Singh J, Spire B, Taylor J, Tolstrup M, Valente S, van Lunzen J, Walensky R, Wilson I, Zack J. International AIDS Society global scientific strategy: towards an HIV cure 2016. Nat Med. 2016;22(8):839-50. Epub 2016/07/12. doi: 10.1038/nm.4108. PubMed PMID: 27400264; PMCID: PMC5322797.

126. Perreau M, Savoye AL, De Crignis E, Corpataux JM, Cubas R, Haddad EK, De Leval L, Graziosi C, Pantaleo G. Follicular helper T cells serve as the major CD4 T cell compartment for HIV-1 infection, replication, and production. J Exp Med. 2013;210(1):143-56. Epub 2012/12/21. doi: 10.1084/jem.20121932. PubMed PMID: 23254284; PMCID: PMC3549706.

127. Chun TW, Davey RT, Jr., Engel D, Lane HC, Fauci AS. Re-emergence of HIV after stopping therapy. Nature. 1999;401(6756):874-5. Epub 1999/11/30. doi: 10.1038/44755. PubMed PMID: 10553903.

128. Chun TW, Stuyver L, Mizell SB, Ehler LA, Mican JA, Baseler M, Lloyd AL, Nowak MA, Fauci AS. Presence of an inducible HIV-1 latent reservoir during highly active antiretroviral therapy. Proc Natl Acad Sci U S A. 1997;94(24):13193-7. Epub 1997/12/16. doi: 10.1073/pnas.94.24.13193. PubMed PMID: 9371822; PMCID: PMC24285.

129. McGary CS, Deleage C, Harper J, Micci L, Ribeiro SP, Paganini S, Kuri-Cervantes L, Benne C, Ryan ES, Balderas R, Jean S, Easley K, Marconi V, Silvestri G, Estes JD, Sekaly RP, Paiardini M. CTLA-4(+)PD-1(-) Memory CD4(+) T Cells Critically Contribute to Viral Persistence

in Antiretroviral Therapy-Suppressed, SIV-Infected Rhesus Macaques. Immunity. 2017;47(4):776-88 e5. Epub 2017/10/19. doi: 10.1016/j.immuni.2017.09.018. PubMed PMID: 29045906; PMCID: PMC5679306.

130. Arts EJ, Hazuda DJ. HIV-1 antiretroviral drug therapy. Cold Spring Harb Perspect Med. 2012;2(4):a007161. Epub 2012/04/05. doi: 10.1101/cshperspect.a007161. PubMed PMID: 22474613; PMCID: PMC3312400.

131. Clotet B, Feinberg J, van Lunzen J, Khuong-Josses MA, Antinori A, Dumitru I, Pokrovskiy V, Fehr J, Ortiz R, Saag M, Harris J, Brennan C, Fujiwara T, Min S, Team INGS. Once-daily dolutegravir versus darunavir plus ritonavir in antiretroviral-naive adults with HIV-1 infection (FLAMINGO): 48 week results from the randomised open-label phase 3b study. Lancet. 2014;383(9936):2222-31. Epub 2014/04/05. doi: 10.1016/S0140-6736(14)60084-2. PubMed PMID: 24698485.

132. Walmsley SL, Antela A, Clumeck N, Duiculescu D, Eberhard A, Gutierrez F, Hocqueloux L, Maggiolo F, Sandkovsky U, Granier C, Pappa K, Wynne B, Min S, Nichols G, Investigators S. Dolutegravir plus abacavir-lamivudine for the treatment of HIV-1 infection. N Engl J Med. 2013;369(19):1807-18. Epub 2013/11/08. doi: 10.1056/NEJMoa1215541. PubMed PMID: 24195548.

133. Lalezari JP, Eron JJ, Carlson M, Cohen C, DeJesus E, Arduino RC, Gallant JE, Volberding P, Murphy RL, Valentine F, Nelson EL, Sista PR, Dusek A, Kilby JM. A phase II clinical study of the long-term safety and antiviral activity of enfuvirtide-based antiretroviral therapy. AIDS. 2003;17(5):691-8. Epub 2003/03/21. doi: 10.1097/00002030-200303280-00007. PubMed PMID: 12646792.

134. Ho DD, Neumann AU, Perelson AS, Chen W, Leonard JM, Markowitz M. Rapid turnover of plasma virions and CD4 lymphocytes in HIV-1 infection. Nature. 1995;373(6510):123-6. Epub 1995/01/12. doi: 10.1038/373123a0. PubMed PMID: 7816094.

135. Perelson AS, Essunger P, Cao Y, Vesanen M, Hurley A, Saksela K, Markowitz M, Ho DD. Decay characteristics of HIV-1-infected compartments during combination therapy. Nature. 1997;387(6629):188-91. Epub 1997/05/08. doi: 10.1038/387188a0. PubMed PMID: 9144290.

136. Wei X, Ghosh SK, Taylor ME, Johnson VA, Emini EA, Deutsch P, Lifson JD, Bonhoeffer S, Nowak MA, Hahn BH, et al. Viral dynamics in human immunodeficiency virus type 1 infection. Nature. 1995;373(6510):117-22. Epub 1995/01/12. doi: 10.1038/373117a0. PubMed PMID: 7529365.

137. Buchbinder SP. Maximizing the Benefits of HIV Preexposure Prophylaxis. Top Antivir Med. 2018;25(4):138-42. Epub 2018/04/25. PubMed PMID: 29689539; PMCID: PMC5935218.

138. Shrestha R, Copenhaver M. Exploring the Use of Pre-exposure Prophylaxis (PrEP) for HIV Prevention Among High-Risk People Who Use Drugs in Treatment. Front Public Health. 2018;6:195. Epub 2018/08/01. doi: 10.3389/fpubh.2018.00195. PubMed PMID: 30062091; PMCID: PMC6054971.

139. Okwundu CI, Uthman OA, Okoromah CA. Antiretroviral pre-exposure prophylaxis (PrEP) for preventing HIV in high-risk individuals. Cochrane Database Syst Rev. 2012(7):CD007189. Epub 2012/07/13. doi: 10.1002/14651858.CD007189.pub3. PubMed PMID: 22786505.

140. Deeks SG, Tracy R, Douek DC. Systemic effects of inflammation on health during chronic HIV infection. Immunity. 2013;39(4):633-45. Epub 2013/10/22. doi: 10.1016/j.immuni.2013.10.001. PubMed PMID: 24138880; PMCID: PMC4012895.

141. Hunt PW, Brenchley J, Sinclair E, McCune JM, Roland M, Page-Shafer K, Hsue P, Emu B, Krone M, Lampiris H, Douek D, Martin JN, Deeks SG. Relationship between T cell activation and CD4+ T cell count in HIV-seropositive individuals with undetectable plasma HIV RNA levels in the absence of therapy. J Infect Dis. 2008;197(1):126-33. Epub 2008/01/04. doi: 10.1086/524143. PubMed PMID: 18171295; PMCID: PMC3466592.

142. Katlama C, Deeks SG, Autran B, Martinez-Picado J, van Lunzen J, Rouzioux C, Miller M, Vella S, Schmitz JE, Ahlers J, Richman DD, Sekaly RP. Barriers to a cure for HIV: new ways to

target and eradicate HIV-1 reservoirs. Lancet. 2013;381(9883):2109-17. Epub 2013/04/02. doi: 10.1016/S0140-6736(13)60104-X. PubMed PMID: 23541541; PMCID: PMC3815451.

143. Phillips AN, Neaton J, Lundgren JD. The role of HIV in serious diseases other than AIDS. AIDS. 2008;22(18):2409-18. Epub 2008/11/14. doi: 10.1097/QAD.0b013e3283174636. PubMed PMID: 19005264; PMCID: PMC2679976.

144. Sauce D, Larsen M, Fastenackels S, Pauchard M, Ait-Mohand H, Schneider L, Guihot A, Boufassa F, Zaunders J, Iguertsira M, Bailey M, Gorochov G, Duvivier C, Carcelain G, Kelleher AD, Simon A, Meyer L, Costagliola D, Deeks SG, Lambotte O, Autran B, Hunt PW, Katlama C, Appay V. HIV disease progression despite suppression of viral replication is associated with exhaustion of lymphopoiesis. Blood. 2011;117(19):5142-51. Epub 2011/03/26. doi: 10.1182/blood-2011-01-331306. PubMed PMID: 21436070; PMCID: PMC3109539.

145. Mouton JP, Cohen K, Maartens G. Key toxicity issues with the WHO-recommended first-line antiretroviral therapy regimen. Expert Rev Clin Pharmacol. 2016;9(11):1493-503. Epub 2016/08/09. doi: 10.1080/17512433.2016.1221760. PubMed PMID: 27498720.

146. Chun TW, Finzi D, Margolick J, Chadwick K, Schwartz D, Siliciano RF. In vivo fate of HIV-1-infected T cells: quantitative analysis of the transition to stable latency. Nat Med. 1995;1(12):1284-90. Epub 1995/12/01. doi: 10.1038/nm1295-1284. PubMed PMID: 7489410.

147. Wong JK, Hezareh M, Gunthard HF, Havlir DV, Ignacio CC, Spina CA, Richman DD. Recovery of replication-competent HIV despite prolonged suppression of plasma viremia. Science. 1997;278(5341):1291-5. Epub 1997/11/21. doi: 10.1126/science.278.5341.1291. PubMed PMID: 9360926.

148. Davey RT, Jr., Bhat N, Yoder C, Chun TW, Metcalf JA, Dewar R, Natarajan V, Lempicki RA, Adelsberger JW, Miller KD, Kovacs JA, Polis MA, Walker RE, Falloon J, Masur H, Gee D, Baseler M, Dimitrov DS, Fauci AS, Lane HC. HIV-1 and T cell dynamics after interruption of highly active antiretroviral therapy (HAART) in patients with a history of sustained viral suppression. Proc

Natl Acad Sci U S A. 1999;96(26):15109-14. Epub 1999/12/28. doi: 10.1073/pnas.96.26.15109. PubMed PMID: 10611346; PMCID: PMC24781.

149. Hill AL, Rosenbloom DI, Fu F, Nowak MA, Siliciano RF. Predicting the outcomes of treatment to eradicate the latent reservoir for HIV-1. Proc Natl Acad Sci U S A. 2014;111(37):13475-80. Epub 2014/08/07. doi: 10.1073/pnas.1406663111. PubMed PMID: 25097264; PMCID: PMC4169952.

150. Crooks AM, Bateson R, Cope AB, Dahl NP, Griggs MK, Kuruc JD, Gay CL, Eron JJ, Margolis DM, Bosch RJ, Archin NM. Precise Quantitation of the Latent HIV-1 Reservoir: Implications for Eradication Strategies. J Infect Dis. 2015;212(9):1361-5. Epub 2015/04/17. doi: 10.1093/infdis/jiv218. PubMed PMID: 25877550; PMCID: PMC4601910.

151. Kaufmann GR, Khanna N, Weber R, Perrin L, Furrer H, Cavassini M, Ledergerber B, Vernazza P, Bernasconi E, Rickenbach M, Hirschel B, Battegay M, Swiss HIVCS. Long-term virological response to multiple sequential regimens of highly active antiretroviral therapy for HIV infection. Antivir Ther. 2004;9(2):263-74. Epub 2004/05/12. PubMed PMID: 15134189.

152. Siliciano JD, Kajdas J, Finzi D, Quinn TC, Chadwick K, Margolick JB, Kovacs C, Gange SJ, Siliciano RF. Long-term follow-up studies confirm the stability of the latent reservoir for HIV-1 in resting CD4+ T cells. Nat Med. 2003;9(6):727-8. Epub 2003/05/20. doi: 10.1038/nm880. PubMed PMID: 12754504.

153. Strain MC, Gunthard HF, Havlir DV, Ignacio CC, Smith DM, Leigh-Brown AJ, Macaranas TR, Lam RY, Daly OA, Fischer M, Opravil M, Levine H, Bacheler L, Spina CA, Richman DD, Wong JK. Heterogeneous clearance rates of long-lived lymphocytes infected with HIV: intrinsic stability predicts lifelong persistence. Proc Natl Acad Sci U S A. 2003;100(8):4819-24. Epub 2003/04/10. doi: 10.1073/pnas.0736332100. PubMed PMID: 12684537; PMCID: PMC153639.

154. Bender AM, Simonetti FR, Kumar MR, Fray EJ, Bruner KM, Timmons AE, Tai KY, Jenike KM, Antar AAR, Liu PT, Ho YC, Raugi DN, Seydi M, Gottlieb GS, Okoye AA, Del Prete GQ, Picker LJ, Mankowski JL, Lifson JD, Siliciano JD, Laird GM, Barouch DH, Clements JE, Siliciano RF.

The Landscape of Persistent Viral Genomes in ART-Treated SIV, SHIV, and HIV-2 Infections. Cell Host Microbe. 2019;26(1):73-85 e4. Epub 2019/07/12. doi: 10.1016/j.chom.2019.06.005. PubMed PMID: 31295427; PMCID: PMC6724192.

155. Bertagnolli LN, White JA, Simonetti FR, Beg SA, Lai J, Tomescu C, Murray AJ, Antar AAR, Zhang H, Margolick JB, Hoh R, Deeks SG, Tebas P, Montaner LJ, Siliciano RF, Laird GM, Siliciano JD. The role of CD32 during HIV-1 infection. Nature. 2018;561(7723):E17-E9. Epub 2018/09/21. doi: 10.1038/s41586-018-0494-3. PubMed PMID: 30232425; PMCID: PMC6442722.

156. Bruner KM, Murray AJ, Pollack RA, Soliman MG, Laskey SB, Capoferri AA, Lai J, Strain MC, Lada SM, Hoh R, Ho YC, Richman DD, Deeks SG, Siliciano JD, Siliciano RF. Defective proviruses rapidly accumulate during acute HIV-1 infection. Nat Med. 2016;22(9):1043-9. Epub 2016/08/09. doi: 10.1038/nm.4156. PubMed PMID: 27500724; PMCID: PMC5014606.

157. Hiener B, Horsburgh BA, Eden JS, Barton K, Schlub TE, Lee E, von Stockenstrom S, Odevall L, Milush JM, Liegler T, Sinclair E, Hoh R, Boritz EA, Douek D, Fromentin R, Chomont N, Deeks SG, Hecht FM, Palmer S. Identification of Genetically Intact HIV-1 Proviruses in Specific CD4(+) T Cells from Effectively Treated Participants. Cell Rep. 2017;21(3):813-22. Epub 2017/10/19. doi: 10.1016/j.celrep.2017.09.081. PubMed PMID: 29045846; PMCID: PMC5960642.

158. Ho YC, Shan L, Hosmane NN, Wang J, Laskey SB, Rosenbloom DI, Lai J, Blankson JN, Siliciano JD, Siliciano RF. Replication-competent noninduced proviruses in the latent reservoir increase barrier to HIV-1 cure. Cell. 2013;155(3):540-51. Epub 2013/11/19. doi: 10.1016/j.cell.2013.09.020. PubMed PMID: 24243014; PMCID: PMC3896327.

159. Imamichi H, Dewar RL, Adelsberger JW, Rehm CA, O'Doherty U, Paxinos EE, Fauci AS, Lane HC. Defective HIV-1 proviruses produce novel protein-coding RNA species in HIV-infected patients on combination antiretroviral therapy. Proc Natl Acad Sci U S A. 2016;113(31):8783-8. Epub 2016/07/20. doi: 10.1073/pnas.1609057113. PubMed PMID: 27432972; PMCID: PMC4978246.

160. Long S, Fennessey CM, Newman L, Reid C, O'Brien SP, Li Y, Del Prete GQ, Lifson JD, Gorelick RJ, Keele BF. Evaluating the Intactness of Persistent Viral Genomes in Simian Immunodeficiency Virus-Infected Rhesus Macaques after Initiating Antiretroviral Therapy within One Year of Infection. J Virol. 2019;94(1). Epub 2019/10/11. doi: 10.1128/JVI.01308-19. PubMed PMID: 31597776; PMCID: PMC6912123.

161. Estes JD, Kityo C, Ssali F, Swainson L, Makamdop KN, Del Prete GQ, Deeks SG, Luciw PA, Chipman JG, Beilman GJ, Hoskuldsson T, Khoruts A, Anderson J, Deleage C, Jasurda J, Schmidt TE, Hafertepe M, Callisto SP, Pearson H, Reimann T, Schuster J, Schoephoerster J, Southern P, Perkey K, Shang L, Wietgrefe SW, Fletcher CV, Lifson JD, Douek DC, McCune JM, Haase AT, Schacker TW. Defining total-body AIDS-virus burden with implications for curative strategies. Nat Med. 2017;23(11):1271-6. Epub 2017/10/03. doi: 10.1038/nm.4411. PubMed PMID: 28967921; PMCID: PMC5831193.

162. Pierson T, Hoffman TL, Blankson J, Finzi D, Chadwick K, Margolick JB, Buck C, Siliciano JD, Doms RW, Siliciano RF. Characterization of chemokine receptor utilization of viruses in the latent reservoir for human immunodeficiency virus type 1. J Virol. 2000;74(17):7824-33. Epub 2000/08/10. doi: 10.1128/jvi.74.17.7824-7833.2000. PubMed PMID: 10933689; PMCID: PMC112312.

163. Doitsh G, Cavrois M, Lassen KG, Zepeda O, Yang Z, Santiago ML, Hebbeler AM, Greene WC. Abortive HIV infection mediates CD4 T cell depletion and inflammation in human lymphoid tissue. Cell. 2010;143(5):789-801. Epub 2010/11/30. doi: 10.1016/j.cell.2010.11.001. PubMed PMID: 21111238; PMCID: PMC3026834.

164. Bleul CC, Wu L, Hoxie JA, Springer TA, Mackay CR. The HIV coreceptors CXCR4 and CCR5 are differentially expressed and regulated on human T lymphocytes. Proc Natl Acad Sci U S A. 1997;94(5):1925-30. Epub 1997/03/04. doi: 10.1073/pnas.94.5.1925. PubMed PMID: 9050881; PMCID: PMC20019.

165. Gornalusse GG, Mummidi S, Gaitan AA, Jimenez F, Ramsuran V, Picton A, Rogers K, Manoharan MS, Avadhanam N, Murthy KK, Martinez H, Molano Murillo A, Chykarenko ZA, Hutt R, Daskalakis D, Shostakovich-Koretskaya L, Abdool Karim S, Martin JN, Deeks SG, Hecht F, Sinclair E, Clark RA, Okulicz J, Valentine FT, Martinson N, Tiemessen CT, Ndung'u T, Hunt PW, He W, Ahuja SK. Epigenetic mechanisms, T-cell activation, and CCR5 genetics interact to regulate T-cell expression of CCR5, the major HIV-1 coreceptor. Proc Natl Acad Sci U S A. 2015;112(34):E4762-71. Epub 2015/08/27. doi: 10.1073/pnas.1423228112. PubMed PMID: 26307764; PMCID: PMC4553789.

166. Shan L, Deng K, Gao H, Xing S, Capoferri AA, Durand CM, Rabi SA, Laird GM, Kim M, Hosmane NN, Yang HC, Zhang H, Margolick JB, Li L, Cai W, Ke R, Flavell RA, Siliciano JD, Siliciano RF. Transcriptional Reprogramming during Effector-to-Memory Transition Renders CD4(+) T Cells Permissive for Latent HIV-1 Infection. Immunity. 2017;47(4):766-75 e3. Epub 2017/10/19. doi: 10.1016/j.immuni.2017.09.014. PubMed PMID: 29045905; PMCID: PMC5948104.

167. Okoye AA, Hansen SG, Vaidya M, Fukazawa Y, Park H, Duell DM, Lum R, Hughes CM, Ventura AB, Ainslie E, Ford JC, Morrow D, Gilbride RM, Legasse AW, Hesselgesser J, Geleziunas R, Li Y, Oswald K, Shoemaker R, Fast R, Bosche WJ, Borate BR, Edlefsen PT, Axthelm MK, Picker LJ, Lifson JD. Early antiretroviral therapy limits SIV reservoir establishment to delay or prevent post-treatment viral rebound. Nat Med. 2018;24(9):1430-40. Epub 2018/08/08. doi: 10.1038/s41591-018-0130-7. PubMed PMID: 30082858; PMCID: PMC6389357.

168. Whitney JB, Hill AL, Sanisetty S, Penaloza-MacMaster P, Liu J, Shetty M, Parenteau L, Cabral C, Shields J, Blackmore S, Smith JY, Brinkman AL, Peter LE, Mathew SI, Smith KM, Borducchi EN, Rosenbloom DI, Lewis MG, Hattersley J, Li B, Hesselgesser J, Geleziunas R, Robb ML, Kim JH, Michael NL, Barouch DH. Rapid seeding of the viral reservoir prior to SIV viraemia in rhesus monkeys. Nature. 2014;512(7512):74-7. Epub 2014/07/22. doi: 10.1038/nature13594. PubMed PMID: 25042999; PMCID: PMC4126858.

169. Whitney JB, Lim SY, Osuna CE, Kublin JL, Chen E, Yoon G, Liu PT, Abbink P, Borducci EN, Hill A, Lewis MG, Geleziunas R, Robb ML, Michael NL, Barouch DH. Prevention of SIVmac251 reservoir seeding in rhesus monkeys by early antiretroviral therapy. Nat Commun. 2018;9(1):5429. Epub 2018/12/24. doi: 10.1038/s41467-018-07881-9. PubMed PMID: 30575753; PMCID: PMC6303321.

170. Chomont N, El-Far M, Ancuta P, Trautmann L, Procopio FA, Yassine-Diab B, Boucher G, Boulassel MR, Ghattas G, Brenchley JM, Schacker TW, Hill BJ, Douek DC, Routy JP, Haddad EK, Sekaly RP. HIV reservoir size and persistence are driven by T cell survival and homeostatic proliferation. Nat Med. 2009;15(8):893-900. Epub 2009/06/23. doi: 10.1038/nm.1972. PubMed PMID: 19543283; PMCID: PMC2859814.

171. Akondy RS, Fitch M, Edupuganti S, Yang S, Kissick HT, Li KW, Youngblood BA, Abdelsamed HA, McGuire DJ, Cohen KW, Alexe G, Nagar S, McCausland MM, Gupta S, Tata P, Haining WN, McElrath MJ, Zhang D, Hu B, Greenleaf WJ, Goronzy JJ, Mulligan MJ, Hellerstein M, Ahmed R. Origin and differentiation of human memory CD8 T cells after vaccination. Nature. 2017;552(7685):362-7. Epub 2017/12/14. doi: 10.1038/nature24633. PubMed PMID: 29236685; PMCID: PMC6037316.

172. Bushar ND, Corbo E, Schmidt M, Maltzman JS, Farber DL. Ablation of SLP-76 signaling after T cell priming generates memory CD4 T cells impaired in steady-state and cytokine-driven homeostasis. Proc Natl Acad Sci U S A. 2010;107(2):827-31. Epub 2010/01/19. doi: 10.1073/pnas.0908126107. PubMed PMID: 20080760; PMCID: PMC2818906.

173. De Boer RJ, Perelson AS. Quantifying T lymphocyte turnover. J Theor Biol. 2013;327:45-87. Epub 2013/01/15. doi: 10.1016/j.jtbi.2012.12.025. PubMed PMID: 23313150; PMCID: PMC3640348.

174. Farber DL, Yudanin NA, Restifo NP. Human memory T cells: generation, compartmentalization and homeostasis. Nat Rev Immunol. 2014;14(1):24-35. Epub 2013/12/18. doi: 10.1038/nri3567. PubMed PMID: 24336101; PMCID: PMC4032067.

175. Hammarlund E, Lewis MW, Hansen SG, Strelow LI, Nelson JA, Sexton GJ, Hanifin JM, Slifka MK. Duration of antiviral immunity after smallpox vaccination. Nat Med. 2003;9(9):1131-7. Epub 2003/08/20. doi: 10.1038/nm917. PubMed PMID: 12925846.

176. Kassiotis G, Garcia S, Simpson E, Stockinger B. Impairment of immunological memory in the absence of MHC despite survival of memory T cells. Nat Immunol. 2002;3(3):244-50. Epub 2002/02/12. doi: 10.1038/ni766. PubMed PMID: 11836529.

177. Macallan DC, Asquith B, Irvine AJ, Wallace DL, Worth A, Ghattas H, Zhang Y, Griffin GE, Tough DF, Beverley PC. Measurement and modeling of human T cell kinetics. Eur J Immunol. 2003;33(8):2316-26. Epub 2003/07/29. doi: 10.1002/eji.200323763. PubMed PMID: 12884307.

178. Macallan DC, Wallace D, Zhang Y, De Lara C, Worth AT, Ghattas H, Griffin GE, Beverley PC, Tough DF. Rapid turnover of effector-memory CD4(+) T cells in healthy humans. J Exp Med. 2004;200(2):255-60. Epub 2004/07/14. doi: 10.1084/jem.20040341. PubMed PMID: 15249595; PMCID: PMC2212011.

179. Vukmanovic-Stejic M, Zhang Y, Cook JE, Fletcher JM, McQuaid A, Masters JE, Rustin MH, Taams LS, Beverley PC, Macallan DC, Akbar AN. Human CD4+ CD25hi Foxp3+ regulatory T cells are derived by rapid turnover of memory populations in vivo. J Clin Invest. 2006;116(9):2423-33. Epub 2006/09/07. doi: 10.1172/JCI28941. PubMed PMID: 16955142; PMCID: PMC1555646.

180. Weng NP, Araki Y, Subedi K. The molecular basis of the memory T cell response: differential gene expression and its epigenetic regulation. Nat Rev Immunol. 2012;12(4):306-15. Epub 2012/03/17. doi: 10.1038/nri3173. PubMed PMID: 22421787; PMCID: PMC4686144.

181. Bailey JR, Sedaghat AR, Kieffer T, Brennan T, Lee PK, Wind-Rotolo M, Haggerty CM, Kamireddi AR, Liu Y, Lee J, Persaud D, Gallant JE, Cofrancesco J, Jr., Quinn TC, Wilke CO, Ray SC, Siliciano JD, Nettles RE, Siliciano RF. Residual human immunodeficiency virus type 1 viremia in some patients on antiretroviral therapy is dominated by a small number of invariant clones

rarely found in circulating CD4+ T cells. J Virol. 2006;80(13):6441-57. Epub 2006/06/16. doi: 10.1128/JVI.00591-06. PubMed PMID: 16775332; PMCID: PMC1488985.

182. Tobin NH, Learn GH, Holte SE, Wang Y, Melvin AJ, McKernan JL, Pawluk DM, Mohan KM, Lewis PF, Mullins JI, Frenkel LM. Evidence that low-level viremias during effective highly active antiretroviral therapy result from two processes: expression of archival virus and replication of virus. J Virol. 2005;79(15):9625-34. Epub 2005/07/15. doi: 10.1128/JVI.79.15.9625-9634.2005. PubMed PMID: 16014925; PMCID: PMC1181593.

183. Bui JK, Sobolewski MD, Keele BF, Spindler J, Musick A, Wiegand A, Luke BT, Shao W, Hughes SH, Coffin JM, Kearney MF, Mellors JW. Proviruses with identical sequences comprise a large fraction of the replication-competent HIV reservoir. PLoS Pathog. 2017;13(3):e1006283. Epub 2017/03/23. doi: 10.1371/journal.ppat.1006283. PubMed PMID: 28328934; PMCID: PMC5378418.

184. Cohn LB, da Silva IT, Valieris R, Huang AS, Lorenzi JCC, Cohen YZ, Pai JA, Butler AL, Caskey M, Jankovic M, Nussenzweig MC. Clonal CD4(+) T cells in the HIV-1 latent reservoir display a distinct gene profile upon reactivation. Nat Med. 2018;24(5):604-9. Epub 2018/04/25. doi: 10.1038/s41591-018-0017-7. PubMed PMID: 29686423; PMCID: PMC5972543.

185. Cohn LB, Silva IT, Oliveira TY, Rosales RA, Parrish EH, Learn GH, Hahn BH, Czartoski JL, McElrath MJ, Lehmann C, Klein F, Caskey M, Walker BD, Siliciano JD, Siliciano RF, Jankovic M, Nussenzweig MC. HIV-1 integration landscape during latent and active infection. Cell. 2015;160(3):420-32. Epub 2015/01/31. doi: 10.1016/j.cell.2015.01.020. PubMed PMID: 25635456; PMCID: PMC4371550.

186. Hosmane NN, Kwon KJ, Bruner KM, Capoferri AA, Beg S, Rosenbloom DI, Keele BF, Ho YC, Siliciano JD, Siliciano RF. Proliferation of latently infected CD4(+) T cells carrying replication-competent HIV-1: Potential role in latent reservoir dynamics. J Exp Med. 2017;214(4):959-72. Epub 2017/03/28. doi: 10.1084/jem.20170193. PubMed PMID: 28341641; PMCID: PMC5379987.

187. Maldarelli F, Wu X, Su L, Simonetti FR, Shao W, Hill S, Spindler J, Ferris AL, Mellors JW, Kearney MF, Coffin JM, Hughes SH. HIV latency. Specific HIV integration sites are linked to clonal expansion and persistence of infected cells. Science. 2014;345(6193):179-83. Epub 2014/06/28. doi: 10.1126/science.1254194. PubMed PMID: 24968937; PMCID: PMC4262401.

188. Simonetti FR, Sobolewski MD, Fyne E, Shao W, Spindler J, Hattori J, Anderson EM, Watters SA, Hill S, Wu X, Wells D, Su L, Luke BT, Halvas EK, Besson G, Penrose KJ, Yang Z, Kwan RW, Van Waes C, Uldrick T, Citrin DE, Kovacs J, Polis MA, Rehm CA, Gorelick R, Piatak M, Keele BF, Kearney MF, Coffin JM, Hughes SH, Mellors JW, Maldarelli F. Clonally expanded CD4+ T cells can produce infectious HIV-1 in vivo. Proc Natl Acad Sci U S A. 2016;113(7):1883-8. Epub 2016/02/10. doi: 10.1073/pnas.1522675113. PubMed PMID: 26858442; PMCID: PMC4763755.

189. von Stockenstrom S, Odevall L, Lee E, Sinclair E, Bacchetti P, Killian M, Epling L, Shao W, Hoh R, Ho T, Faria NR, Lemey P, Albert J, Hunt P, Loeb L, Pilcher C, Poole L, Hatano H, Somsouk M, Douek D, Boritz E, Deeks SG, Hecht FM, Palmer S. Longitudinal Genetic Characterization Reveals That Cell Proliferation Maintains a Persistent HIV Type 1 DNA Pool During Effective HIV Therapy. J Infect Dis. 2015;212(4):596-607. Epub 2015/02/26. doi: 10.1093/infdis/jiv092. PubMed PMID: 25712966; PMCID: PMC4539896.

190. Wagner TA, McLaughlin S, Garg K, Cheung CY, Larsen BB, Styrchak S, Huang HC, Edlefsen PT, Mullins JI, Frenkel LM. HIV latency. Proliferation of cells with HIV integrated into cancer genes contributes to persistent infection. Science. 2014;345(6196):570-3. Epub 2014/07/12. doi: 10.1126/science.1256304. PubMed PMID: 25011556; PMCID: PMC4230336.

191. Vandergeeten C, Fromentin R, DaFonseca S, Lawani MB, Sereti I, Lederman MM, Ramgopal M, Routy JP, Sekaly RP, Chomont N. Interleukin-7 promotes HIV persistence during antiretroviral therapy. Blood. 2013;121(21):4321-9. Epub 2013/04/17. doi: 10.1182/blood-2012-11-465625. PubMed PMID: 23589672; PMCID: PMC3663425.

192. Petrovas C, Ferrando-Martinez S, Gerner MY, Casazza JP, Pegu A, Deleage C, Cooper A, Hataye J, Andrews S, Ambrozak D, Del Rio Estrada PM, Boritz E, Paris R, Moysi E, Boswell KL, Ruiz-Mateos E, Vagios I, Leal M, Ablanedo-Terrazas Y, Rivero A, Gonzalez-Hernandez LA, McDermott AB, Moir S, Reyes-Teran G, Docobo F, Pantaleo G, Douek DC, Betts MR, Estes JD, Germain RN, Mascola JR, Koup RA. Follicular CD8 T cells accumulate in HIV infection and can kill infected cells in vitro via bispecific antibodies. Sci Transl Med. 2017;9(373). Epub 2017/01/20. doi: 10.1126/scitranslmed.aag2285. PubMed PMID: 28100833; PMCID: PMC5497679.

193. Pantaleo G, Graziosi C, Butini L, Pizzo PA, Schnittman SM, Kotler DP, Fauci AS. Lymphoid organs function as major reservoirs for human immunodeficiency virus. Proc Natl Acad Sci U S A. 1991;88(21):9838-42. Epub 1991/11/01. doi: 10.1073/pnas.88.21.9838. PubMed PMID: 1682922; PMCID: PMC52816.

194. Descours B, Petitjean G, Lopez-Zaragoza JL, Bruel T, Raffel R, Psomas C, Reynes J, Lacabaratz C, Levy Y, Schwartz O, Lelievre JD, Benkirane M. CD32a is a marker of a CD4 T-cell HIV reservoir harbouring replication-competent proviruses. Nature. 2017;543(7646):564-7. Epub 2017/03/16. doi: 10.1038/nature21710. PubMed PMID: 28297712.

195. Abdel-Mohsen M, Kuri-Cervantes L, Grau-Exposito J, Spivak AM, Nell RA, Tomescu C, Vadrevu SK, Giron LB, Serra-Peinado C, Genesca M, Castellvi J, Wu G, Del Rio Estrada PM, Gonzalez-Navarro M, Lynn K, King CT, Vemula S, Cox K, Wan Y, Li Q, Mounzer K, Kostman J, Frank I, Paiardini M, Hazuda D, Reyes-Teran G, Richman D, Howell B, Tebas P, Martinez-Picado J, Planelles V, Buzon MJ, Betts MR, Montaner LJ. CD32 is expressed on cells with transcriptionally active HIV but does not enrich for HIV DNA in resting T cells. Sci Transl Med. 2018;10(437). Epub 2018/04/20. doi: 10.1126/scitranslmed.aar6759. PubMed PMID: 29669853; PMCID: PMC6282755.

196. Osuna CE, Lim SY, Kublin JL, Apps R, Chen E, Mota TM, Huang SH, Ren Y, Bachtel ND, Tsibris AM, Ackerman ME, Jones RB, Nixon DF, Whitney JB. Evidence that CD32a does not mark

the HIV-1 latent reservoir. Nature. 2018;561(7723):E20-E8. Epub 2018/09/21. doi: 10.1038/s41586-018-0495-2. PubMed PMID: 30232424; PMCID: PMC6528470.

197. Perez L, Anderson J, Chipman J, Thorkelson A, Chun TW, Moir S, Haase AT, Douek DC, Schacker TW, Boritz EA. Conflicting evidence for HIV enrichment in CD32(+) CD4 T cells. Nature. 2018;561(7723):E9-E16. Epub 2018/09/21. doi: 10.1038/s41586-018-0493-4. PubMed PMID: 30232423; PMCID: PMC6410373.

198. Lee SK, Xu Z, Lieberman J, Shankar P. The functional CD8 T cell response to HIV becomes type-specific in progressive disease. J Clin Invest. 2002;110(9):1339-47. Epub 2002/11/06. doi: 10.1172/JCI16028. PubMed PMID: 12417573; PMCID: PMC151615.

199. Zhang D, Shankar P, Xu Z, Harnisch B, Chen G, Lange C, Lee SJ, Valdez H, Lederman MM, Lieberman J. Most antiviral CD8 T cells during chronic viral infection do not express high levels of perforin and are not directly cytotoxic. Blood. 2003;101(1):226-35. Epub 2002/10/24. doi: 10.1182/blood-2002-03-0791. PubMed PMID: 12393740.

200. McLane LM, Abdel-Hakeem MS, Wherry EJ. CD8 T Cell Exhaustion During Chronic Viral Infection and Cancer. Annu Rev Immunol. 2019;37:457-95. Epub 2019/01/25. doi: 10.1146/annurev-immunol-041015-055318. PubMed PMID: 30676822.

201. Ishida Y, Agata Y, Shibahara K, Honjo T. Induced expression of PD-1, a novel member of the immunoglobulin gene superfamily, upon programmed cell death. EMBO J. 1992;11(11):3887-95. Epub 1992/11/01. PubMed PMID: 1396582; PMCID: PMC556898.

202. Leach DR, Krummel MF, Allison JP. Enhancement of antitumor immunity by CTLA-4 blockade. Science. 1996;271(5256):1734-6. Epub 1996/03/22. doi: 10.1126/science.271.5256.1734. PubMed PMID: 8596936.

203. Gallimore A, Glithero A, Godkin A, Tissot AC, Pluckthun A, Elliott T, Hengartner H, Zinkernagel R. Induction and exhaustion of lymphocytic choriomeningitis virus-specific cytotoxic T lymphocytes visualized using soluble tetrameric major histocompatibility complex class I-

peptide complexes. J Exp Med. 1998;187(9):1383-93. Epub 1998/06/06. doi: 10.1084/jem.187.9.1383. PubMed PMID: 9565631; PMCID: PMC2212278.

204. Moskophidis D, Lechner F, Pircher H, Zinkernagel RM. Virus persistence in acutely infected immunocompetent mice by exhaustion of antiviral cytotoxic effector T cells. Nature. 1993;362(6422):758-61. Epub 1993/04/22. doi: 10.1038/362758a0. PubMed PMID: 8469287.

205. Zajac AJ, Blattman JN, Murali-Krishna K, Sourdive DJ, Suresh M, Altman JD, Ahmed R. Viral immune evasion due to persistence of activated T cells without effector function. J Exp Med. 1998;188(12):2205-13. Epub 1998/12/22. doi: 10.1084/jem.188.12.2205. PubMed PMID: 9858507; PMCID: PMC2212420.

206. Kaech SM, Ahmed R. Memory CD8+ T cell differentiation: initial antigen encounter triggers a developmental program in naive cells. Nat Immunol. 2001;2(5):415-22. Epub 2001/04/27. doi: 10.1038/87720. PubMed PMID: 11323695; PMCID: PMC3760150.

207. Kaech SM, Hemby S, Kersh E, Ahmed R. Molecular and functional profiling of memory CD8 T cell differentiation. Cell. 2002;111(6):837-51. Epub 2003/01/16. doi: 10.1016/s0092-8674(02)01139-x. PubMed PMID: 12526810.

208. Blank CU, Haining WN, Held W, Hogan PG, Kallies A, Lugli E, Lynn RC, Philip M, Rao A, Restifo NP, Schietinger A, Schumacher TN, Schwartzberg PL, Sharpe AH, Speiser DE, Wherry EJ, Youngblood BA, Zehn D. Defining 'T cell exhaustion'. Nat Rev Immunol. 2019;19(11):665-74. Epub 2019/10/02. doi: 10.1038/s41577-019-0221-9. PubMed PMID: 31570879; PMCID: PMC7286441.

209. Kaech SM, Tan JT, Wherry EJ, Konieczny BT, Surh CD, Ahmed R. Selective expression of the interleukin 7 receptor identifies effector CD8 T cells that give rise to long-lived memory cells. Nat Immunol. 2003;4(12):1191-8. Epub 2003/11/20. doi: 10.1038/ni1009. PubMed PMID: 14625547.

210. Ahmed R, Bevan MJ, Reiner SL, Fearon DT. The precursors of memory: models and controversies. Nat Rev Immunol. 2009;9(9):662-8. Epub 2009/08/15. doi: 10.1038/nri2619. PubMed PMID: 19680250.

211. Cui W, Kaech SM. Generation of effector CD8+ T cells and their conversion to memory T cells. Immunol Rev. 2010;236:151-66. Epub 2010/07/20. doi: 10.1111/j.1600-065X.2010.00926.x. PubMed PMID: 20636815; PMCID: PMC4380273.

212. Harty JT, Badovinac VP. Shaping and reshaping CD8+ T-cell memory. Nat Rev Immunol. 2008;8(2):107-19. Epub 2008/01/26. doi: 10.1038/nri2251. PubMed PMID: 18219309.

213. Jameson SC, Masopust D. Diversity in T cell memory: an embarrassment of riches. Immunity. 2009;31(6):859-71. Epub 2010/01/13. doi: 10.1016/j.immuni.2009.11.007. PubMed PMID: 20064446; PMCID: PMC2957815.

214. Kaech SM, Wherry EJ. Heterogeneity and cell-fate decisions in effector and memory CD8+ T cell differentiation during viral infection. Immunity. 2007;27(3):393-405. Epub 2007/09/26. doi: 10.1016/j.immuni.2007.08.007. PubMed PMID: 17892848; PMCID: PMC3431921.

215. Kaech SM, Wherry EJ, Ahmed R. Effector and memory T-cell differentiation: implications for vaccine development. Nat Rev Immunol. 2002;2(4):251-62. Epub 2002/05/11. doi: 10.1038/nri778. PubMed PMID: 12001996.

216. Virgin HW, Wherry EJ, Ahmed R. Redefining chronic viral infection. Cell. 2009;138(1):30-50. Epub 2009/07/15. doi: 10.1016/j.cell.2009.06.036. PubMed PMID: 19596234.

217. Williams MA, Bevan MJ. Effector and memory CTL differentiation. Annu Rev Immunol. 2007;25:171-92. Epub 2006/11/30. doi: 10.1146/annurev.immunol.25.022106.141548. PubMed PMID: 17129182.

218. Boni C, Fisicaro P, Valdatta C, Amadei B, Di Vincenzo P, Giuberti T, Laccabue D, Zerbini A, Cavalli A, Missale G, Bertoletti A, Ferrari C. Characterization of hepatitis B virus (HBV)-specific T-cell dysfunction in chronic HBV infection. J Virol. 2007;81(8):4215-25. Epub 2007/02/09. doi: 10.1128/JVI.02844-06. PubMed PMID: 17287266; PMCID: PMC1866111.

219. El-Far M, Halwani R, Said E, Trautmann L, Doroudchi M, Janbazian L, Fonseca S, van Grevenynghe J, Yassine-Diab B, Sekaly RP, Haddad EK. T-cell exhaustion in HIV infection. Curr HIV/AIDS Rep. 2008;5(1):13-9. Epub 2008/04/18. doi: 10.1007/s11904-008-0003-7. PubMed PMID: 18417030.

220. Reignat S, Webster GJ, Brown D, Ogg GS, King A, Seneviratne SL, Dusheiko G, Williams R, Maini MK, Bertoletti A. Escaping high viral load exhaustion: CD8 cells with altered tetramer binding in chronic hepatitis B virus infection. J Exp Med. 2002;195(9):1089-101. Epub 2002/05/08. doi: 10.1084/jem.20011723. PubMed PMID: 11994415; PMCID: PMC2193712.

221. Wherry EJ, Kurachi M. Molecular and cellular insights into T cell exhaustion. Nat Rev Immunol. 2015;15(8):486-99. Epub 2015/07/25. doi: 10.1038/nri3862. PubMed PMID: 26205583; PMCID: PMC4889009.

222. Wherry EJ, Ahmed R. Memory CD8 T-cell differentiation during viral infection. J Virol. 2004;78(11):5535-45. Epub 2004/05/14. doi: 10.1128/JVI.78.11.5535-5545.2004. PubMed PMID: 15140950; PMCID: PMC415833.

223. Fuller MJ, Zajac AJ. Ablation of CD8 and CD4 T cell responses by high viral loads. J Immunol. 2003;170(1):477-86. Epub 2002/12/24. doi: 10.4049/jimmunol.170.1.477. PubMed PMID: 12496434.

224. Wherry EJ, Blattman JN, Murali-Krishna K, van der Most R, Ahmed R. Viral persistence alters CD8 T-cell immunodominance and tissue distribution and results in distinct stages of functional impairment. J Virol. 2003;77(8):4911-27. Epub 2003/03/29. doi: 10.1128/jvi.77.8.4911-4927.2003. PubMed PMID: 12663797; PMCID: PMC152117.

225. Agnellini P, Wolint P, Rehr M, Cahenzli J, Karrer U, Oxenius A. Impaired NFAT nuclear translocation results in split exhaustion of virus-specific CD8+ T cell functions during chronic viral infection. Proc Natl Acad Sci U S A. 2007;104(11):4565-70. Epub 2007/03/16. doi: 10.1073/pnas.0610335104. PubMed PMID: 17360564; PMCID: PMC1815473.

226. Fuller MJ, Khanolkar A, Tebo AE, Zajac AJ. Maintenance, loss, and resurgence of T cell responses during acute, protracted, and chronic viral infections. J Immunol. 2004;172(7):4204-14. Epub 2004/03/23. doi: 10.4049/jimmunol.172.7.4204. PubMed PMID: 15034033.

227. Mackerness KJ, Cox MA, Lilly LM, Weaver CT, Harrington LE, Zajac AJ. Pronounced virus-dependent activation drives exhaustion but sustains IFN-gamma transcript levels. J Immunol. 2010;185(6):3643-51. Epub 2010/08/20. doi: 10.4049/jimmunol.1000841. PubMed PMID: 20720198; PMCID: PMC2933304.

228. Shin H, Blackburn SD, Intlekofer AM, Kao C, Angelosanto JM, Reiner SL, Wherry EJ. A role for the transcriptional repressor Blimp-1 in CD8(+) T cell exhaustion during chronic viral infection. Immunity. 2009;31(2):309-20. Epub 2009/08/12. doi: 10.1016/j.immuni.2009.06.019. PubMed PMID: 19664943; PMCID: PMC2747257.

229. Chahroudi A, Silvestri G, Lichterfeld M. T memory stem cells and HIV: a long-term relationship. Curr HIV/AIDS Rep. 2015;12(1):33-40. Epub 2015/01/13. doi: 10.1007/s11904-014-0246-4. PubMed PMID: 25578055; PMCID: PMC4370789.

230. Masopust D, Vezys V, Usherwood EJ, Cauley LS, Olson S, Marzo AL, Ward RL, Woodland DL, Lefrancois L. Activated primary and memory CD8 T cells migrate to nonlymphoid tissues regardless of site of activation or tissue of origin. J Immunol. 2004;172(8):4875-82. Epub 2004/04/07. doi: 10.4049/jimmunol.172.8.4875. PubMed PMID: 15067066.

231. Radziewicz H, Ibegbu CC, Fernandez ML, Workowski KA, Obideen K, Wehbi M, Hanson HL, Steinberg JP, Masopust D, Wherry EJ, Altman JD, Rouse BT, Freeman GJ, Ahmed R, Grakoui A. Liver-infiltrating lymphocytes in chronic human hepatitis C virus infection display an exhausted phenotype with high levels of PD-1 and low levels of CD127 expression. J Virol. 2007;81(6):2545-53. Epub 2006/12/22. doi: 10.1128/JVI.02021-06. PubMed PMID: 17182670; PMCID: PMC1865979.

232. Shin H, Blackburn SD, Blattman JN, Wherry EJ. Viral antigen and extensive division maintain virus-specific CD8 T cells during chronic infection. J Exp Med. 2007;204(4):941-9. Epub 2007/04/11. doi: 10.1084/jem.20061937. PubMed PMID: 17420267; PMCID: PMC2118542.

233. Wherry EJ, Barber DL, Kaech SM, Blattman JN, Ahmed R. Antigen-independent memory CD8 T cells do not develop during chronic viral infection. Proc Natl Acad Sci U S A. 2004;101(45):16004-9. Epub 2004/10/27. doi: 10.1073/pnas.0407192101. PubMed PMID: 15505208; PMCID: PMC524220.

234. Wherry EJ, Teichgraber V, Becker TC, Masopust D, Kaech SM, Antia R, von Andrian UH, Ahmed R. Lineage relationship and protective immunity of memory CD8 T cell subsets. Nat Immunol. 2003;4(3):225-34. Epub 2003/02/04. doi: 10.1038/ni889. PubMed PMID: 12563257.

235. Paley MA, Kroy DC, Odorizzi PM, Johnnidis JB, Dolfi DV, Barnett BE, Bikoff EK, Robertson EJ, Lauer GM, Reiner SL, Wherry EJ. Progenitor and terminal subsets of CD8+ T cells cooperate to contain chronic viral infection. Science. 2012;338(6111):1220-5. Epub 2012/12/01. doi: 10.1126/science.1229620. PubMed PMID: 23197535; PMCID: PMC3653769.

236. Im SJ, Hashimoto M, Gerner MY, Lee J, Kissick HT, Burger MC, Shan Q, Hale JS, Lee J, Nasti TH, Sharpe AH, Freeman GJ, Germain RN, Nakaya HI, Xue HH, Ahmed R. Defining CD8+ T cells that provide the proliferative burst after PD-1 therapy. Nature. 2016;537(7620):417-21. Epub 2016/08/09. doi: 10.1038/nature19330. PubMed PMID: 27501248; PMCID: PMC5297183.

237. Gupta PK, Godec J, Wolski D, Adland E, Yates K, Pauken KE, Cosgrove C, Ledderose C, Junger WG, Robson SC, Wherry EJ, Alter G, Goulder PJ, Klenerman P, Sharpe AH, Lauer GM, Haining WN. CD39 Expression Identifies Terminally Exhausted CD8+ T Cells. PLoS Pathog. 2015;11(10):e1005177. Epub 2015/10/21. doi: 10.1371/journal.ppat.1005177. PubMed PMID: 26485519; PMCID: PMC4618999.

238. Ahn E, Araki K, Hashimoto M, Li W, Riley JL, Cheung J, Sharpe AH, Freeman GJ, Irving BA, Ahmed R. Role of PD-1 during effector CD8 T cell differentiation. Proc Natl Acad Sci U S A.

2018;115(18):4749-54. Epub 2018/04/15. doi: 10.1073/pnas.1718217115. PubMed PMID: 29654146; PMCID: PMC5939075.

239. Chen Z, Ji Z, Ngiow SF, Manne S, Cai Z, Huang AC, Johnson J, Staupe RP, Bengsch B, Xu C, Yu S, Kurachi M, Herati RS, Vella LA, Baxter AE, Wu JE, Khan O, Beltra JC, Giles JR, Stelekati E, McLane LM, Lau CW, Yang X, Berger SL, Vahedi G, Ji H, Wherry EJ. TCF-1-Centered Transcriptional Network Drives an Effector versus Exhausted CD8 T Cell-Fate Decision. Immunity. 2019;51(5):840-55 e5. Epub 2019/10/14. doi: 10.1016/j.immuni.2019.09.013. PubMed PMID: 31606264; PMCID: PMC6943829.

240. Hashimoto M, Kamphorst AO, Im SJ, Kissick HT, Pillai RN, Ramalingam SS, Araki K, Ahmed R. CD8 T Cell Exhaustion in Chronic Infection and Cancer: Opportunities for Interventions. Annu Rev Med. 2018;69:301-18. Epub 2018/02/08. doi: 10.1146/annurev-med-012017-043208. PubMed PMID: 29414259.

241. Jadhav RR, Im SJ, Hu B, Hashimoto M, Li P, Lin JX, Leonard WJ, Greenleaf WJ, Ahmed R, Goronzy JJ. Epigenetic signature of PD-1+ TCF1+ CD8 T cells that act as resource cells during chronic viral infection and respond to PD-1 blockade. Proc Natl Acad Sci U S A. 2019;116(28):14113-8. Epub 2019/06/23. doi: 10.1073/pnas.1903520116. PubMed PMID: 31227606; PMCID: PMC6628832.

242. Johnson JL, Georgakilas G, Petrovic J, Kurachi M, Cai S, Harly C, Pear WS, Bhandoola A, Wherry EJ, Vahedi G. Lineage-Determining Transcription Factor TCF-1 Initiates the Epigenetic Identity of T Cells. Immunity. 2018;48(2):243-57 e10. Epub 2018/02/22. doi: 10.1016/j.immuni.2018.01.012. PubMed PMID: 29466756; PMCID: PMC5824646.

243. Kamphorst AO, Wieland A, Nasti T, Yang S, Zhang R, Barber DL, Konieczny BT, Daugherty CZ, Koenig L, Yu K, Sica GL, Sharpe AH, Freeman GJ, Blazar BR, Turka LA, Owonikoko TK, Pillai RN, Ramalingam SS, Araki K, Ahmed R. Rescue of exhausted CD8 T cells by PD-1-targeted therapies is CD28-dependent. Science. 2017;355(6332):1423-7. Epub 2017/03/11. doi: 10.1126/science.aaf0683. PubMed PMID: 28280249; PMCID: PMC5595217.

244. Kanev K, Wu M, Drews A, Roelli P, Wurmser C, von Hosslin M, Zehn D. Proliferation-competent Tcf1+ CD8 T cells in dysfunctional populations are CD4 T cell help independent. Proc Natl Acad Sci U S A. 2019;116(40):20070-6. Epub 2019/09/19. doi: 10.1073/pnas.1902701116. PubMed PMID: 31530725; PMCID: PMC6778176.

245. Li J, Byrne KT, Yan F, Yamazoe T, Chen Z, Baslan T, Richman LP, Lin JH, Sun YH, Rech AJ, Balli D, Hay CA, Sela Y, Merrell AJ, Liudahl SM, Gordon N, Norgard RJ, Yuan S, Yu S, Chao T, Ye S, Eisinger-Mathason TSK, Faryabi RB, Tobias JW, Lowe SW, Coussens LM, Wherry EJ, Vonderheide RH, Stanger BZ. Tumor Cell-Intrinsic Factors Underlie Heterogeneity of Immune Cell Infiltration and Response to Immunotherapy. Immunity. 2018;49(1):178-93 e7. Epub 2018/07/01. doi: 10.1016/j.immuni.2018.06.006. PubMed PMID: 29958801; PMCID: PMC6707727.

246. Man K, Gabriel SS, Liao Y, Gloury R, Preston S, Henstridge DC, Pellegrini M, Zehn D, Berberich-Siebelt F, Febbraio MA, Shi W, Kallies A. Transcription Factor IRF4 Promotes CD8(+) T Cell Exhaustion and Limits the Development of Memory-like T Cells during Chronic Infection. Immunity. 2017;47(6):1129-41 e5. Epub 2017/12/17. doi: 10.1016/j.immuni.2017.11.021. PubMed PMID: 29246443.

247. Philip M, Fairchild L, Sun L, Horste EL, Camara S, Shakiba M, Scott AC, Viale A, Lauer P, Merghoub T, Hellmann MD, Wolchok JD, Leslie CS, Schietinger A. Chromatin states define tumour-specific T cell dysfunction and reprogramming. Nature. 2017;545(7655):452-6. Epub 2017/05/18. doi: 10.1038/nature22367. PubMed PMID: 28514453; PMCID: PMC5693219.

248. Utzschneider DT, Charmoy M, Chennupati V, Pousse L, Ferreira DP, Calderon-Copete S, Danilo M, Alfei F, Hofmann M, Wieland D, Pradervand S, Thimme R, Zehn D, Held W. T Cell Factor 1-Expressing Memory-like CD8(+) T Cells Sustain the Immune Response to Chronic Viral Infections. Immunity. 2016;45(2):415-27. Epub 2016/08/18. doi: 10.1016/j.immuni.2016.07.021. PubMed PMID: 27533016.

249. Wieland D, Kemming J, Schuch A, Emmerich F, Knolle P, Neumann-Haefelin C, Held W, Zehn D, Hofmann M, Thimme R. TCF1(+) hepatitis C virus-specific CD8(+) T cells are maintained after cessation of chronic antigen stimulation. Nat Commun. 2017;8:15050. Epub 2017/05/04. doi: 10.1038/ncomms15050. PubMed PMID: 28466857; PMCID: PMC5418623.

250. Brooks DG, Ha SJ, Elsaesser H, Sharpe AH, Freeman GJ, Oldstone MB. IL-10 and PD-L1 operate through distinct pathways to suppress T-cell activity during persistent viral infection. Proc Natl Acad Sci U S A. 2008;105(51):20428-33. Epub 2008/12/17. doi: 10.1073/pnas.0811139106. PubMed PMID: 19075244; PMCID: PMC2629263.

251. Brooks DG, Trifilo MJ, Edelmann KH, Teyton L, McGavern DB, Oldstone MB. Interleukin-10 determines viral clearance or persistence in vivo. Nat Med. 2006;12(11):1301-9. Epub 2006/10/17. doi: 10.1038/nm1492. PubMed PMID: 17041596; PMCID: PMC2535582.

252. Said EA, Dupuy FP, Trautmann L, Zhang Y, Shi Y, El-Far M, Hill BJ, Noto A, Ancuta P, Peretz Y, Fonseca SG, Van Grevenynghe J, Boulassel MR, Bruneau J, Shoukry NH, Routy JP, Douek DC, Haddad EK, Sekaly RP. Programmed death-1-induced interleukin-10 production by monocytes impairs CD4+ T cell activation during HIV infection. Nat Med. 2010;16(4):452-9. Epub 2010/03/09. doi: 10.1038/nm.2106. PubMed PMID: 20208540; PMCID: PMC4229134.

253. Zarour HM. Reversing T-cell Dysfunction and Exhaustion in Cancer. Clin Cancer Res. 2016;22(8):1856-64. Epub 2016/04/17. doi: 10.1158/1078-0432.CCR-15-1849. PubMed PMID: 27084739; PMCID: PMC4872712.

254. Ejrnaes M, Filippi CM, Martinic MM, Ling EM, Togher LM, Crotty S, von Herrath MG. Resolution of a chronic viral infection after interleukin-10 receptor blockade. J Exp Med. 2006;203(11):2461-72. Epub 2006/10/13. doi: 10.1084/jem.20061462. PubMed PMID: 17030951; PMCID: PMC2118120.

255. Barber DL, Wherry EJ, Masopust D, Zhu B, Allison JP, Sharpe AH, Freeman GJ, Ahmed R. Restoring function in exhausted CD8 T cells during chronic viral infection. Nature. 2006;439(7077):682-7. Epub 2005/12/31. doi: 10.1038/nature04444. PubMed PMID: 16382236.

256. Day CL, Kaufmann DE, Kiepiela P, Brown JA, Moodley ES, Reddy S, Mackey EW, Miller JD, Leslie AJ, DePierres C, Mncube Z, Duraiswamy J, Zhu B, Eichbaum Q, Altfeld M, Wherry EJ, Coovadia HM, Goulder PJ, Klenerman P, Ahmed R, Freeman GJ, Walker BD. PD-1 expression on HIV-specific T cells is associated with T-cell exhaustion and disease progression. Nature. 2006;443(7109):350-4. Epub 2006/08/22. doi: 10.1038/nature05115. PubMed PMID: 16921384.

257. Iwai Y, Ishida M, Tanaka Y, Okazaki T, Honjo T, Minato N. Involvement of PD-L1 on tumor cells in the escape from host immune system and tumor immunotherapy by PD-L1 blockade. Proc Natl Acad Sci U S A. 2002;99(19):12293-7. Epub 2002/09/10. doi: 10.1073/pnas.192461099. PubMed PMID: 12218188; PMCID: PMC129438.

258. Urbani S, Amadei B, Tola D, Massari M, Schivazappa S, Missale G, Ferrari C. PD-1 expression in acute hepatitis C virus (HCV) infection is associated with HCV-specific CD8 exhaustion. J Virol. 2006;80(22):11398-403. Epub 2006/09/08. doi: 10.1128/JVI.01177-06. PubMed PMID: 16956940; PMCID: PMC1642188.

259. Wherry EJ, Ha SJ, Kaech SM, Haining WN, Sarkar S, Kalia V, Subramaniam S, Blattman JN, Barber DL, Ahmed R. Molecular signature of CD8+ T cell exhaustion during chronic viral infection. Immunity. 2007;27(4):670-84. Epub 2007/10/24. doi: 10.1016/j.immuni.2007.09.006. PubMed PMID: 17950003.

260. Hudson WH, Gensheimer J, Hashimoto M, Wieland A, Valanparambil RM, Li P, Lin JX, Konieczny BT, Im SJ, Freeman GJ, Leonard WJ, Kissick HT, Ahmed R. Proliferating Transitory T Cells with an Effector-like Transcriptional Signature Emerge from PD-1(+) Stem-like CD8(+) T Cells during Chronic Infection. Immunity. 2019;51(6):1043-58 e4. Epub 2019/12/08. doi: 10.1016/j.immuni.2019.11.002. PubMed PMID: 31810882; PMCID: PMC6920571.

261. Verma V, Shrimali RK, Ahmad S, Dai W, Wang H, Lu S, Nandre R, Gaur P, Lopez J, Sade-Feldman M, Yizhak K, Bjorgaard SL, Flaherty KT, Wargo JA, Boland GM, Sullivan RJ, Getz G, Hammond SA, Tan M, Qi J, Wong P, Merghoub T, Wolchok J, Hacohen N, Janik JE, Mkrtichyan M, Gupta S, Khleif SN. PD-1 blockade in subprimed CD8 cells induces dysfunctional

PD-1(+)CD38(hi) cells and anti-PD-1 resistance. Nat Immunol. 2019;20(9):1231-43. Epub 2019/07/31. doi: 10.1038/s41590-019-0441-y. PubMed PMID: 31358999; PMCID: PMC7472661.

262. Wang B, Zhang W, Jankovic V, Golubov J, Poon P, Oswald EM, Gurer C, Wei J, Ramos I, Wu Q, Waite J, Ni M, Adler C, Wei Y, Macdonald L, Rowlands T, Brydges S, Siao J, Poueymirou W, MacDonald D, Yancopoulos GD, Sleeman MA, Murphy AJ, Skokos D. Combination cancer immunotherapy targeting PD-1 and GITR can rescue CD8(+) T cell dysfunction and maintain memory phenotype. Sci Immunol. 2018;3(29). Epub 2018/11/06. doi: 10.1126/sciimmunol.aat7061. PubMed PMID: 30389797.

263. Alfei F, Kanev K, Hofmann M, Wu M, Ghoneim HE, Roelli P, Utzschneider DT, von Hoesslin M, Cullen JG, Fan Y, Eisenberg V, Wohlleber D, Steiger K, Merkler D, Delorenzi M, Knolle PA, Cohen CJ, Thimme R, Youngblood B, Zehn D. TOX reinforces the phenotype and longevity of exhausted T cells in chronic viral infection. Nature. 2019;571(7764):265-9. Epub 2019/06/18. doi: 10.1038/s41586-019-1326-9. PubMed PMID: 31207605.

264. Khan O, Giles JR, McDonald S, Manne S, Ngiow SF, Patel KP, Werner MT, Huang AC, Alexander KA, Wu JE, Attanasio J, Yan P, George SM, Bengsch B, Staupe RP, Donahue G, Xu W, Amaravadi RK, Xu X, Karakousis GC, Mitchell TC, Schuchter LM, Kaye J, Berger SL, Wherry EJ. TOX transcriptionally and epigenetically programs CD8(+) T cell exhaustion. Nature. 2019;571(7764):211-8. Epub 2019/06/18. doi: 10.1038/s41586-019-1325-x. PubMed PMID: 31207603; PMCID: PMC6713202.

265. Scott AC, Dundar F, Zumbo P, Chandran SS, Klebanoff CA, Shakiba M, Trivedi P, Menocal L, Appleby H, Camara S, Zamarin D, Walther T, Snyder A, Femia MR, Comen EA, Wen HY, Hellmann MD, Anandasabapathy N, Liu Y, Altorki NK, Lauer P, Levy O, Glickman MS, Kaye J, Betel D, Philip M, Schietinger A. TOX is a critical regulator of tumour-specific T cell differentiation. Nature. 2019;571(7764):270-4. Epub 2019/06/18. doi: 10.1038/s41586-019-1324-y. PubMed PMID: 31207604; PMCID: PMC7698992.

266. Seo H, Chen J, Gonzalez-Avalos E, Samaniego-Castruita D, Das A, Wang YH, Lopez-Moyado IF, Georges RO, Zhang W, Onodera A, Wu CJ, Lu LF, Hogan PG, Bhandoola A, Rao A. TOX and TOX2 transcription factors cooperate with NR4A transcription factors to impose CD8(+) T cell exhaustion. Proc Natl Acad Sci U S A. 2019;116(25):12410-5. Epub 2019/06/04. doi: 10.1073/pnas.1905675116. PubMed PMID: 31152140; PMCID: PMC6589758.

267. Yao C, Sun HW, Lacey NE, Ji Y, Moseman EA, Shih HY, Heuston EF, Kirby M, Anderson S, Cheng J, Khan O, Handon R, Reilley J, Fioravanti J, Hu J, Gossa S, Wherry EJ, Gattinoni L, McGavern DB, O'Shea JJ, Schwartzberg PL, Wu T. Single-cell RNA-seq reveals TOX as a key regulator of CD8(+) T cell persistence in chronic infection. Nat Immunol. 2019;20(7):890-901. Epub 2019/06/19. doi: 10.1038/s41590-019-0403-4. PubMed PMID: 31209400; PMCID: PMC6588409.

268. Hutter G, Nowak D, Mossner M, Ganepola S, Mussig A, Allers K, Schneider T, Hofmann J, Kucherer C, Blau O, Blau IW, Hofmann WK, Thiel E. Long-term control of HIV by CCR5 Delta32/Delta32 stem-cell transplantation. N Engl J Med. 2009;360(7):692-8. Epub 2009/02/14. doi: 10.1056/NEJMoa0802905. PubMed PMID: 19213682.

269. Gupta RK, Abdul-Jawad S, McCoy LE, Mok HP, Peppa D, Salgado M, Martinez-Picado J, Nijhuis M, Wensing AMJ, Lee H, Grant P, Nastouli E, Lambert J, Pace M, Salasc F, Monit C, Innes AJ, Muir L, Waters L, Frater J, Lever AML, Edwards SG, Gabriel IH, Olavarria E. HIV-1 remission following CCR5Delta32/Delta32 haematopoietic stem-cell transplantation. Nature. 2019;568(7751):244-8. Epub 2019/03/06. doi: 10.1038/s41586-019-1027-4. PubMed PMID: 30836379; PMCID: PMC7275870.

270. Ananworanich J, Schuetz A, Vandergeeten C, Sereti I, de Souza M, Rerknimitr R, Dewar R, Marovich M, van Griensven F, Sekaly R, Pinyakorn S, Phanuphak N, Trichavaroj R, Rutvisuttinunt W, Chomchey N, Paris R, Peel S, Valcour V, Maldarelli F, Chomont N, Michael N, Phanuphak P, Kim JH, Group RSS. Impact of multi-targeted antiretroviral treatment on gut T cell depletion and HIV reservoir seeding during acute HIV infection. PLoS One. 2012;7(3):e33948.

Epub 2012/04/06. doi: 10.1371/journal.pone.0033948. PubMed PMID: 22479485; PMCID: PMC3316511.

271. Buzon MJ, Martin-Gayo E, Pereyra F, Ouyang Z, Sun H, Li JZ, Piovoso M, Shaw A, Dalmau J, Zangger N, Martinez-Picado J, Zurakowski R, Yu XG, Telenti A, Walker BD, Rosenberg ES, Lichterfeld M. Long-term antiretroviral treatment initiated at primary HIV-1 infection affects the size, composition, and decay kinetics of the reservoir of HIV-1-infected CD4 T cells. J Virol. 2014;88(17):10056-65. Epub 2014/06/27. doi: 10.1128/JVI.01046-14. PubMed PMID: 24965451; PMCID: PMC4136362.

272. Cheret A, Bacchus-Souffan C, Avettand-Fenoel V, Melard A, Nembot G, Blanc C, Samri A, Saez-Cirion A, Hocqueloux L, Lascoux-Combe C, Allavena C, Goujard C, Valantin MA, Leplatois A, Meyer L, Rouzioux C, Autran B, Group OA-S. Combined ART started during acute HIV infection protects central memory CD4+ T cells and can induce remission. J Antimicrob Chemother. 2015;70(7):2108-20. Epub 2015/04/23. doi: 10.1093/jac/dkv084. PubMed PMID: 25900157.

273. Schuetz A, Deleage C, Sereti I, Rerknimitr R, Phanuphak N, Phuang-Ngern Y, Estes JD, Sandler NG, Sukhumvittaya S, Marovich M, Jongrakthaitae S, Akapirat S, Fletscher JL, Kroon E, Dewar R, Trichavaroj R, Chomchey N, Douek DC, RJ OC, Ngauy V, Robb ML, Phanuphak P, Michael NL, Excler JL, Kim JH, de Souza MS, Ananworanich J, Rv254/Search, Groups RSS. Initiation of ART during early acute HIV infection preserves mucosal Th17 function and reverses HIV-related immune activation. PLoS Pathog. 2014;10(12):e1004543. Epub 2014/12/17. doi: 10.1371/journal.ppat.1004543. PubMed PMID: 25503054; PMCID: PMC4263756.

274. Hogan CM, Degruttola V, Sun X, Fiscus SA, Del Rio C, Hare CB, Markowitz M, Connick E, Macatangay B, Tashima KT, Kallungal B, Camp R, Morton T, Daar ES, Little S, Team AS. The setpoint study (ACTG A5217): effect of immediate versus deferred antiretroviral therapy on virologic set point in recently HIV-1-infected individuals. J Infect Dis. 2012;205(1):87-96. Epub 2011/12/20. doi: 10.1093/infdis/jir699. PubMed PMID: 22180621; PMCID: PMC3242744.

275. Investigators ST, Fidler S, Porter K, Ewings F, Frater J, Ramjee G, Cooper D, Rees H, Fisher M, Schechter M, Kaleebu P, Tambussi G, Kinloch S, Miro JM, Kelleher A, McClure M, Kaye S, Gabriel M, Phillips R, Weber J, Babiker A. Short-course antiretroviral therapy in primary HIV infection. N Engl J Med. 2013;368(3):207-17. Epub 2013/01/18. doi: 10.1056/NEJMoa1110039. PubMed PMID: 23323897; PMCID: PMC4131004.

276. Saez-Cirion A, Bacchus C, Hocqueloux L, Avettand-Fenoel V, Girault I, Lecuroux C, Potard V, Versmisse P, Melard A, Prazuck T, Descours B, Guergnon J, Viard JP, Boufassa F, Lambotte O, Goujard C, Meyer L, Costagliola D, Venet A, Pancino G, Autran B, Rouzioux C, Group AVS. Post-treatment HIV-1 controllers with a long-term virological remission after the interruption of early initiated antiretroviral therapy ANRS VISCONTI Study. PLoS Pathog. 2013;9(3):e1003211. Epub 2013/03/22. doi: 10.1371/journal.ppat.1003211. PubMed PMID: 23516360; PMCID: PMC3597518.

277. Stohr W, Fidler S, McClure M, Weber J, Cooper D, Ramjee G, Kaleebu P, Tambussi G, Schechter M, Babiker A, Phillips RE, Porter K, Frater J. Duration of HIV-1 viral suppression on cessation of antiretroviral therapy in primary infection correlates with time on therapy. PLoS One. 2013;8(10):e78287. Epub 2013/11/10. doi: 10.1371/journal.pone.0078287. PubMed PMID: 24205183; PMCID: PMC3808338.

278. Lim SY, Osuna CE, Hraber PT, Hesselgesser J, Gerold JM, Barnes TL, Sanisetty S, Seaman MS, Lewis MG, Geleziunas R, Miller MD, Cihlar T, Lee WA, Hill AL, Whitney JB. TLR7 agonists induce transient viremia and reduce the viral reservoir in SIV-infected rhesus macaques on antiretroviral therapy. Sci Transl Med. 2018;10(439). Epub 2018/05/04. doi: 10.1126/scitranslmed.aao4521. PubMed PMID: 29720451; PMCID: PMC5973480.

279. McBrien JB, Kumar NA, Silvestri G. Mechanisms of CD8(+) T cell-mediated suppression of HIV/SIV replication. Eur J Immunol. 2018;48(6):898-914. Epub 2018/02/11. doi: 10.1002/eji.201747172. PubMed PMID: 29427516; PMCID: PMC6531861.

280. Cao Y, Cartwright EK, Silvestri G, Perelson AS. CD8+ lymphocyte control of SIV infection during antiretroviral therapy. PLoS Pathog. 2018;14(10):e1007350. Epub 2018/10/12. doi: 10.1371/journal.ppat.1007350. PubMed PMID: 30308068; PMCID: PMC6199003.

281. Cartwright EK, Spicer L, Smith SA, Lee D, Fast R, Paganini S, Lawson BO, Nega M, Easley K, Schmitz JE, Bosinger SE, Paiardini M, Chahroudi A, Vanderford TH, Estes JD, Lifson JD, Derdeyn CA, Silvestri G. CD8(+) Lymphocytes Are Required for Maintaining Viral Suppression in SIV-Infected Macaques Treated with Short-Term Antiretroviral Therapy. Immunity. 2016;45(3):656-68. Epub 2016/09/23. doi: 10.1016/j.immuni.2016.08.018. PubMed PMID: 27653601; PMCID: PMC5087330.

282. Wightman F, Solomon A, Kumar SS, Urriola N, Gallagher K, Hiener B, Palmer S, McNeil C, Garsia R, Lewin SR. Effect of ipilimumab on the HIV reservoir in an HIV-infected individual with metastatic melanoma. AIDS. 2015;29(4):504-6. Epub 2015/01/30. doi: 10.1097/QAD.0000000000000562. PubMed PMID: 25628259; PMCID: PMC4492799.

283. Guihot A, Marcelin AG, Massiani MA, Samri A, Soulie C, Autran B, Spano JP. Drastic decrease of the HIV reservoir in a patient treated with nivolumab for lung cancer. Ann Oncol. 2018;29(2):517-8. Epub 2017/12/06. doi: 10.1093/annonc/mdx696. PubMed PMID: 29206889.

284. Gay CL, Bosch RJ, Ritz J, Hataye JM, Aga E, Tressler RL, Mason SW, Hwang CK, Grasela DM, Ray N, Cyktor JC, Coffin JM, Acosta EP, Koup RA, Mellors JW, Eron JJ, Team ACTS. Clinical Trial of the Anti-PD-L1 Antibody BMS-936559 in HIV-1 Infected Participants on Suppressive Antiretroviral Therapy. J Infect Dis. 2017;215(11):1725-33. Epub 2017/04/22. doi: 10.1093/infdis/jix191. PubMed PMID: 28431010; PMCID: PMC5790148.

285. Velu V, Titanji K, Zhu B, Husain S, Pladevega A, Lai L, Vanderford TH, Chennareddi L, Silvestri G, Freeman GJ, Ahmed R, Amara RR. Enhancing SIV-specific immunity in vivo by PD-1 blockade. Nature. 2009;458(7235):206-10. Epub 2008/12/17. doi: 10.1038/nature07662. PubMed PMID: 19078956; PMCID: PMC2753387.

286. Mylvaganam GH, Chea LS, Tharp GK, Hicks S, Velu V, Iyer SS, Deleage C, Estes JD, Bosinger SE, Freeman GJ, Ahmed R, Amara RR. Combination anti-PD-1 and antiretroviral therapy provides therapeutic benefit against SIV. JCI Insight. 2018;3(18). Epub 2018/09/21. doi: 10.1172/jci.insight.122940. PubMed PMID: 30232277; PMCID: PMC6237231.

287. Ferrando-Martinez S, Moysi E, Pegu A, Andrews S, Nganou Makamdop K, Ambrozak D, McDermott AB, Palesch D, Paiardini M, Pavlakis GN, Brenchley JM, Douek D, Mascola JR, Petrovas C, Koup RA. Accumulation of follicular CD8+ T cells in pathogenic SIV infection. J Clin Invest. 2018;128(5):2089-103. Epub 2018/04/18. doi: 10.1172/JCI96207. PubMed PMID: 29664020; PMCID: PMC5919804.

288. Harper J, Gordon S, Chan CN, Wang H, Lindemuth E, Galardi C, Falcinelli SD, Raines SLM, Read JL, Nguyen K, McGary CS, Nekorchuk M, Busman-Sahay K, Schawalder J, King C, Pino M, Micci L, Cervasi B, Jean S, Sanderson A, Johns B, Koblansky AA, Amrine-Madsen H, Lifson J, Margolis DM, Silvestri G, Bar KJ, Favre D, Estes JD, Paiardini M. CTLA-4 and PD-1 dual blockade induces SIV reactivation without control of rebound after antiretroviral therapy interruption. Nat Med. 2020;26(4):519-28. Epub 2020/04/15. doi: 10.1038/s41591-020-0782-y. PubMed PMID: 32284611; PMCID: PMC7790171.

289. Lu W, Arraes LC, Ferreira WT, Andrieu JM. Therapeutic dendritic-cell vaccine for chronic HIV-1 infection. Nat Med. 2004;10(12):1359-65. Epub 2004/11/30. doi: 10.1038/nm1147. PubMed PMID: 15568033.

290. Borducchi EN, Cabral C, Stephenson KE, Liu J, Abbink P, Ng'ang'a D, Nkolola JP, Brinkman AL, Peter L, Lee BC, Jimenez J, Jetton D, Mondesir J, Mojta S, Chandrashekar A, Molloy K, Alter G, Gerold JM, Hill AL, Lewis MG, Pau MG, Schuitemaker H, Hesselgesser J, Geleziunas R, Kim JH, Robb ML, Michael NL, Barouch DH. Ad26/MVA therapeutic vaccination with TLR7 stimulation in SIV-infected rhesus monkeys. Nature. 2016;540(7632):284-7. Epub 2016/11/15. doi: 10.1038/nature20583. PubMed PMID: 27841870; PMCID: PMC5145754.

291. Bar-On Y, Gruell H, Schoofs T, Pai JA, Nogueira L, Butler AL, Millard K, Lehmann C, Suarez I, Oliveira TY, Karagounis T, Cohen YZ, Wyen C, Scholten S, Handl L, Belblidia S, Dizon JP, Vehreschild JJ, Witmer-Pack M, Shimeliovich I, Jain K, Fiddike K, Seaton KE, Yates NL, Horowitz J, Gulick RM, Pfeifer N, Tomaras GD, Seaman MS, Fatkenheuer G, Caskey M, Klein F, Nussenzweig MC. Safety and antiviral activity of combination HIV-1 broadly neutralizing antibodies in viremic individuals. Nat Med. 2018;24(11):1701-7. Epub 2018/09/28. doi: 10.1038/s41591-018-0186-4. PubMed PMID: 30258217; PMCID: PMC6221973.

292. Mendoza P, Gruell H, Nogueira L, Pai JA, Butler AL, Millard K, Lehmann C, Suarez I, Oliveira TY, Lorenzi JCC, Cohen YZ, Wyen C, Kummerle T, Karagounis T, Lu CL, Handl L, Unson-O'Brien C, Patel R, Ruping C, Schlotz M, Witmer-Pack M, Shimeliovich I, Kremer G, Thomas E, Seaton KE, Horowitz J, West AP, Jr., Bjorkman PJ, Tomaras GD, Gulick RM, Pfeifer N, Fatkenheuer G, Seaman MS, Klein F, Caskey M, Nussenzweig MC. Combination therapy with anti-HIV-1 antibodies maintains viral suppression. Nature. 2018;561(7724):479-84. Epub 2018/09/28. doi: 10.1038/s41586-018-0531-2. PubMed PMID: 30258136; PMCID: PMC6166473.

293. Crowell TA, Colby DJ, Pinyakorn S, Sacdalan C, Pagliuzza A, Intasan J, Benjapornpong K, Tangnaree K, Chomchey N, Kroon E, de Souza MS, Tovanabutra S, Rolland M, Eller MA, Paquin-Proulx D, Bolton DL, Tokarev A, Thomas R, Takata H, Trautmann L, Krebs SJ, Modjarrad K, McDermott AB, Bailer RT, Doria-Rose N, Patel B, Gorelick RJ, Fullmer BA, Schuetz A, Grandin PV, O'Connell RJ, Ledgerwood JE, Graham BS, Tressler R, Mascola JR, Chomont N, Michael NL, Robb ML, Phanuphak N, Ananworanich J, Group RVS. Safety and efficacy of VRC01 broadly neutralising antibodies in adults with acutely treated HIV (RV397): a phase 2, randomised, double-blind, placebo-controlled trial. Lancet HIV. 2019;6(5):e297-e306. Epub 2019/04/20. doi: 10.1016/S2352-3018(19)30053-0. PubMed PMID: 31000477; PMCID: PMC6693657.

294. Lynch RM, Boritz E, Coates EE, DeZure A, Madden P, Costner P, Enama ME, Plummer S, Holman L, Hendel CS, Gordon I, Casazza J, Conan-Cibotti M, Migueles SA, Tressler R, Bailer RT, McDermott A, Narpala S, O'Dell S, Wolf G, Lifson JD, Freemire BA, Gorelick RJ, Pandey JP,

Mohan S, Chomont N, Fromentin R, Chun TW, Fauci AS, Schwartz RM, Koup RA, Douek DC, Hu Z, Capparelli E, Graham BS, Mascola JR, Ledgerwood JE, Team VRCS. Virologic effects of broadly neutralizing antibody VRC01 administration during chronic HIV-1 infection. Sci Transl Med. 2015;7(319):319ra206. Epub 2015/12/25. doi: 10.1126/scitranslmed.aad5752. PubMed PMID: 26702094.

295. Haynes BF, Shaw GM, Korber B, Kelsoe G, Sodroski J, Hahn BH, Borrow P, McMichael AJ. HIV-Host Interactions: Implications for Vaccine Design. Cell Host Microbe. 2016;19(3):292-303. Epub 2016/03/01. doi: 10.1016/j.chom.2016.02.002. PubMed PMID: 26922989; PMCID: PMC4823811.

296. Bonsignori M, Scott E, Wiehe K, Easterhoff D, Alam SM, Hwang KK, Cooper M, Xia SM, Zhang R, Montefiori DC, Henderson R, Nie X, Kelsoe G, Moody MA, Chen X, Joyce MG, Kwong PD, Connors M, Mascola JR, McGuire AT, Stamatatos L, Medina-Ramirez M, Sanders RW, Saunders KO, Kepler TB, Haynes BF. Inference of the HIV-1 VRC01 Antibody Lineage Unmutated Common Ancestor Reveals Alternative Pathways to Overcome a Key Glycan Barrier. Immunity. 2018;49(6):1162-74 e8. Epub 2018/12/16. doi: 10.1016/j.immuni.2018.10.015. PubMed PMID: 30552024; PMCID: PMC6303191.

297. Duan H, Chen X, Boyington JC, Cheng C, Zhang Y, Jafari AJ, Stephens T, Tsybovsky Y, Kalyuzhniy O, Zhao P, Menis S, Nason MC, Normandin E, Mukhamedova M, DeKosky BJ, Wells L, Schief WR, Tian M, Alt FW, Kwong PD, Mascola JR. Glycan Masking Focuses Immune Responses to the HIV-1 CD4-Binding Site and Enhances Elicitation of VRC01-Class Precursor Antibodies. Immunity. 2018;49(2):301-11 e5. Epub 2018/08/05. doi: 10.1016/j.immuni.2018.07.005. PubMed PMID: 30076101; PMCID: PMC6896779.

298. Kwong PD, Mascola JR. HIV-1 Vaccines Based on Antibody Identification, B Cell Ontogeny, and Epitope Structure. Immunity. 2018;48(5):855-71. Epub 2018/05/17. doi: 10.1016/j.immuni.2018.04.029. PubMed PMID: 29768174.

299. Sanders RW, Moore JP. Native-like Env trimers as a platform for HIV-1 vaccine design. Immunol Rev. 2017;275(1):161-82. Epub 2017/01/31. doi: 10.1111/imr.12481. PubMed PMID: 28133806; PMCID: PMC5299501.

300. Hansen SG, Ford JC, Lewis MS, Ventura AB, Hughes CM, Coyne-Johnson L, Whizin N, Oswald K, Shoemaker R, Swanson T, Legasse AW, Chiuchiolo MJ, Parks CL, Axthelm MK, Nelson JA, Jarvis MA, Piatak M, Jr., Lifson JD, Picker LJ. Profound early control of highly pathogenic SIV by an effector memory T-cell vaccine. Nature. 2011;473(7348):523-7. Epub 2011/05/13. doi: 10.1038/nature10003. PubMed PMID: 21562493; PMCID: PMC3102768.

301. Hansen SG, Piatak M, Jr., Ventura AB, Hughes CM, Gilbride RM, Ford JC, Oswald K, Shoemaker R, Li Y, Lewis MS, Gilliam AN, Xu G, Whizin N, Burwitz BJ, Planer SL, Turner JM, Legasse AW, Axthelm MK, Nelson JA, Fruh K, Sacha JB, Estes JD, Keele BF, Edlefsen PT, Lifson JD, Picker LJ. Immune clearance of highly pathogenic SIV infection. Nature. 2013;502(7469):100-4. Epub 2013/09/13. doi: 10.1038/nature12519. PubMed PMID: 24025770; PMCID: PMC3849456.

302. Hansen SG, Marshall EE, Malouli D, Ventura AB, Hughes CM, Ainslie E, Ford JC, Morrow D, Gilbride RM, Bae JY, Legasse AW, Oswald K, Shoemaker R, Berkemeier B, Bosche WJ, Hull M, Womack J, Shao J, Edlefsen PT, Reed JS, Burwitz BJ, Sacha JB, Axthelm MK, Fruh K, Lifson JD, Picker LJ. A live-attenuated RhCMV/SIV vaccine shows long-term efficacy against heterologous SIV challenge. Sci Transl Med. 2019;11(501). Epub 2019/07/19. doi: 10.1126/scitranslmed.aaw2607. PubMed PMID: 31316007; PMCID: PMC6788755.

303. Marshall EE, Malouli D, Hansen SG, Gilbride RM, Hughes CM, Ventura AB, Ainslie E, Selseth AN, Ford JC, Burke D, Kreklywich CN, Womack J, Legasse AW, Axthelm MK, Kahl C, Streblow D, Edlefsen PT, Picker LJ, Fruh K. Enhancing safety of cytomegalovirus-based vaccine vectors by engaging host intrinsic immunity. Sci Transl Med. 2019;11(501). Epub 2019/07/19. doi: 10.1126/scitranslmed.aaw2603. PubMed PMID: 31316006; PMCID: PMC6830438.

304. Etienne L, Nerrienet E, LeBreton M, Bibila GT, Foupouapouognigni Y, Rousset D, Nana A, Djoko CF, Tamoufe U, Aghokeng AF, Mpoudi-Ngole E, Delaporte E, Peeters M, Wolfe ND, Ayouba A. Characterization of a new simian immunodeficiency virus strain in a naturally infected Pan troglodytes troglodytes chimpanzee with AIDS related symptoms. Retrovirology. 2011;8:4. Epub 2011/01/15. doi: 10.1186/1742-4690-8-4. PubMed PMID: 21232091; PMCID: PMC3034674.

305. Gray RH, Wawer MJ, Brookmeyer R, Sewankambo NK, Serwadda D, Wabwire-Mangen F, Lutalo T, Li X, vanCott T, Quinn TC, Rakai Project T. Probability of HIV-1 transmission per coital act in monogamous, heterosexual, HIV-1-discordant couples in Rakai, Uganda. Lancet. 2001;357(9263):1149-53. Epub 2001/04/27. doi: 10.1016/S0140-6736(00)04331-2. PubMed PMID: 11323041.

306. Keele BF, Jones JH, Terio KA, Estes JD, Rudicell RS, Wilson ML, Li Y, Learn GH, Beasley TM, Schumacher-Stankey J, Wroblewski E, Mosser A, Raphael J, Kamenya S, Lonsdorf EV, Travis DA, Mlengeya T, Kinsel MJ, Else JG, Silvestri G, Goodall J, Sharp PM, Shaw GM, Pusey AE, Hahn BH. Increased mortality and AIDS-like immunopathology in wild chimpanzees infected with SIVcpz. Nature. 2009;460(7254):515-9. Epub 2009/07/25. doi: 10.1038/nature08200. PubMed PMID: 19626114; PMCID: PMC2872475.

307. Novembre FJ, Saucier M, Anderson DC, Klumpp SA, O'Neil SP, Brown CR, 2nd, Hart CE, Guenthner PC, Swenson RB, McClure HM. Development of AIDS in a chimpanzee infected with human immunodeficiency virus type 1. J Virol. 1997;71(5):4086-91. Epub 1997/05/01. doi: 10.1128/JVI.71.5.4086-4091.1997. PubMed PMID: 9094687; PMCID: PMC191562.

308. Muthukumar A, Zhou D, Paiardini M, Barry AP, Cole KS, McClure HM, Staprans SI, Silvestri G, Sodora DL. Timely triggering of homeostatic mechanisms involved in the regulation of T-cell levels in SIVsm-infected sooty mangabeys. Blood. 2005;106(12):3839-45. Epub 2005/08/18. doi: 10.1182/blood-2005-01-0394. PubMed PMID: 16105985; PMCID: PMC1895113.

309. Paiardini M, Cervasi B, Sumpter B, McClure HM, Sodora DL, Magnani M, Staprans SI, Piedimonte G, Silvestri G. Perturbations of cell cycle control in T cells contribute to the different outcomes of simian immunodeficiency virus infection in rhesus macaques and sooty mangabeys. J Virol. 2006;80(2):634-42. Epub 2005/12/28. doi: 10.1128/JVI.80.2.634-642.2006. PubMed PMID: 16378966; PMCID: PMC1346860.

310. Paiardini M, Pandrea I, Apetrei C, Silvestri G. Lessons learned from the natural hosts of HIV-related viruses. Annu Rev Med. 2009;60:485-95. Epub 2009/07/28. doi: 10.1146/annurev.med.60.041807.123753. PubMed PMID: 19630581.

311. Silvestri G. Naturally SIV-infected sooty mangabeys: are we closer to understanding why they do not develop AIDS? J Med Primatol. 2005;34(5-6):243-52. Epub 2005/09/01. doi: 10.1111/j.1600-0684.2005.00122.x. PubMed PMID: 16128919.

312. Silvestri G, Paiardini M, Pandrea I, Lederman MM, Sodora DL. Understanding the benign nature of SIV infection in natural hosts. J Clin Invest. 2007;117(11):3148-54. Epub 2007/11/03. doi: 10.1172/JCI33034. PubMed PMID: 17975656; PMCID: PMC2045617.

313. Silvestri G, Sodora DL, Koup RA, Paiardini M, O'Neil SP, McClure HM, Staprans SI, Feinberg MB. Nonpathogenic SIV infection of sooty mangabeys is characterized by limited bystander immunopathology despite chronic high-level viremia. Immunity. 2003;18(3):441-52. Epub 2003/03/22. doi: 10.1016/s1074-7613(03)00060-8. PubMed PMID: 12648460.

314. Paiardini M, Cervasi B, Reyes-Aviles E, Micci L, Ortiz AM, Chahroudi A, Vinton C, Gordon SN, Bosinger SE, Francella N, Hallberg PL, Cramer E, Schlub T, Chan ML, Riddick NE, Collman RG, Apetrei C, Pandrea I, Else J, Munch J, Kirchhoff F, Davenport MP, Brenchley JM, Silvestri G. Low levels of SIV infection in sooty mangabey central memory CD(4)(+) T cells are associated with limited CCR5 expression. Nat Med. 2011;17(7):830-6. Epub 2011/06/28. doi: 10.1038/nm.2395. PubMed PMID: 21706028; PMCID: PMC3253129.

315. Palesch D, Bosinger SE, Tharp GK, Vanderford TH, Paiardini M, Chahroudi A, Johnson ZP, Kirchhoff F, Hahn BH, Norgren RB, Patel NB, Sodora DL, Dawoud RA, Stewart CB, Seepo

SM, Harris RA, Liu Y, Raveendran M, Han Y, English A, Thomas GWC, Hahn MW, Pipes L, Mason CE, Muzny DM, Gibbs RA, Sauter D, Worley K, Rogers J, Silvestri G. Sooty mangabey genome sequence provides insight into AIDS resistance in a natural SIV host. Nature. 2018;553(7686):77-81. Epub 2018/01/05. doi: 10.1038/nature25140. PubMed PMID: 29300007; PMCID: PMC5843367.

316. Chahroudi A, Bosinger SE, Vanderford TH, Paiardini M, Silvestri G. Natural SIV hosts: showing AIDS the door. Science. 2012;335(6073):1188-93. Epub 2012/03/10. doi: 10.1126/science.1217550. PubMed PMID: 22403383; PMCID: PMC3822437.

317. Hatziioannou T, Evans DT. Animal models for HIV/AIDS research. Nat Rev Microbiol. 2012;10(12):852-67. Epub 2012/11/17. doi: 10.1038/nrmicro2911. PubMed PMID: 23154262; PMCID: PMC4334372.

318. Kumar N, Chahroudi A, Silvestri G. Animal models to achieve an HIV cure. Curr Opin HIV AIDS. 2016;11(4):432-41. Epub 2016/05/07. doi: 10.1097/COH.0000000000000290. PubMed PMID: 27152962; PMCID: PMC4922307.

319. Wu JT, Leung K, Leung GM. Nowcasting and forecasting the potential domestic and international spread of the 2019-nCoV outbreak originating in Wuhan, China: a modelling study. Lancet. 2020;395(10225):689-97. Epub 2020/02/06. doi: 10.1016/S0140-6736(20)30260-9. PubMed PMID: 32014114; PMCID: PMC7159271.

320. Zhu N, Zhang D, Wang W, Li X, Yang B, Song J, Zhao X, Huang B, Shi W, Lu R, Niu P, Zhan F, Ma X, Wang D, Xu W, Wu G, Gao GF, Tan W, China Novel Coronavirus I, Research T. A Novel Coronavirus from Patients with Pneumonia in China, 2019. N Engl J Med. 2020;382(8):727-33. Epub 2020/01/25. doi: 10.1056/NEJMoa2001017. PubMed PMID: 31978945; PMCID: PMC7092803.

321. Gralinski LE, Menachery VD. Return of the Coronavirus: 2019-nCoV. Viruses. 2020;12(2). Epub 2020/01/30. doi: 10.3390/v12020135. PubMed PMID: 31991541; PMCID: PMC7077245.

322. Wu F, Zhao S, Yu B, Chen YM, Wang W, Song ZG, Hu Y, Tao ZW, Tian JH, Pei YY, Yuan ML, Zhang YL, Dai FH, Liu Y, Wang QM, Zheng JJ, Xu L, Holmes EC, Zhang YZ. A new coronavirus associated with human respiratory disease in China. Nature. 2020;579(7798):265-9. Epub 2020/02/06. doi: 10.1038/s41586-020-2008-3. PubMed PMID: 32015508; PMCID: PMC7094943.

323. Zhou P, Yang XL, Wang XG, Hu B, Zhang L, Zhang W, Si HR, Zhu Y, Li B, Huang CL, Chen HD, Chen J, Luo Y, Guo H, Jiang RD, Liu MQ, Chen Y, Shen XR, Wang X, Zheng XS, Zhao K, Chen QJ, Deng F, Liu LL, Yan B, Zhan FX, Wang YY, Xiao GF, Shi ZL. A pneumonia outbreak associated with a new coronavirus of probable bat origin. Nature. 2020;579(7798):270-3. Epub 2020/02/06. doi: 10.1038/s41586-020-2012-7. PubMed PMID: 32015507; PMCID: PMC7095418.

324. Wang R, Zhang X, Irwin DM, Shen Y. Emergence of SARS-like coronavirus poses new challenge in China. J Infect. 2020;80(3):350-71. Epub 2020/02/03. doi: 10.1016/j.jinf.2020.01.017. PubMed PMID: 32007524; PMCID: PMC7126811.

325. Lu R, Zhao X, Li J, Niu P, Yang B, Wu H, Wang W, Song H, Huang B, Zhu N, Bi Y, Ma X, Zhan F, Wang L, Hu T, Zhou H, Hu Z, Zhou W, Zhao L, Chen J, Meng Y, Wang J, Lin Y, Yuan J, Xie Z, Ma J, Liu WJ, Wang D, Xu W, Holmes EC, Gao GF, Wu G, Chen W, Shi W, Tan W. Genomic characterisation and epidemiology of 2019 novel coronavirus: implications for virus origins and receptor binding. Lancet. 2020;395(10224):565-74. Epub 2020/02/03. doi: 10.1016/S0140-6736(20)30251-8. PubMed PMID: 32007145; PMCID: PMC7159086.

326. Andersen KG, Rambaut A, Lipkin WI, Holmes EC, Garry RF. The proximal origin of SARS-CoV-2. Nat Med. 2020;26(4):450-2. Epub 2020/04/15. doi: 10.1038/s41591-020-0820-9. PubMed PMID: 32284615; PMCID: PMC7095063.

327. Hoffmann M, Kleine-Weber H, Schroeder S, Kruger N, Herrler T, Erichsen S, Schiergens TS, Herrler G, Wu NH, Nitsche A, Muller MA, Drosten C, Pohlmann S. SARS-CoV-2 Cell Entry Depends on ACE2 and TMPRSS2 and Is Blocked by a Clinically Proven Protease Inhibitor. Cell.

2020;181(2):271-80 e8. Epub 2020/03/07. doi: 10.1016/j.cell.2020.02.052. PubMed PMID: 32142651; PMCID: PMC7102627.

328. Chandrashekar A, Liu J, Martinot AJ, McMahan K, Mercado NB, Peter L, Tostanoski LH, Yu J, Maliga Z, Nekorchuk M, Busman-Sahay K, Terry M, Wrijil LM, Ducat S, Martinez DR, Atyeo C, Fischinger S, Burke JS, Slein MD, Pessaint L, Van Ry A, Greenhouse J, Taylor T, Blade K, Cook A, Finneyfrock B, Brown R, Teow E, Velasco J, Zahn R, Wegmann F, Abbink P, Bondzie EA, Dagotto G, Gebre MS, He X, Jacob-Dolan C, Kordana N, Li Z, Lifton MA, Mahrokhian SH, Maxfield LF, Nityanandam R, Nkolola JP, Schmidt AG, Miller AD, Baric RS, Alter G, Sorger PK, Estes JD, Andersen H, Lewis MG, Barouch DH. SARS-CoV-2 infection protects against rechallenge in rhesus macaques. Science. 2020;369(6505):812-7. Epub 2020/05/22. doi: 10.1126/science.abc4776. PubMed PMID: 32434946; PMCID: PMC7243369.

329. Hoang TN, Pino M, Boddapati AK, Viox EG, Starke CE, Upadhyay AA, Gumber S, Nekorchuk M, Busman-Sahay K, Strongin Z, Harper JL, Tharp GK, Pellegrini KL, Kirejczyk S, Zandi K, Tao S, Horton TR, Beagle EN, Mahar EA, Lee MYH, Cohen J, Jean SM, Wood JS, Connor-Stroud F, Stammen RL, Delmas OM, Wang S, Cooney KA, Sayegh MN, Wang L, Filev PD, Weiskopf D, Silvestri G, Waggoner J, Piantadosi A, Kasturi SP, Al-Shakhshir H, Ribeiro SP, Sekaly RP, Levit RD, Estes JD, Vanderford TH, Schinazi RF, Bosinger SE, Paiardini M. Baricitinib treatment resolves lower-airway macrophage inflammation and neutrophil recruitment in SARS-CoV-2-infected rhesus macaques. Cell. 2021;184(2):460-75 e21. Epub 2020/12/06. doi: 10.1016/j.cell.2020.11.007. PubMed PMID: 33278358; PMCID: PMC7654323.

330. Shi J, Wen Z, Zhong G, Yang H, Wang C, Huang B, Liu R, He X, Shuai L, Sun Z, Zhao Y, Liu P, Liang L, Cui P, Wang J, Zhang X, Guan Y, Tan W, Wu G, Chen H, Bu Z. Susceptibility of ferrets, cats, dogs, and other domesticated animals to SARS-coronavirus 2. Science. 2020;368(6494):1016-20. Epub 2020/04/10. doi: 10.1126/science.abb7015. PubMed PMID: 32269068; PMCID: PMC7164390.

331. Upadhyay AA, Hoang TN, Pino M, Boddapati AK, Viox EG, Lee MYH, Corry J, Strongin Z, Cowan DA, Beagle EN, Horton TR, Hamilton S, Aoued H, Harper JL, Nguyen K, Pellegrini KL, Tharp GK, Piantadosi A, Levit RD, Amara RR, Barratt-Boyes SM, Ribeiro SP, Sekaly RP, Vanderford TH, Schinazi RF, Paiardini M, Bosinger SE. TREM2+ and interstitial macrophages orchestrate airway inflammation in SARS-CoV-2 infection in rhesus macaques. bioRxiv. 2021. Epub 2021/10/14. doi: 10.1101/2021.10.05.463212. PubMed PMID: 34642693; PMCID: PMC8509096.

332. Ou X, Liu Y, Lei X, Li P, Mi D, Ren L, Guo L, Guo R, Chen T, Hu J, Xiang Z, Mu Z, Chen X, Chen J, Hu K, Jin Q, Wang J, Qian Z. Characterization of spike glycoprotein of SARS-CoV-2 on virus entry and its immune cross-reactivity with SARS-CoV. Nat Commun. 2020;11(1):1620. Epub 2020/03/30. doi: 10.1038/s41467-020-15562-9. PubMed PMID: 32221306; PMCID: PMC7100515.

333. Ziegler CGK, Allon SJ, Nyquist SK, Mbano IM, Miao VN, Tzouanas CN, Cao Y, Yousif AS, Bals J, Hauser BM, Feldman J, Muus C, Wadsworth MH, 2nd, Kazer SW, Hughes TK, Doran B, Gatter GJ, Vukovic M, Taliaferro F, Mead BE, Guo Z, Wang JP, Gras D, Plaisant M, Ansari M, Angelidis I, Adler H, Sucre JMS, Taylor CJ, Lin B, Waghray A, Mitsialis V, Dwyer DF, Buchheit KM, Boyce JA, Barrett NA, Laidlaw TM, Carroll SL, Colonna L, Tkachev V, Peterson CW, Yu A, Zheng HB, Gideon HP, Winchell CG, Lin PL, Bingle CD, Snapper SB, Kropski JA, Theis FJ, Schiller HB, Zaragosi LE, Barbry P, Leslie A, Kiem HP, Flynn JL, Fortune SM, Berger B, Finberg RW, Kean LS, Garber M, Schmidt AG, Lingwood D, Shalek AK, Ordovas-Montanes J, lung-network@humancellatlas.org HCALBNEa, Network HCALB. SARS-CoV-2 Receptor ACE2 Is an Interferon-Stimulated Gene in Human Airway Epithelial Cells and Is Detected in Specific Cell Subsets across Tissues. Cell. 2020;181(5):1016-35 e19. Epub 2020/05/16. doi: 10.1016/j.cell.2020.04.035. PubMed PMID: 32413319; PMCID: PMC7252096.

334. V'Kovski P, Kratzel A, Steiner S, Stalder H, Thiel V. Coronavirus biology and replication: implications for SARS-CoV-2. Nat Rev Microbiol. 2021;19(3):155-70. Epub 2020/10/30. doi: 10.1038/s41579-020-00468-6. PubMed PMID: 33116300; PMCID: PMC7592455.

335. Chen N, Zhou M, Dong X, Qu J, Gong F, Han Y, Qiu Y, Wang J, Liu Y, Wei Y, Xia J, Yu T, Zhang X, Zhang L. Epidemiological and clinical characteristics of 99 cases of 2019 novel coronavirus pneumonia in Wuhan, China: a descriptive study. Lancet. 2020;395(10223):507-13. Epub 2020/02/03. doi: 10.1016/S0140-6736(20)30211-7. PubMed PMID: 32007143; PMCID: PMC7135076.

336. Wu Z, McGoogan JM. Characteristics of and Important Lessons From the Coronavirus Disease 2019 (COVID-19) Outbreak in China: Summary of a Report of 72314 Cases From the Chinese Center for Disease Control and Prevention. JAMA. 2020;323(13):1239-42. Epub 2020/02/25. doi: 10.1001/jama.2020.2648. PubMed PMID: 32091533.

337. Fehr AR, Perlman S. Coronaviruses: an overview of their replication and pathogenesis. Methods Mol Biol. 2015;1282:1-23. Epub 2015/02/28. doi: 10.1007/978-1-4939-2438-7_1. PubMed PMID: 25720466; PMCID: PMC4369385.

338. Huang C, Wang Y, Li X, Ren L, Zhao J, Hu Y, Zhang L, Fan G, Xu J, Gu X, Cheng Z, Yu T, Xia J, Wei Y, Wu W, Xie X, Yin W, Li H, Liu M, Xiao Y, Gao H, Guo L, Xie J, Wang G, Jiang R, Gao Z, Jin Q, Wang J, Cao B. Clinical features of patients infected with 2019 novel coronavirus in Wuhan, China. Lancet. 2020;395(10223):497-506. Epub 2020/01/28. doi: 10.1016/S0140-6736(20)30183-5. PubMed PMID: 31986264; PMCID: PMC7159299.

339. Kuri-Cervantes L, Pampena MB, Meng W, Rosenfeld AM, Ittner CAG, Weisman AR, Agyekum RS, Mathew D, Baxter AE, Vella LA, Kuthuru O, Apostolidis SA, Bershaw L, Dougherty J, Greenplate AR, Pattekar A, Kim J, Han N, Gouma S, Weirick ME, Arevalo CP, Bolton MJ, Goodwin EC, Anderson EM, Hensley SE, Jones TK, Mangalmurti NS, Luning Prak ET, Wherry EJ, Meyer NJ, Betts MR. Comprehensive mapping of immune perturbations associated with

severe COVID-19. Sci Immunol. 2020;5(49). Epub 2020/07/17. doi: 10.1126/sciimmunol.abd7114. PubMed PMID: 32669287; PMCID: PMC7402634.

340. Mathew D, Giles JR, Baxter AE, Oldridge DA, Greenplate AR, Wu JE, Alanio C, Kuri-Cervantes L, Pampena MB, D'Andrea K, Manne S, Chen Z, Huang YJ, Reilly JP, Weisman AR, Ittner CAG, Kuthuru O, Dougherty J, Nzingha K, Han N, Kim J, Pattekar A, Goodwin EC, Anderson EM, Weirick ME, Gouma S, Arevalo CP, Bolton MJ, Chen F, Lacey SF, Ramage H, Cherry S, Hensley SE, Apostolidis SA, Huang AC, Vella LA, Unit UPCP, Betts MR, Meyer NJ, Wherry EJ. Deep immune profiling of COVID-19 patients reveals distinct immunotypes with therapeutic implications. Science. 2020;369(6508). Epub 2020/07/17. doi: 10.1126/science.abc8511. PubMed PMID: 32669297; PMCID: PMC7402624.

341. Vella LA, Giles JR, Baxter AE, Oldridge DA, Diorio C, Kuri-Cervantes L, Alanio C, Pampena MB, Wu JE, Chen Z, Huang YJ, Anderson EM, Gouma S, McNerney KO, Chase J, Burudpakdee C, Lee JH, Apostolidis SA, Huang AC, Mathew D, Kuthuru O, Goodwin EC, Weirick ME, Bolton MJ, Arevalo CP, Ramos A, Jasen CJ, Conrey PE, Sayed S, Giannini HM, D'Andrea K, Unit UPCP, Meyer NJ, Behrens EM, Bassiri H, Hensley SE, Henrickson SE, Teachey DT, Betts MR, Wherry EJ. Deep immune profiling of MIS-C demonstrates marked but transient immune activation compared to adult and pediatric COVID-19. Sci Immunol. 2021;6(57). Epub 2021/03/04. doi: 10.1126/sciimmunol.abf7570. PubMed PMID: 33653907; PMCID: PMC8128303.

342. Zhang B, Zhou X, Qiu Y, Song Y, Feng F, Feng J, Song Q, Jia Q, Wang J. Clinical characteristics of 82 cases of death from COVID-19. PLoS One. 2020;15(7):e0235458. Epub 2020/07/10. doi: 10.1371/journal.pone.0235458. PubMed PMID: 32645044; PMCID: PMC7347130.

343. Jia HP, Look DC, Shi L, Hickey M, Pewe L, Netland J, Farzan M, Wohlford-Lenane C, Perlman S, McCray PB, Jr. ACE2 receptor expression and severe acute respiratory syndrome coronavirus infection depend on differentiation of human airway epithelia. J Virol.

2005;79(23):14614-21. Epub 2005/11/12. doi: 10.1128/JVI.79.23.14614-14621.2005. PubMed PMID: 16282461; PMCID: PMC1287568.

344. Xu H, Zhong L, Deng J, Peng J, Dan H, Zeng X, Li T, Chen Q. High expression of ACE2 receptor of 2019-nCoV on the epithelial cells of oral mucosa. Int J Oral Sci. 2020;12(1):8. Epub 2020/02/26. doi: 10.1038/s41368-020-0074-x. PubMed PMID: 32094336; PMCID: PMC7039956.

345. Kuba K, Imai Y, Penninger JM. Angiotensin-converting enzyme 2 in lung diseases. Curr Opin Pharmacol. 2006;6(3):271-6. Epub 2006/04/04. doi: 10.1016/j.coph.2006.03.001. PubMed PMID: 16581295; PMCID: PMC7106490.

346. Chen IY, Moriyama M, Chang MF, Ichinohe T. Severe Acute Respiratory Syndrome Coronavirus Viroporin 3a Activates the NLRP3 Inflammasome. Front Microbiol. 2019;10:50. Epub 2019/02/15. doi: 10.3389/fmicb.2019.00050. PubMed PMID: 30761102; PMCID: PMC6361828.

347. Fink SL, Cookson BT. Apoptosis, pyroptosis, and necrosis: mechanistic description of dead and dying eukaryotic cells. Infect Immun. 2005;73(4):1907-16. Epub 2005/03/24. doi: 10.1128/IAI.73.4.1907-1916.2005. PubMed PMID: 15784530; PMCID: PMC1087413.

348. Xu Z, Shi L, Wang Y, Zhang J, Huang L, Zhang C, Liu S, Zhao P, Liu H, Zhu L, Tai Y, Bai C, Gao T, Song J, Xia P, Dong J, Zhao J, Wang FS. Pathological findings of COVID-19 associated with acute respiratory distress syndrome. Lancet Respir Med. 2020;8(4):420-2. Epub 2020/02/23. doi: 10.1016/S2213-2600(20)30076-X. PubMed PMID: 32085846; PMCID: PMC7164771.

349. Cohen KW, Linderman SL, Moodie Z, Czartoski J, Lai L, Mantus G, Norwood C, Nyhoff LE, Edara VV, Floyd K, De Rosa SC, Ahmed H, Whaley R, Patel SN, Prigmore B, Lemos MP, Davis CW, Furth S, O'Keefe JB, Gharpure MP, Gunisetty S, Stephens K, Antia R, Zarnitsyna VI, Stephens DS, Edupuganti S, Rouphael N, Anderson EJ, Mehta AK, Wrammert J, Suthar MS, Ahmed R, McElrath MJ. Longitudinal analysis shows durable and broad immune memory after SARS-CoV-2 infection with persisting antibody responses and memory B and T cells. Cell Rep Med. 2021;2(7):100354. Epub 2021/07/13. doi: 10.1016/j.xcrm.2021.100354. PubMed PMID: 34250512; PMCID: PMC8253687.

350. Jung JH, Rha MS, Sa M, Choi HK, Jeon JH, Seok H, Park DW, Park SH, Jeong HW, Choi WS, Shin EC. SARS-CoV-2-specific T cell memory is sustained in COVID-19 convalescent patients for 10 months with successful development of stem cell-like memory T cells. Nat Commun. 2021;12(1):4043. Epub 2021/07/02. doi: 10.1038/s41467-021-24377-1. PubMed PMID: 34193870; PMCID: PMC8245549.

351. Tan AT, Linster M, Tan CW, Le Bert N, Chia WN, Kunasegaran K, Zhuang Y, Tham CYL, Chia A, Smith GJD, Young B, Kalimuddin S, Low JGH, Lye D, Wang LF, Bertoletti A. Early induction of functional SARS-CoV-2-specific T cells associates with rapid viral clearance and mild disease in COVID-19 patients. Cell Rep. 2021;34(6):108728. Epub 2021/02/01. doi: 10.1016/j.celrep.2021.108728. PubMed PMID: 33516277; PMCID: PMC7826084.

352. Miller JD, van der Most RG, Akondy RS, Glidewell JT, Albott S, Masopust D, Murali-Krishna K, Mahar PL, Edupuganti S, Lalor S, Germon S, Del Rio C, Mulligan MJ, Staprans SI, Altman JD, Feinberg MB, Ahmed R. Human effector and memory CD8+ T cell responses to smallpox and yellow fever vaccines. Immunity. 2008;28(5):710-22. Epub 2008/05/13. doi: 10.1016/j.immuni.2008.02.020. PubMed PMID: 18468462.

353. Saini SK, Hersby DS, Tamhane T, Povlsen HR, Amaya Hernandez SP, Nielsen M, Gang AO, Hadrup SR. SARS-CoV-2 genome-wide T cell epitope mapping reveals immunodominance and substantial CD8(+) T cell activation in COVID-19 patients. Sci Immunol. 2021;6(58). Epub 2021/04/16. doi: 10.1126/sciimmunol.abf7550. PubMed PMID: 33853928; PMCID: PMC8139428.

354. Sekine T, Perez-Potti A, Rivera-Ballesteros O, Stralin K, Gorin JB, Olsson A, Llewellyn-Lacey S, Kamal H, Bogdanovic G, Muschiol S, Wullimann DJ, Kammann T, Emgard J, Parrot T, Folkesson E, Karolinska C-SG, Rooyackers O, Eriksson LI, Henter JI, Sonnerborg A, Allander T, Albert J, Nielsen M, Klingstrom J, Gredmark-Russ S, Bjorkstrom NK, Sandberg JK, Price DA, Ljunggren HG, Aleman S, Buggert M. Robust T Cell Immunity in Convalescent Individuals with Asymptomatic or Mild COVID-19. Cell. 2020;183(1):158-68 e14. Epub 2020/09/28. doi: 10.1016/j.cell.2020.08.017. PubMed PMID: 32979941; PMCID: PMC7427556.

355. Song JW, Zhang C, Fan X, Meng FP, Xu Z, Xia P, Cao WJ, Yang T, Dai XP, Wang SY, Xu RN, Jiang TJ, Li WG, Zhang DW, Zhao P, Shi M, Agrati C, Ippolito G, Maeurer M, Zumla A, Wang FS, Zhang JY. Immunological and inflammatory profiles in mild and severe cases of COVID-19. Nat Commun. 2020;11(1):3410. Epub 2020/07/10. doi: 10.1038/s41467-020-17240-2. PubMed PMID: 32641700; PMCID: PMC7343781.

356. Zheng HY, Zhang M, Yang CX, Zhang N, Wang XC, Yang XP, Dong XQ, Zheng YT. Elevated exhaustion levels and reduced functional diversity of T cells in peripheral blood may predict severe progression in COVID-19 patients. Cell Mol Immunol. 2020;17(5):541-3. Epub 2020/03/24. doi: 10.1038/s41423-020-0401-3. PubMed PMID: 32203186; PMCID: PMC7091621.

357. Rha MS, Jeong HW, Ko JH, Choi SJ, Seo IH, Lee JS, Sa M, Kim AR, Joo EJ, Ahn JY, Kim JH, Song KH, Kim ES, Oh DH, Ahn MY, Choi HK, Jeon JH, Choi JP, Kim HB, Kim YK, Park SH, Choi WS, Choi JY, Peck KR, Shin EC. PD-1-Expressing SARS-CoV-2-Specific CD8(+) T Cells Are Not Exhausted, but Functional in Patients with COVID-19. Immunity. 2021;54(1):44-52 e3. Epub 2020/12/19. doi: 10.1016/j.immuni.2020.12.002. PubMed PMID: 33338412; PMCID: PMC7834198.

358. Juno JA, Tan HX, Lee WS, Reynaldi A, Kelly HG, Wragg K, Esterbauer R, Kent HE, Batten CJ, Mordant FL, Gherardin NA, Pymm P, Dietrich MH, Scott NE, Tham WH, Godfrey DI, Subbarao K, Davenport MP, Kent SJ, Wheatley AK. Humoral and circulating follicular helper T cell responses in recovered patients with COVID-19. Nat Med. 2020;26(9):1428-34. Epub 2020/07/15. doi: 10.1038/s41591-020-0995-0. PubMed PMID: 32661393.

359. Rydyznski Moderbacher C, Ramirez SI, Dan JM, Grifoni A, Hastie KM, Weiskopf D, Belanger S, Abbott RK, Kim C, Choi J, Kato Y, Crotty EG, Kim C, Rawlings SA, Mateus J, Tse LPV, Frazier A, Baric R, Peters B, Greenbaum J, Ollmann Saphire E, Smith DM, Sette A, Crotty S. Antigen-Specific Adaptive Immunity to SARS-CoV-2 in Acute COVID-19 and Associations with Age and Disease Severity. Cell. 2020;183(4):996-1012 e19. Epub 2020/10/05. doi: 10.1016/j.cell.2020.09.038. PubMed PMID: 33010815; PMCID: PMC7494270.

360. Dan JM, Mateus J, Kato Y, Hastie KM, Yu ED, Faliti CE, Grifoni A, Ramirez SI, Haupt S, Frazier A, Nakao C, Rayaprolu V, Rawlings SA, Peters B, Krammer F, Simon V, Saphire EO, Smith DM, Weiskopf D, Sette A, Crotty S. Immunological memory to SARS-CoV-2 assessed for up to 8 months after infection. Science. 2021;371(6529). Epub 2021/01/08. doi: 10.1126/science.abf4063. PubMed PMID: 33408181; PMCID: PMC7919858.

361. Grifoni A, Weiskopf D, Ramirez SI, Mateus J, Dan JM, Moderbacher CR, Rawlings SA, Sutherland A, Premkumar L, Jadi RS, Marrama D, de Silva AM, Frazier A, Carlin AF, Greenbaum JA, Peters B, Krammer F, Smith DM, Crotty S, Sette A. Targets of T Cell Responses to SARS-CoV-2 Coronavirus in Humans with COVID-19 Disease and Unexposed Individuals. Cell. 2020;181(7):1489-501 e15. Epub 2020/05/31. doi: 10.1016/j.cell.2020.05.015. PubMed PMID: 32473127; PMCID: PMC7237901.

362. Peng Y, Mentzer AJ, Liu G, Yao X, Yin Z, Dong D, Dejnirattisai W, Rostron T, Supasa P, Liu C, Lopez-Camacho C, Slon-Campos J, Zhao Y, Stuart DI, Paesen GC, Grimes JM, Antson AA, Bayfield OW, Hawkins D, Ker DS, Wang B, Turtle L, Subramaniam K, Thomson P, Zhang P, Dold C, Ratcliff J, Simmonds P, de Silva T, Sopp P, Wellington D, Rajapaksa U, Chen YL, Salio M, Napolitani G, Paes W, Borrow P, Kessler BM, Fry JW, Schwabe NF, Semple MG, Baillie JK, Moore SC, Openshaw PJM, Ansari MA, Dunachie S, Barnes E, Frater J, Kerr G, Goulder P, Lockett T, Levin R, Zhang Y, Jing R, Ho LP, Oxford Immunology Network Covid-19 Response TcC, Investigators IC, Cornall RJ, Conlon CP, Klenerman P, Screaton GR, Mongkolsapaya J, McMichael A, Knight JC, Ogg G, Dong T. Broad and strong memory CD4(+) and CD8(+) T cells induced by SARS-CoV-2 in UK convalescent individuals following COVID-19. Nat Immunol. 2020;21(11):1336-45. Epub 2020/09/06. doi: 10.1038/s41590-020-0782-6. PubMed PMID: 32887977; PMCID: PMC7611020.

363. Hansen CH, Michlmayr D, Gubbels SM, Molbak K, Ethelberg S. Assessment of protection against reinfection with SARS-CoV-2 among 4 million PCR-tested individuals in Denmark in 2020:

a population-level observational study. Lancet. 2021;397(10280):1204-12. Epub 2021/03/21. doi: 10.1016/S0140-6736(21)00575-4. PubMed PMID: 33743221; PMCID: PMC7969130.

364. Le Bert N, Clapham HE, Tan AT, Chia WN, Tham CYL, Lim JM, Kunasegaran K, Tan LWL, Dutertre CA, Shankar N, Lim JME, Sun LJ, Zahari M, Tun ZM, Kumar V, Lim BL, Lim SH, Chia A, Tan YJ, Tambyah PA, Kalimuddin S, Lye D, Low JGH, Wang LF, Wan WY, Hsu LY, Bertoletti A, Tam CC. Highly functional virus-specific cellular immune response in asymptomatic SARS-CoV-2 infection. J Exp Med. 2021;218(5). Epub 2021/03/02. doi: 10.1084/jem.20202617. PubMed PMID: 33646265; PMCID: PMC7927662 SARS-CoV-2-specific T cells in biological samples pending. W.N. Chia reported a patent for a sublicense agreement with GenScript for the surrogate virus neutralization test pending (Duke-NUS). P. Tambyah reported grants from Arcturus, Roche, Shionogi, Sanofi-Pasteur, and Aj Biologics outside the submitted work. L. Wang reported a patent application on sVNT pending. A. Bertoletti reported personal fees from Oxford Immunotech and Qiagen outside the submitted work; in addition, A. Bertoletti had a patent for the use of peptide pools in whole blood for detection of SARS-CoV-2 T cells pending. C.C. Tam reported grants from Roche and personal fees from Verivax outside the submitted work. No other disclosures were reported.

365. Long QX, Tang XJ, Shi QL, Li Q, Deng HJ, Yuan J, Hu JL, Xu W, Zhang Y, Lv FJ, Su K, Zhang F, Gong J, Wu B, Liu XM, Li JJ, Qiu JF, Chen J, Huang AL. Clinical and immunological assessment of asymptomatic SARS-CoV-2 infections. Nat Med. 2020;26(8):1200-4. Epub 2020/06/20. doi: 10.1038/s41591-020-0965-6. PubMed PMID: 32555424.

366. Ogbe A, Kronsteiner B, Skelly DT, Pace M, Brown A, Adland E, Adair K, Akhter HD, Ali M, Ali SE, Angyal A, Ansari MA, Arancibia-Carcamo CV, Brown H, Chinnakannan S, Conlon C, de Lara C, de Silva T, Dold C, Dong T, Donnison T, Eyre D, Flaxman A, Fletcher H, Gardner J, Grist JT, Hackstein CP, Jaruthamsophon K, Jeffery K, Lambe T, Lee L, Li W, Lim N, Matthews PC, Mentzer AJ, Moore SC, Naisbitt DJ, Ogese M, Ogg G, Openshaw P, Pirmohamed M, Pollard AJ, Ramamurthy N, Rongkard P, Rowland-Jones S, Sampson O, Screaton G, Sette A, Stafford

L, Thompson C, Thomson PJ, Thwaites R, Vieira V, Weiskopf D, Zacharopoulou P, Oxford Immunology Network Covid-19 Response TCC, Oxford Protective TCIfC-CT, Turtle L, Klenerman P, Goulder P, Frater J, Barnes E, Dunachie S. T cell assays differentiate clinical and subclinical SARS-CoV-2 infections from cross-reactive antiviral responses. Nat Commun. 2021;12(1):2055. Epub 2021/04/08. doi: 10.1038/s41467-021-21856-3. PubMed PMID: 33824342; PMCID: PMC8024333.

367. Wang Z, Yang X, Zhong J, Zhou Y, Tang Z, Zhou H, He J, Mei X, Tang Y, Lin B, Chen Z, McCluskey J, Yang J, Corbett AJ, Ran P. Exposure to SARS-CoV-2 generates T-cell memory in the absence of a detectable viral infection. Nat Commun. 2021;12(1):1724. Epub 2021/03/21. doi: 10.1038/s41467-021-22036-z. PubMed PMID: 33741972; PMCID: PMC7979809.

368. Bacher P, Rosati E, Esser D, Martini GR, Saggau C, Schiminsky E, Dargvainiene J, Schroder I, Wieters I, Khodamoradi Y, Eberhardt F, Vehreschild M, Neb H, Sonntagbauer M, Conrad C, Tran F, Rosenstiel P, Markewitz R, Wandinger KP, Augustin M, Rybniker J, Kochanek M, Leypoldt F, Cornely OA, Koehler P, Franke A, Scheffold A. Low-Avidity CD4(+) T Cell Responses to SARS-CoV-2 in Unexposed Individuals and Humans with Severe COVID-19. Immunity. 2020;53(6):1258-71 e5. Epub 2020/12/10. doi: 10.1016/j.immuni.2020.11.016. PubMed PMID: 33296686; PMCID: PMC7689350.

369. Braun J, Loyal L, Frentsch M, Wendisch D, Georg P, Kurth F, Hippenstiel S, Dingeldey M, Kruse B, Fauchere F, Baysal E, Mangold M, Henze L, Lauster R, Mall MA, Beyer K, Rohmel J, Voigt S, Schmitz J, Miltenyi S, Demuth I, Muller MA, Hocke A, Witzenrath M, Suttorp N, Kern F, Reimer U, Wenschuh H, Drosten C, Corman VM, Giesecke-Thiel C, Sander LE, Thiel A. SARS-CoV-2-reactive T cells in healthy donors and patients with COVID-19. Nature. 2020;587(7833):270-4. Epub 2020/07/30. doi: 10.1038/s41586-020-2598-9. PubMed PMID: 32726801.

370. Le Bert N, Tan AT, Kunasegaran K, Tham CYL, Hafezi M, Chia A, Chng MHY, Lin M, Tan N, Linster M, Chia WN, Chen MI, Wang LF, Ooi EE, Kalimuddin S, Tambyah PA, Low JG, Tan

YJ, Bertoletti A. SARS-CoV-2-specific T cell immunity in cases of COVID-19 and SARS, and uninfected controls. Nature. 2020;584(7821):457-62. Epub 2020/07/16. doi: 10.1038/s41586-020-2550-z. PubMed PMID: 32668444.

371. Low JS, Vaqueirinho D, Mele F, Foglierini M, Jerak J, Perotti M, Jarrossay D, Jovic S, Perez L, Cacciatore R, Terrot T, Pellanda AF, Biggiogero M, Garzoni C, Ferrari P, Ceschi A, Lanzavecchia A, Sallusto F, Cassotta A. Clonal analysis of immunodominance and cross-reactivity of the CD4 T cell response to SARS-CoV-2. Science. 2021;372(6548):1336-41. Epub 2021/05/20. doi: 10.1126/science.abg8985. PubMed PMID: 34006597; PMCID: PMC8168615.

372. Loyal L, Braun J, Henze L, Kruse B, Dingeldey M, Reimer U, Kern F, Schwarz T, Mangold M, Unger C, Dorfler F, Kadler S, Rosowski J, Gurcan K, Uyar-Aydin Z, Frentsch M, Kurth F, Schnatbaum K, Eckey M, Hippenstiel S, Hocke A, Muller MA, Sawitzki B, Miltenyi S, Paul F, Mall MA, Wenschuh H, Voigt S, Drosten C, Lauster R, Lachman N, Sander LE, Corman VM, Rohmel J, Meyer-Arndt L, Thiel A, Giesecke-Thiel C. Cross-reactive CD4(+) T cells enhance SARS-CoV-2 immune responses upon infection and vaccination. Science. 2021;374(6564):eabh1823. Epub 2021/09/02. doi: 10.1126/science.abh1823. PubMed PMID: 34465633.

373. Mateus J, Grifoni A, Tarke A, Sidney J, Ramirez SI, Dan JM, Burger ZC, Rawlings SA, Smith DM, Phillips E, Mallal S, Lammers M, Rubiro P, Quiambao L, Sutherland A, Yu ED, da Silva Antunes R, Greenbaum J, Frazier A, Markmann AJ, Premkumar L, de Silva A, Peters B, Crotty S, Sette A, Weiskopf D. Selective and cross-reactive SARS-CoV-2 T cell epitopes in unexposed humans. Science. 2020;370(6512):89-94. Epub 2020/08/06. doi: 10.1126/science.abd3871. PubMed PMID: 32753554; PMCID: PMC7574914.

374. Meckiff BJ, Ramirez-Suastegui C, Fajardo V, Chee SJ, Kusnadi A, Simon H, Eschweiler S, Grifoni A, Pelosi E, Weiskopf D, Sette A, Ay F, Seumois G, Ottensmeier CH, Vijayanand P. Imbalance of Regulatory and Cytotoxic SARS-CoV-2-Reactive CD4(+) T Cells in COVID-19. Cell. 2020;183(5):1340-53 e16. Epub 2020/10/24. doi: 10.1016/j.cell.2020.10.001. PubMed PMID: 33096020; PMCID: PMC7534589.

375. Nelde A, Bilich T, Heitmann JS, Maringer Y, Salih HR, Roerden M, Lubke M, Bauer J, Rieth J, Wacker M, Peter A, Horber S, Traenkle B, Kaiser PD, Rothbauer U, Becker M, Junker D, Krause G, Strengert M, Schneiderhan-Marra N, Templin MF, Joos TO, Kowalewski DJ, Stos-Zweifel V, Fehr M, Rabsteyn A, Mirakaj V, Karbach J, Jager E, Graf M, Gruber LC, Rachfalski D, Preuss B, Hagelstein I, Marklin M, Bakchoul T, Gouttefangeas C, Kohlbacher O, Klein R, Stevanovic S, Rammensee HG, Walz JS. SARS-CoV-2-derived peptides define heterologous and COVID-19-induced T cell recognition. Nat Immunol. 2021;22(1):74-85. Epub 2020/10/02. doi: 10.1038/s41590-020-00808-x. PubMed PMID: 32999467.

376. Weiskopf D, Schmitz KS, Raadsen MP, Grifoni A, Okba NMA, Endeman H, van den Akker JPC, Molenkamp R, Koopmans MPG, van Gorp ECM, Haagmans BL, de Swart RL, Sette A, de Vries RD. Phenotype and kinetics of SARS-CoV-2-specific T cells in COVID-19 patients with acute respiratory distress syndrome. Sci Immunol. 2020;5(48). Epub 2020/06/28. doi: 10.1126/sciimmunol.abd2071. PubMed PMID: 32591408; PMCID: PMC7319493.

377. Dykema AG, Zhang B, Woldemeskel BA, Garliss CC, Cheung LS, Choudhury D, Zhang J, Aparicio L, Bom S, Rashid R, Caushi JX, Hsiue EH, Cascino K, Thompson EA, Kwaa AK, Singh D, Thapa S, Ordonez AA, Pekosz A, D'Alessio FR, Powell JD, Yegnasubramanian S, Zhou S, Pardoll DM, Ji H, Cox AL, Blankson JN, Smith KN. Functional characterization of CD4+ T cell receptors crossreactive for SARS-CoV-2 and endemic coronaviruses. J Clin Invest. 2021;131(10). Epub 2021/04/09. doi: 10.1172/JCI146922. PubMed PMID: 33830946; PMCID: PMC8121515.

378. Clute SC, Watkin LB, Cornberg M, Naumov YN, Sullivan JL, Luzuriaga K, Welsh RM, Selin LK. Cross-reactive influenza virus-specific CD8+ T cells contribute to lymphoproliferation in Epstein-Barr virus-associated infectious mononucleosis. J Clin Invest. 2005;115(12):3602-12. Epub 2005/11/26. doi: 10.1172/JCI25078. PubMed PMID: 16308574; PMCID: PMC1288832.

379. Koutsakos M, Illing PT, Nguyen THO, Mifsud NA, Crawford JC, Rizzetto S, Eltahla AA, Clemens EB, Sant S, Chua BY, Wong CY, Allen EK, Teng D, Dash P, Boyd DF, Grzelak L, Zeng

W, Hurt AC, Barr I, Rockman S, Jackson DC, Kotsimbos TC, Cheng AC, Richards M, Westall GP, Loudovaris T, Mannering SI, Elliott M, Tangye SG, Wakim LM, Rossjohn J, Vijaykrishna D, Luciani F, Thomas PG, Gras S, Purcell AW, Kedzierska K. Human CD8(+) T cell cross-reactivity across influenza A, B and C viruses. Nat Immunol. 2019;20(5):613-25. Epub 2019/02/20. doi: 10.1038/s41590-019-0320-6. PubMed PMID: 30778243.

380. Lipsitch M, Grad YH, Sette A, Crotty S. Cross-reactive memory T cells and herd immunity to SARS-CoV-2. Nat Rev Immunol. 2020;20(11):709-13. Epub 2020/10/08. doi: 10.1038/s41577-020-00460-4. PubMed PMID: 33024281; PMCID: PMC7537578.

381. Zhao J, Zhao J, Mangalam AK, Channappanavar R, Fett C, Meyerholz DK, Agnihothram S, Baric RS, David CS, Perlman S. Airway Memory CD4(+) T Cells Mediate Protective Immunity against Emerging Respiratory Coronaviruses. Immunity. 2016;44(6):1379-91. Epub 2016/06/12. doi: 10.1016/j.immuni.2016.05.006. PubMed PMID: 27287409; PMCID: PMC4917442.

382. Grau-Exposito J, Sanchez-Gaona N, Massana N, Suppi M, Astorga-Gamaza A, Perea D, Rosado J, Falco A, Kirkegaard C, Torrella A, Planas B, Navarro J, Suanzes P, Alvarez-Sierra D, Ayora A, Sansano I, Esperalba J, Andres C, Anton A, Ramon YCS, Almirante B, Pujol-Borrell R, Falco V, Burgos J, Buzon MJ, Genesca M. Peripheral and lung resident memory T cell responses against SARS-CoV-2. Nat Commun. 2021;12(1):3010. Epub 2021/05/23. doi: 10.1038/s41467-021-23333-3. PubMed PMID: 34021148; PMCID: PMC8140108.

383. Pizzolla A, Nguyen THO, Smith JM, Brooks AG, Kedzieska K, Heath WR, Reading PC, Wakim LM. Resident memory CD8(+) T cells in the upper respiratory tract prevent pulmonary influenza virus infection. Sci Immunol. 2017;2(12). Epub 2017/08/08. doi: 10.1126/sciimmunol.aam6970. PubMed PMID: 28783656.

384. Slutter B, Van Braeckel-Budimir N, Abboud G, Varga SM, Salek-Ardakani S, Harty JT. Dynamics of influenza-induced lung-resident memory T cells underlie waning heterosubtypic immunity. Sci Immunol. 2017;2(7). Epub 2017/08/08. doi: 10.1126/sciimmunol.aag2031. PubMed PMID: 28783666; PMCID: PMC5590757.

385. McMahan K, Yu J, Mercado NB, Loos C, Tostanoski LH, Chandrashekar A, Liu J, Peter L, Atyeo C, Zhu A, Bondzie EA, Dagotto G, Gebre MS, Jacob-Dolan C, Li Z, Nampanya F, Patel S, Pessaint L, Van Ry A, Blade K, Yalley-Ogunro J, Cabus M, Brown R, Cook A, Teow E, Andersen H, Lewis MG, Lauffenburger DA, Alter G, Barouch DH. Correlates of protection against SARS-CoV-2 in rhesus macaques. Nature. 2021;590(7847):630-4. Epub 2020/12/05. doi: 10.1038/s41586-020-03041-6. PubMed PMID: 33276369; PMCID: PMC7906955.

386. Hasenkrug KJ, Feldmann F, Myers L, Santiago ML, Guo K, Barrett BS, Mickens KL, Carmody A, Okumura A, Rao D, Collins MM, Messer RJ, Lovaglio J, Shaia C, Rosenke R, van Doremalen N, Clancy C, Saturday G, Hanley P, Smith BJ, Meade-White K, Shupert WL, Hawman DW, Feldmann H. Recovery from Acute SARS-CoV-2 Infection and Development of Anamnestic Immune Responses in T Cell-Depleted Rhesus Macaques. mBio. 2021;12(4):e0150321. Epub 2021/07/28. doi: 10.1128/mBio.01503-21. PubMed PMID: 34311582; PMCID: PMC8406331.

387. Barnes CO, Jette CA, Abernathy ME, Dam KA, Esswein SR, Gristick HB, Malyutin AG, Sharaf NG, Huey-Tubman KE, Lee YE, Robbiani DF, Nussenzweig MC, West AP, Jr., Bjorkman PJ. SARS-CoV-2 neutralizing antibody structures inform therapeutic strategies. Nature. 2020;588(7839):682-7. Epub 2020/10/13. doi: 10.1038/s41586-020-2852-1. PubMed PMID: 33045718; PMCID: PMC8092461.

388. Barnes CO, West AP, Jr., Huey-Tubman KE, Hoffmann MAG, Sharaf NG, Hoffman PR, Koranda N, Gristick HB, Gaebler C, Muecksch F, Lorenzi JCC, Finkin S, Hagglof T, Hurley A, Millard KG, Weisblum Y, Schmidt F, Hatziioannou T, Bieniasz PD, Caskey M, Robbiani DF, Nussenzweig MC, Bjorkman PJ. Structures of Human Antibodies Bound to SARS-CoV-2 Spike Reveal Common Epitopes and Recurrent Features of Antibodies. Cell. 2020;182(4):828-42 e16. Epub 2020/07/10. doi: 10.1016/j.cell.2020.06.025. PubMed PMID: 32645326; PMCID: PMC7311918.

389. Gaebler C, Wang Z, Lorenzi JCC, Muecksch F, Finkin S, Tokuyama M, Cho A, Jankovic M, Schaefer-Babajew D, Oliveira TY, Cipolla M, Viant C, Barnes CO, Bram Y, Breton G, Hagglof

T, Mendoza P, Hurley A, Turroja M, Gordon K, Millard KG, Ramos V, Schmidt F, Weisblum Y, Jha D, Tankelevich M, Martinez-Delgado G, Yee J, Patel R, Dizon J, Unson-O'Brien C, Shimeliovich I, Robbiani DF, Zhao Z, Gazumyan A, Schwartz RE, Hatziioannou T, Bjorkman PJ, Mehandru S, Bieniasz PD, Caskey M, Nussenzweig MC. Evolution of antibody immunity to SARS-CoV-2. Nature. 2021;591(7851):639-44. Epub 2021/01/19. doi: 10.1038/s41586-021-03207-w. PubMed PMID: 33461210; PMCID: PMC8221082.

390. Kaplonek P, Wang C, Bartsch Y, Fischinger S, Gorman MJ, Bowman K, Kang J, Dayal D, Martin P, Nowak RP, Villani AC, Hsieh CL, Charland NC, Gonye ALK, Gushterova I, Khanna HK, LaSalle TJ, Lavin-Parsons KM, Lilley BM, Lodenstein CL, Manakongtreecheep K, Margolin JD, McKaig BN, Rojas-Lopez M, Russo BC, Sharma N, Tantivit J, Thomas MF, Sade-Feldman M, Feldman J, Julg B, Nilles EJ, Musk ER, Menon AS, Fischer ES, McLellan JS, Schmidt A, Goldberg MB, Filbin MR, Hacohen N, Lauffenburger DA, Alter G. Early cross-coronavirus reactive signatures of humoral immunity against COVID-19. Sci Immunol. 2021;6(64):eabj2901. Epub 2021/10/16. doi: 10.1126/sciimmunol.abj2901. PubMed PMID: 34652962.

391. Muecksch F, Weisblum Y, Barnes CO, Schmidt F, Schaefer-Babajew D, Wang Z, JC CL, Flyak AI, DeLaitsch AT, Huey-Tubman KE, Hou S, Schiffer CA, Gaebler C, Da Silva J, Poston D, Finkin S, Cho A, Cipolla M, Oliveira TY, Millard KG, Ramos V, Gazumyan A, Rutkowska M, Caskey M, Nussenzweig MC, Bjorkman PJ, Hatziioannou T, Bieniasz PD. Affinity maturation of SARS-CoV-2 neutralizing antibodies confers potency, breadth, and resilience to viral escape mutations. Immunity. 2021;54(8):1853-68 e7. Epub 2021/08/01. doi: 10.1016/j.immuni.2021.07.008. PubMed PMID: 34331873; PMCID: PMC8323339.

392. Robbiani DF, Gaebler C, Muecksch F, Lorenzi JCC, Wang Z, Cho A, Agudelo M, Barnes CO, Gazumyan A, Finkin S, Hagglof T, Oliveira TY, Viant C, Hurley A, Hoffmann HH, Millard KG, Kost RG, Cipolla M, Gordon K, Bianchini F, Chen ST, Ramos V, Patel R, Dizon J, Shimeliovich I, Mendoza P, Hartweger H, Nogueira L, Pack M, Horowitz J, Schmidt F, Weisblum Y, Michailidis E, Ashbrook AW, Waltari E, Pak JE, Huey-Tubman KE, Koranda N, Hoffman PR, West AP, Jr.,

Rice CM, Hatziioannou T, Bjorkman PJ, Bieniasz PD, Caskey M, Nussenzweig MC. Convergent antibody responses to SARS-CoV-2 in convalescent individuals. Nature. 2020;584(7821):437-42. Epub 2020/06/20. doi: 10.1038/s41586-020-2456-9. PubMed PMID: 32555388; PMCID: PMC7442695.

393. Roltgen K, Powell AE, Wirz OF, Stevens BA, Hogan CA, Najeeb J, Hunter M, Wang H, Sahoo MK, Huang C, Yamamoto F, Manohar M, Manalac J, Otrelo-Cardoso AR, Pham TD, Rustagi A, Rogers AJ, Shah NH, Blish CA, Cochran JR, Jardetzky TS, Zehnder JL, Wang TT, Narasimhan B, Gombar S, Tibshirani R, Nadeau KC, Kim PS, Pinsky BA, Boyd SD. Defining the features and duration of antibody responses to SARS-CoV-2 infection associated with disease severity and outcome. Sci Immunol. 2020;5(54). Epub 2020/12/09. doi: 10.1126/sciimmunol.abe0240. PubMed PMID: 33288645; PMCID: PMC7857392.

394. Turner JS, Kim W, Kalaidina E, Goss CW, Rauseo AM, Schmitz AJ, Hansen L, Haile A, Klebert MK, Pusic I, O'Halloran JA, Presti RM, Ellebedy AH. SARS-CoV-2 infection induces long-lived bone marrow plasma cells in humans. Nature. 2021;595(7867):421-5. Epub 2021/05/25. doi: 10.1038/s41586-021-03647-4. PubMed PMID: 34030176.

395. Wang Z, Muecksch F, Schaefer-Babajew D, Finkin S, Viant C, Gaebler C, Hoffmann HH, Barnes CO, Cipolla M, Ramos V, Oliveira TY, Cho A, Schmidt F, Da Silva J, Bednarski E, Aguado L, Yee J, Daga M, Turroja M, Millard KG, Jankovic M, Gazumyan A, Zhao Z, Rice CM, Bieniasz PD, Caskey M, Hatziioannou T, Nussenzweig MC. Naturally enhanced neutralizing breadth against SARS-CoV-2 one year after infection. Nature. 2021;595(7867):426-31. Epub 2021/06/15. doi: 10.1038/s41586-021-03696-9. PubMed PMID: 34126625; PMCID: PMC8277577.

396. Liu W, Russell RM, Bibollet-Ruche F, Skelly AN, Sherrill-Mix S, Freeman DA, Stoltz R, Lindemuth E, Lee FH, Sterrett S, Bar KJ, Erdmann N, Gouma S, Hensley SE, Ketas T, Cupo A, Cruz Portillo VM, Moore JP, Bieniasz PD, Hatziioannou T, Massey G, Minyard MB, Saag MS, Davis RS, Shaw GM, Britt WJ, Leal SM, Jr., Goepfert P, Hahn BH. Predictors of

Nonseroconversion after SARS-CoV-2 Infection. Emerg Infect Dis. 2021;27(9):2454-8. Epub 2021/07/02. doi: 10.3201/eid2709.211042. PubMed PMID: 34193339; PMCID: PMC8386781.

397. Aldridge RW, Lewer D, Beale S, Johnson AM, Zambon M, Hayward AC, Fragaszy EB, Flu Watch G. Seasonality and immunity to laboratory-confirmed seasonal coronaviruses (HCoV-NL63, HCoV-OC43, and HCoV-229E): results from the Flu Watch cohort study. Wellcome Open Res. 2020;5:52. Epub 2021/01/19. doi: 10.12688/wellcomeopenres.15812.2. PubMed PMID: 33447664; PMCID: PMC7786426.2.

398. Sariol A, Perlman S. Lessons for COVID-19 Immunity from Other Coronavirus Infections. Immunity. 2020;53(2):248-63. Epub 2020/07/28. doi: 10.1016/j.immuni.2020.07.005. PubMed PMID: 32717182; PMCID: PMC7359787.

399. Anderson EM, Goodwin EC, Verma A, Arevalo CP, Bolton MJ, Weirick ME, Gouma S, McAllister CM, Christensen SR, Weaver J, Hicks P, Manzoni TB, Oniyide O, Ramage H, Mathew D, Baxter AE, Oldridge DA, Greenplate AR, Wu JE, Alanio C, D'Andrea K, Kuthuru O, Dougherty J, Pattekar A, Kim J, Han N, Apostolidis SA, Huang AC, Vella LA, Kuri-Cervantes L, Pampena MB, Unit UPCP, Betts MR, Wherry EJ, Meyer NJ, Cherry S, Bates P, Rader DJ, Hensley SE. Seasonal human coronavirus antibodies are boosted upon SARS-CoV-2 infection but not associated with protection. Cell. 2021;184(7):1858-64 e10. Epub 2021/02/26. doi: 10.1016/j.cell.2021.02.010. PubMed PMID: 33631096; PMCID: PMC7871851.

400. Ng KW, Faulkner N, Cornish GH, Rosa A, Harvey R, Hussain S, Ulferts R, Earl C, Wrobel AG, Benton DJ, Roustan C, Bolland W, Thompson R, Agua-Doce A, Hobson P, Heaney J, Rickman H, Paraskevopoulou S, Houlihan CF, Thomson K, Sanchez E, Shin GY, Spyer MJ, Joshi D, O'Reilly N, Walker PA, Kjaer S, Riddell A, Moore C, Jebson BR, Wilkinson M, Marshall LR, Rosser EC, Radziszewska A, Peckham H, Ciurtin C, Wedderburn LR, Beale R, Swanton C, Gandhi S, Stockinger B, McCauley J, Gamblin SJ, McCoy LE, Cherepanov P, Nastouli E, Kassiotis G. Preexisting and de novo humoral immunity to SARS-CoV-2 in humans. Science.

2020;370(6522):1339-43. Epub 2020/11/08. doi: 10.1126/science.abe1107. PubMed PMID: 33159009; PMCID: PMC7857411.

401. Wec AZ, Wrapp D, Herbert AS, Maurer DP, Haslwanter D, Sakharkar M, Jangra RK, Dieterle ME, Lilov A, Huang D, Tse LV, Johnson NV, Hsieh CL, Wang N, Nett JH, Champney E, Burnina I, Brown M, Lin S, Sinclair M, Johnson C, Pudi S, Bortz R, 3rd, Wirchnianski AS, Laudermilch E, Florez C, Fels JM, O'Brien CM, Graham BS, Nemazee D, Burton DR, Baric RS, Voss JE, Chandran K, Dye JM, McLellan JS, Walker LM. Broad neutralization of SARS-related viruses by human monoclonal antibodies. Science. 2020;369(6504):731-6. Epub 2020/06/17. doi: 10.1126/science.abc7424. PubMed PMID: 32540900; PMCID: PMC7299279.

402. Jaimes JA, Andre NM, Chappie JS, Millet JK, Whittaker GR. Phylogenetic Analysis and Structural Modeling of SARS-CoV-2 Spike Protein Reveals an Evolutionary Distinct and Proteolytically Sensitive Activation Loop. J Mol Biol. 2020;432(10):3309-25. Epub 2020/04/23. doi: 10.1016/j.jmb.2020.04.009. PubMed PMID: 32320687; PMCID: PMC7166309.

403. Nguyen-Contant P, Embong AK, Kanagaiah P, Chaves FA, Yang H, Branche AR, Topham DJ, Sangster MY. S Protein-Reactive IgG and Memory B Cell Production after Human SARS-CoV-2 Infection Includes Broad Reactivity to the S2 Subunit. mBio. 2020;11(5). Epub 2020/09/27. doi: 10.1128/mBio.01991-20. PubMed PMID: 32978311; PMCID: PMC7520599.

404. Chi X, Yan R, Zhang J, Zhang G, Zhang Y, Hao M, Zhang Z, Fan P, Dong Y, Yang Y, Chen Z, Guo Y, Zhang J, Li Y, Song X, Chen Y, Xia L, Fu L, Hou L, Xu J, Yu C, Li J, Zhou Q, Chen W. A neutralizing human antibody binds to the N-terminal domain of the Spike protein of SARS-CoV-2. Science. 2020;369(6504):650-5. Epub 2020/06/24. doi: 10.1126/science.abc6952. PubMed PMID: 32571838; PMCID: PMC7319273.

405. McCallum M, De Marco A, Lempp FA, Tortorici MA, Pinto D, Walls AC, Beltramello M, Chen A, Liu Z, Zatta F, Zepeda S, di Iulio J, Bowen JE, Montiel-Ruiz M, Zhou J, Rosen LE, Bianchi S, Guarino B, Fregni CS, Abdelnabi R, Foo SC, Rothlauf PW, Bloyet LM, Benigni F, Cameroni E, Neyts J, Riva A, Snell G, Telenti A, Whelan SPJ, Virgin HW, Corti D, Pizzuto MS, Veesler D. N-

terminal domain antigenic mapping reveals a site of vulnerability for SARS-CoV-2. Cell. 2021;184(9):2332-47 e16. Epub 2021/03/25. doi: 10.1016/j.cell.2021.03.028. PubMed PMID: 33761326; PMCID: PMC7962585.

406. Poh CM, Carissimo G, Wang B, Amrun SN, Lee CY, Chee RS, Fong SW, Yeo NK, Lee WH, Torres-Ruesta A, Leo YS, Chen MI, Tan SY, Chai LYA, Kalimuddin S, Kheng SSG, Thien SY, Young BE, Lye DC, Hanson BJ, Wang CI, Renia L, Ng LFP. Two linear epitopes on the SARS-CoV-2 spike protein that elicit neutralising antibodies in COVID-19 patients. Nat Commun. 2020;11(1):2806. Epub 2020/06/03. doi: 10.1038/s41467-020-16638-2. PubMed PMID: 32483236; PMCID: PMC7264175.

407. Iyer AS, Jones FK, Nodoushani A, Kelly M, Becker M, Slater D, Mills R, Teng E, Kamruzzaman M, Garcia-Beltran WF, Astudillo M, Yang D, Miller TE, Oliver E, Fischinger S, Atyeo C, Iafrate AJ, Calderwood SB, Lauer SA, Yu J, Li Z, Feldman J, Hauser BM, Caradonna TM, Branda JA, Turbett SE, LaRocque RC, Mellon G, Barouch DH, Schmidt AG, Azman AS, Alter G, Ryan ET, Harris JB, Charles RC. Persistence and decay of human antibody responses to the receptor binding domain of SARS-CoV-2 spike protein in COVID-19 patients. Sci Immunol. 2020;5(52). Epub 2020/10/10. doi: 10.1126/sciimmunol.abe0367. PubMed PMID: 33033172; PMCID: PMC7857394.

408. Long QX, Liu BZ, Deng HJ, Wu GC, Deng K, Chen YK, Liao P, Qiu JF, Lin Y, Cai XF, Wang DQ, Hu Y, Ren JH, Tang N, Xu YY, Yu LH, Mo Z, Gong F, Zhang XL, Tian WG, Hu L, Zhang XX, Xiang JL, Du HX, Liu HW, Lang CH, Luo XH, Wu SB, Cui XP, Zhou Z, Zhu MM, Wang J, Xue CJ, Li XF, Wang L, Li ZJ, Wang K, Niu CC, Yang QJ, Tang XJ, Zhang Y, Liu XM, Li JJ, Zhang DC, Zhang F, Liu P, Yuan J, Li Q, Hu JL, Chen J, Huang AL. Antibody responses to SARS-CoV-2 in patients with COVID-19. Nat Med. 2020;26(6):845-8. Epub 2020/05/01. doi: 10.1038/s41591-020-0897-1. PubMed PMID: 32350462.

409. Ibarrondo FJ, Fulcher JA, Goodman-Meza D, Elliott J, Hofmann C, Hausner MA, Ferbas KG, Tobin NH, Aldrovandi GM, Yang OO. Rapid Decay of Anti-SARS-CoV-2 Antibodies in

Persons with Mild Covid-19. N Engl J Med. 2020;383(11):1085-7. Epub 2020/07/25. doi: 10.1056/NEJMc2025179. PubMed PMID: 32706954; PMCID: PMC7397184.

410. Isho B, Abe KT, Zuo M, Jamal AJ, Rathod B, Wang JH, Li Z, Chao G, Rojas OL, Bang YM, Pu A, Christie-Holmes N, Gervais C, Ceccarelli D, Samavarchi-Tehrani P, Guvenc F, Budylowski P, Li A, Paterson A, Yue FY, Marin LM, Caldwell L, Wrana JL, Colwill K, Sicheri F, Mubareka S, Gray-Owen SD, Drews SJ, Siqueira WL, Barrios-Rodiles M, Ostrowski M, Rini JM, Durocher Y, McGeer AJ, Gommerman JL, Gingras AC. Persistence of serum and saliva antibody responses to SARS-CoV-2 spike antigens in COVID-19 patients. Sci Immunol. 2020;5(52). Epub 2020/10/10. doi: 10.1126/sciimmunol.abe5511. PubMed PMID: 33033173; PMCID: PMC8050884.

411. Lucas C, Klein J, Sundaram ME, Liu F, Wong P, Silva J, Mao T, Oh JE, Mohanty S, Huang J, Tokuyama M, Lu P, Venkataraman A, Park A, Israelow B, Vogels CBF, Muenker MC, Chang CH, Casanovas-Massana A, Moore AJ, Zell J, Fournier JB, Yale IRT, Wyllie AL, Campbell M, Lee AI, Chun HJ, Grubaugh ND, Schulz WL, Farhadian S, Dela Cruz C, Ring AM, Shaw AC, Wisnewski AV, Yildirim I, Ko AI, Omer SB, Iwasaki A. Delayed production of neutralizing antibodies correlates with fatal COVID-19. Nat Med. 2021;27(7):1178-86. Epub 2021/05/07. doi: 10.1038/s41591-021-01355-0. PubMed PMID: 33953384.

412. Bok K, Sitar S, Graham BS, Mascola JR. Accelerated COVID-19 vaccine development: milestones, lessons, and prospects. Immunity. 2021;54(8):1636-51. Epub 2021/08/05. doi: 10.1016/j.immuni.2021.07.017. PubMed PMID: 34348117; PMCID: PMC8328682 and patent application: WO/2018/081318 Prefusion Coronavirus Spike Proteins and their use; PCT Patent Application No. PCT/US2021/017709, filed on February 11, 2021, entitled "SARS-CoV-2 VACCINE." J.M. and B.G. are listed as inventors on the following patent application: U.S. Provisional Patent Application No. 63/140,250, filed on January 21, 2021, entitled "NEWCASTLE DISEASE VIRUS-LIKE PARTICLE DISPLAYING PREFUSION-STABILIZED SARS-COV-2 SPIKE AND ITS USE.".

413. Levin EG, Lustig Y, Cohen C, Fluss R, Indenbaum V, Amit S, Doolman R, Asraf K, Mendelson E, Ziv A, Rubin C, Freedman L, Kreiss Y, Regev-Yochay G. Waning Immune Humoral Response to BNT162b2 Covid-19 Vaccine over 6 Months. N Engl J Med. 2021. Epub 2021/10/07. doi: 10.1056/NEJMoa2114583. PubMed PMID: 34614326; PMCID: PMC8522797.

414. Plante JA, Mitchell BM, Plante KS, Debbink K, Weaver SC, Menachery VD. The variant gambit: COVID-19's next move. Cell Host Microbe. 2021;29(4):508-15. Epub 2021/04/01. doi: 10.1016/j.chom.2021.02.020. PubMed PMID: 33789086; PMCID: PMC7919536.

415. Wu A, Wang L, Zhou HY, Ji CY, Xia SZ, Cao Y, Meng J, Ding X, Gold S, Jiang T, Cheng G. One year of SARS-CoV-2 evolution. Cell Host Microbe. 2021;29(4):503-7. Epub 2021/03/08. doi: 10.1016/j.chom.2021.02.017. PubMed PMID: 33676588; PMCID: PMC7903908.

416. Yurkovetskiy L, Wang X, Pascal KE, Tomkins-Tinch C, Nyalile TP, Wang Y, Baum A, Diehl WE, Dauphin A, Carbone C, Veinotte K, Egri SB, Schaffner SF, Lemieux JE, Munro JB, Rafique A, Barve A, Sabeti PC, Kyratsous CA, Dudkina NV, Shen K, Luban J. Structural and Functional Analysis of the D614G SARS-CoV-2 Spike Protein Variant. Cell. 2020;183(3):739-51 e8. Epub 2020/09/30. doi: 10.1016/j.cell.2020.09.032. PubMed PMID: 32991842; PMCID: PMC7492024.

417. Chen RE, Zhang X, Case JB, Winkler ES, Liu Y, VanBlargan LA, Liu J, Errico JM, Xie X, Suryadevara N, Gilchuk P, Zost SJ, Tahan S, Droit L, Turner JS, Kim W, Schmitz AJ, Thapa M, Wang D, Boon ACM, Presti RM, O'Halloran JA, Kim AHJ, Deepak P, Pinto D, Fremont DH, Crowe JE, Jr., Corti D, Virgin HW, Ellebedy AH, Shi PY, Diamond MS. Resistance of SARS-CoV-2 variants to neutralization by monoclonal and serum-derived polyclonal antibodies. Nat Med. 2021;27(4):717-26. Epub 2021/03/06. doi: 10.1038/s41591-021-01294-w. PubMed PMID: 33664494; PMCID: PMC8058618.

418. Edara VV, Norwood C, Floyd K, Lai L, Davis-Gardner ME, Hudson WH, Mantus G, Nyhoff LE, Adelman MW, Fineman R, Patel S, Byram R, Gomes DN, Michael G, Abdullahi H, Beydoun N, Panganiban B, McNair N, Hellmeister K, Pitts J, Winters J, Kleinhenz J, Usher J, O'Keefe JB, Piantadosi A, Waggoner JJ, Babiker A, Stephens DS, Anderson EJ, Edupuganti S, Rouphael N,

Ahmed R, Wrammert J, Suthar MS. Infection- and vaccine-induced antibody binding and neutralization of the B.1.351 SARS-CoV-2 variant. Cell Host Microbe. 2021;29(4):516-21 e3. Epub 2021/04/03. doi: 10.1016/j.chom.2021.03.009. PubMed PMID: 33798491; PMCID: PMC7980225.

419. Greaney AJ, Loes AN, Crawford KHD, Starr TN, Malone KD, Chu HY, Bloom JD. Comprehensive mapping of mutations in the SARS-CoV-2 receptor-binding domain that affect recognition by polyclonal human plasma antibodies. Cell Host Microbe. 2021;29(3):463-76 e6. Epub 2021/02/17. doi: 10.1016/j.chom.2021.02.003. PubMed PMID: 33592168; PMCID: PMC7869748.

420. Wu K, Werner AP, Koch M, Choi A, Narayanan E, Stewart-Jones GBE, Colpitts T, Bennett H, Boyoglu-Barnum S, Shi W, Moliva JI, Sullivan NJ, Graham BS, Carfi A, Corbett KS, Seder RA, Edwards DK. Serum Neutralizing Activity Elicited by mRNA-1273 Vaccine. N Engl J Med. 2021;384(15):1468-70. Epub 2021/03/18. doi: 10.1056/NEJMc2102179. PubMed PMID: 33730471; PMCID: PMC8008744.

421. Muik A, Wallisch AK, Sanger B, Swanson KA, Muhl J, Chen W, Cai H, Maurus D, Sarkar R, Tureci O, Dormitzer PR, Sahin U. Neutralization of SARS-CoV-2 lineage B.1.1.7 pseudovirus by BNT162b2 vaccine-elicited human sera. Science. 2021;371(6534):1152-3. Epub 2021/01/31. doi: 10.1126/science.abg6105. PubMed PMID: 33514629; PMCID: PMC7971771.

422. Starr TN, Greaney AJ, Hilton SK, Ellis D, Crawford KHD, Dingens AS, Navarro MJ, Bowen JE, Tortorici MA, Walls AC, King NP, Veesler D, Bloom JD. Deep Mutational Scanning of SARS-CoV-2 Receptor Binding Domain Reveals Constraints on Folding and ACE2 Binding. Cell. 2020;182(5):1295-310 e20. Epub 2020/08/26. doi: 10.1016/j.cell.2020.08.012. PubMed PMID: 32841599; PMCID: PMC7418704.

423. Wall EC, Wu M, Harvey R, Kelly G, Warchal S, Sawyer C, Daniels R, Hobson P, Hatipoglu E, Ngai Y, Hussain S, Nicod J, Goldstone R, Ambrose K, Hindmarsh S, Beale R, Riddell A, Gamblin S, Howell M, Kassiotis G, Libri V, Williams B, Swanton C, Gandhi S, Bauer DL.

Neutralising antibody activity against SARS-CoV-2 VOCs B.1.617.2 and B.1.351 by BNT162b2 vaccination. Lancet. 2021;397(10292):2331-3. Epub 2021/06/07. doi: 10.1016/S0140-6736(21)01290-3. PubMed PMID: 34090624; PMCID: PMC8175044 Roche-Ventana, Pfizer and Archer Dx, unrelated to this Correspondence; personal fees from Genentech, Sarah Canon Research Institute, Medicxi, Bicycle Therapeutics, GRAIL, Amgen, AstraZeneca, BMS, Illumina, GlaxoSmithKline, MSD, and Roche-Ventana, unrelated to this Correspondence; and stock options from Apogen Biotech, Epic Biosciences, GRAIL, and Achilles Therapeutics, unrelated to this Correspondence. All other authors declare no competing interests. ECW, MW, SG, and DLVB contributed equally. GKa, CSw, SGan, and DLVB are joint senior authors. RB and DLVB are members of the Genotype-to-Phenotype UK National Virology Consortium. Funding details and acknowledgments can be found in the appendix. All data (anonymised) and full R code to produce all figures and statistical analysis presented in this Correspondence are available online on Github.

424. Bastard P, Rosen LB, Zhang Q, Michailidis E, Hoffmann HH, Zhang Y, Dorgham K, Philippot Q, Rosain J, Beziat V, Manry J, Shaw E, Haljasmagi L, Peterson P, Lorenzo L, Bizien L, Trouillet-Assant S, Dobbs K, de Jesus AA, Belot A, Kallaste A, Catherinot E, Tandjaoui-Lambiotte Y, Le Pen J, Kerner G, Bigio B, Seeleuthner Y, Yang R, Bolze A, Spaan AN, Delmonte OM, Abers MS, Aiuti A, Casari G, Lampasona V, Piemonti L, Ciceri F, Bilguvar K, Lifton RP, Vasse M, Smadja DM, Migaud M, Hadjadj J, Terrier B, Duffy D, Quintana-Murci L, van de Beek D, Roussel L, Vinh DC, Tangye SG, Haerynck F, Dalmau D, Martinez-Picado J, Brodin P, Nussenzweig MC, Boisson-Dupuis S, Rodriguez-Gallego C, Vogt G, Mogensen TH, Oler AJ, Gu J, Burbelo PD, Cohen JI, Biondi A, Bettini LR, D'Angio M, Bonfanti P, Rossignol P, Mayaux J, Rieux-Laucat F, Husebye ES, Fusco F, Ursini MV, Imberti L, Sottini A, Paghera S, Quiros-Roldan E, Rossi C, Castagnoli R, Montagna D, Licari A, Marseglia GL, Duval X, Ghosn J, Lab H, Group N-UIRtC, Clinicians C, Clinicians C-S, Imagine CG, French CCSG, Milieu Interieur C, Co VCC, Amsterdam UMCC-B, Effort CHG, Tsang JS, Goldbach-Mansky R, Kisand K, Lionakis MS, Puel

A, Zhang SY, Holland SM, Gorochov G, Jouanguy E, Rice CM, Cobat A, Notarangelo LD, Abel L, Su HC, Casanova JL. Autoantibodies against type I IFNs in patients with life-threatening COVID-19. Science. 2020;370(6515). Epub 2020/09/26. doi: 10.1126/science.abd4585. PubMed PMID: 32972996; PMCID: PMC7857397.

425. Zhang Q, Bastard P, Liu Z, Le Pen J, Moncada-Velez M, Chen J, Ogishi M, Sabli IKD, Hodeib S, Korol C, Rosain J, Bilguvar K, Ye J, Bolze A, Bigio B, Yang R, Arias AA, Zhou Q, Zhang Y, Onodi F, Korniotis S, Karpf L, Philippot Q, Chbihi M, Bonnet-Madin L, Dorgham K, Smith N, Schneider WM, Razooky BS, Hoffmann HH, Michailidis E, Moens L, Han JE, Lorenzo L, Bizien L, Meade P, Neehus AL, Ugurbil AC, Corneau A, Kerner G, Zhang P, Rapaport F, Seeleuthner Y, Manry J, Masson C, Schmitt Y, Schluter A, Le Voyer T, Khan T, Li J, Fellay J, Roussel L, Shahrooei M, Alosaimi MF, Mansouri D, Al-Saud H, Al-Mulla F, Almourfi F, Al-Muhsen SZ, Alsohime F, Al Turki S, Hasanato R, van de Beek D, Biondi A, Bettini LR, D'Angio M, Bonfanti P, Imberti L, Sottini A, Paghera S, Quiros-Roldan E, Rossi C, Oler AJ, Tompkins MF, Alba C, Vandernoot I, Goffard JC, Smits G, Migeotte I, Haerynck F, Soler-Palacin P, Martin-Nalda A, Colobran R, Morange PE, Keles S, Colkesen F, Ozcelik T, Yasar KK, Senoglu S, Karabela SN, Rodriguez-Gallego C, Novelli G, Hraiech S, Tandjaoui-Lambiotte Y, Duval X, Laouenan C, Clinicians C-S, Clinicians C, Imagine CG, French CCSG, Co VCC, Amsterdam UMCC-B, Effort CHG, Group N-UTCI, Snow AL, Dalgard CL, Milner JD, Vinh DC, Mogensen TH, Marr N, Spaan AN, Boisson B, Boisson-Dupuis S, Bustamante J, Puel A, Ciancanelli MJ, Meyts I, Maniatis T, Soumelis V, Amara A, Nussenzweig M, Garcia-Sastre A, Krammer F, Pujol A, Duffy D, Lifton RP, Zhang SY, Gorochov G, Beziat V, Jouanguy E, Sancho-Shimizu V, Rice CM, Abel L, Notarangelo LD, Cobat A, Su HC, Casanova JL. Inborn errors of type I IFN immunity in patients with life-threatening COVID-19. Science. 2020;370(6515). Epub 2020/09/26. doi: 10.1126/science.abd4570. PubMed PMID: 32972995; PMCID: PMC7857407.

426. Schoggins JW, Wilson SJ, Panis M, Murphy MY, Jones CT, Bieniasz P, Rice CM. A diverse range of gene products are effectors of the type I interferon antiviral response. Nature.

2011;472(7344):481-5. Epub 2011/04/12. doi: 10.1038/nature09907. PubMed PMID: 21478870; PMCID: PMC3409588.

427. Guarda G, Braun M, Staehli F, Tardivel A, Mattmann C, Forster I, Farlik M, Decker T, Du Pasquier RA, Romero P, Tschopp J. Type I interferon inhibits interleukin-1 production and inflammasome activation. Immunity. 2011;34(2):213-23. Epub 2011/02/26. doi: 10.1016/j.immuni.2011.02.006. PubMed PMID: 21349431.

428. Pillai PS, Molony RD, Martinod K, Dong H, Pang IK, Tal MC, Solis AG, Bielecki P, Mohanty S, Trentalange M, Homer RJ, Flavell RA, Wagner DD, Montgomery RR, Shaw AC, Staeheli P, Iwasaki A. Mx1 reveals innate pathways to antiviral resistance and lethal influenza disease. Science. 2016;352(6284):463-6. Epub 2016/04/23. doi: 10.1126/science.aaf3926. PubMed PMID: 27102485; PMCID: PMC5465864.

429. Hadjadj J, Yatim N, Barnabei L, Corneau A, Boussier J, Smith N, Pere H, Charbit B, Bondet V, Chenevier-Gobeaux C, Breillat P, Carlier N, Gauzit R, Morbieu C, Pene F, Marin N, Roche N, Szwebel TA, Merkling SH, Treluyer JM, Veyer D, Mouthon L, Blanc C, Tharaux PL, Rozenberg F, Fischer A, Duffy D, Rieux-Laucat F, Kerneis S, Terrier B. Impaired type I interferon activity and inflammatory responses in severe COVID-19 patients. Science. 2020;369(6504):718-24. Epub 2020/07/15. doi: 10.1126/science.abc6027. PubMed PMID: 32661059; PMCID: PMC7402632.

430. Blanco-Melo D, Nilsson-Payant BE, Liu WC, Uhl S, Hoagland D, Moller R, Jordan TX, Oishi K, Panis M, Sachs D, Wang TT, Schwartz RE, Lim JK, Albrecht RA, tenOever BR. Imbalanced Host Response to SARS-CoV-2 Drives Development of COVID-19. Cell. 2020;181(5):1036-45 e9. Epub 2020/05/18. doi: 10.1016/j.cell.2020.04.026. PubMed PMID: 32416070; PMCID: PMC7227586.

431. Combes AJ, Courau T, Kuhn NF, Hu KH, Ray A, Chen WS, Chew NW, Cleary SJ, Kushnoor D, Reeder GC, Shen A, Tsui J, Hiam-Galvez KJ, Munoz-Sandoval P, Zhu WS, Lee DS, Sun Y, You R, Magnen M, Rodriguez L, Im KW, Serwas NK, Leligdowicz A, Zamecnik CR,

Loudermilk RP, Wilson MR, Ye CJ, Fragiadakis GK, Looney MR, Chan V, Ward A, Carrillo S, Consortium UC, Matthay M, Erle DJ, Woodruff PG, Langelier C, Kangelaris K, Hendrickson CM, Calfee C, Rao AA, Krummel MF. Global absence and targeting of protective immune states in severe COVID-19. Nature. 2021;591(7848):124-30. Epub 2021/01/26. doi: 10.1038/s41586-021-03234-7. PubMed PMID: 33494096; PMCID: PMC8567458.

432. Klein J, Brito A, Trubin P, Lu P, Wong P, Alpert T, Pena-Hernandez M, Haynes W, Kamath K, Liu F, Vogels C, Fauver J, Lucas C, Oh JE, Mao T, Silva J, Wyllie A, Muenker MC, Casanovas-Massana A, Moore A, Petrone M, Kalinich C, Yale Impact Research T, Cruz CD, Farhadian S, Ring A, Shon J, Ko A, Grubaugh N, Goldman-Israelow B, Iwasaki A, Azar M. Longitudinal immune profiling of a SARS-CoV-2 reinfection in a solid organ transplant recipient. Res Sq. 2021. Epub 2021/05/21. doi: 10.21203/rs.3.rs-405958/v1. PubMed PMID: 34013255; PMCID: PMC8132249.

433. Sposito B, Broggi A, Pandolfi L, Crotta S, Clementi N, Ferrarese R, Sisti S, Criscuolo E, Spreafico R, Long JM, Ambrosi A, Liu E, Frangipane V, Saracino L, Bozzini S, Marongiu L, Facchini FA, Bottazzi A, Fossali T, Colombo R, Clementi M, Tagliabue E, Chou J, Pontiroli AE, Meloni F, Wack A, Mancini N, Zanoni I. The interferon landscape along the respiratory tract impacts the severity of COVID-19. Cell. 2021;184(19):4953-68 e16. Epub 2021/09/08. doi: 10.1016/j.cell.2021.08.016. PubMed PMID: 34492226; PMCID: PMC8373821.

434. Kramer B, Knoll R, Bonaguro L, ToVinh M, Raabe J, Astaburuaga-Garcia R, Schulte-Schrepping J, Kaiser KM, Rieke GJ, Bischoff J, Monin MB, Hoffmeister C, Schlabe S, De Domenico E, Reusch N, Handler K, Reynolds G, Bluthgen N, Hack G, Finnemann C, Nischalke HD, Strassburg CP, Stephenson E, Su Y, Gardner L, Yuan D, Chen D, Goldman J, Rosenstiel P, Schmidt SV, Latz E, Hrusovsky K, Ball AJ, Johnson JM, Koenig PA, Schmidt FI, Haniffa M, Heath JR, Kummerer BM, Keitel V, Jensen B, Stubbemann P, Kurth F, Sander LE, Sawitzki B, Deutsche C-OI, Aschenbrenner AC, Schultze JL, Nattermann J. Early IFN-alpha signatures and persistent dysfunction are distinguishing features of NK cells in severe COVID-19. Immunity.

2021;54(11):2650-69 e14. Epub 2021/10/01. doi: 10.1016/j.immuni.2021.09.002. PubMed PMID: 34592166; PMCID: PMC8416549.

435. Broggi A, Ghosh S, Sposito B, Spreafico R, Balzarini F, Lo Cascio A, Clementi N, De Santis M, Mancini N, Granucci F, Zanoni I. Type III interferons disrupt the lung epithelial barrier upon viral recognition. Science. 2020;369(6504):706-12. Epub 2020/06/13. doi: 10.1126/science.abc3545. PubMed PMID: 32527925; PMCID: PMC7292499.

436. Major J, Crotta S, Llorian M, McCabe TM, Gad HH, Priestnall SL, Hartmann R, Wack A. Type I and III interferons disrupt lung epithelial repair during recovery from viral infection. Science. 2020;369(6504):712-7. Epub 2020/06/13. doi: 10.1126/science.abc2061. PubMed PMID: 32527928; PMCID: PMC7292500.

437. Lempp FA, Soriaga LB, Montiel-Ruiz M, Benigni F, Noack J, Park YJ, Bianchi S, Walls AC, Bowen JE, Zhou J, Kaiser H, Joshi A, Agostini M, Meury M, Dellota E, Jr., Jaconi S, Cameroni E, Martinez-Picado J, Vergara-Alert J, Izquierdo-Useros N, Virgin HW, Lanzavecchia A, Veesler D, Purcell LA, Telenti A, Corti D. Lectins enhance SARS-CoV-2 infection and influence neutralizing antibodies. Nature. 2021;598(7880):342-7. Epub 2021/09/01. doi: 10.1038/s41586-021-03925-1. PubMed PMID: 34464958.

438. Baum A, Ajithdoss D, Copin R, Zhou A, Lanza K, Negron N, Ni M, Wei Y, Mohammadi K, Musser B, Atwal GS, Oyejide A, Goez-Gazi Y, Dutton J, Clemmons E, Staples HM, Bartley C, Klaffke B, Alfson K, Gazi M, Gonzalez O, Dick E, Jr., Carrion R, Jr., Pessaint L, Porto M, Cook A, Brown R, Ali V, Greenhouse J, Taylor T, Andersen H, Lewis MG, Stahl N, Murphy AJ, Yancopoulos GD, Kyratsous CA. REGN-COV2 antibodies prevent and treat SARS-CoV-2 infection in rhesus macaques and hamsters. Science. 2020;370(6520):1110-5. Epub 2020/10/11. doi: 10.1126/science.abe2402. PubMed PMID: 33037066; PMCID: PMC7857396.

439. De Gasparo R, Pedotti M, Simonelli L, Nickl P, Muecksch F, Cassaniti I, Percivalle E, Lorenzi JCC, Mazzola F, Magri D, Michalcikova T, Haviernik J, Honig V, Mrazkova B, Polakova N, Fortova A, Tureckova J, Iatsiuk V, Di Girolamo S, Palus M, Zudova D, Bednar P, Bukova I,

Bianchini F, Mehn D, Nencka R, Strakova P, Pavlis O, Rozman J, Gioria S, Sammartino JC, Giardina F, Gaiarsa S, Pan-Hammarstrom Q, Barnes CO, Bjorkman PJ, Calzolai L, Piralla A, Baldanti F, Nussenzweig MC, Bieniasz PD, Hatziioannou T, Prochazka J, Sedlacek R, Robbiani DF, Ruzek D, Varani L. Bispecific IgG neutralizes SARS-CoV-2 variants and prevents escape in mice. Nature. 2021;593(7859):424-8. Epub 2021/03/27. doi: 10.1038/s41586-021-03461-y. PubMed PMID: 33767445.

440. Pinto D, Park YJ, Beltramello M, Walls AC, Tortorici MA, Bianchi S, Jaconi S, Culap K, Zatta F, De Marco A, Peter A, Guarino B, Spreafico R, Cameroni E, Case JB, Chen RE, Havenar-Daughton C, Snell G, Telenti A, Virgin HW, Lanzavecchia A, Diamond MS, Fink K, Veesler D, Corti D. Cross-neutralization of SARS-CoV-2 by a human monoclonal SARS-CoV antibody. Nature. 2020;583(7815):290-5. Epub 2020/05/19. doi: 10.1038/s41586-020-2349-y. PubMed PMID: 32422645.

441. Pinto D, Sauer MM, Czudnochowski N, Low JS, Tortorici MA, Housley MP, Noack J, Walls AC, Bowen JE, Guarino B, Rosen LE, di Iulio J, Jerak J, Kaiser H, Islam S, Jaconi S, Sprugasci N, Culap K, Abdelnabi R, Foo C, Coelmont L, Bartha I, Bianchi S, Silacci-Fregni C, Bassi J, Marzi R, Vetti E, Cassotta A, Ceschi A, Ferrari P, Cippa PE, Giannini O, Ceruti S, Garzoni C, Riva A, Benigni F, Cameroni E, Piccoli L, Pizzuto MS, Smithey M, Hong D, Telenti A, Lempp FA, Neyts J, Havenar-Daughton C, Lanzavecchia A, Sallusto F, Snell G, Virgin HW, Beltramello M, Corti D, Veesler D. Broad betacoronavirus neutralization by a stem helix-specific human antibody. Science. 2021;373(6559):1109-16. Epub 2021/08/05. doi: 10.1126/science.abj3321. PubMed PMID: 34344823.

442. Starr TN, Czudnochowski N, Liu Z, Zatta F, Park YJ, Addetia A, Pinto D, Beltramello M, Hernandez P, Greaney AJ, Marzi R, Glass WG, Zhang I, Dingens AS, Bowen JE, Tortorici MA, Walls AC, Wojcechowskyj JA, De Marco A, Rosen LE, Zhou J, Montiel-Ruiz M, Kaiser H, Dillen JR, Tucker H, Bassi J, Silacci-Fregni C, Housley MP, di Iulio J, Lombardo G, Agostini M, Sprugasci N, Culap K, Jaconi S, Meury M, Dellota E, Jr., Abdelnabi R, Foo SC, Cameroni E,

Stumpf S, Croll TI, Nix JC, Havenar-Daughton C, Piccoli L, Benigni F, Neyts J, Telenti A, Lempp FA, Pizzuto MS, Chodera JD, Hebner CM, Virgin HW, Whelan SPJ, Veesler D, Corti D, Bloom JD, Snell G. SARS-CoV-2 RBD antibodies that maximize breadth and resistance to escape. Nature. 2021;597(7874):97-102. Epub 2021/07/15. doi: 10.1038/s41586-021-03807-6. PubMed PMID: 34261126.

443. Tortorici MA, Beltramello M, Lempp FA, Pinto D, Dang HV, Rosen LE, McCallum M, Bowen J, Minola A, Jaconi S, Zatta F, De Marco A, Guarino B, Bianchi S, Lauron EJ, Tucker H, Zhou J, Peter A, Havenar-Daughton C, Wojcechowskyj JA, Case JB, Chen RE, Kaiser H, Montiel-Ruiz M, Meury M, Czudnochowski N, Spreafico R, Dillen J, Ng C, Sprugasci N, Culap K, Benigni F, Abdelnabi R, Foo SC, Schmid MA, Cameroni E, Riva A, Gabrieli A, Galli M, Pizzuto MS, Neyts J, Diamond MS, Virgin HW, Snell G, Corti D, Fink K, Veesler D. Ultrapotent human antibodies protect against SARS-CoV-2 challenge via multiple mechanisms. Science. 2020;370(6519):950-7. Epub 2020/09/26. doi: 10.1126/science.abe3354. PubMed PMID: 32972994; PMCID: PMC7857395.

444. Tortorici MA, Czudnochowski N, Starr TN, Marzi R, Walls AC, Zatta F, Bowen JE, Jaconi S, Di Iulio J, Wang Z, De Marco A, Zepeda SK, Pinto D, Liu Z, Beltramello M, Bartha I, Housley MP, Lempp FA, Rosen LE, Dellota E, Jr., Kaiser H, Montiel-Ruiz M, Zhou J, Addetia A, Guarino B, Culap K, Sprugasci N, Saliba C, Vetti E, Giacchetto-Sasselli I, Fregni CS, Abdelnabi R, Foo SC, Havenar-Daughton C, Schmid MA, Benigni F, Cameroni E, Neyts J, Telenti A, Virgin HW, Whelan SPJ, Snell G, Bloom JD, Corti D, Veesler D, Pizzuto MS. Broad sarbecovirus neutralization by a human monoclonal antibody. Nature. 2021;597(7874):103-8. Epub 2021/07/20. doi: 10.1038/s41586-021-03817-4. PubMed PMID: 34280951.

445. Van Rompay KKA, Olstad KJ, Sammak RL, Dutra J, Watanabe JK, Usachenko JL, Immareddy R, Verma A, Shaan Lakshmanappa Y, Schmidt BA, Roh JW, Elizaldi SR, Allen AM, Muecksch F, Lorenzi JCC, Lockwood S, Pollard RE, Yee JL, Nham PB, Ardeshir A, Deere JD, Patterson J, Dang Q, Hatziioannou T, Bieniasz PD, Iyer SS, Hartigan-O'Connor DJ, Nussenzweig

MC, Reader JR. Early treatment with a combination of two potent neutralizing antibodies improves clinical outcomes and reduces virus replication and lung inflammation in SARS-CoV-2 infected macaques. PLoS Pathog. 2021;17(7):e1009688. Epub 2021/07/07. doi: 10.1371/journal.ppat.1009688. PubMed PMID: 34228761; PMCID: PMC8284825 following competing interests: Rockefeller University has submitted a patent application for C135-LS and C144-LS on which MCN is an inventor. MCN and PDB are HHMI investigators.

446. Verma A, Hawes CE, Lakshmanappa YS, Roh JW, Schmidt BA, Dutra J, Louie W, Liu H, Ma ZM, Watanabe JK, Usachenko JL, Immareddy R, Sammak RL, Pollard R, Reader JR, Olstad KJ, Coffey LL, Kozlowski PA, Hartigan-O'Connor DJ, Nussenzweig M, Van Rompay KKA, Morrison JH, Iyer SS. Monoclonal antibodies protect aged rhesus macaques from SARS-CoV-2-induced immune activation and neuroinflammation. Cell Rep. 2021;37(5):109942. Epub 2021/10/28. doi: 10.1016/j.celrep.2021.109942. PubMed PMID: 34706272; PMCID: PMC8523485.

447. Owen DR, Allerton CMN, Anderson AS, Aschenbrenner L, Avery M, Berritt S, Boras B, Cardin RD, Carlo A, Coffman KJ, Dantonio A, Di L, Eng H, Ferre R, Gajiwala KS, Gibson SA, Greasley SE, Hurst BL, Kadar EP, Kalgutkar AS, Lee JC, Lee J, Liu W, Mason SW, Noell S, Novak JJ, Obach RS, Ogilvie K, Patel NC, Pettersson M, Rai DK, Reese MR, Sammons MF, Sathish JG, Singh RSP, Steppan CM, Stewart AE, Tuttle JB, Updyke L, Verhoest PR, Wei L, Yang Q, Zhu Y. An oral SARS-CoV-2 M(pro) inhibitor clinical candidate for the treatment of COVID-19. Science. 2021:eabl4784. Epub 2021/11/03. doi: 10.1126/science.abl4784. PubMed PMID: 34726479.

448. Tahir Ul Qamar M, Alqahtani SM, Alamri MA, Chen LL. Structural basis of SARS-CoV-2 3CL(pro) and anti-COVID-19 drug discovery from medicinal plants. J Pharm Anal. 2020;10(4):313-9. Epub 2020/04/17. doi: 10.1016/j.jpha.2020.03.009. PubMed PMID: 32296570; PMCID: PMC7156227.

449. Wang M, Cao R, Zhang L, Yang X, Liu J, Xu M, Shi Z, Hu Z, Zhong W, Xiao G. Remdesivir and chloroquine effectively inhibit the recently emerged novel coronavirus (2019-nCoV) in vitro. Cell Res. 2020;30(3):269-71. Epub 2020/02/06. doi: 10.1038/s41422-020-0282-0. PubMed PMID: 32020029; PMCID: PMC7054408.

450. Williamson BN, Feldmann F, Schwarz B, Meade-White K, Porter DP, Schulz J, van Doremalen N, Leighton I, Yinda CK, Perez-Perez L, Okumura A, Lovaglio J, Hanley PW, Saturday G, Bosio CM, Anzick S, Barbian K, Cihlar T, Martens C, Scott DP, Munster VJ, de Wit E. Clinical benefit of remdesivir in rhesus macaques infected with SARS-CoV-2. Nature. 2020;585(7824):273-6. Epub 2020/06/10. doi: 10.1038/s41586-020-2423-5. PubMed PMID: 32516797; PMCID: PMC7486271.

451. Wahl A, Gralinski LE, Johnson CE, Yao W, Kovarova M, Dinnon KH, 3rd, Liu H, Madden VJ, Krzystek HM, De C, White KK, Gully K, Schafer A, Zaman T, Leist SR, Grant PO, Bluemling GR, Kolykhalov AA, Natchus MG, Askin FB, Painter G, Browne EP, Jones CD, Pickles RJ, Baric RS, Garcia JV. SARS-CoV-2 infection is effectively treated and prevented by EIDD-2801. Nature. 2021;591(7850):451-7. Epub 2021/02/10. doi: 10.1038/s41586-021-03312-w. PubMed PMID: 33561864; PMCID: PMC7979515.

452. Beigel JH, Tomashek KM, Dodd LE, Mehta AK, Zingman BS, Kalil AC, Hohmann E, Chu HY, Luetkemeyer A, Kline S, Lopez de Castilla D, Finberg RW, Dierberg K, Tapson V, Hsieh L, Patterson TF, Paredes R, Sweeney DA, Short WR, Touloumi G, Lye DC, Ohmagari N, Oh MD, Ruiz-Palacios GM, Benfield T, Fatkenheuer G, Kortepeter MG, Atmar RL, Creech CB, Lundgren J, Babiker AG, Pett S, Neaton JD, Burgess TH, Bonnett T, Green M, Makowski M, Osinusi A, Nayak S, Lane HC, Members A-SG. Remdesivir for the Treatment of Covid-19 - Final Report. N Engl J Med. 2020;383(19):1813-26. Epub 2020/05/24. doi: 10.1056/NEJMoa2007764. PubMed PMID: 32445440; PMCID: PMC7262788.

453. Kalil AC, Patterson TF, Mehta AK, Tomashek KM, Wolfe CR, Ghazaryan V, Marconi VC, Ruiz-Palacios GM, Hsieh L, Kline S, Tapson V, Iovine NM, Jain MK, Sweeney DA, El Sahly HM,

Branche AR, Regalado Pineda J, Lye DC, Sandkovsky U, Luetkemeyer AF, Cohen SH, Finberg RW, Jackson PEH, Taiwo B, Paules CI, Arguinchona H, Erdmann N, Ahuja N, Frank M, Oh MD, Kim ES, Tan SY, Mularski RA, Nielsen H, Ponce PO, Taylor BS, Larson L, Rouphael NG, Saklawi Y, Cantos VD, Ko ER, Engemann JJ, Amin AN, Watanabe M, Billings J, Elie MC, Davey RT, Burgess TH, Ferreira J, Green M, Makowski M, Cardoso A, de Bono S, Bonnett T, Proschan M, Deye GA, Dempsey W, Nayak SU, Dodd LE, Beigel JH, Members A-SG. Baricitinib plus Remdesivir for Hospitalized Adults with Covid-19. N Engl J Med. 2021;384(9):795-807. Epub 2020/12/12. doi: 10.1056/NEJMoa2031994. PubMed PMID: 33306283; PMCID: PMC7745180.

454. Group RC, Horby P, Lim WS, Emberson JR, Mafham M, Bell JL, Linsell L, Staplin N, Brightling C, Ustianowski A, Elmahi E, Prudon B, Green C, Felton T, Chadwick D, Rege K, Fegan C, Chappell LC, Faust SN, Jaki T, Jeffery K, Montgomery A, Rowan K, Juszczak E, Baillie JK, Haynes R, Landray MJ. Dexamethasone in Hospitalized Patients with Covid-19. N Engl J Med. 2021;384(8):693-704. Epub 2020/07/18. doi: 10.1056/NEJMoa2021436. PubMed PMID: 32678530; PMCID: PMC7383595.

455. Xu X, Han M, Li T, Sun W, Wang D, Fu B, Zhou Y, Zheng X, Yang Y, Li X, Zhang X, Pan A, Wei H. Effective treatment of severe COVID-19 patients with tocilizumab. Proc Natl Acad Sci U S A. 2020;117(20):10970-5. Epub 2020/05/01. doi: 10.1073/pnas.2005615117. PubMed PMID: 32350134; PMCID: PMC7245089.

456. Marconi VC, Ramanan AV, de Bono S, Kartman CE, Krishnan V, Liao R, Piruzeli MLB, Goldman JD, Alatorre-Alexander J, de Cassia Pellegrini R, Estrada V, Som M, Cardoso A, Chakladar S, Crowe B, Reis P, Zhang X, Adams DH, Ely EW, Group C-BS. Efficacy and safety of baricitinib for the treatment of hospitalised adults with COVID-19 (COV-BARRIER): a randomised, double-blind, parallel-group, placebo-controlled phase 3 trial. Lancet Respir Med. 2021. Epub 2021/09/05. doi: 10.1016/S2213-2600(21)00331-3. PubMed PMID: 34480861; PMCID: PMC8409066 Disease Control and Prevention (CDC), Gilead Sciences, the US National Institutes of Health (NIH), Veterans Affairs, and ViiV; received honoraria from Eli Lilly and

Company; served as an advisory board member for Eli Lilly and Company and Novartis; and participated as a study section chair for the NIH. AVR received research grants from Eli Lilly and Company; and served as a speaker or consultant for AbbVie, Eli Lilly and Company, Novartis, Pfizer, Roche, Sobi, and Union Chimique Belge. SB, CEK, VK, RL, MLBP, AC, SC, BC, PR, XZ, and DHA are employees and shareholders of Eli Lilly and Company. JDG received research support from Eli Lilly and Company, Regeneron Pharmaceuticals, and Gilead Sciences; grants from Eurofins Viracor and the Biomedical Advanced Research and Development Authority (administered by Merck); speaker fees from Eli Lilly and Company, Gilead Sciences, and Mylan Pharmaceuticals; and advisory board fees from Gilead Sciences. JAA served as a speaker and scientific advisor for AstraZeneca, Boehringer Ingelheim, BMS, Eli Lilly and Company, Foundation Medicine, Novartis, MSD, Roche, and Takeda. VE received a research grant from Eli Lilly and Company. MS received research grants from Eli Lilly and Company, NIAID, and Novartis; and served as a board member for NBOME, Osteopathic Founders Foundation, and COGMED. EWE received research grants from the CDC, NIH, and Veterans Affairs; and served as an unpaid consultant for Eli Lilly and Company. RDP declares no competing interests.

457. Stockman LJ, Bellamy R, Garner P. SARS: systematic review of treatment effects. PLoS Med. 2006;3(9):e343. Epub 2006/09/14. doi: 10.1371/journal.pmed.0030343. PubMed PMID: 16968120; PMCID: PMC1564166.

458. Park A, Iwasaki A. Type I and Type III Interferons - Induction, Signaling, Evasion, and Application to Combat COVID-19. Cell Host Microbe. 2020;27(6):870-8. Epub 2020/05/29. doi: 10.1016/j.chom.2020.05.008. PubMed PMID: 32464097; PMCID: PMC7255347.

459. Mantlo E, Bukreyeva N, Maruyama J, Paessler S, Huang C. Antiviral activities of type I interferons to SARS-CoV-2 infection. Antiviral Res. 2020;179:104811. Epub 2020/05/04. doi: 10.1016/j.antiviral.2020.104811. PubMed PMID: 32360182; PMCID: PMC7188648.

460. Sadoff J, Gray G, Vandebosch A, Cardenas V, Shukarev G, Grinsztejn B, Goepfert PA, Truyers C, Fennema H, Spiessens B, Offergeld K, Scheper G, Taylor KL, Robb ML, Treanor J,

Barouch DH, Stoddard J, Ryser MF, Marovich MA, Neuzil KM, Corey L, Cauwenberghs N, Tanner T, Hardt K, Ruiz-Guinazu J, Le Gars M, Schuitemaker H, Van Hoof J, Struyf F, Douoguih M, Group ES. Safety and Efficacy of Single-Dose Ad26.COV2.S Vaccine against Covid-19. N Engl J Med. 2021;384(23):2187-201. Epub 2021/04/22. doi: 10.1056/NEJMoa2101544. PubMed PMID: 33882225; PMCID: PMC8220996.

461. Polack FP, Thomas SJ, Kitchin N, Absalon J, Gurtman A, Lockhart S, Perez JL, Perez Marc G, Moreira ED, Zerbini C, Bailey R, Swanson KA, Roychoudhury S, Koury K, Li P, Kalina WV, Cooper D, Frenck RW, Jr., Hammitt LL, Tureci O, Nell H, Schaefer A, Unal S, Tresnan DB, Mather S, Dormitzer PR, Sahin U, Jansen KU, Gruber WC, Group CCT. Safety and Efficacy of the BNT162b2 mRNA Covid-19 Vaccine. N Engl J Med. 2020;383(27):2603-15. Epub 2020/12/11. doi: 10.1056/NEJMoa2034577. PubMed PMID: 33301246; PMCID: PMC7745181.

462. Baden LR, El Sahly HM, Essink B, Kotloff K, Frey S, Novak R, Diemert D, Spector SA, Rouphael N, Creech CB, McGettigan J, Khetan S, Segall N, Solis J, Brosz A, Fierro C, Schwartz H, Neuzil K, Corey L, Gilbert P, Janes H, Follmann D, Marovich M, Mascola J, Polakowski L, Ledgerwood J, Graham BS, Bennett H, Pajon R, Knightly C, Leav B, Deng W, Zhou H, Han S, Ivarsson M, Miller J, Zaks T, Group CS. Efficacy and Safety of the mRNA-1273 SARS-CoV-2 Vaccine. N Engl J Med. 2021;384(5):403-16. Epub 2020/12/31. doi: 10.1056/NEJMoa2035389. PubMed PMID: 33378609; PMCID: PMC7787219.

463. Valenzuela P, Medina A, Rutter WJ, Ammerer G, Hall BD. Synthesis and assembly of hepatitis B virus surface antigen particles in yeast. Nature. 1982;298(5872):347-50. Epub 1982/07/22. doi: 10.1038/298347a0. PubMed PMID: 7045698.

464. Plotkin SA. Vaccines: the fourth century. Clin Vaccine Immunol. 2009;16(12):1709-19. Epub 2009/10/02. doi: 10.1128/CVI.00290-09. PubMed PMID: 19793898; PMCID: PMC2786381.

465. Hilleman MR. Vaccines in historic evolution and perspective: a narrative of vaccine discoveries. J Hum Virol. 2000;3(2):63-76. Epub 2000/06/13. PubMed PMID: 10850891.

466. Gerberding JL, Haynes BF. Vaccine Innovations - Past and Future. N Engl J Med. 2021;384(5):393-6. Epub 2021/02/04. doi: 10.1056/NEJMp2029466. PubMed PMID: 33535287.

467. Pardi N, Hogan MJ, Porter FW, Weissman D. mRNA vaccines - a new era in vaccinology. Nat Rev Drug Discov. 2018;17(4):261-79. Epub 2018/01/13. doi: 10.1038/nrd.2017.243. PubMed PMID: 29326426; PMCID: PMC5906799.

468. Cohen AA, Gnanapragasam PNP, Lee YE, Hoffman PR, Ou S, Kakutani LM, Keeffe JR, Wu HJ, Howarth M, West AP, Barnes CO, Nussenzweig MC, Bjorkman PJ. Mosaic nanoparticles elicit cross-reactive immune responses to zoonotic coronaviruses in mice. Science. 2021;371(6530):735-41. Epub 2021/01/14. doi: 10.1126/science.abf6840. PubMed PMID: 33436524; PMCID: PMC7928838.

469. Liu L, Wang P, Nair MS, Yu J, Rapp M, Wang Q, Luo Y, Chan JF, Sahi V, Figueroa A, Guo XV, Cerutti G, Bimela J, Gorman J, Zhou T, Chen Z, Yuen KY, Kwong PD, Sodroski JG, Yin MT, Sheng Z, Huang Y, Shapiro L, Ho DD. Potent neutralizing antibodies against multiple epitopes on SARS-CoV-2 spike. Nature. 2020;584(7821):450-6. Epub 2020/07/23. doi: 10.1038/s41586-020-2571-7. PubMed PMID: 32698192.

470. Saunders KO, Lee E, Parks R, Martinez DR, Li D, Chen H, Edwards RJ, Gobeil S, Barr M, Mansouri K, Alam SM, Sutherland LL, Cai F, Sanzone AM, Berry M, Manne K, Bock KW, Minai M, Nagata BM, Kapingidza AB, Azoitei M, Tse LV, Scobey TD, Spreng RL, Rountree RW, DeMarco CT, Denny TN, Woods CW, Petzold EW, Tang J, Oguin TH, 3rd, Sempowski GD, Gagne M, Douek DC, Tomai MA, Fox CB, Seder R, Wiehe K, Weissman D, Pardi N, Golding H, Khurana S, Acharya P, Andersen H, Lewis MG, Moore IN, Montefiori DC, Baric RS, Haynes BF. Neutralizing antibody vaccine for pandemic and pre-emergent coronaviruses. Nature. 2021;594(7864):553-9. Epub 2021/05/11. doi: 10.1038/s41586-021-03594-0. PubMed PMID: 33971664; PMCID: PMC8528238.

471. Wrapp D, Wang N, Corbett KS, Goldsmith JA, Hsieh CL, Abiona O, Graham BS, McLellan JS. Cryo-EM structure of the 2019-nCoV spike in the prefusion conformation. Science.

2020;367(6483):1260-3. Epub 2020/02/23. doi: 10.1126/science.abb2507. PubMed PMID: 32075877; PMCID: PMC7164637.

472. Barouch DH, Stephenson KE, Sadoff J, Yu J, Chang A, Gebre M, McMahan K, Liu J, Chandrashekar A, Patel S, Le Gars M, de Groot AM, Heerwegh D, Struyf F, Douoguih M, van Hoof J, Schuitemaker H. Durable Humoral and Cellular Immune Responses Following Ad26.COV2.S Vaccination for COVID-19. medRxiv. 2021. Epub 2021/07/17. doi: 10.1101/2021.07.05.21259918. PubMed PMID: 34268527; PMCID: PMC8282116.

473. Doria-Rose N, Suthar MS, Makowski M, O'Connell S, McDermott AB, Flach B, Ledgerwood JE, Mascola JR, Graham BS, Lin BC, O'Dell S, Schmidt SD, Widge AT, Edara VV, Anderson EJ, Lai L, Floyd K, Rouphael NG, Zarnitsyna V, Roberts PC, Makhene M, Buchanan W, Luke CJ, Beigel JH, Jackson LA, Neuzil KM, Bennett H, Leav B, Albert J, Kunwar P, m RNASG. Antibody Persistence through 6 Months after the Second Dose of mRNA-1273 Vaccine for Covid-19. N Engl J Med. 2021;384(23):2259-61. Epub 2021/04/07. doi: 10.1056/NEJMc2103916. PubMed PMID: 33822494; PMCID: PMC8524784.

474. Widge AT, Rouphael NG, Jackson LA, Anderson EJ, Roberts PC, Makhene M, Chappell JD, Denison MR, Stevens LJ, Pruijssers AJ, McDermott AB, Flach B, Lin BC, Doria-Rose NA, O'Dell S, Schmidt SD, Neuzil KM, Bennett H, Leav B, Makowski M, Albert J, Cross K, Edara VV, Floyd K, Suthar MS, Buchanan W, Luke CJ, Ledgerwood JE, Mascola JR, Graham BS, Beigel JH, m RNASG. Durability of Responses after SARS-CoV-2 mRNA-1273 Vaccination. N Engl J Med. 2021;384(1):80-2. Epub 2020/12/04. doi: 10.1056/NEJMc2032195. PubMed PMID: 33270381; PMCID: PMC7727324.

475. Pegu A, O'Connell SE, Schmidt SD, O'Dell S, Talana CA, Lai L, Albert J, Anderson E, Bennett H, Corbett KS, Flach B, Jackson L, Leav B, Ledgerwood JE, Luke CJ, Makowski M, Nason MC, Roberts PC, Roederer M, Rebolledo PA, Rostad CA, Rouphael NG, Shi W, Wang L, Widge AT, Yang ES, m RNASGss, Beigel JH, Graham BS, Mascola JR, Suthar MS, McDermott AB, Doria-Rose NA, Arega J, Beigel JH, Buchanan W, Elsafy M, Hoang B, Lampley R, Kolhekar

A, Koo H, Luke C, Makhene M, Nayak S, Pikaart-Tautges R, Roberts PC, Russell J, Sindall E, Albert J, Kunwar P, Makowski M, Anderson EJ, Bechnak A, Bower M, Camacho-Gonzalez AF, Collins M, Drobeniuc A, Edara VV, Edupuganti S, Floyd K, Gibson T, Ackerley CMG, Johnson B, Kamidani S, Kao C, Kelley C, Lai L, Macenczak H, McCullough MP, Peters E, Phadke VK, Rebolledo PA, Rostad CA, Rouphael N, Scherer E, Sherman A, Stephens K, Suthar MS, Teherani M, Traenkner J, Winston J, Yildirim I, Barr L, Benoit J, Carste B, Choe J, Dunstan M, Erolin R, Ffitch J, Fields C, Jackson LA, Kiniry E, Lasicka S, Lee S, Nguyen M, Pimienta S, Suyehira J, Witte M, Bennett H, Altaras NE, Carfi A, Hurley M, Leav B, Pajon R, Sun W, Zaks T, Coler RN, Larsen SE, Neuzil KM, Lindesmith LC, Martinez DR, Munt J, Mallory M, Edwards C, Baric RS, Berkowitz NM, Boritz EA, Carlton K, Corbett KS, Costner P, Creanga A, Doria-Rose NA, Douek DC, Flach B, Gaudinski M, Gordon I, Graham BS, Holman L, Ledgerwood JE, Leung K, Lin BC, Louder MK, Mascola JR, McDermott AB, Morabito KM, Novik L, O'Connell S, O'Dell S, Padilla M, Pegu A, Schmidt SD, Shi W, Swanson PA, 2nd, Talana CA, Wang L, Widge AT, Yang ES, Zhang Y, Chappell JD, Denison MR, Hughes T, Lu X, Pruijssers AJ, Stevens LJ, Posavad CM, Gale M, Jr., Menachery V, Shi PY. Durability of mRNA-1273 vaccine-induced antibodies against SARS-CoV-2 variants. Science. 2021;373(6561):1372-7. Epub 2021/08/14. doi: 10.1126/science.abj4176. PubMed PMID: 34385356.

476. Callaway E. The coronavirus is mutating - does it matter? Nature. 2020;585(7824):174-7. Epub 2020/09/10. doi: 10.1038/d41586-020-02544-6. PubMed PMID: 32901123.

477. Krause PR, Fleming TR, Longini IM, Peto R, Briand S, Heymann DL, Beral V, Snape MD, Rees H, Ropero AM, Balicer RD, Cramer JP, Munoz-Fontela C, Gruber M, Gaspar R, Singh JA, Subbarao K, Van Kerkhove MD, Swaminathan S, Ryan MJ, Henao-Restrepo AM. SARS-CoV-2 Variants and Vaccines. N Engl J Med. 2021;385(2):179-86. Epub 2021/06/24. doi: 10.1056/NEJMsr2105280. PubMed PMID: 34161052; PMCID: PMC8262623.

478. Mascola JR, Graham BS, Fauci AS. SARS-CoV-2 Viral Variants-Tackling a Moving Target. JAMA. 2021;325(13):1261-2. Epub 2021/02/12. doi: 10.1001/jama.2021.2088. PubMed PMID: 33571363.

479. Walensky RP, Walke HT, Fauci AS. SARS-CoV-2 Variants of Concern in the United States-Challenges and Opportunities. JAMA. 2021;325(11):1037-8. Epub 2021/02/18. doi: 10.1001/jama.2021.2294. PubMed PMID: 33595644.

480. Choi A, Koch M, Wu K, Dixon G, Oestreicher J, Legault H, Stewart-Jones GBE, Colpitts T, Pajon R, Bennett H, Carfi A, Edwards DK. Serum Neutralizing Activity of mRNA-1273 against SARS-CoV-2 Variants. J Virol. 2021;95(23):e0131321. Epub 2021/09/23. doi: 10.1128/JVI.01313-21. PubMed PMID: 34549975.

481. Edara VV, Hudson WH, Xie X, Ahmed R, Suthar MS. Neutralizing Antibodies Against SARS-CoV-2 Variants After Infection and Vaccination. JAMA. 2021;325(18):1896-8. Epub 2021/03/20. doi: 10.1001/jama.2021.4388. PubMed PMID: 33739374; PMCID: PMC7980146.

482. Edara VV, Pinsky BA, Suthar MS, Lai L, Davis-Gardner ME, Floyd K, Flowers MW, Wrammert J, Hussaini L, Ciric CR, Bechnak S, Stephens K, Graham BS, Bayat Mokhtari E, Mudvari P, Boritz E, Creanga A, Pegu A, Derrien-Colemyn A, Henry AR, Gagne M, Douek DC, Sahoo MK, Sibai M, Solis D, Webby RJ, Jeevan T, Fabrizio TP. Infection and Vaccine-Induced Neutralizing-Antibody Responses to the SARS-CoV-2 B.1.617 Variants. N Engl J Med. 2021;385(7):664-6. Epub 2021/07/08. doi: 10.1056/NEJMc2107799. PubMed PMID: 34233096; PMCID: PMC8279090.

483. Corbett KS, Werner AP, Connell SO, Gagne M, Lai L, Moliva JI, Flynn B, Choi A, Koch M, Foulds KE, Andrew SF, Flebbe DR, Lamb E, Nurmukhambetova ST, Provost SJ, Bock KW, Minai M, Nagata BM, Ry AV, Flinchbaugh Z, Johnston TS, Mokhtari EB, Mudvari P, Henry AR, Laboune F, Chang B, Porto M, Wear J, Alvarado GS, Boyoglu-Barnum S, Todd JM, Bart B, Cook A, Dodson A, Pessaint L, Steingrebe K, Elbashir S, Sriparna M, Pekosz A, Andersen H, Wu K, Edwards DK, Kar S, Lewis MG, Boritz E, Moore IN, Carfi A, Suthar MS, McDermott A, Roederer M, Nason MC,

Sullivan NJ, Douek DC, Graham BS, Seder RA. mRNA-1273 protects against SARS-CoV-2 beta infection in nonhuman primates. Nat Immunol. 2021;22(10):1306-15. Epub 2021/08/22. doi: 10.1038/s41590-021-01021-0. PubMed PMID: 34417590; PMCID: PMC8488000.

484. Alter G, Yu J, Liu J, Chandrashekar A, Borducchi EN, Tostanoski LH, McMahan K, Jacob-Dolan C, Martinez DR, Chang A, Anioke T, Lifton M, Nkolola J, Stephenson KE, Atyeo C, Shin S, Fields P, Kaplan I, Robins H, Amanat F, Krammer F, Baric RS, Le Gars M, Sadoff J, de Groot AM, Heerwegh D, Struyf F, Douoguih M, van Hoof J, Schuitemaker H, Barouch DH. Immunogenicity of Ad26.COV2.S vaccine against SARS-CoV-2 variants in humans. Nature. 2021;596(7871):268-72. Epub 2021/06/10. doi: 10.1038/s41586-021-03681-2. PubMed PMID: 34107529; PMCID: PMC8357629.

485. Barros-Martins J, Hammerschmidt SI, Cossmann A, Odak I, Stankov MV, Morillas Ramos G, Dopfer-Jablonka A, Heidemann A, Ritter C, Friedrichsen M, Schultze-Florey C, Ravens I, Willenzon S, Bubke A, Ristenpart J, Janssen A, Ssebyatika G, Bernhardt G, Munch J, Hoffmann M, Pohlmann S, Krey T, Bosnjak B, Forster R, Behrens GMN. Immune responses against SARS-CoV-2 variants after heterologous and homologous ChAdOx1 nCoV-19/BNT162b2 vaccination. Nat Med. 2021;27(9):1525-9. Epub 2021/07/16. doi: 10.1038/s41591-021-01449-9. PubMed PMID: 34262158; PMCID: PMC8440184.

486. Ewer KJ, Barrett JR, Belij-Rammerstorfer S, Sharpe H, Makinson R, Morter R, Flaxman A, Wright D, Bellamy D, Bittaye M, Dold C, Provine NM, Aboagye J, Fowler J, Silk SE, Alderson J, Aley PK, Angus B, Berrie E, Bibi S, Cicconi P, Clutterbuck EA, Chelysheva I, Folegatti PM, Fuskova M, Green CM, Jenkin D, Kerridge S, Lawrie A, Minassian AM, Moore M, Mujadidi Y, Plested E, Poulton I, Ramasamy MN, Robinson H, Song R, Snape MD, Tarrant R, Voysey M, Watson MEE, Douglas AD, Hill AVS, Gilbert SC, Pollard AJ, Lambe T, Oxford CVTG. T cell and antibody responses induced by a single dose of ChAdOx1 nCoV-19 (AZD1222) vaccine in a phase 1/2 clinical trial. Nat Med. 2021;27(2):270-8. Epub 2020/12/19. doi: 10.1038/s41591-020-01194-5. PubMed PMID: 33335323.

487. Jackson LA, Anderson EJ, Rouphael NG, Roberts PC, Makhene M, Coler RN, McCullough MP, Chappell JD, Denison MR, Stevens LJ, Pruijssers AJ, McDermott A, Flach B, Doria-Rose NA, Corbett KS, Morabito KM, O'Dell S, Schmidt SD, Swanson PA, 2nd, Padilla M, Mascola JR, Neuzil KM, Bennett H, Sun W, Peters E, Makowski M, Albert J, Cross K, Buchanan W, Pikaart-Tautges R, Ledgerwood JE, Graham BS, Beigel JH, m RNASG. An mRNA Vaccine against SARS-CoV-2 - Preliminary Report. N Engl J Med. 2020;383(20):1920-31. Epub 2020/07/15. doi: 10.1056/NEJMoa2022483. PubMed PMID: 32663912; PMCID: PMC7377258.

488. Sahin U, Muik A, Derhovanessian E, Vogler I, Kranz LM, Vormehr M, Baum A, Pascal K, Quandt J, Maurus D, Brachtendorf S, Lorks V, Sikorski J, Hilker R, Becker D, Eller AK, Grutzner J, Boesler C, Rosenbaum C, Kuhnle MC, Luxemburger U, Kemmer-Bruck A, Langer D, Bexon M, Bolte S, Kariko K, Palanche T, Fischer B, Schultz A, Shi PY, Fontes-Garfias C, Perez JL, Swanson KA, Loschko J, Scully IL, Cutler M, Kalina W, Kyratsous CA, Cooper D, Dormitzer PR, Jansen KU, Tureci O. COVID-19 vaccine BNT162b1 elicits human antibody and TH1 T cell responses. Nature. 2020;586(7830):594-9. Epub 2020/10/01. doi: 10.1038/s41586-020-2814-7. PubMed PMID: 32998157.

489. Bhaskaran K, Hamouda O, Sannes M, Boufassa F, Johnson AM, Lambert PC, Porter K, Collaboration C. Changes in the risk of death after HIV seroconversion compared with mortality in the general population. JAMA. 2008;300(1):51-9. Epub 2008/07/03. doi: 10.1001/jama.300.1.51. PubMed PMID: 18594040.

490. Cooper DA. Life and death in the cART era. Lancet. 2008;372(9635):266-7. Epub 2008/07/29. doi: 10.1016/S0140-6736(08)61086-7. PubMed PMID: 18657689.

491. Zeng D, Hoffmann P, Lan F, Huie P, Higgins J, Strober S. Unique patterns of surface receptors, cytokine secretion, and immune functions distinguish T cells in the bone marrow from those in the periphery: impact on allogeneic bone marrow transplantation. Blood. 2002;99(4):1449-57. Epub 2002/02/07. doi: 10.1182/blood.v99.4.1449. PubMed PMID: 11830499.

492. Di Rosa F, Pabst R. The bone marrow: a nest for migratory memory T cells. Trends Immunol. 2005;26(7):360-6. Epub 2005/06/28. doi: 10.1016/j.it.2005.04.011. PubMed PMID: 15978522.

493. Westermann J, Pabst R. Distribution of lymphocyte subsets and natural killer cells in the human body. Clin Investig. 1992;70(7):539-44. Epub 1992/07/01. doi: 10.1007/BF00184787. PubMed PMID: 1392422.

494. Becker TC, Coley SM, Wherry EJ, Ahmed R. Bone marrow is a preferred site for homeostatic proliferation of memory CD8 T cells. J Immunol. 2005;174(3):1269-73. Epub 2005/01/22. doi: 10.4049/jimmunol.174.3.1269. PubMed PMID: 15661882.

495. Masopust D, Vezys V, Marzo AL, Lefrancois L. Preferential localization of effector memory cells in nonlymphoid tissue. Science. 2001;291(5512):2413-7. Epub 2001/03/27. doi: 10.1126/science.1058867. PubMed PMID: 11264538.

496. Slifka MK, Whitmire JK, Ahmed R. Bone marrow contains virus-specific cytotoxic T lymphocytes. Blood. 1997;90(5):2103-8. Epub 1997/09/18. PubMed PMID: 9292550.

497. Herndler-Brandstetter D, Landgraf K, Tzankov A, Jenewein B, Brunauer R, Laschober GT, Parson W, Kloss F, Gassner R, Lepperdinger G, Grubeck-Loebenstein B. The impact of aging on memory T cell phenotype and function in the human bone marrow. J Leukoc Biol. 2012;91(2):197-205. Epub 2011/10/21. doi: 10.1189/jlb.0611299. PubMed PMID: 22013229.

498. Price PW, Cerny J. Characterization of CD4+ T cells in mouse bone marrow. I. Increased activated/memory phenotype and altered TCR Vbeta repertoire. Eur J Immunol. 1999;29(3):1051-6. Epub 1999/03/26. doi: 10.1002/(SICI)1521-4141(199903)29:03<1051::AID-IMMU1051>3.0.CO;2-Y. PubMed PMID: 10092110.

499. Sallusto F, Lenig D, Forster R, Lipp M, Lanzavecchia A. Two subsets of memory T lymphocytes with distinct homing potentials and effector functions. Nature. 1999;401(6754):708-12. Epub 1999/10/28. doi: 10.1038/44385. PubMed PMID: 10537110.

500. Zou L, Barnett B, Safah H, Larussa VF, Evdemon-Hogan M, Mottram P, Wei S, David O, Curiel TJ, Zou W. Bone marrow is a reservoir for CD4+CD25+ regulatory T cells that traffic through CXCL12/CXCR4 signals. Cancer Res. 2004;64(22):8451-5. Epub 2004/11/19. doi: 10.1158/0008-5472.CAN-04-1987. PubMed PMID: 15548717.

501. Parretta E, Cassese G, Barba P, Santoni A, Guardiola J, Di Rosa F. CD8 cell division maintaining cytotoxic memory occurs predominantly in the bone marrow. J Immunol. 2005;174(12):7654-64. Epub 2005/06/10. doi: 10.4049/jimmunol.174.12.7654. PubMed PMID: 15944266.

502. Alpdogan O, Eng JM, Muriglan SJ, Willis LM, Hubbard VM, Tjoe KH, Terwey TH, Kochman A, van den Brink MR. Interleukin-15 enhances immune reconstitution after allogeneic bone marrow transplantation. Blood. 2005;105(2):865-73. Epub 2004/07/29. doi: 10.1182/blood-2003-09-3344. PubMed PMID: 15280205.

503. Goldrath AW, Sivakumar PV, Glaccum M, Kennedy MK, Bevan MJ, Benoist C, Mathis D, Butz EA. Cytokine requirements for acute and Basal homeostatic proliferation of naive and memory CD8+ T cells. J Exp Med. 2002;195(12):1515-22. Epub 2002/06/19. doi: 10.1084/jem.20020033. PubMed PMID: 12070279; PMCID: PMC2193554.

504. Mackall CL, Fry TJ, Bare C, Morgan P, Galbraith A, Gress RE. IL-7 increases both thymic-dependent and thymic-independent T-cell regeneration after bone marrow transplantation. Blood. 2001;97(5):1491-7. Epub 2001/02/27. doi: 10.1182/blood.v97.5.1491. PubMed PMID: 11222398.

505. Suda T, Okada S, Suda J, Miura Y, Ito M, Sudo T, Hayashi S, Nishikawa S, Nakauchi H. A stimulatory effect of recombinant murine interleukin-7 (IL-7) on B-cell colony formation and an inhibitory effect of IL-1 alpha. Blood. 1989;74(6):1936-41. Epub 1989/11/01. PubMed PMID: 2804342.

506. Herndler-Brandstetter D, Landgraf K, Jenewein B, Tzankov A, Brunauer R, Brunner S, Parson W, Kloss F, Gassner R, Lepperdinger G, Grubeck-Loebenstein B. Human bone marrow hosts polyfunctional memory CD4+ and CD8+ T cells with close contact to IL-15-producing cells.

J Immunol. 2011;186(12):6965-71. Epub 2011/05/13. doi: 10.4049/jimmunol.1100243. PubMed PMID: 21562158.

507. Thiebot H, Vaslin B, Derdouch S, Bertho JM, Mouthon F, Prost S, Gras G, Ducouret P, Dormont D, Le Grand R. Impact of bone marrow hematopoiesis failure on T-cell generation during pathogenic simian immunodeficiency virus infection in macaques. Blood. 2005;105(6):2403-9. Epub 2004/09/25. doi: 10.1182/blood-2004-01-0025. PubMed PMID: 15388577.

508. Yamakami K, Honda M, Takei M, Ami Y, Kitamura N, Nishinarita S, Sawada S, Horie T. Early bone marrow hematopoietic defect in simian/human immunodeficiency virus C2/1-infected macaques and relevance to advance of disease. J Virol. 2004;78(20):10906-10. Epub 2004/09/29. doi: 10.1128/JVI.78.20.10906-10910.2004. PubMed PMID: 15452210; PMCID: PMC521857.

509. Sui Y, Frey B, Wang Y, Billeskov R, Kulkarni S, McKinnon K, Rourke T, Fritts L, Miller CJ, Berzofsky JA. Paradoxical myeloid-derived suppressor cell reduction in the bone marrow of SIV chronically infected macaques. PLoS Pathog. 2017;13(5):e1006395. Epub 2017/05/13. doi: 10.1371/journal.ppat.1006395. PubMed PMID: 28498847; PMCID: PMC5448820.

510. Ceroni F, Aguilera-Garcia D, Chassaing N, Bax DA, Blanco-Kelly F, Ramos P, Tarilonte M, Villaverde C, da Silva LRJ, Ballesta-Martinez MJ, Sanchez-Soler MJ, Holt RJ, Cooper-Charles L, Bruty J, Wallis Y, McMullan D, Hoffman J, Bunyan D, Stewart A, Stewart H, Lachlan K, Study DDD, Fryer A, McKay V, Roume J, Dureau P, Saggar A, Griffiths M, Calvas P, Ayuso C, Corton M, Ragge NK. New GJA8 variants and phenotypes highlight its critical role in a broad spectrum of eye anomalies. Hum Genet. 2019;138(8-9):1027-42. Epub 2018/02/22. doi: 10.1007/s00439-018-1875-2. PubMed PMID: 29464339.

511. Kaufmann DE, Kavanagh DG, Pereyra F, Zaunders JJ, Mackey EW, Miura T, Palmer S, Brockman M, Rathod A, Piechocka-Trocha A, Baker B, Zhu B, Le Gall S, Waring MT, Ahern R, Moss K, Kelleher AD, Coffin JM, Freeman GJ, Rosenberg ES, Walker BD. Upregulation of CTLA-4 by HIV-specific CD4+ T cells correlates with disease progression and defines a reversible

immune dysfunction. Nat Immunol. 2007;8(11):1246-54. Epub 2007/10/02. doi: 10.1038/ni1515. PubMed PMID: 17906628.

512. Paris RM, Petrovas C, Ferrando-Martinez S, Moysi E, Boswell KL, Archer E, Yamamoto T, Ambrozak D, Casazza JP, Haubrich R, Connors M, Ake J, Kim JH, Koup RA. Selective Loss of Early Differentiated, Highly Functional PD1high CD4 T Cells with HIV Progression. PLoS One. 2015;10(12):e0144767. Epub 2015/12/19. doi: 10.1371/journal.pone.0144767. PubMed PMID: 26678998; PMCID: PMC4692060.

513. Caby F, Guihot A, Lambert-Niclot S, Guiguet M, Boutolleau D, Agher R, Valantin MA, Tubiana R, Calvez V, Marcelin AG, Carcelain G, Autran B, Costagliola D, Katlama C. Determinants of a Low CD4/CD8 Ratio in HIV-1-Infected Individuals Despite Long-term Viral Suppression. Clin Infect Dis. 2016;62(10):1297-303. Epub 2016/02/26. doi: 10.1093/cid/ciw076. PubMed PMID: 26908792.

514. Deeks SG. HIV infection, inflammation, immunosenescence, and aging. Annu Rev Med. 2011;62:141-55. Epub 2010/11/26. doi: 10.1146/annurev-med-042909-093756. PubMed PMID: 21090961; PMCID: PMC3759035.

515. Lu W, Mehraj V, Vyboh K, Cao W, Li T, Routy JP. CD4:CD8 ratio as a frontier marker for clinical outcome, immune dysfunction and viral reservoir size in virologically suppressed HIV-positive patients. J Int AIDS Soc. 2015;18:20052. Epub 2015/07/02. doi: 10.7448/IAS.18.1.20052. PubMed PMID: 26130226; PMCID: PMC4486418.

516. Fromentin R, Bakeman W, Lawani MB, Khoury G, Hartogensis W, DaFonseca S, Killian M, Epling L, Hoh R, Sinclair E, Hecht FM, Bacchetti P, Deeks SG, Lewin SR, Sekaly RP, Chomont N. CD4+ T Cells Expressing PD-1, TIGIT and LAG-3 Contribute to HIV Persistence during ART. PLoS Pathog. 2016;12(7):e1005761. Epub 2016/07/16. doi: 10.1371/journal.ppat.1005761. PubMed PMID: 27415008; PMCID: PMC4944956.

517. Amara RR, Villinger F, Altman JD, Lydy SL, O'Neil SP, Staprans SI, Montefiori DC, Xu Y, Herndon JG, Wyatt LS, Candido MA, Kozyr NL, Earl PL, Smith JM, Ma HL, Grimm BD, Hulsey

ML, Miller J, McClure HM, McNicholl JM, Moss B, Robinson HL. Control of a mucosal challenge and prevention of AIDS by a multiprotein DNA/MVA vaccine. Science. 2001;292(5514):69-74. Epub 2001/06/08. doi: 10.1126/science.1058915. PubMed PMID: 11393868.

518. Guan WJ, Ni ZY, Hu Y, Liang WH, Ou CQ, He JX, Liu L, Shan H, Lei CL, Hui DSC, Du B, Li LJ, Zeng G, Yuen KY, Chen RC, Tang CL, Wang T, Chen PY, Xiang J, Li SY, Wang JL, Liang ZJ, Peng YX, Wei L, Liu Y, Hu YH, Peng P, Wang JM, Liu JY, Chen Z, Li G, Zheng ZJ, Qiu SQ, Luo J, Ye CJ, Zhu SY, Zhong NS, China Medical Treatment Expert Group for C. Clinical Characteristics of Coronavirus Disease 2019 in China. N Engl J Med. 2020;382(18):1708-20. Epub 2020/02/29. doi: 10.1056/NEJMoa2002032. PubMed PMID: 32109013; PMCID: PMC7092819.

519. Estes JD, Wong SW, Brenchley JM. Nonhuman primate models of human viral infections. Nat Rev Immunol. 2018;18(6):390-404. Epub 2018/03/21. doi: 10.1038/s41577-018-0005-7. PubMed PMID: 29556017; PMCID: PMC5970954.

520. Munster VJ, Feldmann F, Williamson BN, van Doremalen N, Perez-Perez L, Schulz J, Meade-White K, Okumura A, Callison J, Brumbaugh B, Avanzato VA, Rosenke R, Hanley PW, Saturday G, Scott D, Fischer ER, de Wit E. Respiratory disease in rhesus macaques inoculated with SARS-CoV-2. Nature. 2020;585(7824):268-72. Epub 2020/05/13. doi: 10.1038/s41586-020-2324-7. PubMed PMID: 32396922; PMCID: PMC7486227.

521. Rockx B, Kuiken T, Herfst S, Bestebroer T, Lamers MM, Oude Munnink BB, de Meulder D, van Amerongen G, van den Brand J, Okba NMA, Schipper D, van Run P, Leijten L, Sikkema R, Verschoor E, Verstrepen B, Bogers W, Langermans J, Drosten C, Fentener van Vlissingen M, Fouchier R, de Swart R, Koopmans M, Haagmans BL. Comparative pathogenesis of COVID-19, MERS, and SARS in a nonhuman primate model. Science. 2020;368(6494):1012-5. Epub 2020/04/19. doi: 10.1126/science.abb7314. PubMed PMID: 32303590; PMCID: PMC7164679.

522. Yu J, Tostanoski LH, Peter L, Mercado NB, McMahan K, Mahrokhian SH, Nkolola JP, Liu J, Li Z, Chandrashekar A, Martinez DR, Loos C, Atyeo C, Fischinger S, Burke JS, Slein MD, Chen

Y, Zuiani A, Lelis FJN, Travers M, Habibi S, Pessaint L, Van Ry A, Blade K, Brown R, Cook A, Finneyfrock B, Dodson A, Teow E, Velasco J, Zahn R, Wegmann F, Bondzie EA, Dagotto G, Gebre MS, He X, Jacob-Dolan C, Kirilova M, Kordana N, Lin Z, Maxfield LF, Nampanya F, Nityanandam R, Ventura JD, Wan H, Cai Y, Chen B, Schmidt AG, Wesemann DR, Baric RS, Alter G, Andersen H, Lewis MG, Barouch DH. DNA vaccine protection against SARS-CoV-2 in rhesus macaques. Science. 2020;369(6505):806-11. Epub 2020/05/22. doi: 10.1126/science.abc6284. PubMed PMID: 32434945; PMCID: PMC7243363.

523. Keystone EC, Taylor PC, Drescher E, Schlichting DE, Beattie SD, Berclaz PY, Lee CH, Fidelus-Gort RK, Luchi ME, Rooney TP, Macias WL, Genovese MC. Safety and efficacy of baricitinib at 24 weeks in patients with rheumatoid arthritis who have had an inadequate response to methotrexate. Ann Rheum Dis. 2015;74(2):333-40. Epub 2014/11/29. doi: 10.1136/annrheumdis-2014-206478. PubMed PMID: 25431052; PMCID: PMC4316868.

524. Cantini F, Niccoli L, Matarrese D, Nicastri E, Stobbione P, Goletti D. Baricitinib therapy in COVID-19: A pilot study on safety and clinical impact. J Infect. 2020;81(2):318-56. Epub 2020/04/26. doi: 10.1016/j.jinf.2020.04.017. PubMed PMID: 32333918; PMCID: PMC7177073.

525. Richardson P, Griffin I, Tucker C, Smith D, Oechsle O, Phelan A, Rawling M, Savory E, Stebbing J. Baricitinib as potential treatment for 2019-nCoV acute respiratory disease. Lancet. 2020;395(10223):e30-e1. Epub 2020/02/08. doi: 10.1016/S0140-6736(20)30304-4. PubMed PMID: 32032529; PMCID: PMC7137985.

526. Stebbing J, Krishnan V, de Bono S, Ottaviani S, Casalini G, Richardson PJ, Monteil V, Lauschke VM, Mirazimi A, Youhanna S, Tan YJ, Baldanti F, Sarasini A, Terres JAR, Nickoloff BJ, Higgs RE, Rocha G, Byers NL, Schlichting DE, Nirula A, Cardoso A, Corbellino M, Sacco Baricitinib Study G. Mechanism of baricitinib supports artificial intelligence-predicted testing in COVID-19 patients. EMBO Mol Med. 2020;12(8):e12697. Epub 2020/05/31. doi: 10.15252/emmm.202012697. PubMed PMID: 32473600; PMCID: PMC7300657.

527. Titanji BK, Farley MM, Mehta A, Connor-Schuler R, Moanna A, Cribbs SK, O'Shea J, DeSilva K, Chan B, Edwards A, Gavegnano C, Schinazi RF, Marconi VC. Use of Baricitinib in Patients With Moderate to Severe Coronavirus Disease 2019. Clin Infect Dis. 2021;72(7):1247-50. Epub 2020/07/01. doi: 10.1093/cid/ciaa879. PubMed PMID: 32597466; PMCID: PMC7337637.

528. Chertow DS, Kindrachuk J, Sheng ZM, Pujanauski LM, Cooper K, Nogee D, Claire MS, Solomon J, Perry D, Sayre P, Janosko KB, Lackemeyer MG, Bohannon JK, Kash JC, Jahrling PB, Taubenberger JK. Influenza A and methicillin-resistant Staphylococcus aureus co-infection in rhesus macaques - A model of severe pneumonia. Antiviral Res. 2016;129:120-9. Epub 2016/03/01. doi: 10.1016/j.antiviral.2016.02.013. PubMed PMID: 26923881; PMCID: PMC6617511.

529. Qin C, Zhou L, Hu Z, Zhang S, Yang S, Tao Y, Xie C, Ma K, Shang K, Wang W, Tian DS. Dysregulation of Immune Response in Patients With Coronavirus 2019 (COVID-19) in Wuhan, China. Clin Infect Dis. 2020;71(15):762-8. Epub 2020/03/13. doi: 10.1093/cid/ciaa248. PubMed PMID: 32161940; PMCID: PMC7108125.

530. Ruan Q, Yang K, Wang W, Jiang L, Song J. Clinical predictors of mortality due to COVID-19 based on an analysis of data of 150 patients from Wuhan, China. Intensive Care Med. 2020;46(5):846-8. Epub 2020/03/04. doi: 10.1007/s00134-020-05991-x. PubMed PMID: 32125452; PMCID: PMC7080116.

531. Subramanian A, Tamayo P, Mootha VK, Mukherjee S, Ebert BL, Gillette MA, Paulovich A, Pomeroy SL, Golub TR, Lander ES, Mesirov JP. Gene set enrichment analysis: a knowledge-based approach for interpreting genome-wide expression profiles. Proc Natl Acad Sci U S A. 2005;102(43):15545-50. Epub 2005/10/04. doi: 10.1073/pnas.0506580102. PubMed PMID: 16199517; PMCID: PMC1239896.

532. Arunachalam PS, Wimmers F, Mok CKP, Perera R, Scott M, Hagan T, Sigal N, Feng Y, Bristow L, Tak-Yin Tsang O, Wagh D, Coller J, Pellegrini KL, Kazmin D, Alaaeddine G, Leung

WS, Chan JMC, Chik TSH, Choi CYC, Huerta C, Paine McCullough M, Lv H, Anderson E, Edupuganti S, Upadhyay AA, Bosinger SE, Maecker HT, Khatri P, Rouphael N, Peiris M, Pulendran B. Systems biological assessment of immunity to mild versus severe COVID-19 infection in humans. Science. 2020;369(6508):1210-20. Epub 2020/08/14. doi: 10.1126/science.abc6261. PubMed PMID: 32788292; PMCID: PMC7665312.

533. Schulte-Schrepping J, Reusch N, Paclik D, Bassler K, Schlickeiser S, Zhang B, Kramer B, Krammer T, Brumhard S, Bonaguro L, De Domenico E, Wendisch D, Grasshoff M, Kapellos TS, Beckstette M, Pecht T, Saglam A, Dietrich O, Mei HE, Schulz AR, Conrad C, Kunkel D, Vafadarnejad E, Xu CJ, Horne A, Herbert M, Drews A, Thibeault C, Pfeiffer M, Hippenstiel S, Hocke A, Muller-Redetzky H, Heim KM, Machleidt F, Uhrig A, Bosquillon de Jarcy L, Jurgens L, Stegemann M, Glosenkamp CR, Volk HD, Goffinet C, Landthaler M, Wyler E, Georg P, Schneider M, Dang-Heine C, Neuwinger N, Kappert K, Tauber R, Corman V, Raabe J, Kaiser KM, Vinh MT, Rieke G, Meisel C, Ulas T, Becker M, Geffers R, Witzenrath M, Drosten C, Suttorp N, von Kalle C, Kurth F, Handler K, Schultze JL, Aschenbrenner AC, Li Y, Nattermann J, Sawitzki B, Saliba AE, Sander LE, Deutsche C-OI. Severe COVID-19 Is Marked by a Dysregulated Myeloid Cell Compartment. Cell. 2020;182(6):1419-40 e23. Epub 2020/08/19. doi: 10.1016/j.cell.2020.08.001. PubMed PMID: 32810438; PMCID: PMC7405822.

534. Silvin A, Chapuis N, Dunsmore G, Goubet AG, Dubuisson A, Derosa L, Almire C, Henon C, Kosmider O, Droin N, Rameau P, Catelain C, Alfaro A, Dussiau C, Friedrich C, Sourdeau E, Marin N, Szwebel TA, Cantin D, Mouthon L, Borderie D, Deloger M, Bredel D, Mouraud S, Drubay D, Andrieu M, Lhonneur AS, Saada V, Stoclin A, Willekens C, Pommeret F, Griscelli F, Ng LG, Zhang Z, Bost P, Amit I, Barlesi F, Marabelle A, Pene F, Gachot B, Andre F, Zitvogel L, Ginhoux F, Fontenay M, Solary E. Elevated Calprotectin and Abnormal Myeloid Cell Subsets Discriminate Severe from Mild COVID-19. Cell. 2020;182(6):1401-18 e18. Epub 2020/08/19. doi: 10.1016/j.cell.2020.08.002. PubMed PMID: 32810439; PMCID: PMC7405878.

535. Bost P, Giladi A, Liu Y, Bendjelal Y, Xu G, David E, Blecher-Gonen R, Cohen M, Medaglia C, Li H, Deczkowska A, Zhang S, Schwikowski B, Zhang Z, Amit I. Host-Viral Infection Maps Reveal Signatures of Severe COVID-19 Patients. Cell. 2020;181(7):1475-88 e12. Epub 2020/06/02. doi: 10.1016/j.cell.2020.05.006. PubMed PMID: 32479746; PMCID: PMC7205692.

536. Chua RL, Lukassen S, Trump S, Hennig BP, Wendisch D, Pott F, Debnath O, Thurmann L, Kurth F, Volker MT, Kazmierski J, Timmermann B, Twardziok S, Schneider S, Machleidt F, Muller-Redetzky H, Maier M, Krannich A, Schmidt S, Balzer F, Liebig J, Loske J, Suttorp N, Eils J, Ishaque N, Liebert UG, von Kalle C, Hocke A, Witzenrath M, Goffinet C, Drosten C, Laudi S, Lehmann I, Conrad C, Sander LE, Eils R. COVID-19 severity correlates with airway epithelium-immune cell interactions identified by single-cell analysis. Nat Biotechnol. 2020;38(8):970-9. Epub 2020/06/28. doi: 10.1038/s41587-020-0602-4. PubMed PMID: 32591762.

537. Liao M, Liu Y, Yuan J, Wen Y, Xu G, Zhao J, Cheng L, Li J, Wang X, Wang F, Liu L, Amit I, Zhang S, Zhang Z. Single-cell landscape of bronchoalveolar immune cells in patients with COVID-19. Nat Med. 2020;26(6):842-4. Epub 2020/05/14. doi: 10.1038/s41591-020-0901-9. PubMed PMID: 32398875.

538. de Lang A, Baas T, Teal T, Leijten LM, Rain B, Osterhaus AD, Haagmans BL, Katze MG. Functional genomics highlights differential induction of antiviral pathways in the lungs of SARS-CoV-infected macaques. PLoS Pathog. 2007;3(8):e112. Epub 2007/08/19. doi: 10.1371/journal.ppat.0030112. PubMed PMID: 17696609; PMCID: PMC1941749.

539. Laing AG, Lorenc A, Del Molino Del Barrio I, Das A, Fish M, Monin L, Munoz-Ruiz M, McKenzie DR, Hayday TS, Francos-Quijorna I, Kamdar S, Joseph M, Davies D, Davis R, Jennings A, Zlatareva I, Vantourout P, Wu Y, Sofra V, Cano F, Greco M, Theodoridis E, Freedman JD, Gee S, Chan JNE, Ryan S, Bugallo-Blanco E, Peterson P, Kisand K, Haljasmagi L, Chadli L, Moingeon P, Martinez L, Merrick B, Bisnauthsing K, Brooks K, Ibrahim MAA, Mason J, Lopez Gomez F, Babalola K, Abdul-Jawad S, Cason J, Mant C, Seow J, Graham C, Doores KJ, Di Rosa F, Edgeworth J, Shankar-Hari M, Hayday AC. A dynamic COVID-19 immune signature includes

associations with poor prognosis. Nat Med. 2020;26(10):1623-35. Epub 2020/08/19. doi: 10.1038/s41591-020-1038-6. PubMed PMID: 32807934.

540. Tang NL, Chan PK, Wong CK, To KF, Wu AK, Sung YM, Hui DS, Sung JJ, Lam CW. Early enhanced expression of interferon-inducible protein-10 (CXCL-10) and other chemokines predicts adverse outcome in severe acute respiratory syndrome. Clin Chem. 2005;51(12):2333-40. Epub 2005/10/01. doi: 10.1373/clinchem.2005.054460. PubMed PMID: 16195357; PMCID: PMC7108146.

541. Skendros P, Mitsios A, Chrysanthopoulou A, Mastellos DC, Metallidis S, Rafailidis P, Ntinopoulou M, Sertaridou E, Tsironidou V, Tsigalou C, Tektonidou M, Konstantinidis T, Papagoras C, Mitroulis I, Germanidis G, Lambris JD, Ritis K. Complement and tissue factor-enriched neutrophil extracellular traps are key drivers in COVID-19 immunothrombosis. J Clin Invest. 2020;130(11):6151-7. Epub 2020/08/08. doi: 10.1172/JCI141374. PubMed PMID: 32759504; PMCID: PMC7598040.

542. Bronte V, Ugel S, Tinazzi E, Vella A, De Sanctis F, Cane S, Batani V, Trovato R, Fiore A, Petrova V, Hofer F, Barouni RM, Musiu C, Caligola S, Pinton L, Torroni L, Polati E, Donadello K, Friso S, Pizzolo F, Iezzi M, Facciotti F, Pelicci PG, Righetti D, Bazzoni P, Rampudda M, Comel A, Mosaner W, Lunardi C, Olivieri O. Baricitinib restrains the immune dysregulation in patients with severe COVID-19. J Clin Invest. 2020;130(12):6409-16. Epub 2020/08/19. doi: 10.1172/JCI141772. PubMed PMID: 32809969; PMCID: PMC8016181.

543. Loo YM, Fornek J, Crochet N, Bajwa G, Perwitasari O, Martinez-Sobrido L, Akira S, Gill MA, Garcia-Sastre A, Katze MG, Gale M, Jr. Distinct RIG-I and MDA5 signaling by RNA viruses in innate immunity. J Virol. 2008;82(1):335-45. Epub 2007/10/19. doi: 10.1128/JVI.01080-07. PubMed PMID: 17942531; PMCID: PMC2224404.

544. Loo YM, Gale M, Jr. Immune signaling by RIG-I-like receptors. Immunity. 2011;34(5):680-92. Epub 2011/05/28. doi: 10.1016/j.immuni.2011.05.003. PubMed PMID: 21616437; PMCID: PMC3177755.

545. Zevini A, Olagnier D, Hiscott J. Crosstalk between Cytoplasmic RIG-I and STING Sensing Pathways. Trends Immunol. 2017;38(3):194-205. Epub 2017/01/12. doi: 10.1016/j.it.2016.12.004. PubMed PMID: 28073693; PMCID: PMC5329138.

546. Davidson AD, Williamson MK, Lewis S, Shoemark D, Carroll MW, Heesom KJ, Zambon M, Ellis J, Lewis PA, Hiscox JA, Matthews DA. Characterisation of the transcriptome and proteome of SARS-CoV-2 reveals a cell passage induced in-frame deletion of the furin-like cleavage site from the spike glycoprotein. Genome Med. 2020;12(1):68. Epub 2020/07/30. doi: 10.1186/s13073-020-00763-0. PubMed PMID: 32723359; PMCID: PMC7386171.

547. Waggoner JJ, Stittleburg V, Pond R, Saklawi Y, Sahoo MK, Babiker A, Hussaini L, Kraft CS, Pinsky BA, Anderson EJ, Rouphael N. Triplex Real-Time RT-PCR for Severe Acute Respiratory Syndrome Coronavirus 2. Emerg Infect Dis. 2020;26(7):1633-5. Epub 2020/04/16. doi: 10.3201/eid2607.201285. PubMed PMID: 32294051; PMCID: PMC7323516.

548. Zheng GX, Terry JM, Belgrader P, Ryvkin P, Bent ZW, Wilson R, Ziraldo SB, Wheeler TD, McDermott GP, Zhu J, Gregory MT, Shuga J, Montesclaros L, Underwood JG, Masquelier DA, Nishimura SY, Schnall-Levin M, Wyatt PW, Hindson CM, Bharadwaj R, Wong A, Ness KD, Beppu LW, Deeg HJ, McFarland C, Loeb KR, Valente WJ, Ericson NG, Stevens EA, Radich JP, Mikkelsen TS, Hindson BJ, Bielas JH. Massively parallel digital transcriptional profiling of single cells. Nat Commun. 2017;8:14049. Epub 2017/01/17. doi: 10.1038/ncomms14049. PubMed PMID: 28091601; PMCID: PMC5241818 L.M., D.A.M., S.Y.N., M.S.L., P.W.W., C.M.H., R.B., A.W., K.D.N., T.S.M. and B.J.H. are employees of 10x Genomics.

549. Dobin A, Davis CA, Schlesinger F, Drenkow J, Zaleski C, Jha S, Batut P, Chaisson M, Gingeras TR. STAR: ultrafast universal RNA-seq aligner. Bioinformatics (Oxford, England). 2013;29(1):15-21. Epub 2012/10/30. doi: 10.1093/bioinformatics/bts635. PubMed PMID: 23104886; PMCID: PMC3530905.

550. Love MI, Huber W, Anders S. Moderated estimation of fold change and dispersion for RNA-seq data with DESeq2. Genome Biol. 2014;15(12):550. Epub 2014/12/18. doi: 10.1186/s13059-014-0550-8. PubMed PMID: 25516281; PMCID: PMC4302049.

551. Gu Z, Eils R, Schlesner M. Complex heatmaps reveal patterns and correlations in multidimensional genomic data. Bioinformatics. 2016;32(18):2847-9. Epub 2016/05/22. doi: 10.1093/bioinformatics/btw313. PubMed PMID: 27207943.

552. Satija R, Butler A, Hoffman P. Seurat: Tools for Single Cell Genomics. R package version. 2018;2(0).

553. McGinnis CS, Murrow LM, Gartner ZJ. DoubletFinder: Doublet Detection in Single-Cell RNA Sequencing Data Using Artificial Nearest Neighbors. Cell Syst. 2019;8(4):329-37 e4. Epub 2019/04/08. doi: 10.1016/j.cels.2019.03.003. PubMed PMID: 30954475; PMCID: PMC6853612.

554. McInnes L, Healy J, Melville J. Umap: Uniform manifold approximation and projection for dimension reduction. arXiv preprint arXiv:180203426. 2018.

555. Aran D, Looney AP, Liu L, Wu E, Fong V, Hsu A, Chak S, Naikawadi RP, Wolters PJ, Abate AR, Butte AJ, Bhattacharya M. Reference-based analysis of lung single-cell sequencing reveals a transitional profibrotic macrophage. Nat Immunol. 2019;20(2):163-72. Epub 2019/01/16. doi: 10.1038/s41590-018-0276-y. PubMed PMID: 30643263; PMCID: PMC6340744.

556. Finak G, McDavid A, Yajima M, Deng J, Gersuk V, Shalek AK, Slichter CK, Miller HW, McElrath MJ, Prlic M, Linsley PS, Gottardo R. MAST: a flexible statistical framework for assessing transcriptional changes and characterizing heterogeneity in single-cell RNA sequencing data. Genome Biol. 2015;16:278. Epub 2015/12/15. doi: 10.1186/s13059-015-0844-5. PubMed PMID: 26653891; PMCID: PMC4676162.

557. Wickham H. ggplot2: elegant graphics for data analysis: springer; 2016.

558. Pino M, Paganini S, Deleage C, Padhan K, Harper JL, King CT, Micci L, Cervasi B, Mudd JC, Gill KP, Jean SM, Easley K, Silvestri G, Estes JD, Petrovas C, Lederman MM, Paiardini M. Fingolimod retains cytolytic T cells and limits T follicular helper cell infection in lymphoid sites of

SIV persistence. PLoS Pathog. 2019;15(10):e1008081. Epub 2019/10/19. doi: 10.1371/journal.ppat.1008081. PubMed PMID: 31626660; PMCID: PMC6834281.

559. Kasturi SP, Rasheed MAU, Havenar-Daughton C, Pham M, Legere T, Sher ZJ, Kovalenkov Y, Gumber S, Huang JY, Gottardo R, Fulp W, Sato A, Sawant S, Stanfield-Oakley S, Yates N, LaBranche C, Alam SM, Tomaras G, Ferrari G, Montefiori D, Wrammert J, Villinger F, Tomai M, Vasilakos J, Fox CB, Reed SG, Haynes BF, Crotty S, Ahmed R, Pulendran B. 3M-052, a synthetic TLR-7/8 agonist, induces durable HIV-1 envelope-specific plasma cells and humoral immunity in nonhuman primates. Sci Immunol. 2020;5(48). Epub 2020/06/21. doi: 10.1126/sciimmunol.abb1025. PubMed PMID: 32561559; PMCID: PMC8109745.

560. Mulligan MJ, Lyke KE, Kitchin N, Absalon J, Gurtman A, Lockhart S, Neuzil K, Raabe V, Bailey R, Swanson KA, Li P, Koury K, Kalina W, Cooper D, Fontes-Garfias C, Shi PY, Tureci O, Tompkins KR, Walsh EE, Frenck R, Falsey AR, Dormitzer PR, Gruber WC, Sahin U, Jansen KU. Phase I/II study of COVID-19 RNA vaccine BNT162b1 in adults. Nature. 2020;586(7830):589-93. Epub 2020/08/14. doi: 10.1038/s41586-020-2639-4. PubMed PMID: 32785213.

561. Carvalho T, Krammer F, Iwasaki A. The first 12 months of COVID-19: a timeline of immunological insights. Nat Rev Immunol. 2021;21(4):245-56. Epub 2021/03/17. doi: 10.1038/s41577-021-00522-1. PubMed PMID: 33723416; PMCID: PMC7958099.

562. Wichmann D, Sperhake JP, Lutgehetmann M, Steurer S, Edler C, Heinemann A, Heinrich F, Mushumba H, Kniep I, Schroder AS, Burdelski C, de Heer G, Nierhaus A, Frings D, Pfefferle S, Becker H, Bredereke-Wiedling H, de Weerth A, Paschen HR, Sheikhzadeh-Eggers S, Stang A, Schmiedel S, Bokemeyer C, Addo MM, Aepfelbacher M, Puschel K, Kluge S. Autopsy Findings and Venous Thromboembolism in Patients With COVID-19: A Prospective Cohort Study. Ann Intern Med. 2020;173(4):268-77. Epub 2020/05/07. doi: 10.7326/M20-2003. PubMed PMID: 32374815; PMCID: PMC7240772.

563. Moore JB, June CH. Cytokine release syndrome in severe COVID-19. Science. 2020;368(6490):473-4. Epub 2020/04/19. doi: 10.1126/science.abb8925. PubMed PMID: 32303591.

564. Munoz-Fontela C, Dowling WE, Funnell SGP, Gsell PS, Riveros-Balta AX, Albrecht RA, Andersen H, Baric RS, Carroll MW, Cavaleri M, Qin C, Crozier I, Dallmeier K, de Waal L, de Wit E, Delang L, Dohm E, Duprex WP, Falzarano D, Finch CL, Frieman MB, Graham BS, Gralinski LE, Guilfoyle K, Haagmans BL, Hamilton GA, Hartman AL, Herfst S, Kaptein SJF, Klimstra WB, Knezevic I, Krause PR, Kuhn JH, Le Grand R, Lewis MG, Liu WC, Maisonnasse P, McElroy AK, Munster V, Oreshkova N, Rasmussen AL, Rocha-Pereira J, Rockx B, Rodriguez E, Rogers TF, Salguero FJ, Schotsaert M, Stittelaar KJ, Thibaut HJ, Tseng CT, Vergara-Alert J, Beer M, Brasel T, Chan JFW, Garcia-Sastre A, Neyts J, Perlman S, Reed DS, Richt JA, Roy CJ, Segales J, Vasan SS, Henao-Restrepo AM, Barouch DH. Animal models for COVID-19. Nature. 2020;586(7830):509-15. Epub 2020/09/24. doi: 10.1038/s41586-020-2787-6. PubMed PMID: 32967005; PMCID: PMC8136862.

565. Corbett KS, Flynn B, Foulds KE, Francica JR, Boyoglu-Barnum S, Werner AP, Flach B, O'Connell S, Bock KW, Minai M, Nagata BM, Andersen H, Martinez DR, Noe AT, Douek N, Donaldson MM, Nji NN, Alvarado GS, Edwards DK, Flebbe DR, Lamb E, Doria-Rose NA, Lin BC, Louder MK, O'Dell S, Schmidt SD, Phung E, Chang LA, Yap C, Todd JM, Pessaint L, Van Ry A, Browne S, Greenhouse J, Putman-Taylor T, Strasbaugh A, Campbell TA, Cook A, Dodson A, Steingrebe K, Shi W, Zhang Y, Abiona OM, Wang L, Pegu A, Yang ES, Leung K, Zhou T, Teng IT, Widge A, Gordon I, Novik L, Gillespie RA, Loomis RJ, Moliva JI, Stewart-Jones G, Himansu S, Kong WP, Nason MC, Morabito KM, Ruckwardt TJ, Ledgerwood JE, Gaudinski MR, Kwong PD, Mascola JR, Carfi A, Lewis MG, Baric RS, McDermott A, Moore IN, Sullivan NJ, Roederer M, Seder RA, Graham BS. Evaluation of the mRNA-1273 Vaccine against SARS-CoV-2 in Nonhuman Primates. N Engl J Med. 2020;383(16):1544-55. Epub 2020/07/30. doi: 10.1056/NEJMoa2024671. PubMed PMID: 32722908; PMCID: PMC7449230.

566. Mercado NB, Zahn R, Wegmann F, Loos C, Chandrashekar A, Yu J, Liu J, Peter L, McMahan K, Tostanoski LH, He X, Martinez DR, Rutten L, Bos R, van Manen D, Vellinga J, Custers J, Langedijk JP, Kwaks T, Bakkers MJG, Zuijdgeest D, Rosendahl Huber SK, Atyeo C, Fischinger S, Burke JS, Feldman J, Hauser BM, Caradonna TM, Bondzie EA, Dagotto G, Gebre MS, Hoffman E, Jacob-Dolan C, Kirilova M, Li Z, Lin Z, Mahrokhian SH, Maxfield LF, Nampanya F, Nityanandam R, Nkolola JP, Patel S, Ventura JD, Verrington K, Wan H, Pessaint L, Van Ry A, Blade K, Strasbaugh A, Cabus M, Brown R, Cook A, Zouantchangadou S, Teow E, Andersen H, Lewis MG, Cai Y, Chen B, Schmidt AG, Reeves RK, Baric RS, Lauffenburger DA, Alter G, Stoffels P, Mammen M, Van Hoof J, Schuitemaker H, Barouch DH. Single-shot Ad26 vaccine protects against SARS-CoV-2 in rhesus macaques. Nature. 2020;586(7830):583-8. Epub 2020/07/31. doi: 10.1038/s41586-020-2607-z. PubMed PMID: 32731257; PMCID: PMC7581548.

567. Routhu NK, Cheedarla N, Gangadhara S, Bollimpelli VS, Boddapati AK, Shiferaw A, Rahman SA, Sahoo A, Edara VV, Lai L, Floyd K, Wang S, Fischinger S, Atyeo C, Shin SA, Gumber S, Kirejczyk S, Cohen J, Jean SM, Wood JS, Connor-Stroud F, Stammen RL, Upadhyay AA, Pellegrini K, Montefiori D, Shi PY, Menachery VD, Alter G, Vanderford TH, Bosinger SE, Suthar MS, Amara RR. A modified vaccinia Ankara vector-based vaccine protects macaques from SARS-CoV-2 infection, immune pathology, and dysfunction in the lungs. Immunity. 2021;54(3):542-56 e9. Epub 2021/02/26. doi: 10.1016/j.immuni.2021.02.001. PubMed PMID: 33631118; PMCID: PMC7859620.

568. Singh DK, Singh B, Ganatra SR, Gazi M, Cole J, Thippeshappa R, Alfson KJ, Clemmons E, Gonzalez O, Escobedo R, Lee TH, Chatterjee A, Goez-Gazi Y, Sharan R, Gough M, Alvarez C, Blakley A, Ferdin J, Bartley C, Staples H, Parodi L, Callery J, Mannino A, Klaffke B, Escareno P, Platt RN, 2nd, Hodara V, Scordo J, Gautam S, Vilanova AG, Olmo-Fontanez A, Schami A, Oyejide A, Ajithdoss DK, Copin R, Baum A, Kyratsous C, Alvarez X, Ahmed M, Rosa B, Goodroe A, Dutton J, Hall-Ursone S, Frost PA, Voges AK, Ross CN, Sayers K, Chen C, Hallam C, Khader SA, Mitreva M, Anderson TJC, Martinez-Sobrido L, Patterson JL, Turner J, Torrelles JB, Dick EJ,

Jr., Brasky K, Schlesinger LS, Giavedoni LD, Carrion R, Jr., Kaushal D. Responses to acute infection with SARS-CoV-2 in the lungs of rhesus macaques, baboons and marmosets. Nat Microbiol. 2021;6(1):73-86. Epub 2020/12/20. doi: 10.1038/s41564-020-00841-4. PubMed PMID: 33340034; PMCID: PMC7890948.

569. Aid M, Busman-Sahay K, Vidal SJ, Maliga Z, Bondoc S, Starke C, Terry M, Jacobson CA, Wrijil L, Ducat S, Brook OR, Miller AD, Porto M, Pellegrini KL, Pino M, Hoang TN, Chandrashekar A, Patel S, Stephenson K, Bosinger SE, Andersen H, Lewis MG, Hecht JL, Sorger PK, Martinot AJ, Estes JD, Barouch DH. Vascular Disease and Thrombosis in SARS-CoV-2-Infected Rhesus Macaques. Cell. 2020;183(5):1354-66 e13. Epub 2020/10/17. doi: 10.1016/j.cell.2020.10.005. PubMed PMID: 33065030; PMCID: PMC7546181.

570. Fahlberg MD, Blair RV, Doyle-Meyers LA, Midkiff CC, Zenere G, Russell-Lodrigue KE, Monjure CJ, Haupt EH, Penney TP, Lehmicke G, Threeton BM, Golden N, Datta PK, Roy CJ, Bohm RP, Maness NJ, Fischer T, Rappaport J, Vaccari M. Cellular events of acute, resolving or progressive COVID-19 in SARS-CoV-2 infected non-human primates. Nat Commun. 2020;11(1):6078. Epub 2020/11/29. doi: 10.1038/s41467-020-19967-4. PubMed PMID: 33247138; PMCID: PMC7695721.

571. Speranza E, Williamson BN, Feldmann F, Sturdevant GL, Perez-Perez L, Meade-White K, Smith BJ, Lovaglio J, Martens C, Munster VJ, Okumura A, Shaia C, Feldmann H, Best SM, de Wit E. Single-cell RNA sequencing reveals SARS-CoV-2 infection dynamics in lungs of African green monkeys. Sci Transl Med. 2021;13(578). Epub 2021/01/13. doi: 10.1126/scitranslmed.abe8146. PubMed PMID: 33431511; PMCID: PMC7875333.

572. Schultze JL, Aschenbrenner AC. COVID-19 and the human innate immune system. Cell. 2021;184(7):1671-92. Epub 2021/03/21. doi: 10.1016/j.cell.2021.02.029. PubMed PMID: 33743212; PMCID: PMC7885626.

573. Chakarov S, Lim HY, Tan L, Lim SY, See P, Lum J, Zhang XM, Foo S, Nakamizo S, Duan K, Kong WT, Gentek R, Balachander A, Carbajo D, Bleriot C, Malleret B, Tam JKC, Baig S,

Shabeer M, Toh SES, Schlitzer A, Larbi A, Marichal T, Malissen B, Chen J, Poidinger M, Kabashima K, Bajenoff M, Ng LG, Angeli V, Ginhoux F. Two distinct interstitial macrophage populations coexist across tissues in specific subtissular niches. Science. 2019;363(6432). Epub 2019/03/16. doi: 10.1126/science.aau0964. PubMed PMID: 30872492.

574. Gibbings SL, Thomas SM, Atif SM, McCubbrey AL, Desch AN, Danhorn T, Leach SM, Bratton DL, Henson PM, Janssen WJ, Jakubzick CV. Three Unique Interstitial Macrophages in the Murine Lung at Steady State. Am J Respir Cell Mol Biol. 2017;57(1):66-76. Epub 2017/03/04. doi: 10.1165/rcmb.2016-0361OC. PubMed PMID: 28257233; PMCID: PMC5516280.

575. Schyns J, Bai Q, Ruscitti C, Radermecker C, De Schepper S, Chakarov S, Farnir F, Pirottin D, Ginhoux F, Boeckxstaens G, Bureau F, Marichal T. Non-classical tissue monocytes and two functionally distinct populations of interstitial macrophages populate the mouse lung. Nat Commun. 2019;10(1):3964. Epub 2019/09/05. doi: 10.1038/s41467-019-11843-0. PubMed PMID: 31481690; PMCID: PMC6722135.

576. Ural BB, Yeung ST, Damani-Yokota P, Devlin JC, de Vries M, Vera-Licona P, Samji T, Sawai CM, Jang G, Perez OA, Pham Q, Maher L, Loke P, Dittmann M, Reizis B, Khanna KM. Identification of a nerve-associated, lung-resident interstitial macrophage subset with distinct localization and immunoregulatory properties. Sci Immunol. 2020;5(45). Epub 2020/03/30. doi: 10.1126/sciimmunol.aax8756. PubMed PMID: 32220976; PMCID: PMC7717505.

577. Esaulova E, Das S, Singh DK, Choreno-Parra JA, Swain A, Arthur L, Rangel-Moreno J, Ahmed M, Singh B, Gupta A, Fernandez-Lopez LA, de la Luz Garcia-Hernandez M, Bucsan A, Moodley C, Mehra S, Garcia-Latorre E, Zuniga J, Atkinson J, Kaushal D, Artyomov MN, Khader SA. The immune landscape in tuberculosis reveals populations linked to disease and latency. Cell Host Microbe. 2021;29(2):165-78 e8. Epub 2020/12/20. doi: 10.1016/j.chom.2020.11.013. PubMed PMID: 33340449; PMCID: PMC7878437.

578. Hao Y, Hao S, Andersen-Nissen E, Mauck WM, 3rd, Zheng S, Butler A, Lee MJ, Wilk AJ, Darby C, Zager M, Hoffman P, Stoeckius M, Papalexi E, Mimitou EP, Jain J, Srivastava A, Stuart

T, Fleming LM, Yeung B, Rogers AJ, McElrath JM, Blish CA, Gottardo R, Smibert P, Satija R. Integrated analysis of multimodal single-cell data. Cell. 2021;184(13):3573-87 e29. Epub 2021/06/02. doi: 10.1016/j.cell.2021.04.048. PubMed PMID: 34062119; PMCID: PMC8238499.

579. Cai Y, Sugimoto C, Arainga M, Alvarez X, Didier ES, Kuroda MJ. In vivo characterization of alveolar and interstitial lung macrophages in rhesus macaques: implications for understanding lung disease in humans. J Immunol. 2014;192(6):2821-9. Epub 2014/02/19. doi: 10.4049/jimmunol.1302269. PubMed PMID: 24534529; PMCID: PMC3959879.

580. O'Shea NR, Chew TS, Dunne J, Marnane R, Nedjat-Shokouhi B, Smith PJ, Bloom SL, Smith AM, Segal AW. Critical Role of the Disintegrin Metalloprotease ADAM-like Decysin-1 [ADAMDEC1] for Intestinal Immunity and Inflammation. J Crohns Colitis. 2016;10(12):1417-27. Epub 2016/05/27. doi: 10.1093/ecco-jcc/jjw111. PubMed PMID: 27226416; PMCID: PMC5174729.

581. Coillard A, Segura E. In vivo Differentiation of Human Monocytes. Front Immunol. 2019;10:1907. Epub 2019/08/29. doi: 10.3389/fimmu.2019.01907. PubMed PMID: 31456804; PMCID: PMC6700358.

582. Vanderheiden A, Thomas J, Soung AL, Davis-Gardner ME, Floyd K, Jin F, Cowan DA, Pellegrini K, Creanga A, Pegu A, Derrien-Colemyn A, Shi PY, Grakoui A, Klein RS, Bosinger SE, Kohlmeier JE, Menachery VD, Suthar MS. CCR2-dependent monocyte-derived cells restrict SARS-CoV-2 infection. bioRxiv. 2021. Epub 2021/05/12. doi: 10.1101/2021.05.03.442538. PubMed PMID: 33972938; PMCID: PMC8109197.

583. Ren X, Wen W, Fan X, Hou W, Su B, Cai P, Li J, Liu Y, Tang F, Zhang F, Yang Y, He J, Ma W, He J, Wang P, Cao Q, Chen F, Chen Y, Cheng X, Deng G, Deng X, Ding W, Feng Y, Gan R, Guo C, Guo W, He S, Jiang C, Liang J, Li YM, Lin J, Ling Y, Liu H, Liu J, Liu N, Liu SQ, Luo M, Ma Q, Song Q, Sun W, Wang G, Wang F, Wang Y, Wen X, Wu Q, Xu G, Xie X, Xiong X, Xing X, Xu H, Yin C, Yu D, Yu K, Yuan J, Zhang B, Zhang P, Zhang T, Zhao J, Zhao P, Zhou J, Zhou W, Zhong S, Zhong X, Zhang S, Zhu L, Zhu P, Zou B, Zou J, Zuo Z, Bai F, Huang X, Zhou P,

Jiang Q, Huang Z, Bei JX, Wei L, Bian XW, Liu X, Cheng T, Li X, Zhao P, Wang FS, Wang H, Su B, Zhang Z, Qu K, Wang X, Chen J, Jin R, Zhang Z. COVID-19 immune features revealed by a large-scale single-cell transcriptome atlas. Cell. 2021;184(7):1895-913 e19. Epub 2021/03/04. doi: 10.1016/j.cell.2021.01.053. PubMed PMID: 33657410; PMCID: PMC7857060.

584. Liegeois M, Legrand C, Desmet CJ, Marichal T, Bureau F. The interstitial macrophage: A long-neglected piece in the puzzle of lung immunity. Cell Immunol. 2018;330:91-6. Epub 2018/02/21. doi: 10.1016/j.cellimm.2018.02.001. PubMed PMID: 29458975.

585. Hoppstadter J, Diesel B, Zarbock R, Breinig T, Monz D, Koch M, Meyerhans A, Gortner L, Lehr CM, Huwer H, Kiemer AK. Differential cell reaction upon Toll-like receptor 4 and 9 activation in human alveolar and lung interstitial macrophages. Respir Res. 2010;11:124. Epub 2010/09/17. doi: 10.1186/1465-9921-11-124. PubMed PMID: 20843333; PMCID: PMC2949727.

586. Asano T, Boisson B, Onodi F, Matuozzo D, Moncada-Velez M, Maglorius Renkilaraj MRL, Zhang P, Meertens L, Bolze A, Materna M, Korniotis S, Gervais A, Talouarn E, Bigio B, Seeleuthner Y, Bilguvar K, Zhang Y, Neehus AL, Ogishi M, Pelham SJ, Le Voyer T, Rosain J, Philippot Q, Soler-Palacin P, Colobran R, Martin-Nalda A, Riviere JG, Tandjaoui-Lambiotte Y, Chaibi K, Shahrooei M, Darazam IA, Olyaei NA, Mansouri D, Hatipoglu N, Palabiyik F, Ozcelik T, Novelli G, Novelli A, Casari G, Aiuti A, Carrera P, Bondesan S, Barzaghi F, Rovere-Querini P, Tresoldi C, Franco JL, Rojas J, Reyes LF, Bustos IG, Arias AA, Morelle G, Christele K, Troya J, Planas-Serra L, Schluter A, Gut M, Pujol A, Allende LM, Rodriguez-Gallego C, Flores C, Cabrera-Marante O, Pleguezuelo DE, de Diego RP, Keles S, Aytekin G, Akcan OM, Bryceson YT, Bergman P, Brodin P, Smole D, Smith CIE, Norlin AC, Campbell TM, Covill LE, Hammarstrom L, Pan-Hammarstrom Q, Abolhassani H, Mane S, Marr N, Ata M, Al Ali F, Khan T, Spaan AN, Dalgard CL, Bonfanti P, Biondi A, Tubiana S, Burdet C, Nussbaum R, Kahn-Kirby A, Snow AL, Effort CHG, Clinicians C-S, Clinicians C, Imagine CG, French CCSG, Co VCC, Amsterdam UMCC, Biobank, Group N-UCS, Bustamante J, Puel A, Boisson-Dupuis S, Zhang SY, Beziat V, Lifton RP, Bastard P, Notarangelo LD, Abel L, Su HC, Jouanguy E, Amara A, Soumelis V, Cobat

A, Zhang Q, Casanova JL. X-linked recessive TLR7 deficiency in ~1% of men under 60 years old with life-threatening COVID-19. Sci Immunol. 2021;6(62). Epub 2021/08/21. doi: 10.1126/sciimmunol.abl4348. PubMed PMID: 34413140; PMCID: PMC8532080.

587. Bastard P, Orlova E, Sozaeva L, Levy R, James A, Schmitt MM, Ochoa S, Kareva M, Rodina Y, Gervais A, Le Voyer T, Rosain J, Philippot Q, Neehus AL, Shaw E, Migaud M, Bizien L, Ekwall O, Berg S, Beccuti G, Ghizzoni L, Thiriez G, Pavot A, Goujard C, Fremond ML, Carter E, Rothenbuhler A, Linglart A, Mignot B, Comte A, Cheikh N, Hermine O, Breivik L, Husebye ES, Humbert S, Rohrlich P, Coaquette A, Vuoto F, Faure K, Mahlaoui N, Kotnik P, Battelino T, Trebusak Podkrajsek K, Kisand K, Ferre EMN, DiMaggio T, Rosen LB, Burbelo PD, McIntyre M, Kann NY, Shcherbina A, Pavlova M, Kolodkina A, Holland SM, Zhang SY, Crow YJ, Notarangelo LD, Su HC, Abel L, Anderson MS, Jouanguy E, Neven B, Puel A, Casanova JL, Lionakis MS. Preexisting autoantibodies to type I IFNs underlie critical COVID-19 pneumonia in patients with APS-1. J Exp Med. 2021;218(7). Epub 2021/04/24. doi: 10.1084/jem.20210554. PubMed PMID: 33890986; PMCID: PMC8077172 reported a patent to 63/055,155 pending and a patent to 63/141,669 pending. No other disclosures were reported.

588. Froberg A, Kjellenberg K, Lindroos AK, Nyberg G. Self-reported physical activity and sedentary behaviour amongst adolescents in Sweden vary depending on sex, age and parental education. Acta Paediatr. 2021;110(11):3097-104. Epub 2021/08/20. doi: 10.1111/apa.16077. PubMed PMID: 34411339.

589. Lopez J, Mommert M, Mouton W, Pizzorno A, Brengel-Pesce K, Mezidi M, Villard M, Lina B, Richard JC, Fassier JB, Cheynet V, Padey B, Duliere V, Julien T, Paul S, Bastard P, Belot A, Bal A, Casanova JL, Rosa-Calatrava M, Morfin F, Walzer T, Trouillet-Assant S. Correction: Early nasal type I IFN immunity against SARS-CoV-2 is compromised in patients with autoantibodies against type I IFNs. J Exp Med. 2021;218(10). Epub 2021/08/21. doi: 10.1084/jem.2021121108132021c. PubMed PMID: 34415984; PMCID: PMC8493864.

590. Solanich X, Rigo-Bonnin R, Gumucio VD, Bastard P, Rosain J, Philippot Q, Perez-Fernandez XL, Fuset-Cabanes MP, Gordillo-Benitez MA, Suarez-Cuartin G, Boza-Hernandez E, Riera-Mestre A, Parra-Martinez A, Colobran R, Antoli A, Navarro S, Rocamora-Blanch G, Framil M, Calatayud L, Corbella X, Casanova JL, Morandeira F, Sabater-Riera J. Pre-existing Autoantibodies Neutralizing High Concentrations of Type I Interferons in Almost 10% of COVID-19 Patients Admitted to Intensive Care in Barcelona. J Clin Immunol. 2021. Epub 2021/09/28. doi: 10.1007/s10875-021-01136-x. PubMed PMID: 34570326; PMCID: PMC8475877.

591. van der Wijst MGP, Vazquez SE, Hartoularos GC, Bastard P, Grant T, Bueno R, Lee DS, Greenland JR, Sun Y, Perez R, Ogorodnikov A, Ward A, Mann SA, Lynch KL, Yun C, Havlir DV, Chamie G, Marquez C, Greenhouse B, Lionakis MS, Norris PJ, Dumont LJ, Kelly K, Zhang P, Zhang Q, Gervais A, Le Voyer T, Whatley A, Si Y, Byrne A, Combes AJ, Rao AA, Song YS, Fragiadakis GK, Kangelaris K, Calfee CS, Erle DJ, Hendrickson C, Krummel MF, Woodruff PG, Langelier CR, Casanova JL, Derisi JL, Anderson MS, Ye CJ, consortium UC. Type I interferon autoantibodies are associated with systemic immune alterations in patients with COVID-19. Sci Transl Med. 2021;13(612):eabh2624. Epub 2021/08/26. doi: 10.1126/scitranslmed.abh2624. PubMed PMID: 34429372.

592. Liu C, Martins AJ, Lau WW, Rachmaninoff N, Chen J, Imberti L, Mostaghimi D, Fink DL, Burbelo PD, Dobbs K, Delmonte OM, Bansal N, Failla L, Sottini A, Quiros-Roldan E, Han KL, Sellers BA, Cheung F, Sparks R, Chun TW, Moir S, Lionakis MS, Consortium NC, Clinicians C, Rossi C, Su HC, Kuhns DB, Cohen JI, Notarangelo LD, Tsang JS. Time-resolved systems immunology reveals a late juncture linked to fatal COVID-19. Cell. 2021;184(7):1836-57 e22. Epub 2021/03/14. doi: 10.1016/j.cell.2021.02.018. PubMed PMID: 33713619; PMCID: PMC7874909.

593. Wolfel R, Corman VM, Guggemos W, Seilmaier M, Zange S, Muller MA, Niemeyer D, Jones TC, Vollmar P, Rothe C, Hoelscher M, Bleicker T, Brunink S, Schneider J, Ehmann R, Zwirglmaier K, Drosten C, Wendtner C. Virological assessment of hospitalized patients with

COVID-2019. Nature. 2020;581(7809):465-9. Epub 2020/04/03. doi: 10.1038/s41586-020-2196-x. PubMed PMID: 32235945.

594. Blighe K, Rana S, Lewis M. EnhancedVolcano: Publication-ready volcano plots with 667 enhanced colouring and labeling. R package version 1.6. 0. 668 https://github. com/kevinblighe. EnhancedVolcano; 2020.

595. Butler A, Hoffman P, Smibert P, Papalexi E, Satija R. Integrating single-cell transcriptomic data across different conditions, technologies, and species. Nat Biotechnol. 2018;36(5):411-20. Epub 2018/04/03. doi: 10.1038/nbt.4096. PubMed PMID: 29608179; PMCID: PMC6700744.

596. Burke DC, Isaacs A. Further studies on interferon. Br J Exp Pathol. 1958;39(1):78-84. Epub 1958/02/01. PubMed PMID: 13510551; PMCID: PMC2082203.

597. Isaacs A, Burke DC. Mode of action of interferon. Nature. 1958;182(4642):1073-4. Epub 1958/10/18. doi: 10.1038/1821073a0. PubMed PMID: 13590226.

598. Isaacs A, Lindenmann J. Virus interference. I. The interferon. Proc R Soc Lond B Biol Sci. 1957;147(927):258-67. Epub 1957/09/12. doi: 10.1098/rspb.1957.0048. PubMed PMID: 13465720.

599. Isaacs A, Lindenmann J, Valentine RC. Virus interference. II. Some properties of interferon. Proc R Soc Lond B Biol Sci. 1957;147(927):268-73. Epub 1957/09/12. doi: 10.1098/rspb.1957.0049. PubMed PMID: 13465721.

600. Lindenmann J, Burke DC, Isaacs A. Studies on the production, mode of action and properties of interferon. Br J Exp Pathol. 1957;38(5):551-62. Epub 1957/10/01. PubMed PMID: 13479681; PMCID: PMC2082625.

601. Povysil G, Butler-Laporte G, Shang N, Wang C, Khan A, Alaamery M, Nakanishi T, Zhou S, Forgetta V, Eveleigh RJ, Bourgey M, Aziz N, Jones SJ, Knoppers B, Scherer SW, Strug LJ, Lepage P, Ragoussis J, Bourque G, Alghamdi J, Aljawini N, Albes N, Al-Afghani HM, Alghamdi B, Almutairi MS, Mahmoud ES, Abu-Safieh L, El Bardisy H, Harthi FSA, Alshareef A, Suliman BA, Alqahtani SA, Almalik A, Alrashed MM, Massadeh S, Mooser V, Lathrop M, Fawzy M, Arabi YM,

Mbarek H, Saad C, Al-Muftah W, Jung J, Mangul S, Badji R, Thani AA, Ismail SI, Gharavi AG, Abedalthagafi MS, Richards JB, Goldstein DB, Kiryluk K. Rare loss-of-function variants in type I IFN immunity genes are not associated with severe COVID-19. J Clin Invest. 2021;131(14). Epub 2021/05/28. doi: 10.1172/JCI147834. PubMed PMID: 34043590; PMCID: PMC8279578.

602. Lee JS, Park S, Jeong HW, Ahn JY, Choi SJ, Lee H, Choi B, Nam SK, Sa M, Kwon JS, Jeong SJ, Lee HK, Park SH, Park SH, Choi JY, Kim SH, Jung I, Shin EC. Immunophenotyping of COVID-19 and influenza highlights the role of type I interferons in development of severe COVID-19. Sci Immunol. 2020;5(49). Epub 2020/07/12. doi: 10.1126/sciimmunol.abd1554. PubMed PMID: 32651212; PMCID: PMC7402635.

603. Prelli Bozzo C, Nchioua R, Volcic M, Koepke L, Kruger J, Schutz D, Heller S, Sturzel CM, Kmiec D, Conzelmann C, Muller J, Zech F, Braun E, Gross R, Wettstein L, Weil T, Weiss J, Diofano F, Rodriguez Alfonso AA, Wiese S, Sauter D, Munch J, Goffinet C, Catanese A, Schon M, Boeckers TM, Stenger S, Sato K, Just S, Kleger A, Sparrer KMJ, Kirchhoff F. IFITM proteins promote SARS-CoV-2 infection and are targets for virus inhibition in vitro. Nat Commun. 2021;12(1):4584. Epub 2021/07/30. doi: 10.1038/s41467-021-24817-y. PubMed PMID: 34321474; PMCID: PMC8319209.

604. Levin D, Schneider WM, Hoffmann HH, Yarden G, Busetto AG, Manor O, Sharma N, Rice CM, Schreiber G. Multifaceted activities of type I interferon are revealed by a receptor antagonist. Sci Signal. 2014;7(327):ra50. Epub 2014/05/29. doi: 10.1126/scisignal.2004998. PubMed PMID: 24866020; PMCID: PMC4311876.

605. Pan M, Kalie E, Scaglione BJ, Raveche ES, Schreiber G, Langer JA. Mutation of the IFNAR-1 receptor binding site of human IFN-alpha2 generates type I IFN competitive antagonists. Biochemistry. 2008;47(46):12018-27. Epub 2008/10/22. doi: 10.1021/bi801588g. PubMed PMID: 18937499.

606. Urin V, Levin D, Sharma N, Harari D, Schreiber G. Fine Tuning of a Type 1 Interferon Antagonist. PLoS One. 2015;10(7):e0130797. Epub 2015/07/15. doi: 10.1371/journal.pone.0130797. PubMed PMID: 26158644; PMCID: PMC4497658.

607. Perez-Zsolt D, Munoz-Basagoiti J, Rodon J, Elosua-Bayes M, Raich-Regue D, Risco C, Sachse M, Pino M, Gumber S, Paiardini M, Chojnacki J, Erkizia I, Muniz-Trabudua X, Ballana E, Riveira-Munoz E, Noguera-Julian M, Paredes R, Trinite B, Tarres-Freixas F, Blanco I, Guallar V, Carrillo J, Blanco J, Telenti A, Heyn H, Segales J, Clotet B, Martinez-Picado J, Vergara-Alert J, Izquierdo-Useros N. SARS-CoV-2 interaction with Siglec-1 mediates trans-infection by dendritic cells. Cell Mol Immunol. 2021. Epub 2021/11/17. doi: 10.1038/s41423-021-00794-6. PubMed PMID: 34782760.

608. Doehn JM, Tabeling C, Biesen R, Saccomanno J, Madlung E, Pappe E, Gabriel F, Kurth F, Meisel C, Corman VM, Hanitsch LG, Treskatsch S, Heim K, Stegemann MS, Ruwwe-Glosenkamp C, Muller-Redetzky HC, Uhrig A, Somasundaram R, Spies C, von Bernuth H, Hofmann J, Drosten C, Suttorp N, Witzenrath M, Sander LE, Hubner RH. CD169/SIGLEC1 is expressed on circulating monocytes in COVID-19 and expression levels are associated with disease severity. Infection. 2021;49(4):757-62. Epub 2021/04/08. doi: 10.1007/s15010-021-01606-9. PubMed PMID: 33825125; PMCID: PMC8023546.